Universiteit
Leiden
The Netherlands

# Off the wall: characterisation and exploitation of a cell wall-deficient life style in filamentous actinomycetes

Ramijan Carmiol, A.K.

**Citation**
Ramijan Carmiol, A. K. (2019, September 17). *Off the wall: characterisation and exploitation of a cell wall-deficient life style in filamentous actinomycetes*. Retrieved from https://hdl.handle.net/1887/75618

| | |
|---|---|
| Version: | Publisher's Version |
| License: | Licence agreement concerning inclusion of doctoral thesis in the Institutional Repository of the University of Leiden |
| Downloaded from: | https://hdl.handle.net/1887/75618 |

**Note:** To cite this publication please use the final published version (if applicable).

Cover Page

Universiteit Leiden

The handle http://hdl.handle.net/1887/75618 holds various files of this Leiden University dissertation.

**Author**: Ramijan, Carmiol A.K.
**Title**: Off the wall: characterisation and exploitation of a cell wall-deficient life style in filamentous actinomycetes
**Issue Date**: 2019-09-17

# Off the wall:

## characterisation and exploitation of a cell wall-deficient life style in filamentous actinomycetes

**Proefschrift**

ter verkrijging van
de graad van Doctor aan de Universiteit Leiden,
op gezag van Rector Magnificus prof.mr. C.J.J.M. Stolker,
volgens besluit van het College voor Promoties
te verdedigen op dinsdag 17 september 2019
klokke 10.00 uur

**door**

Ana Karina Ramijan Carmiol
geboren te San José, Costa Rica
in 18 June 1985

| | |
|---|---|
| **Promotores:** | Prof. dr. G.P. van Wezel<br>Dr. D. Claessen |
| **Promotiecommissie:** | Prof. dr. A. H. Meijer (voorzitter)<br>Prof. dr. N. I. Martin (secretaris) |
| **Overige commissieleden:** | Prof. dr. A. Briegel<br>Dr. T. den Blaauwen<br>Dr. L. J. Wu |

This research was part of the project 12957 funded by the
Applied and Engineering Sciences division TTW,
a domain of the Netherlands Organization for Scientific Research (NWO).

An electronic version of this dissertation is available at:
http://hdl.handle.net/1887/75618

*A mi familia*

## Contents


**Chapter 1** General Introduction .....7

**Chapter 2** Genome rearrangements and megaplasmid loss co-occur with protoplast formation and regeneration in the filamentous bacterium *Kitasatospora viridifaciens* .....19

**Chapter 3** Stress-induced formation of cell wall-deficient cells in filamentous actinomycetes .....39

**Chapter 4** Exploitation of a shape-shifting *Kitasatospora viridifaciens* strain identifies a MurG-like protein required for peptidoglycan synthesis .....75

**Chapter 5** Application of cell wall-deficient variants of the filamentous actinomycete *Kitasatospora viridifaciens* as microbial cell factories .....105

**Chapter 6** Summary and General Discussion.....119

Nederlandse Sammenvating.....131

References.....145

Curriculum vitae.....166

Publications.....168

# Chapter 1
# General Introduction



Part of this chapter was published as: Ultee, E., Ramijan, K. *et al*. “Stress-induced adaptive morphogenesis in bacteria”. *Advances in Microbial Physiology* **74** (2019)

## Filamentous actinomycetes

Actinobacteria constitute one of the largest phyla within the bacterial domain. This phylum contains Gram-positive species with a high GC content and a range of different morphologies, including cocci, rods, or mycelia[1,2]. The fragmented hyphal shape was used to name the Actinomycetales order as the term derives from the Greek words, *aktis* (ray) and *mukēs* (fungi)[2]. Actinomycetes species that form sporulating aerial hyphae are classified within the *Streptomycetaceae* family[3]. Novel taxonomic markers and the increasing number of genome-sequencing projects have helped in the classification of the different actinomycetes belonging to the *Streptomycetaceae* family. Recent phylogenetic analysis have validated *Kitasatospora*[4,5] and *Streptacidiphilus*[6] as sister genera of *Streptomyces*, which collectively comprise this family. All members of the *Streptomycetaceae* share a canonical life cycle[7] (see Fig. 1).

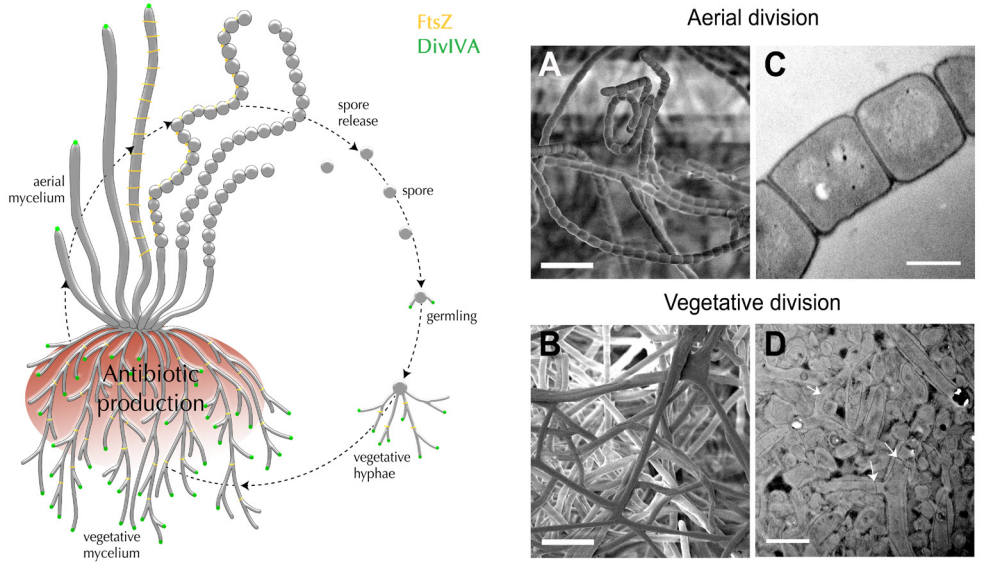


**Figure 1. The developmental life cycle in the *Streptomycetaceae* family.** The cycle starts with the germination of spores and the formation of germ tubes that grow by tip extension, a process coordinated by DivIVA. After a period of vegetative growth, aerial hyphae are formed, which will ultimately sepatate into chains of spores. Sporulation requires FtsZ, which assembles into rings that uniformly compartmentalize the aerial hyphae. Following their formation, spores are dispersed to establish colonies elsewhere. The scanning electron micrographs shows the aerial (**A**) and the vegetative (**B**) hyphae of *Kitasatospora viridifaciens* and depict the two distinct modes of cell division, namely septation during sporulation (**C**) and cross-wall formation during vegetative growth (**D**). Scale bar represents 5 µm (**A, B**), 500 nm (**C**) and 2 µm (**D**). Schematic life cycle adapted with permission of Lizah van der Aart. The scanning electron micrographs were taken with the assistance of Joost Willemse.

The life cycle starts with the germination of spores, leading to the formation of germ tubes that grow by tip extension. New tips are formed by lateral branching, which generates a vegetative mycelium[8]. The vegetative mycelium contains multinucleated compartments, formed by widely spaced cross-walls[9]. Upon nutrient depletion, a complex developmental program initiates both the reproductive growth phase and antibiotic production[10]. During this stage, programmed cell death (PCD) induces the degradation of the vegetative mycelium, causing the release of building blocks required for formation of aerial hyphae[2]. Ultimately, the aerial hyphae develop into thick-walled and grey-pigmented spores[11]. These spores can be dispersed again to establish new colonies elsewhere.

The developmental transitions from vegetative to aerial growth and sporulation are tightly controlled. For instance, the *bld* (bald) genes regulate the onset of aerial growth (Table 1). Null mutations in these genes give a comparable phenotype: a smooth ("hairless") colony surface where formation of aerial hyphae is blocked[12,13]. Likewise, spore formation is controlled by the *whi* (white) genes (Table 1), as sporulation-defective mutants are unable to form the characteristic grey-pigmented spores and remain white[14,15]. The *bld* and *whi* genes encode mostly regulatory proteins[16]. In addition, several structural proteins have been characterized that are required for the formation of aerial hyphae: the spore-associated protein B (SapB), the chaplins and the rodlins[17-22], which collectively render aerial hyphae hydrophobic. Additionally, a surface-associated glycan is required for aerial growth. The proteins responsible for synthesis of this glycan are encoded in the *cslA-glxA* operon, which act in conjunction with a series of copper-related proteins[23-28]. Table 1 provides a selected overview of genes that cause defects in morphological development in *Streptomyces*, genes required for cell division and cell wall synthesis are discussed in the following sections.

**Table 1.** List of genes affecting development in *Streptomyces*. Please note that the list only shows a selection of genes known to influence morphogenesis.

| Locus | Gene product | Reference |
|---|---|---|
| ***Cell division genes*** | | |
| *ftsZ* | Tubulin-like protein | 29,30 |
| *ftsQ (divIB)* | Small membrane protein required for sporulation septa | 31 |
| *ftsW** | Integral membrane protein required for sporulation septa | 32,33 |
| *ftsI** | Penicillin binding protein | 32 |
| *ftsL** | Membrane protein required for sporulation septa | 34 |
| *ssgA* | Cytoplasmic protein that activates septum formation | 35,36 |
| *ssgB* | Cytoplasmic protein that recruits FtsZ during sporulation | 37-39 |
| ***bld* genes** | | |
| *bldA* | Leucyl tRNA | 40,41 |
| *bldB* | Small DNA-binding protein | 42-44 |
| *bldC* | Transcriptional regulator of the MerR family | 45,46 |
| *bldD* | Small DNA-binding protein that binds to promoters of *whiG, bldN* and *sigH* | 47-49 |
| *bldG* | Anti-anti-sigma factor | 50,51 |
| *bldH* | AraC-like regulator (also called *adpA*) | 13 |
| *bldK* | Oligopeptide ABC transporter | 52-54 |
| *bldJ* | Extracellular signaling molecule imported by BldK | 52 |
| *bldM* | Two component response regulator (BldM-WhiI) | 55,56 |
| *bldN* | ECF sigma factor | 57-59 |
| ***whi* genes** | | |
| *whiA* | Transcription factor with WhiB | 60,61 |
| *whiB* | Transcription factor with WhiA | 61,62 |
| *whiD* | Transcription factor (also called *wblB*) | 63,64 |
| *whiE* | 8 gene locus for grey polyketide spore pigment | 65 |
| *whiG* | RNA polymerase sigma factor | 66,67 |
| *whiH* | Transcriptional repressor of the GntR family | 68 |
| *whiI* | Response regulator | 69,70 |
| *whiJ*$^{+}$ | DNA-binding protein, repressor of development. | 71,72 |
| **Hydrophobic sheath components** | | |
| *ramCSABR* | Gene cluster involved in the synthesis of the SapB precursor | 73-75 |
| *chpA-H* | Chaplin proteins | 19-21 |
| *rdlAB* | Rodlin proteins | 18,22 |
| **Cell surface polymers** | | |
| *cslA* | Cellulose synthase-like protein | 24,26 |
| *glxA* | Radical-copper oxidase | 25,26 |
| *sco** | Copper metallochaperone | 76 |
| *dtpA** | DyP-type Peroxidase A | 77 |

$^{+}$Grey phenotype, *Defective sporulation is medium dependent, ECF: extracytoplasmic function

## Filamentous growth and cell division in actinomycetes

The cell wall is a highly dynamic structure. In order for cells to grow, incorporation of new cell wall material into the pre-existing PG needs to be spatially and temporary controlled. Filamentous actinomycetes grow by apical tip extension, in which nascent PG is incorporated at the hyphal tip[78]. Tip growth relies on DivIVA (Green foci in hyphae Fig. 1), which is a coiled-coil protein preferring negatively-curved membranes and in actinobacteria it is an essential protein[78-81]. In *Streptomyces coelicolor*, DivIVA forms a multiprotein complex together with cytoskeletal proteins Scy and FilP, called the polarisome. This complex guides PG synthesis at existing hyphal tips and induces new tips during branching[82,83]. This makes the role of DivIVA in actinobacteria strikingly different from that in firmicutes, where DivIVA is not essential and mostly involved in correct placement of the septum[84,85].

Cell division in filamentous actinomycetes is markedly different between the vegetative and reproductive growth phases. During vegetative growth cell division leads to the formation of permeable cross-walls (Fig. 1) that allow diffusion of molecules[86-88] between the compartments, which remain physically connected to one another. Although the deletion of the conserved cell division gene *ftsZ* abolishes cross-wall formation, it is not lethal[29]. How mycelial networks are organized in the absence of cross-walls is under debate, but may involve membranous structures that compartmentalize the vegetative mycelium[86,87]. FtsZ has a second important role in actinomycetes during sporulation (Fig. 1), where it is necessary for assembling the cell division machinery driving constriction and separation[9]. In this way FtsZ has a more similar function to that in unicellular bacteria, where cell division starts with the positioning of FtsZ at midcell[89,90]. In *Escherichia coli* and *Bacillus subtilis*, FtsZ localization is controlled by the activity of the Min system and nucleoid exclusion[91-93]. These systems exert their effect on FtsZ positioning by preventing polymerization at unwanted sites in the cell. Contrary to these mechanisms in unicellular bacteria, positioning of FtsZ is positively controlled in actinomycetes. Actinomycetes use SsgB to localize FtsZ to the sites where cell division septa will be formed[39]. Following assembly of the other required divisome members, a thick cell wall is synthesized.

## Peptidoglycan synthesis

An important constituent of the cell wall is peptidoglycan (PG). The PG forms a meshwork-like structure that envelopes the cell, and which in essence forms a single gigantic molecule called the murein sacculus[94]. Peptidoglycan strands are composed of monomers of N-acetylglucosamine (GlcNAc) and N-acetylmuramic acid (MurNAc). These strands are covalently cross-linked via peptide stems that emerge from the MurNAc subunits. The composition of the peptide stem and the degree of cross-linking varies tremendously among bacterial species and can also vary along with changes in environmental conditions[95,96].

The PG biosynthetic pathway can be spatially divided into three phases: a cytoplasmic phase, a membrane-associated phase and a periplasmic phase. In the cytosolic phase, precursor molecules UDP-GlcNAc and UDP-MurNAc-pentapeptide are formed. All steps are regulated by a cascade of mainly Mur enzymes: a family of transferases (MurA), dehydrogenases (MurB), amino acid ligases (MurC, MurD, MurE, MurG, and Ddl), racemases (Alr, DadX, and MurI) and glycosyltransferases (MraY, MurG)[97,98]. In the next phase, the cytoplasmic product UDP-MurNAc-pentapeptide is tethered to the lipid membrane via the transport lipid bactoprenol (C55- isoprenoid undecaprenyl phosphate), thereby forming the precursor lipid I. Attachment of UDP-GlcNAc to lipid I via MurG leads to the formation of lipid II. Lipid II is then transported to the other side of the cytoplasmic membrane. The identity of the transporter or flippase in the PG biosynthesis pathway remains controversial, although studies highlight FtsW[99], MurJ[100,101] and/or Amj[102] as possible candidates.

In the final phase of PG synthesis, lipid II monomers are polymerized into PG strands by glycosyltransferases in the periplasmic space[98]. These glycan strands are then incorporated into the pre-existing sacculus structure and cross-linked by transpeptidases. These glycosyltransferases and transpeptidases are referred to as penicillin binding proteins (PBPs) after their affinity for the antibiotic penicillin, which inhibits the activity of these PG synthases[103,104]. Recently, a new family of PG synthases was described: the SEDS (shape, elongation, division and sporulation) proteins[105-107]. In contrast to the PBPs, the SEDS proteins are relatively insensitive to antibiotics known to inhibit PBPs. Instead, the SEDS are affected by a different class of bioactive compounds, and thus may be an interesting target for novel antibiotics[108].

## Adaptive morphogenesis

The cell wall is a highly dynamic structure, which can be altered in response to the cell's requirement. For example, alpha-proteobacteria, like *Caulobacter crescentus* can synthesize a single stalk as part of their dimorphic life cycle[109]. Other bacterial cells can undergo morphological changes

to move to new environments. For instance, when motile bacteria are challenged by dry surroundings or increased viscosity, they can differentiate into swarmer cells, which are elongated and have typically an increase number of flagella[110,111].

Sudden temperature shocks, changes in the pH or changes in the amount of osmolytes can also stress the cell envelope and lead to changes[112]. In both Gram-positive and Gram-negative bacteria, perturbations in the integrity of the cell envelope often initiate a so-called cell envelope stress response (CESR)[113,114]. In Gram-negative bacteria, the CESR is also triggered when cell envelope proteins in the periplasm are damaged or malfunctioning[114]. Upon activation, the CESR-linked regulatory systems will try to counteract the induced damage. The regulatory systems underlying this stress response are conserved, and the best-known ones are two component systems (TCS) and extracytoplasmic function (ECF) sigma factors. TCS are comprised of a membrane-associated sensor kinase that autophosphorylates before transferring the phosphoryl group to its cognate response regulator[115]. A good example of how TCS affects cell wall homeostasis, and thereby cellular morphology, has been described for *Corynebacterium glutamicum* . Under the influence of hyperosmotic conditions, the *mtrAB* two component system is involved in the regulation of cell wall metabolism and osmoregulation. Depletion of *mtrAB* caused a morphogenic switch from rod-shape to segmented cells and conferred resistance to ethambutol[116]. This two-component system is also present in *Mycobacterium tuberculosis*, where it is involved in the virulence response of this bacterium[117,118].

Microorganisms inhabiting environments where sudden environmental changes occur often have specific adaptation mechanisms. For instance, microorganisms in snow and ice habitats have to cope with fluctuating seasonal changes, which include variations in temperatures, UV radiation and availability of nutrients and water[119]. These physical and chemical conditions may lead to desiccation caused by rapid loss of cytoplasmic water and the increase in intracellular ions, which affects cell size homeostasis and compromises membrane integrity[120]. An example of a specific adaptation to cope with this stress is found in *Arthrobacter* strain A3 isolated from the alpine permafrost. Upon cold shock, this strain accumulates the non-reducing disaccharide trehalose that acts as an intracellular osmoprotectant[121]. The OstA protein is involved in the synthesis of trehalose but also acts as an osmotic stress-sensing morphogenetic protein. Depletion of OstA not only reduced the intracellular content of trehalose but also arrested the morphological switch from rod-shaped to myceloid cells[122].

Another specific adaptation mechanism is observed in microorganisms which are abruptly exposed to acid

stress. Bacteria used as probiotics entering the stomach get challenged with extreme acid stress and require a fast response to survive the sudden exposure to hydrochloric acid. For instance, when *Propionibacterium freundenreichii* strain SI41 was exposed to an acidic environment of pH 2, the cells underwent severe mortality, and changed their morphology from rod-shaped to segmented cells. If transient exposure to pH 5 in a chemically defined medium is allowed, the acid tolerance response takes place and there is no significant loss of viability or dramatic change in morphology[123].

In response to a large variety of environmental stresses, several bacteria transit into a so-called viable but non-culturable (VBNC) state[124]. In this state, the cells remain metabolically active but do not proliferate when transferred to nutrient-rich environments. Bacteria in environmental reservoirs can transition into the VBNC state, but also pathogenic bacteria can change into the VBNC within their host[125]. For instance, the gastric disease and ulcer-causing bacterium *Helicobacter pylori* transitions from its characteristic spiral shape to a coccoid VBNC state, under starvation conditions, aerobiosis and acid stress[126]. Some studies report structural modifications of the peptidoglycan that accompany this morphological transformation. Analysis of PG architecture revealed a substantial accumulation of the dipeptide monomers (N-acetylglucosaminyl-N-acetylmuramyl–L-Ala–D-Glu), and a decrease of tripeptide monomers (N-acetylglucosaminyl-N-acetylmuramyl–L-Ala–D-Glu-mesoDAP) in coccoid cells compared to the spiral form[127]. The PG hydrolase AmiA is responsible for the dipeptide monomer accumulation. This PG modification provides an escape from the immune sensor (nucleotide oligomerization domain) Nod1, which only senses murein tripeptides or longer and is unable to recognize dipeptides[128].

Adaptive morphogenesis is not restricted to bacteria. Also in Archaea modification of the cell envelope is a common strategy to cope with extreme environmental changes. Several species from the *Methanosarcina* genus adapt to elevated osmolarity, during which they transition from multicellular aggregates to spherical single cells as they lose the methanochondroitin outer layer[129]. Also, *Haloarchaea* species from the Deep Lake community in Antarctica adapt to cold-water temperatures, by changing the N-acetylation of the S-layer and forming biofilms[130]. Altogether, these examples demonstrate that cell envelope changes are common in microorganisms when they are exposed to stress-causing conditions.

## Life without a cell wall

Although the cell wall provides mechanical protection to virtually all bacteria[98,104], several species can adapt to a transient or permanent life style without this protective envelope. For instance, the multidrug resistance pathogen *Pseudomonas aeruginosa* can transition from rod-shaped to spherical cell wall-deficient (CWD) cells when treated

with β-lactams, which provides a mechanism to escape from the bactericidal effect. When the antibiotic is removed, the entire population of cells reverts to the walled state[131]. Likewise, the rod-shaped bacterium *Mycobacterium bovis* undergoes a dramatic morphological transition when exposed to harsh conditions such as cryogenic stress and nutrient starvation, leading to the formation of giant filamentous structures that produce and release spherical CWD cells[132]. These morphological variances offer an alternative route for the cell to survive and reproduce whilst exposed to stress.

Interestingly, several bacterial species evade the stress of cell wall-targeting antibiotic by adopting a cell wall-deficient life style as so-called L-forms. The first L-forms were described in 1935 and named in honor of the Lister Institute where they were discovered[133]. Following the first studies on L-forms, many terms have been used interchangeably to describe morphologically similar cells such as L-phase bacteria, L-variants, and CWD forms. L-forms can be broadly described as mutant forms of walled bacteria that are able to grow and divide indefinitely without a cell wall. L-form bacteria require an isotonic environment since they lack the turgor-withstanding cell wall. A few clinical reports have described L-form cells in patient samples[134], and some studies have reported bacterial L-forms in plant tissue[135].

L-forms are generated in laboratory settings by cultivation of walled cells in osmoprotective media together with agents that degrade or interfere with cell wall synthesis, such as lysozyme and penicillin G[136-138]. Prolonged exposure in such media can cause bacterial cells to accumulate mutations, which promote a cell wall-deficient (CWD) life style[136,138-140]. These mutations fall in two separate classes. In the first class of mutation the cell membrane formation is stimulated either by blocking PG synthesis or directly activating the synthesis of fatty acids. In the tractable *B. subtilis* L-form system the expression of the *murE* operon was repressed, and in combination with penicillin treatment yielded cells that were able to proliferate without the cell wall[139]. Successful conversion to L-forms was also possible by deleting individual genes (*murC* and *dal*), which also blocked the PG precursor pathway[141]. Proliferation of L-forms was also benefited by a single point mutation in *accDA* or the overexpression of the AccDA protein. Both *accA* and *accD* are part of the protein complex acetyl-CoA carboxylase, which catalyze the first step in fatty acid synthesis[142]. Overexpression of these subunits increased the membrane lipid accumulation, benefiting the L-form mode-of-proliferation. The second class of mutations is important to reduce the oxidative stress caused by repression of cell wall synthesis. Kawai *et al* (2015) demonstrated that inhibition of PG synthesis stimulates the flux through the electron transport chain, which increases reactive oxygen species (ROS). This was based on three observations: 1) ROS levels are abnormally elevated in CWD cells, 2) repres-

sion of antioxidant systems in L-forms severely inhibited their proliferation and 3) anaerobic cultures or addition of ROS scavengers promote L-form growth in Gram-positive and Gram-negative bacteria[143].

Other studies have shared insights on how the transition to the L-form state requires the designated step of escape from the cell wall sacculus. For instance, the isolation of a *B. subtilis* strain that efficiently switches between the L-form and rod-shape state led to the identification of two mutations required for L-form escape. The first one mutation was identified in the *walR* transcription regulator, while a second mutation was identified in the cell division gene *sepF*[144].

Unlike walled bacteria, L-forms are able to propagate independently of the FtsZ-based division machinery[139]. Instead, these cells use a so-called extrusion-resolution system for proliferation, during which numerous progeny cells are more or less simultaneously released from the mother cell. Additionally, L-form cells may propagate by means of blebbing, tubulation and vesiculation, which give rise to a morphologically heterogeneous population of cells[139,140,145-149]. The mode by which L-forms proliferate is conserved in Gram-positive and Gram-negative bacteria and appears to be based solely on biophysical principles. The excessive membrane production in L-form cells drives an imbalance between the growth of the cell surface area and internal volume, leading to vesicle extrusion[140].

Although the biology of L-forms has been addressed in considerable detail, little is known about the relevance of these cells in wild bacteria, and whether the numerous examples of wall-less bacteria identified in patient[150-155] and plant[135,156-158] samples have accumulated mutations or contained a natural adaptation response system.

## Outline of thesis chapters

Filamentous actinomycetes have spurred much interest due to their ability to synthesize a wide diversity of natural products. Although these microorganisms have a canonical life cycle (Fig.1) and a characteristic multicellular mode-of-growth, they are able to transition to a unicellular, CWD state. In this thesis, the filamentous actinomycetes *Kitasatospora viridifaciens* DSM 40239 was chosen to study three distinct types of CWD cells: protoplasts, stress-induced S-cells (see below) and L-forms (Fig. 2). As a source to analyse genetic changes caused by the switch from a walled to a wall-deficient state, the genome sequence of *K. viridifaciens* was determined (**Chapter 2**). *In silico* analysis combined with PFGE approaches revealed that *K. viridifaciens* contains a linear chromosome and a megaplasmid KVP1. Unexpectedly, protoplast formation and regeneration often caused dramatic chromosomal rearrangements and loss of KVP1, which potentially provide a source for creating genetic diversity.

**Chapter 3** describes the response of filamentous actinomycetes to high levels of osmolytes in the environment. Such elevated osmolyte concentrations causes hyperosmotic stress, leading to a reduction in growth, an excess in membrane synthesis and hypercondensation of DNA. Strikingly though, were the spherical CWD S-cells that were extruded under these conditions in the culture. S-cell formation was found in many filamentous actinomycetes, inferring that this response is common. These S-cells are only transiently CWD and eventually establish new mycelia. Notably, prolonged exposure to hyperosomotic stress converted S-cells to mutant L-form variants that proliferate without a wall.

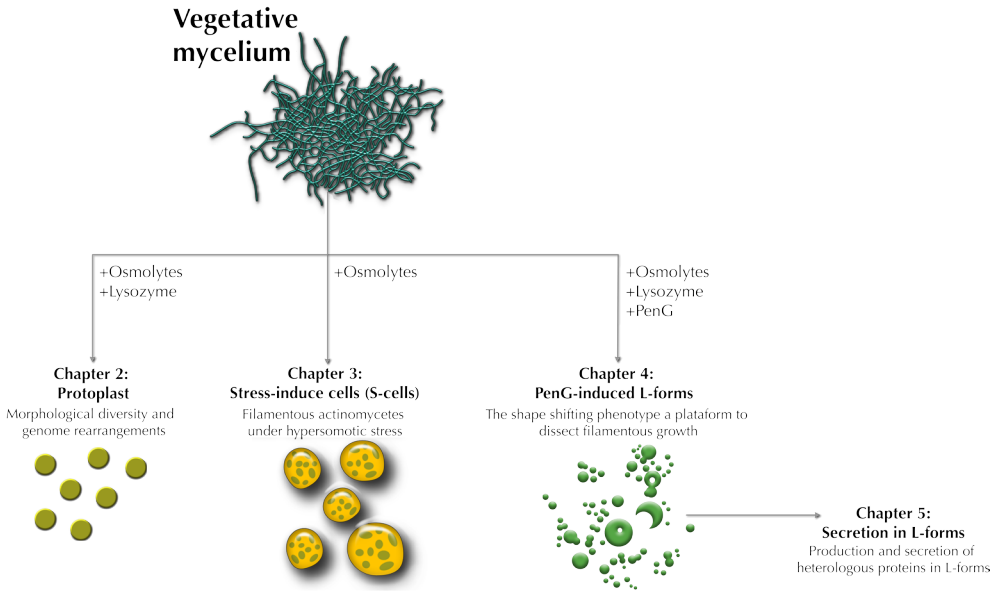


**Figure 2. Schematic outline of this thesis and the three types of CWD cells investigated.** The three types of CWD cells were formed in a osmoprotective environment with sucrose and magnesium chloride. Protoplast were obtained by lysozyme treatment which generates cells uniform in size. The Stress-induced cells formed as consequence of the hyperosmotic stress caused by excess of osmolytes, these CWD cells are heterogeneous in size. L-forms are mutants created after prolonged exposure to Penicillin G and lysozyme, they are not homogeneous in size.

**Chapter 4** investigates the use of a PenG-induced L-form strain of *K. viridifaciens* as a platform to identify genes required for the switch to the walled state. This strain, called *alpha*, has the unique ability to switch between a CWD and walled state, depending on the growth conditions. Using this strain allowed us to disrupt the polar growth determinant *divIVA* or part of the *dcw* gene cluster, which contains a number of genes involved in cell division and cell wall synthesis, including the essential gene *murG*. The absence of *divIVA* or the *dcw* gene cluster prevented *alpha* from switching to the walled state. Strikingly, complementation of the *dcw* mutant with solely the *divIVA* gene restored the switch to filamentous mode-of growth. An *in silico* analysis identified a *murG*-like gene in the genome of *K. viridifaciens*, hereinafter named *murG2*. Reduction of *murG2* in the absence of *murG* dramatically reduced the ability of *alpha* to switch to the filamentous mode-of-growth, implying that MurG2 provides lipid II synthase activity in the absence of MurG.

**Chapter 5** explores the capacity of *alpha* for the secretion of antibiotics and enzymes. We introduced a reporter plasmid with a cellulase gene, and we exploited the shape shifting capacity of *alpha* to compare the secretion in the L-form and mycelial state. The results demonstrate that secretion of secondary metabolites is not affected by the absence of the cell wall, and that DivIVA is not essential for secretion. Altogether these results are the first indications that *alpha* can be further improved as production platform.

A general conclusion to this thesis is provided in **Chapter 6**.

# Chapter 2
# Genome rearrangements and megaplasmid loss co-occur with protoplast formation and regeneration in the filamentous bacterium *Kitasatospora viridifaciens*

K. Ramijan, Z. Zhang, G.P. van Wezel and D. Claessen

## Abstract

Filamentous actinomycetes are multicellular bacteria with linear replicons. Here, we present the genome sequence of *Kitasatospora viridifaciens* DSM 40239, which contains a linear 7.8 Mb chromosome and an autonomously replicating plasmid KVP1 of 1.7 Mb. We observed that disruption of the multinucleated mycelium with lysozyme created morphological diversity after regeneration of protoplasts. Characterization and sequencing of an individual revertant colony that had lost the ability to differentiate coincided with loss of KVP1 and lesions in the right arm of the chromosome. Strikingly, the chromosomal lesion site is preceded by an insertion sequence (IS) element, suggesting that the genomic rearrangement may have been caused by replicative transposition and homologous recombination between both replicons. Altogether, these data indicate that protoplast formation is a stressful process that can lead to profound genetic changes.

Part of this chapter was published as: Ramijan, K. *et al.* Genome sequence of the filamentous actinomycete *Kitasatospora viridifaciens*. *Genome Announc* **5** (2017)

## Introduction

Filamentous actinomycetes are prolific producers of bioactive compounds. These metabolites are mostly used as weapons that provide protection against other microorganisms and phages in the environment[159,160]. This is particularly useful for filamentous organisms, given that they generally lack the ability to make flagella for escaping dangerous situations. In addition, these bacteria are able to generate resistant spores that can invade new environments after their dispersal. Germination of spores leads to the formation of 1-2 germ tubes, which grow by tip extension, thereby establishing filamentous cells called hyphae. Branching of hyphae leads to the formation of a multinucleated vegetative mycelium[161], which forages and acquires nutrients by decomposing polymeric substances. Stressful conditions (such as nutrient depletion) induce programmed cell death (PCD) of the mycelium, which in turn triggers morphological and chemical differentiation. This developmental transition leads to the formation of specialized hyphae that grow into the air, and the onset of production of a suite of bioactive compounds[2]. Eventually, the aerial hyphae metamorphose into chains of grey-pigmented spores[10]. Mutants that are unable to establish an aerial mycelium are called bald (*bld*), while those that are not capable to form spores are called white (*whi*) after their whitish color[162].

Genome mining has been an important tool for the discovery of novel natural products[163,164], many of which are contained on giant linear plasmids[165-168]. Although linear replicons are typically rare in bacteria, they are common in filamentous actinomycetes[169,170]. In fact, *Streptomyces* chromosomes (between 8 and 10 Mb in size) are also linear and typically comprise a “core region” containing the essential genes, and two variable “arms” with lengths ranging from 1.5 Mb to 2.3 Mb[171]. Like linear plasmids, the linear chromosomes are capped by terminal proteins bound to the 5’ end of the DNA[172]. Interestingly, the chromosomal ends are genetically unstable. Large (up to 2 Mb) DNA rearrangements including deletions or amplifications can occur within both chromosomal ends. Such rearrangements can lead to circularization of the chromosome, exchange of chromosomal arms or the formation of hybrid chromosomes due to recombination between the linear plasmids and the chromosome[173]. This wide range of genomic rearrangements is believed to be caused by transposition or homologous recombination, occurring actively within the chromosome or between the chromosome and linear plasmids[174]. Not surprisingly, these changes have profound effects on differentiation and secondary metabolism[175].

In this chapter we characterized genetic instability in the filamentous actinomycete *Kitasatospora viridifaciens*. Although this tetracycline producer strain was previously classified within the *Streptomyces* genus, it was suggested to belong to the *Kitasatospora* genus[176]. We show that protoplast formation and regeneration lead to the emergence of colonies that are no longer able to differentiate, which we attribute to the deletion of a 1.5 Mb segment of the right chromosomal arm and concomitant loss of most of the sequences contained on the large megaplasmid KVP1.

## Results

### Genomic characterization of *Kitasatospora viridifaciens*

To gain more insights in the phylogeny and with the prospect to further exploit *K. viridifaciens*, we extracted genomic DNA and performed whole genome sequencing using a combined Illumina/PacBio approach (see Methods for details). The genome comprised 9,560,682 bp with a G+C content of 72.20%, and revealed signature hallmarks of members of the *Kitasatospora* genus, such as a *Kitasatospora*-specific SsgB protein and the presence of DapF[176]. The whole genome sequence was assembled into four scaffolds (Table 1), with 112 gaps. The major part of the chromosome is contained on Scaffold 2 consisting of 7,834,366 bp and with a total of 7,143 predicted coding sequences (CDSs).

**Table 1.** Genome architecture of *K. viridifaciens* DSM40239

| | Scaffold 1 (KVP1) | Scaffold 2 (Chromosome) | Scaffold 3 | Scaffold 4 |
|---|---|---|---|---|
| Sequence length (bp) | 1,710,701 | 7,834,366 | 15,139 | 476 |
| GC content (%) | 70.9 | 72.5 | 71.4 | 71.4 |
| Coding sequences | 1638 | 7143 | 3 | 0 |
| rRNA | 0 | 31 | 0 | 0 |
| tRNA | 0 | 59 | 0 | 0 |
| ncRNA | 0 | 2 | 0 | 0 |
| tmRNA | 0 | 1 | 0 | 0 |

tmRNA: transfer messenger RNA, ncRNA: non-coding RNA

Further investigation revealed that Scaffold 1 represents a megaplasmid, hereinafter termed KVP1, consisting of 1,710,701 bp and carrying 1,516 genes. Consistent with other linear plasmids described for *Streptomyces*[167,177], KVP1 contains an autonomous replication origin that is centrally located. We found two genes encoding a possible replication protein (BOQ63_RS04290) and a putative plasmid DNA primase/helicase-like gene (BOQ63_RS04295) with an identity of 82 and 76% to Orf1 and Orf2 of the megaplasmid pSCL4 from *Streptomyces clavuligerus*, respectively[168]. Furthermore, KVP1 contains a *traA* gene for conjugative transfer (BOQ63_RS00360), as well as *parA* (BOQ63_RS04095) and *parB* (BOQ63_RS04100) required for DNA segregation. Analysis of the biosynthetic gene clusters (BGCs) using antiSMASH 5.0[178] located 11 BGCs on KVP1 and 33 clusters on the chromosome (Fig. S1). One of the BGCs showed high homology to the BGC for chlortetracycline (Fig. S2).

To test experimentally whether KVP1 is indeed a plasmid, we analysed genomic DNA of the wild-type strain with Pulsed-Field Gel Electrophoresis (PFGE). In the lane containing uncut DNA, a fragment with an estimated size between 1,600,000 and 2,200,000 bp (Fig. 1A, boxed region) was evident. This fragment would be consistent with a genetic element that migrates independently of the chromosomal DNA. When the DNA was digested with AseI, we observed multiple bands with estimated sizes smaller than 1,000,000 bp (Fig. 1A). However, two expected fragments of around 1,600,000 bp, based on an *in silico* prediction (Fig. 1E, 1F), were not observed, possibly due to low amounts of DNA (Fig. 1A). We therefore changed the growth conditions for the wild-type strain and in this manner were able to increase the total amount of DNA in the plug. Consequently, we were able to detect the expected fragments of 1,541,168 and 1,695,864 bp (see arrowheads in Fig. 1B). By further adjusting the switching time to 2.2-75 seconds, well-separated fragments with sizes ranging from 565,000 and 945,000 bp were identified (arrowheads Fig. 1C). Combining these different PFGE runs allowed us to map the AseI fragment spectrum to the *in silico* genome assembly of *K. viridifaciens* (Fig. 1E, 1F). Altogether, these results confirmed that KVP1 is a megaplasmid and verified the predicted AseI sites in the chromosome.

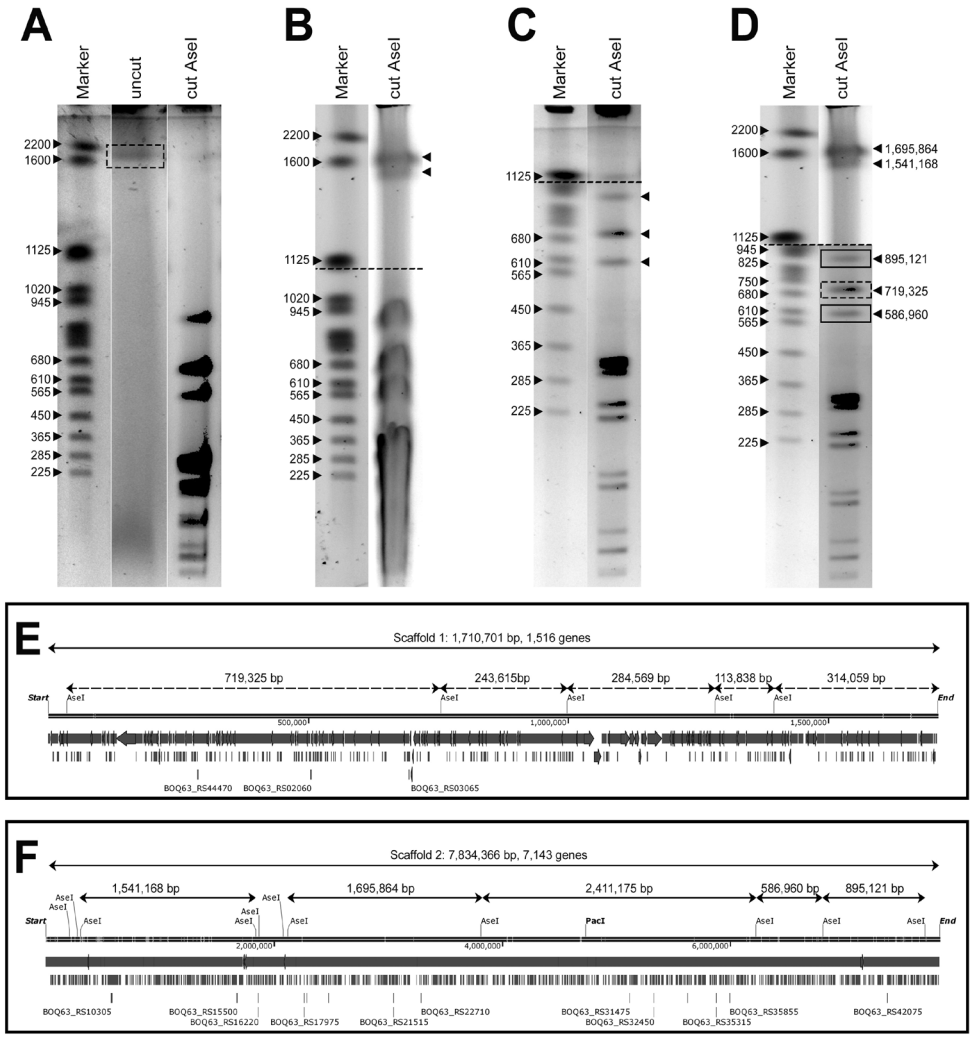


**Figure 1. KVP1 of *K. viridifaciens* is a megaplasmid.** PFGE of genomic DNA of *K. viridifaciens* grown in TSBS (**A, C**) or LPB (**B**) medium. DNA was separated using switching times of 60-125 seconds for 20 hours (**A, B**) or 2,2-75 seconds for 19 hours (**C**). (**D**) The composite gel shows fragments larger than 1,125,000 bp (from upper gel shown in panel **B**), and fragments smaller than 1,020,000 bp (from lower gel in panel **C**). The solid rectangles indicate fragments derived from the chromosome, while the dashed rectangles indicate fragments derived from KVP1. Predicted *in silico* maps of the KVP1 megaplasmid (Scaffold 1) and chromosome (Scaffold 2) of *K. viridifaciens* are shown in panels (**E**) and (**F**), respectively.

## Protoplast formation and regeneration leads to morphological diversity due to lesions and rearrangements in the chromosome and KVP1

The identification of KVP1 as a megaplasmid prompted us to analyse if it was distributed homogenously throughout the mycelium, by dissecting the mycelium into distinct protoplasts. If all protoplasts would carry an intact chromosome and KVP1 plasmid, regenerated colonies derived from them would in principle be wild-type. Notably, regenerated protoplasts yielded colonies with dramatic developmental defects. Although the majority of colonies formed grey-pigmented spores (yellow circles Fig. 2A), a significant number of colonies was brown and bald (red circles Fig. 2A). Sub-culturing of these bald colonies (referred to as "B" in Fig. 2C) indicated that they could be classified in three types based on their appearance: some gave rise to normally-appearing grey-pigmented colonies (B1), while others remained bald (B2) or yielded colonies with a wide variety of phenotypes, including colonies that again were bald (see dashed circles in panel B3).

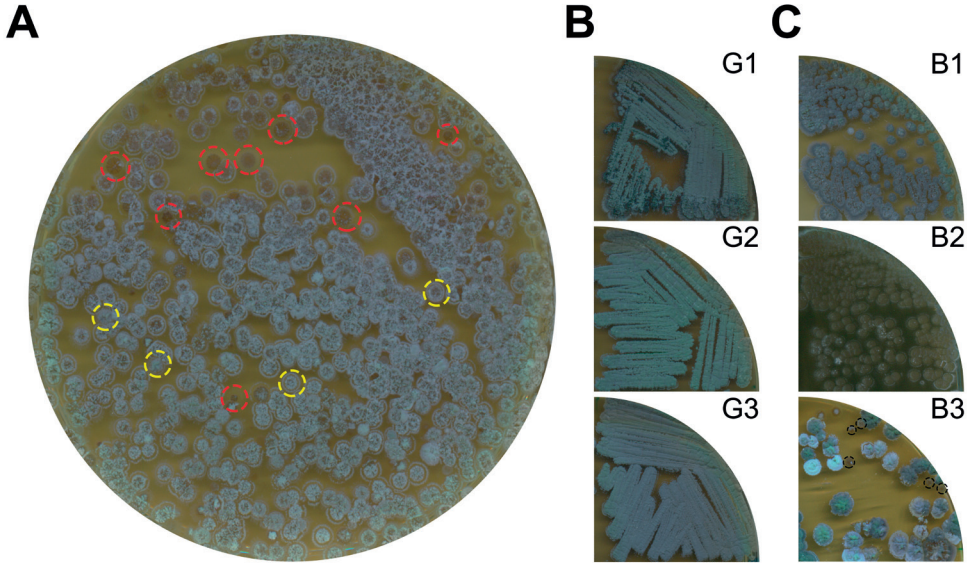


**Figure 2. Protoplast formation and regeneration yield colonies with developmental defects** (**A**) Protoplasts of *K. viridifaciens* regenerated on MYM medium yields grey-pigmented colonies (yellow dotted circles) and brown colonies (red dotted circles). The grey colonies retain their morphology in subsequent subcultures (**B**). Subculturing of the brown colonies (**C**) reveals morphological heterogeneity: some colonies appear grey-pigmented (B1), while others are bald (B2) or display a variety of phenotypes (B3), including again bald colonies (indicated with black dashed circles).

To exclude the possibility that regeneration of protoplasts on the used MYM medium, which lacks osmoprotectants, was causing the observed defects in development, we also analysed the phenotypes of colonies regenerated from protoplasts on R5 medium, which is more commonly used[179]. We observed that regenerated colonies were unable to differentiate on R5 medium (Fig. S3A). We therefore picked 149 random colonies from R5 medium and analysed their phenotype subsequently on MYM medium (Fig. S3B). After 7 days of growth on MYM medium, 77% of the colonies had a (near) wild-type morphology and produced grey-pigmented spores, while 23% of the colonies were defective in development. This demonstrated that the observed morphological heterogeneity detected after protoplast formation and regeneration is medium-independent.

We reasoned that (partial) loss of KVP1 could explain some of the morphological defects observed in the regenerated colonies[180]. To test this assumption, we sub-cultured three B3-type bald colonies (encircled in Fig. 2C) on MYM medium (Fig. 3A). The resulting strains showed severe morphological defects, and even after 14 days of cultivation these stains failed to produce grey-pigmented spores (Fig. 3A). We extracted genomic DNA from the independent lineages (B3.1, B3.2, B3.3), and investigated the presence of genes located in the chromosome and on the KVP1 megaplasmid. Quantitative real-time PCR detected the chromosomal gene *infB* in the wild-type strain and the three tested lineages before the 20$^{th}$ cycle (Fig. 3B). Conversely, the *allC* gene located on the KVP1 plasmid was only detected in the wild-type strain (Fig. 3C). Similarly, we were unable to detect the KVP1-specific genes *orf1*, *parA* and *tetR* (Fig. 3D). These results suggest that the megaplasmid KVP1 had been lost in the bald colonies from the B3-type.

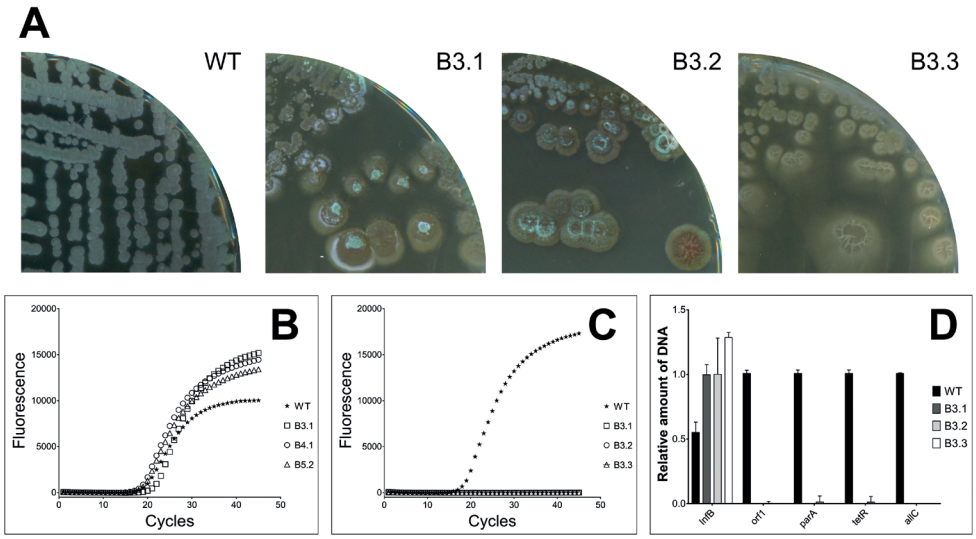


**Figure 3. Bald colonies have lost the KVP1 megaplasmid.** (**A**) Three independently isolated bald strains (B3.1, B3.2 and B3.3) are unable to sporulate on MYM medium, unlike the wild-type strain. Quantitative real-time PCR showed the presence of chromosomal gene *infB* (**B**) in both the wild-type and bald strains. In contrast, the *allC* gene (**C**) located on KVP1 is only present in the wild-type strain. (**D**) The relative abundance of four megaplasmid genes (*orf1*, *parA*, *tetR*, *allC*) in comparison to the abundance of the chromosomal gene *infB* suggest that KVP1 is lost in strains B3.1, B3.2 and B3.3.

To analyse if the entire KVP1 megaplasmid was lost, we performed whole genome sequencing of strain B3.1. Contrary to the wild-type strain, the number of reads mapping to the KVP1 megaplasmid was almost 10-fold reduced in B3.1 (Fig. 4A, right column); while 1,112,768 Illumina reads in the sequenced wild-type strain mapped to KVP1, only 143,387 reads were identified in B3.1. Interestingly, the vast majority of reads mapped to the right arm of the plasmid (dashed black rectangle in Fig. 4A). Remarkably, also the number of reads mapping to the right arm of the chromosome was dramatically decreased in the mutant strain (dashed red rectangle in right column Fig. 4B). A more detailed analysis indicated that most chromosomal sequences between 6,261,000 bp and 7,725,700 bp (Fig. 4C, arrow) were absent in B3.1. Apparently, strain B3.1 had not only lost the majority of sequences contained on KVP1, but also a major part of its right chromosomal arm. Further investigation revealed the lesion site (lower pannel Fig. 4D and E), and immediately adjacent to the chromosomal deletion start (around 6,261,000 bp) the presence of an insertion sequence (IS) (Table 2). This IS contains the BOQ63_RS37135 gene encoding the transposase likely involved in moving this element. Furthermore, a detailed inspection of KVP1 sequences still present in strain B3.1 (164,769 bp

in total) revealed numerous transposition elements in the right arm of KVP1, from them five had a high homology to the IS element encoded by BOQ63_RS37135 (see asterisks in Table 3). Altogether, these results indicate that major chromosomal and megaplasmid rearrangements and DNA loss occur during protoplast formation and regeneration, which may relate to the presence of IS elements.

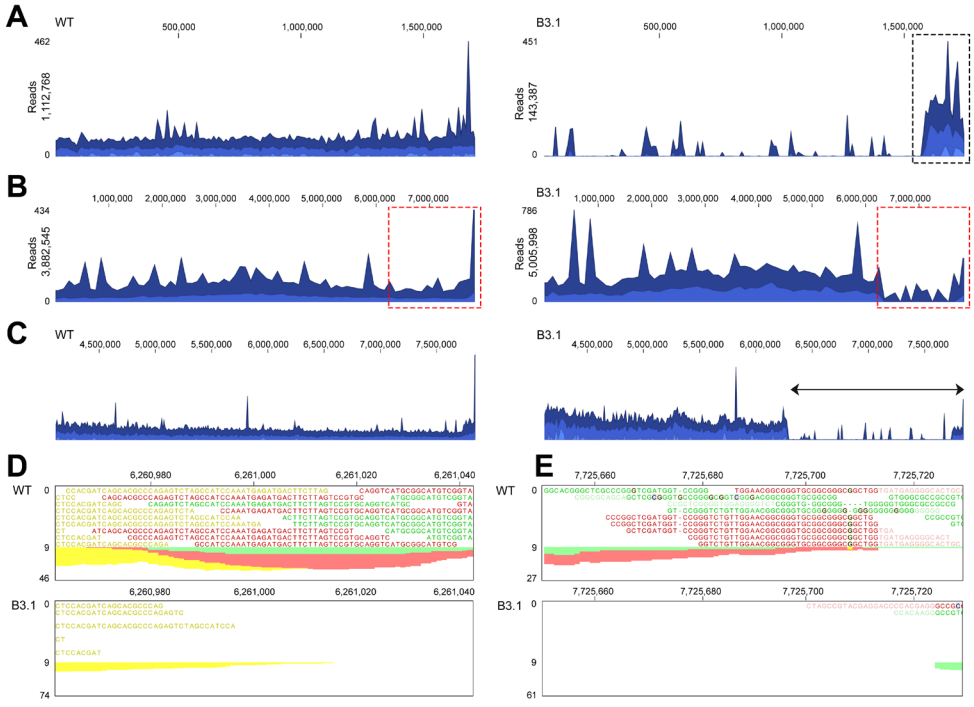


**Figure 4. Whole genome sequencing reveals major chromosomal and megaplasmid lesions in strain B3.1.** Alignment of Illumina reads of the wild type (left) and B3.1 strain (right) against KVP1 (**A**) and the chromosome (**B**). Please note the high coverage of KVP1 sequences detected in the wild type (1,112,768 reads) compared to those of strain B3.1 (143,387 reads). Similarly, a high coverage in the right arm of the chromosome (dashed red rectangle) is observed for the wild-type (**B**, left panel) in comparison to strain B3.1 (**B**, right panel). (**C-E**) A more detailed characterization reveals the lession site that reads between 6,261,000 and 7,725,700 are absent in the right arm of the chromosome of strain B3.1.

**Table 2.** Transposition elements in the chromosome of *K. viridifaciens*

| Locus | Product | Location | |
|---|---|---|---|
| | | Start | Finish |
| BOQ63_RS09605 | IS5/IS1182 family transposase | 408,874 | 409,442 |
| BOQ63_RS10710 | transposase | 656,353 | 657,240 |
| BOQ63_RS10725 | IS256 family transposase | 659,679 | 660,950 |
| BOQ63_RS45020 | IS5/IS1182 family transposase | 1,013,156 | 1,014,156 |
| BOQ63_RS12740 | IS110 family transposase | 1,086,937 | 1,088,178 |
| BOQ63_RS12750 | IS5/IS1182 family transposase | 1,088,200 | 1,088,903 |
| BOQ63_RS15035 | IS200/IS605 family transposase | 1,569,116 | 1,569,363 |
| BOQ63_RS15720 | transposase | 1,761,237 | 1,761,554 |
| BOQ63_RS15725 | transposase | 1,761,551 | 1,762,465 |
| BOQ63_RS17065 | transposase | 2,044,875 | 2,046,032 |
| BOQ63_RS20605 | transposase | 2,847,519 | 2,848,817 |
| BOQ63_RS25160 | transposase | 3,812,365 | 3,813,189 |
| BOQ63_RS25165 | IS21 family transposase | 3,813,189 | 3,814,457 |
| BOQ63_RS25685 | transposase | 3,933,744 | 3,934,664 |
| BOQ63_RS25690 | transposase | 3,934,661 | 3,934,972 |
| BOQ63_RS26595 | IS21 family transposase | 4,116,603 | 4,117,871 |
| BOQ63_RS26600 | transposase | 4,117,871 | 4,118,695 |
| BOQ63_RS26675 | IS5/IS1182 family transposase | 4,131,168 | 4,132,061 |
| BOQ63_RS29050 | transposase | 4,605,449 | 4,606,369 |
| BOQ63_RS32225 | IS630 family transposase | 5,238,044 | 5,284,135 |
| BOQ63_RS34385 | transposase | 5,704,658 | 5,705,617 |
| **BOQ63_RS37135*** | **IS5/IS1182 family transposase** | **6,260,623** | **6,260,976** |
| BOQ63_RS37400 | IS110 family transposase | 6,329,086 | 6,330,300 |
| BOQ63_RS40925 | transposase | 7,097,036 | 7,097,923 |
| BOQ63_RS40980 | IS5/IS1182 family transposase | 7,106,937 | 7,107,098 |
| BOQ63_RS41025 | IS481 family transposase | 7,118,421 | 7,118,739 |
| BOQ63_RS41195 | IS21 family transposase | 7,174,951 | 7,176,219 |
| BOQ63_RS41200 | transposase | 7,176,219 | 7,177,037 |
| BOQ63_RS41470 | IS110 family transposase | 7,239,487 | 7,240,701 |
| BOQ63_RS42020 | transposase | 7,367,798 | 7,369,021 |

*Transposase found upstream chromosomal right arm deletion in bald strain B3.1

**Table 3.** Transposition elements in the right arm of KVP1 megaplasmid of *K. viridifaciens*

| Locus | Product | Location | |
|---|---|---|---|
| | | Start | Finish |
| BOQ63_RS06800 | IS5/IS1182 family transposase | 1,545,936 | 1,546,388 |
| **BOQ63_RS06805*** | **IS5/IS1182 family transposase** | **1,546,385** | **1,546,738** |
| BOQ63_RS06815 | transposase | 1,547,179 | 1,548,066 |
| **BOQ63_RS06880*** | **IS5/IS1182 family transposase** | **1,558,369** | **1,558,722** |
| BOQ63_RS06915 | transposase | 1,564,436 | 1,564,969 |
| BOQ63_RS06940 | IS5/IS1182 family transposase | 1,568,415 | 1,569,308 |
| **BOQ63_RS07050*** | **IS5/IS1182 family transposase** | **1,586,628** | **1,586,981** |
| BOQ63_RS07055 | IS5/IS1182 family transposase | 1,586,978 | 1,587,430 |
| BOQ63_RS07060 | IS5/IS1182 family transposase | 1,587,553 | 1,588,391 |
| BOQ63_RS07125 | IS110 family transposase | 1,600,675 | 1,600,800 |
| BOQ63_RS07220 | IS5/IS1182 family transposase | 1,621,157 | 1,622,011 |
| BOQ63_RS07225 | IS5/IS1182 family transposase | 1,622,341 | 1,623,179 |
| BOQ63_RS07245 | IS5/IS1182 family transposase | 1,624,729 | 1,625,079 |
| BOQ63_RS07255 | IS110 family transposase | 1,625,394 | 1,626,635 |
| **BOQ63_RS07260*** | **IS5/IS1182 family transposase** | **1,627,012** | **1,627,365** |
| BOQ63_RS07280 | IS5/IS1182 family transposase | 1,630,283 | 1,630,534 |
| BOQ63_RS07290 | transposase | 1,631,323 | 1,632,114 |
| BOQ63_RS07295 | transposase | 1,632,285 | 1,633,493 |
| BOQ63_RS07305 | site-specific integrase | 1,634,154 | 1,635,464 |
| BOQ63_RS07320 | DNA invertase | 1,636,936 | 1,637,601 |
| BOQ63_RS07335 | DDE transposase | 1,640,507 | 1,643,533 |
| BOQ63_RS07345 | integrase | 1,645,074 | 1,646,333 |
| BOQ63_RS07380 | integrase | 1,652,931 | 1,654,022 |
| BOQ63_RS07400 | resolvase | 1,656,203 | 1,656,996 |
| BOQ63_RS07425 | transposase | 1,658,975 | 1,659,889 |
| BOQ63_RS07430 | DDE transposase | 1,660,210 | 1,661,212 |
| BOQ63_RS07440 | transposase | 1,661,565 | 1,662,452 |
| BOQ63_RS07445 | IS30 family transposase | 1,662,486 | 1,662,824 |
| BOQ63_RS07475 | IS21 family transposase | 1,665,953 | 1,667,221 |
| BOQ63_RS07480 | IS21 family transposase | 1,667,436 | 1,668,701 |
| BOQ63_RS07485 | transposase | 1,668,701 | 1,669,546 |
| BOQ63_RS07550 | transposase | 1,689,112 | 1,689,999 |
| BOQ63_RS07585 | transposase | 1,695,301 | 1,695,435 |
| BOQ63_RS07615 | IS5/IS1182 family transposase | 1,699,532 | 1,699,984 |
| **BOQ63_RS07620*** | **IS5/IS1182 family transposase** | **1,699,981** | **1,700,334** |
| BOQ63_RS07635 | transposase | 1,704,820 | 1,706,307 |
| BOQ63_RS07640 | TnsA-like heteromeric transposase endonuclease subunit | 1,706,304 | 1,706,978 |

*Homologous copies to the transposase encoded by BOQ63_RS37135

## Discussion

Protoplasts are routinely used for transformation procedures[181]. Here, we provide evidence that protoplast formation and regeneration in *K. viridifaciens* can lead to profound genomic rearrangements in the chromosome, co-occurring with frequent loss of large plasmids. These genomic rearrangements translate into major phenotypic variations, which may turn out to be beneficial for filamentous actinomycetes when facing different environmental conditions.

Filamentous actinomycetes grow by tip extension and develop multinucleated mycelia. Little is known about how streptomycetes regulate the abundance and spatial distribution of chromosomes and extrachromosomal plasmids. Maintaining large plasmids such as KVP1 is costly, given that such elements can comprise about a fifth of the entire genome. Megaplasmids such as KVP1 and pSCL4 are reservoirs for biosynthetic gene clusters, and their interactions with the chromosome have been suggested to be a driving force for horizontal gene transfer[165]. Loss of such plasmids not only affect morphological development but may also influence the production of secondary metabolites in the chromosome. In *S. hygroscopicus* elimination of pSHJG1 increased the production of validamycin A[182], while holomycin yield was boosted when pSCL4 was lost in *S. clavuligerus*[180,183]. Whether the loss of KVP1 has a similar effect on antibiotic production in *K. viridifaciens* remains to be elucidated.

We observed that a surprisingly high number of the colonies derived from regenerated protoplasts (around 23%) were defective in aerial growth and sporulation. Similar morphological defects have been described for *S. clavuligerus*, *S. lividans* and *S. coelicolor* upon loss of their plasmids[180,184]. While the loss of KVP1 may contribute to the inability to form aerial hyphae and spores, we here for the first time show that loss of this plasmid may also co-occur with profound rearrangements in the chromosome, which could equally well contribute to this phenotype. By sequencing one revertant that had lost KVP1 we found that this strain had also lost approximately 1.5 Mb of the right arm of the chromosome. Such chromosomal lesions have been described before and are caused by chromosomal instability, which in streptomycetes can affect morphological differentiation, but also other phenotypic traits like pigmentation, antibiotic resistance and antibiotic production[175,185]. Transposable elements were suggested as the principal cause of genetic instability[186]. The simultaneous occurrence of the loss of KVP1 and the chromosomal lesions in the right arm could be the consequence of replicative transposition between the chromosome and the megaplasmid (Fig. 5). Notably, while most KVP1-located sequences were absent in the sequenced strain, including those required for autonomous replication of this megaplasmid, we identified a high coverage of

sequences originally located in the right arm of KVP1. This could be explained by an exchange of the right arm of the chromosome by the right arm of KVP1. A replicative transposition event between two linear replicons often results in the loss of chromosomal terminal regions and recombination of transposable elements[174]. The presence of IS elements located at the chromosome and plasmid termini could provide the basis for homologous recombination between these DNA molecules. It has been previously shown that homologous copies of IS elements could serve as substrates for the recombination machinery, creating chromosomal rearrangements in the genomes of *Lactococcus lactis* and *Escherichia coli*[187,188]. In the case of the B3.1 protoplast revertant, our results suggest that a possible cause of the genomic rearrangement was the replicative transposition of an IS, exerted by the BOQ63_RS37135 transposase (black arrow in Fig. 5).

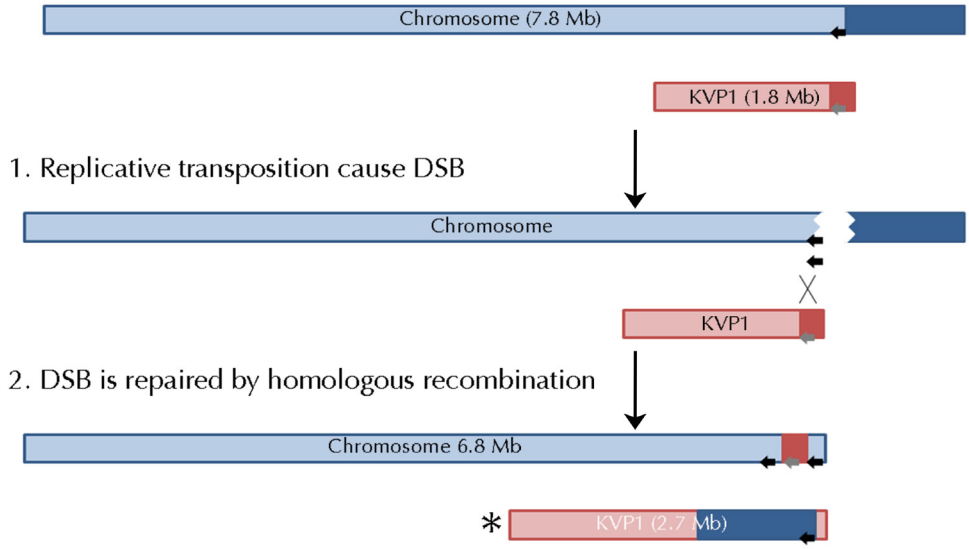


**Figure 5. Proposed model for the genomic rearrangements and lesions identified in strain B3.1.** Replicative transposition of a transposable element (black arrow) located on the chromosome creates a double-stranded break (DSB). Subsequent repair of the DSB by homologous recombination between the chromosome and KVP1 plasmid (grey arrow represents an homologous copy of the transposable element located in KVP1), leads to an exchange of the right arms of both replicons and changes in their size. *Please note that the larger KVP1 megaplasmid variant is lost in strain B3.1.

Following replicative transposition, a double-stranded break (DSB) occurs at the site of transposon excision. This DSB is repaired by recombination with homologous genes located on IS elements present in the right arm of KVP1 (shown as a grey arrow in the KVP1 right arm), which are abundantly present. This recombination might force the interchange of terminal arms. This hypothetical model would explain the genome size reduction of B3.1 (6,787,546 bp).

The frequency of aberrant phenotypes after protoplast regeneration is higher than the phenotypic heterogeneity obtained after outgrowth of spores, which typically is in the order of 1%[173,185,186,189-191]. An explanation for the high frequency of aberrant mutants in protoplasts possibly relates to the activation of transposable elements contained in the terminal regions of the chromosome and/or the KVP1 plasmid. The activation of transposases are typically stimulated by stressful conditions, such as radiation, oxidative stress, temperature or inhibitory concentrations of metals and antibiotics[192]. We recently demonstrated that elevated levels of osmolytes induces hyperosmotic stress[193,194], which are conditions that are also used during preparation of protoplasts. This stress could also stimulate transposition events and consequently chromosomal rearrangements. Consistent with this idea is that other cell wall-deficient cells, called L-forms, which have likewise been exposed to osmotic stress conditions, are genetically instable. In this context it is interesting to note that we found lesions in the right arm of the chromosomal and loss of KVP1, in three independent L-form lineages[194]. These three strains retained a similar region of KVP1 in their genomes, with a size of 164, 773 for *alpha* and M1, and 164,642 bp for M2. These are very similar to the KVP1-sequences remaining (164,769 bp) in the bald protoplast regenerant B3.1 in terms of length and content.

Chromosomal rearrangements are often detrimental for the fitness of a unicellular organism. However, it was recently shown that in *Streptomyces* chromosomal rearrangements may increase the diversity and production of secondary metabolites, including antibiotics. A division of labour strategy would allow a colony to have a mixture of a mutant and wild-type chromosomes, where the mutant cells are virtually sterile and become specialized in the production of antibiotics, while the cells containing wild-type chromosomes are efficient spore producers[185]. The work described here reveals dramatic variations when a mycelium is separated in individual protoplasts. While the stress of protoplasting itself may stimulate these chromosomal changes, we speculate that some variation is likely already present in the mycelium before generating protoplasts. This study provides a starting point to further characterize these changes and to investigate their consequences, which may lead to exciting new insights into the biology of these prolific antibiotic producers.

## Methods

### Strains and media

The strains (Supplementary Table 1) used in this study are derivatives of the *K. viridifaciens* DSM40239 (DSMZ). For protoplast preparation a spore suspension ($10^6$ spores·$ml^{-1}$) was grown for 48 hours in a mixture of TSBS-YEME (1:1 v/v) supplemented with 5 mM $MgCl_2$ and 0.5% glycine. Protoplasts were prepared according to[179], with the difference that the lysozyme concentration was increased to 10 mg·$ml^{-1}$. Serial dilutions of protoplasts were plated on R5[179] or MYM medium[195] at 30°C. Regenerated protoplasts were streaked twice to single colonies on MYM before selecting the three independent bald colonies (B3.1, B3.2, and B3.3) that were further analysed. Bald colonies were used as inoculum on liquid cultures of TSBS. Genomic DNA was isolated after two days of growth at 30°C.

### Whole genome sequencing

For genomic DNA isolation strains were grown in Tryptic Soy Broth medium containing 10% sucrose until mid-exponential phase. Next, chromosomal DNA was isolated as described previously[179] and sequenced by BaseClear (Leiden, The Netherlands) using a combined Illumina/PacBio sequencing approach. The quality of the Illumina FASTQ sequences was enhanced by trimming off low-quality bases and assembled into contigs using CLC Genomics Workbench (version 8.0). The optimal k-mer size was automatically determined using kMerGenie[196]. Contigs were organized into scaffolds based on the alignment of the PacBio continuous long reads (CLR) using BLASR[197]. From the alignment, the orientation, order, and distance between the contigs were estimated using the SSPACE-LongRead scaffolder version 1.0[198]. Gapped regions within the superscaffolds were (partially) closed in an automated manner using GapFiller version 1.10[199]. The genome sequence has been deposited at DDBJ/ENA/GenBank under the accession no. MPLE00000000.

### Alignment of Illumina sequences

Alignments of Illumina reads were performed using CLC Genomics Workbench 8.5.1 (Qiagen, the Netherlands). Raw Illumina (Hiseq2500 system) sequences of the wild-type and the bald strain B3.1 were imported and mapped to the reference genome of *K. viridifaciens* DSM40239 (NCBI reference sequence: NZ_MPLE00000000.1) through the “Map reads to reference” function in the NGS core tools. Mismatch cost was set to 2 and non-specific matches were handled by mapping them randomly.

### Pulse Field Gel Electrophoresis

For PFGE, $10^6$ spores·$ml^{-1}$ of *K. viridifaciens* were inoculated in 25 ml of TSBS with 0.5% glycine or LPB[194]. Cultures were grown at 30°C agitating at 200 rpm for 16 and 40 hours, respectively. Mycelial pellets were harvested by centrifuga-

tion at 4000 rpm for 15min. The preparation of plugs for PFGE was performed as previously described[185]. Plugs were made with SeaKem Gold agarose (Lonza, Switzerland), and the genomic DNA in the plugs was cut with AseI. Plugs were run using a CHEF-DR II Pulse Field Electrophoresis system (Biorad, USA). For efficient separation of fragments, samples were run in two conditions: a switching time of 60-125 seconds for 20 hours, or a switching time of 2.2-75 seconds for 19 hours, both at 200 V.

**Quantitative real time PCR**

Aliquots of 5 ng of DNA were used as a template in quantitative real time PCR. We used primers for both chromosomal (*atpD* and *infB*) and KVP1 (*allC*, *tetR*, *parA* and *orf1*) genes (Supplementary Table 2). The PCR reactions were performed with the iTaq Universal SYBR Green Supermix Mix (Bio-Rad) using 5% DMSO, according to the manufacturer's instructions. Reactions was performed in duplicate using a CFX96 Touch Real-Time PCR Detection System (Bio-Rad). To normalize the relative amount of DNA, the wild-type strain was used as a control, using the *atpD* gene as a reference.

## Supplementary information

**A**

The following regions are from record MPLE01000001.1 (Streptomyces viridifaciens):

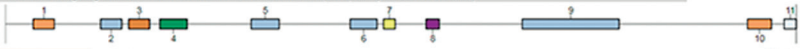

| Region | Type | From | To | Most similar known cluster | | Similarity | MIBiG BGC-ID |
|---|---|---|---|---|---|---|---|
| Region 1 | T3pks | 55019 | 96101 | Actinomycin | NRPS | 10% | BGC0000296 |
| Region 2 | Lanthipeptide - Nrpsfragment | 186747 | 228158 | Viomycin | NRPS | 9% | BGC0000458 |
| Region 3 | Arylpolyene | 241651 | 282784 | WS9326 | NRPS | 5% | BGC0001297 |
| Region 4 | Nrps | 302617 | 356025 | | | | |
| Region 5 | Nrps - Nucleoside | 481446 | 536185 | Tunicamycin | other | 42% | BGC0000880 |
| Region 6 | T1pks - Nrps | 675210 | 727626 | Oxazolomycin | hybrid | 15% | BGC0001106 |
| Region 7 | Lanthipeptide | 740507 | 763068 | | | | |
| Region 8 | Terpene | 823523 | 849476 | Carotenoid | terpene | 45% | BGC0000633 |
| Region 9 | Nrps - T1pks | 1011856 | 1201449 | Candicidin | polyketide | 76% | BGC0000034 |
| Region 10 | T1pks | 1452695 | 1499210 | | | | |
| Region 11 | Blactam | 1524280 | 1547868 | Clavams | other | 64% | BGC0001151 |

**B**

The following regions are from record MPLE01000004.1 (Streptomyces viridifaciens):

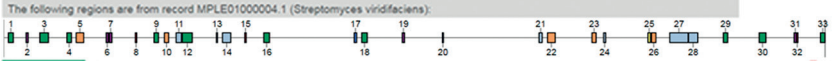

| Region | Type | From | To | Most similar known cluster | | Similarity | MIBiG BGC-ID |
|---|---|---|---|---|---|---|---|
| Region 1 | Nrps | 43540 | 90359 | Capreomycin | NRPS | 9% | BGC0000316 |
| Region 2 | Terpene | 211185 | 230997 | | | | |
| Region 3 | Nrps | 340765 | 421797 | Lipopeptide 8D1-1 / lipopeptide 8D1-2 | NRPS | 15% | BGC0001370 |
| Region 4 | Nrpsfragment | 596569 | 638812 | Meilingmycin | polyketide | 4% | BGC0000093 |
| Region 5 | T2pks | 683975 | 754674 | Spore pigment | polyketide | 83% | BGC0000271 |
| Region 6 | Terpene | 966842 | 986462 | Acarviostatin | saccharide | 11% | BGC0000804 |
| Region 7 | Terpene | 996986 | 1021419 | Hopene | terpene | 61% | BGC0000663 |
| Region 8 | Siderophore | 1241877 | 1255028 | | | | |
| Region 9 | Nrpsfragment | 1418560 | 1460286 | | | | |
| Region 10 | Otherks | 1515975 | 1556086 | Kijanimicin | polyketide | 4% | BGC0000082 |
| Region 11 | Nrpsfragment - T1pks | 1626509 | 1677101 | Vancomycin | NRPS | 17% | BGC0000455 |
| Region 12 | Nrps | 1684526 | 1779221 | Friulimicin | NRPS | 24% | BGC0000354 |
| Region 13 | Bacteriocin | 2007281 | 2017303 | | | | |
| Region 14 | Nrps - Betalactone | 2064569 | 2142082 | Lomaiviticin | polyketide | 6% | BGC0000240 |
| Region 15 | Siderophore | 2274617 | 2287884 | | | | |
| Region 16 | Nrps | 2453955 | 2507665 | Teleocidin B | hybrid | 50% | BGC0001085 |
| Region 17 | Lap | 3307340 | 3330204 | | | | |
| Region 18 | Nrps | 3378027 | 3430494 | Skyllamycin | NRPS | 20% | BGC0000429 |
| Region 19 | Terpene | 3760799 | 3781772 | Geosmin | other | 100% | BGC0001181 |
| Region 20 | Butyrolactone | 4138981 | 4149459 | Pristinamycin | hybrid | 3% | BGC0000952 |
| Region 21 | Thiopeptide - Lap | 5051227 | 5080751 | | | | |
| Region 22 | T2pks | 5131444 | 5203500 | Chlortetracycline | polyketide | 88% | BGC0000209 |
| Region 23 | T3pks | 5550533 | 5589534 | Herboxidiene | polyketide | 2% | BGC0001065 |
| Region 24 | Bacteriocin - Butyrolactone | 5660652 | 5680142 | Methylenomycin | other | 28% | BGC0000914 |
| Region 25 | Lanthipeptide | 6078936 | 6101773 | A54145 | NRPS | 5% | BGC0000291 |
| Region 26 | T3pks | 6112996 | 6154051 | Naringenin | terpene | 100% | BGC0001310 |
| Region 27 | Nrps - T1pks | 6284704 | 6457666 | Gobichelin | NRPS | 27% | BGC0000366 |
| Region 28 | Nrps - Otherks | 6461811 | 6548854 | | | | |
| Region 29 | Nrpsfragment | 6790211 | 6831191 | | | | |
| Region 30 | Nrps | 7128111 | 7192080 | Cyclomarin | NRPS | 8% | BGC0000333 |
| Region 31 | Terpene | 7457995 | 7479215 | 2-methylisoborneol | terpene | 100% | BGC0000658 |
| Region 32 | Siderophore | 7480413 | 7493514 | | | | |
| Region 33 | Nrpsfragment | 7706433 | 7750347 | Herboxidiene | polyketide | 3% | BGC0001065 |

**Supplementary Figure 1. AntiSMASH 5.0 output revealing the biosynthetic gene clusters contained on the megaplasmid (top) and chromosome (bottom) of *K. viridifaciens*.** The biosynthetic gene clusters are numbered according to their localization on the replicon.

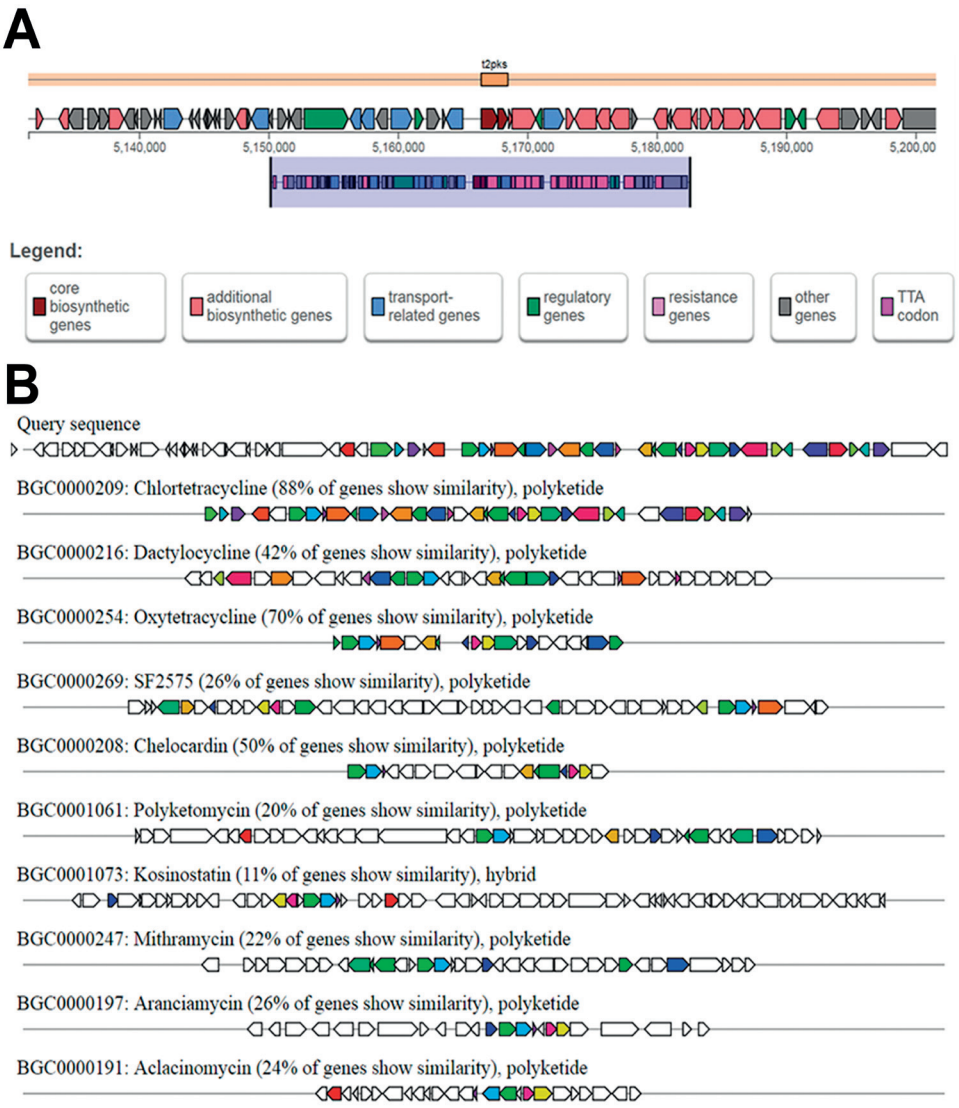


**Supplementary Figure 2. AntiSMASH 5.0 homology search of the *K. viridifaciens* tetracycline biosynthetic gene cluster.** (**A**) Localization of the putative chlorotetracycline BGC in the chromosome of *K. viridifaciens*. (**B**) Comparison of the *K. viridifaciens* tetracyclin biosynthetic gene cluster with known tetracycline gene clusters from *Streptomyces aureofaciens* (BGC0000209), *Dactylosporangium sp*. SC14051 (BGC0000216), *S. rimosus* (BGC0000254), *Streptomyces sp*. SF2575 (BGC0000269), *Amycolatopsis sulphurea* (BGC0000208), *S. diastatochromogenes* (BGC0001061), *Micromonospora sp*. TP-A0468 (BGC0001073), S. *argillaceus* (BGC0000247), *S. echinatus* (BGC0000197), *S. galilaeus* (BGC0000197).

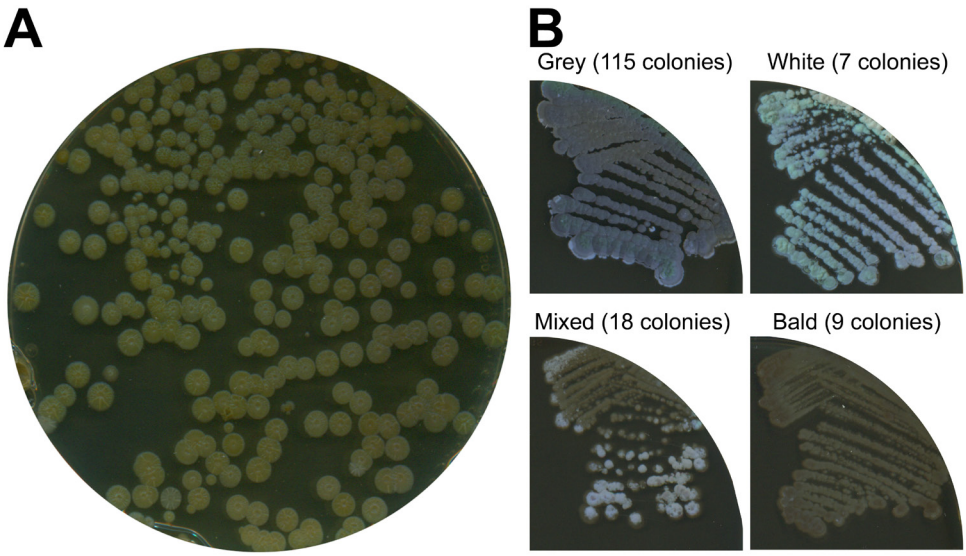


**Supplementary Figure 3. Protoplast regeneration generates morphological diversity in osmotically balanced medium.** (**A**) Protoplasts regenerated on R5 medium yielded colonies that are unable to sporulate due to the high sucrose levels. (**B**) Subculturing of 149 randomly-picked colonies on MYM medium revealed dramatic developmental defects in 23% of the colonies. Whereas 77% of the colonies were able to form grey-pigmented sporulating colonies (similar to the wild-type), 5% of the colonies were white, 6% were bald, while 12% had a mixed appearance.

**Supplementary Table 1.** Strains used in this study

| Strain | Characteristics | Genotype | Reference |
|---|---|---|---|
| *K. viridifaciens* DSM40239 | Sporulating parent strain | Wild-type | DSMZ, This work |
| G1-G3 | Sporulating protoplast revertant | Wild-type | This work |
| B1 | Bald protoplast revertant that recovered the ability to sporulate in the second subculture | N.D. | This work |
| B2 | Bald protoplast revertant | N.D. | This work |
| B3 | Bald protoplast revertant with a mixed colony morphology | Segregation of this type gave KVP1minus colonies | This work |
| B3.1 | Bald protoplast revertant | KVP1 minus, 1 Mb deletion in right arm of the chromosomal | This work |
| B3.2 | Bald protoplast revertant | KVP1 minus | This work |
| B3.3 | Bald protoplast revertant | KVP1 minus | This work |

ND: Not determined

**Supplementary Table 2**: Quantitative real time PCR Primers

| Primer | Sequence |
|---|---|
| qPCR_*infB*-Fw | GTCACGTCGACCACGGTAAG |
| qPCR_*infB*-Rv | CACCGATGTGCTGGGTGATG |
| qPCR_*atpD*-Fw | TTCGGACAGCTCGTCCATAC |
| qPCR_*atpD*-Rv | ACATCGCGCAGAACCACTAC |
| qPCR_*parA*-Fw | CGGTCGTCACCCAGTACAAG |
| qPCR-*parA*-Rv | TAACCGAGTTCGAGGGACAG |
| qPCR-*orf1*-Fw | GAGGGAGCCAATCCCGTATC |
| qPCR-*orf1*-Rv | GGCTGTTGGACAGGACCATC |
| qPCR-*allC*-Fw | CGGCGATAGCGGAGACTAAG |
| qPCR-*allC*-Rv | CCACTGGTGGGACCAGAAAG |
| qPCR-*tetR*-Fw | TGCTCGACCAGCTGTTGAAG |
| qPCR-*tetR*-Rv | TGGCGAGCATGAAGTCGTAG |

# Chapter 3
# Stress-induced formation of cell wall-deficient cells in filamentous actinomycetes

K. Ramijan, E. Ultee, J. Willemse, Z. Zhang, A.J. Wondergem, A. van der Meij, D. Heinrich, A. Briegel, G.P. van Wezel and D. Claessen

## Abstract

The cell wall is a shape-defining structure that envelopes almost all bacteria and protects them from environmental stresses. Bacteria can be forced to grow without a cell wall under certain conditions that interfere with cell wall synthesis, but the relevance of these wall-less cells (known as L-forms) is unclear. Here, we show that several species of filamentous actinomycetes have a natural ability to generate wall-deficient cells in response to hyperosmotic stress, which we call S-cells. This wall-deficient state is transient, as S-cells are able to switch to the normal mycelial mode of growth. However, prolonged exposure of S-cells to hyperosmotic stress yields variants that are able to proliferate indefinitely without their cell wall, similarly to L-forms. We propose that formation of wall-deficient cells in actinomycetes may serve as an adaptation to osmotic stress.



This chapter was published as: Ramijan, K. *et al*. Stress-induced formation of cell wall-deficient cells in filamentous actinomycetes. *Nat Commun* **9**, 5164 (2018).

## Introduction

All free-living bacteria are challenged by constant changes in their environment, and their survival depends on the ability to adapt to sudden exposure to stressful conditions. For instance, soil bacteria can encounter rapid osmotic fluctuations caused by rain, flooding, or desiccation. Bacterial cells typically respond to osmotic changes by rapidly modulating the osmotic potential within the cell, either by importing or exporting ions and compatible solutes[200]. While these responses typically occur immediately after cells have been exposed to the changed environment, they are also able to tune the expression of metabolic pathways or critical enzymes[201].

How such osmotic changes affect cellular morphology is not well known. The cells' shape is largely dictated by the cell wall, which is a highly dynamic structure that acts as the main barrier that provides osmotic protection[202]. The synthesis of its major constituent, peptidoglycan (PG), involves the activity of large protein complexes that cooperatively build and incorporate new PG precursors into the growing glycan strands at the cell surface[98,106,203,204]. These strands are then cross-linked to form a single, giant sacculus that envelops the cell[94]. The sites for the incorporation of new PG is a major difference between the planktonic firmicutes that grow by extension of the lateral wall, and Actinobacteria, which grow via apical extension and thereby incorporating new PG at the cell poles[8,205].

Actinobacteria display a wide diversity of morphologies, including cocci (*Rhodococcus*), rods (*Mycobacterium* and *Corynebacterium*) and mycelia (*Streptomyces* and *Kitasatospora*), or even multiple shapes (*Arthrobacter*)[2,122]. Species belonging to these genera are able to change their morphology to adapt to extreme environments. For example, *Rhodococcus* species that are commonly found in arid environments are able to adapt to desiccation by modulating their lipid content and form short-fragmented cells[206]. *Arthrobacter* species also exhibit high resistance to desiccation and cold stresses. Upon hyperosmotic stress, these cells can modulate the synthesis of osmoprotectants and switch between rod-shaped and myceloid cells[122].

While the cell wall is considered an essential component of virtually all bacteria, most species can be manipulated under laboratory conditions to produce so-called L-forms that are able to propagate without their wall[133,139,148,207]. Typically, L-forms are generated by exposing walled bacteria to high levels of lysozyme combined with antibiotics that target cell wall synthesis in media containing high levels of osmolytes[138,208]. Stable *B. subtilis* L-forms that can propagate indefinitely without the cell wall require two mutations that fall in separate classes[138]. The first class of mutations leads to an increase in membrane synthesis, either directly by increasing fatty acid biosynthesis, or indirectly by

reducing cell wall synthesis[141]. The second class of mutations reduces oxidative damage caused by reactive oxygen species, which are detrimental to proliferation of L-forms[143]. Notably, proliferation of L-forms is independent of the FtsZ-based division machinery[139,140]. Instead, their proliferation can be explained solely by biophysical processes, in which an imbalance between the cell surface area to volume ratio leads to spontaneous blebbing and the subsequent generation of progeny cells[141]. Such a purely biophysical mechanism of L-form proliferation is not species-specific. This observation has led to the hypothesis that early life forms propagated in a similar fashion well before the cell wall had evolved[137,139,141]. Whether L-forms have functional relevance in modern bacteria, however, is unclear.

Here we present evidence that filamentous actinobacteria have a natural ability to extrude cell wall-deficient (CWD) cells when exposed to high levels of osmolytes. These newly-identified cells, which we call S-cells, synthesize PG precursors and are able to switch to the canonical mycelial mode-of-growth. Remarkably, upon prolonged exposure to hyperosmotic stress conditions, S-cells can acquire mutations that enable them to proliferate in the CWD state as L-forms. These results infer that the extrusion of S-cells and their transition into proliferating L-forms is a natural adaptation strategy in filamentous actinobacteria caused by prolonged exposure to osmotic stress.

## Results

### Hyperosmotic stress induces formation of wall-deficient cells

Recent work suggests that hyperosmotic stress conditions affects apical growth in streptomycetes[193]. Consistent with these observations, we noticed that growth was progressively disturbed in the filamentous actinomycete *Kitasatospora viridifaciens*, when high levels of sucrose were added to the medium (Fig. 1A). In liquid-grown cultures containing more than 0.5 M sucrose, initiation of growth was delayed by at least 5 h compared to media with low levels of sucrose. A similar retardation in growth was observed on solid medium supplemented with high levels of osmolytes, evident from the size decrease of colonies (Fig. 1B, C). On average, their size decreased from 12.8 $mm^2$ (n= 278) to 1.4 $mm^2$ (n=184) after 7 days of growth. Notably, the high osmolarity also reduced the number of colony forming units (CFU) by 33%, from $9.3x10^8$ CFU $ml^{-1}$ to 6.1 $x10^8$ CFU $ml^{-1}$, as deduced by plating serial dilutions of spores in triplicate. In order to study the morphological changes accompanying this growth reduction, we stained the mycelium after 48 h of growth with the membrane dye FM5-95 and the DNA stain SYTO-9 (Fig. 1D, E). The high levels of osmolytes had a dramatic effect on mycelial morphology. The hyphae showed indentations along the cylindrical part of the leading hyphae, reminiscent of initiation of sporulation (see BF panel in Fig. 1E).

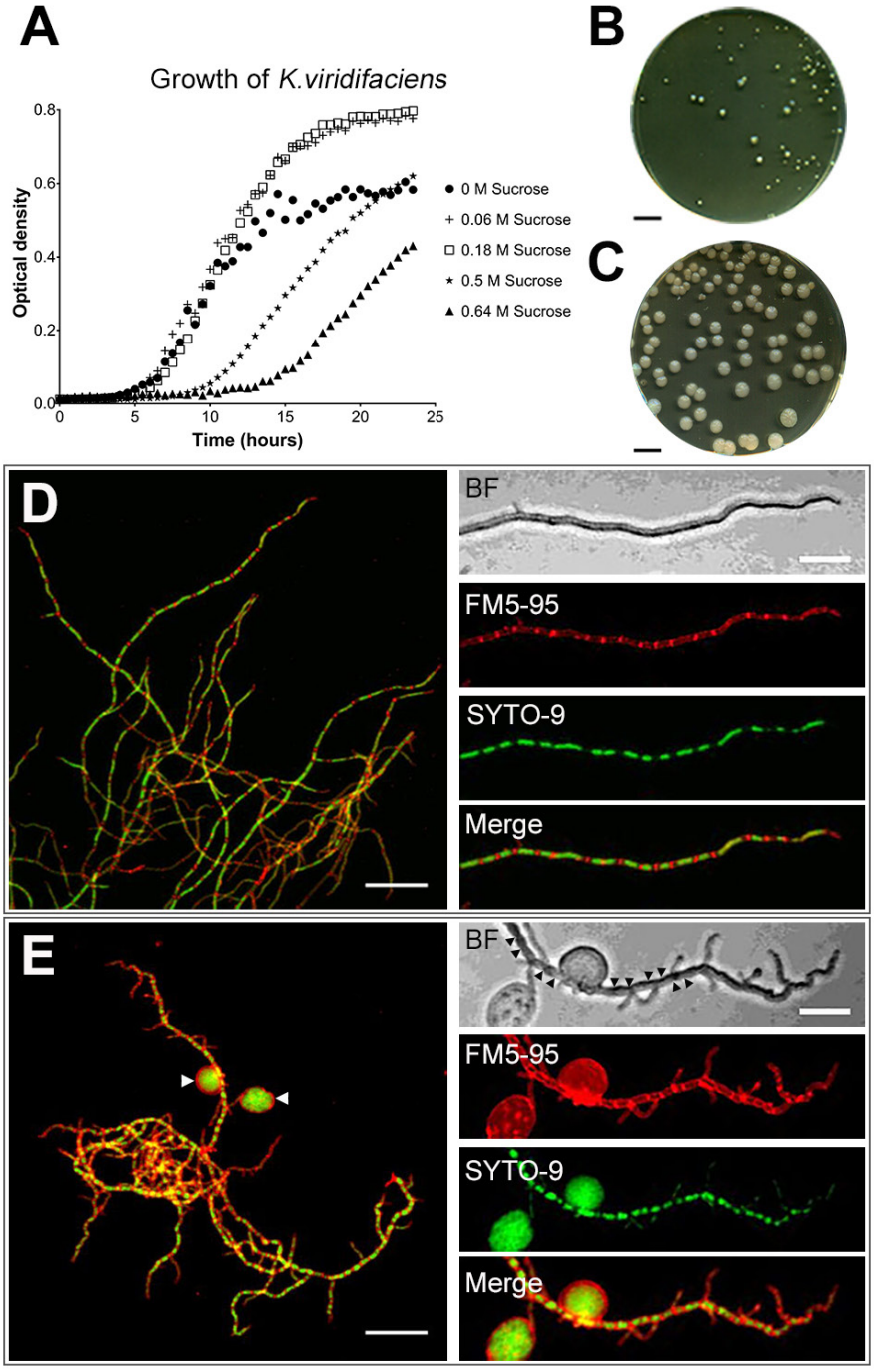
A
Growth of K.viridifaciens
Optical density
Time (hours)
0 M Sucrose
0.06 M Sucrose
0.18 M Sucrose
0.5 M Sucrose
0.64 M Sucrose
B
C
D
BF
FM5-95
SYTO-9
Merge
E
BF
FM5-95
SYTO-9
Merge

**Figure 1. High levels of sucrose affect growth and morphology of *K. viridifaciens*.** (**A**) Growth curves of *K. viridifaciens* in LPB medium supplemented with increasing amounts of sucrose. Values represent the average of five independent replicates. High levels of osmolytes reduce the number and size of colonies (**B**) in comparison to media without osmolytes (**C**). Mycelial morphology *K. viridifaciens* grown in LPB without sucrose (**D**) and with 0.64 M of sucrose (**E**). Mycelium was stained with FM5-95 and SYTO-9 to visualize membranes and DNA, respectively. Please note the S-cells (white arrowheads in **E**) and indentations along the cylindrical part of the hypha, indicated with black arrowheads in the bright field (BF) section, formed in medium containing high levels of sucrose. Scale bars represent 10 mm (**B**, **C**), 20 µm (left panels in **D**, **E**) and 10 µm (magnified section in **D** and **E**).

In addition, the branching frequency increased by more than three-fold in the presence of high levels of osmolytes (Supplementary Fig. 1A, H; Supplementary Table 1, 2; Student's T-test, P-value =0,0010). Additionally, we noticed that these stressed hyphae contained an excess of membrane (compare FM5-95 panels in Fig. 1D, E). The proportion of the hyphae that were stained with FM5-95 increased from 10% to 21% in the presence of 0.64 M Sucrose (Supplementary Fig. 1E, L; Supplementary Table 1, 2; Student's T-test, P-value <0,0001). Simultaneously, the average surface area occupied by the nucleoid decreased from 2.59 $\mu m^2$ to 1.83 $\mu m^2$, indicative of DNA condensation (Supplementary Fig. 1G, N; Supplementary Table 1, 2; Student's T-test, P-value =0.0074). Strikingly, we observed large DNA-containing vesicles surrounding the mycelial networks (indicated by arrowheads in Fig. 1E). High levels of the osmolytes NaCl (0.6 M) and sorbitol (1 M) caused a comparable growth defect (Supplementary Fig. 2A) and also led to the formation of DNA-containing vesicles (Supplementary Fig. 2B-D). Notably, addition of high concentrations of salt (0.6 M NaCl) differently affected morphology and yielded mycelial particles that were small and very dense (Supplementary Fig. 3). *K. viridifaciens* was no longer able to grow when the NaCl concentration was increased to more than 0.6 M (not shown). The formation of DNA-containing vesicles in the presence of both ionic (NaCl) and non-ionic, organic osmolytes (sucrose and sorbitol) indicate that the hyphae form a previously uncharacterized cell type upon hyperosmotic stress, which we hereinafter will refer to as S-cells, for stress-induced cells.

To distinguish S-cells from other cell wall-deficient (CWD) variants of *K. viridifaciens*, we compared them to fresh protoplasts and L-form cells obtained after classical induction with high levels of lysozyme and penicillin (see Methods). Size measurements from 2D images revealed that S-cells had an average surface area of 20.73 $\mu m^2$ (n=213) and were larger than protoplasts (n=514) and L-forms (n=678), which had an average surface area of 4.01 $\mu m^2$ and 7.06 $\mu m^2$, respectively (Table 1). Vancomycin-BODIPY staining ($van^{FL}$, Fig. 2A) revealed a heterogeneous pattern of nascent PG synthesis in these cells, while in L-forms mostly detached wall material was observed. By contrast, no staining was detected when freshly prepared protoplasts were used (Fig. 2A). When protoplasts were maintained in LPB for 48 hours, their average surface area increased to 7.49+2.21$\mu m^2$, which is smaller than that of S-cells (Table 1). Furthermore, protoplasts regenerated a more uniform cell wall while S-cells showed a disordered, non-uniform pattern of cell-wall assembly, whereby wall material was sometimes found to be detached from the cell surface (Fig. 2B, Table 1).

**Table 1.** Comparison between *K. viridifaciens* cell wall-deficient cells

| Characteristics | Protoplast | L-form | S-cell |
|---|---|---|---|
| Origin | Osmoprotective conditions combined with lysozyme treatment | Osmoprotective conditions combined with prolonged exposure to lysozyme and penicillin G | Osmoprotective conditions |
| Area ($\mu m^2$) | 4.01±1.93 | 7,06±5.87 | 20.73±11.53 |
| Cell wall | Homogeneous regeneration. Wall material mostly associated with the cell surface | Not uniform, disordered assembly. Wall material often detached from the cell surface | Not uniform, disordered assembly. Wall material sometimes detached from the cell surface |
| Genotype | Wild type | Mutant | Wild-type |

Bacteria can be forced to grow without a cell wall if cell wall synthesis is inhibited. Here we show that in filamentous actinomycetes, hyperosmotic stress induces formation of wall-deficient cells that can switch to normal mycelial growth, or mutate and proliferate indefinitely as wall-less forms.

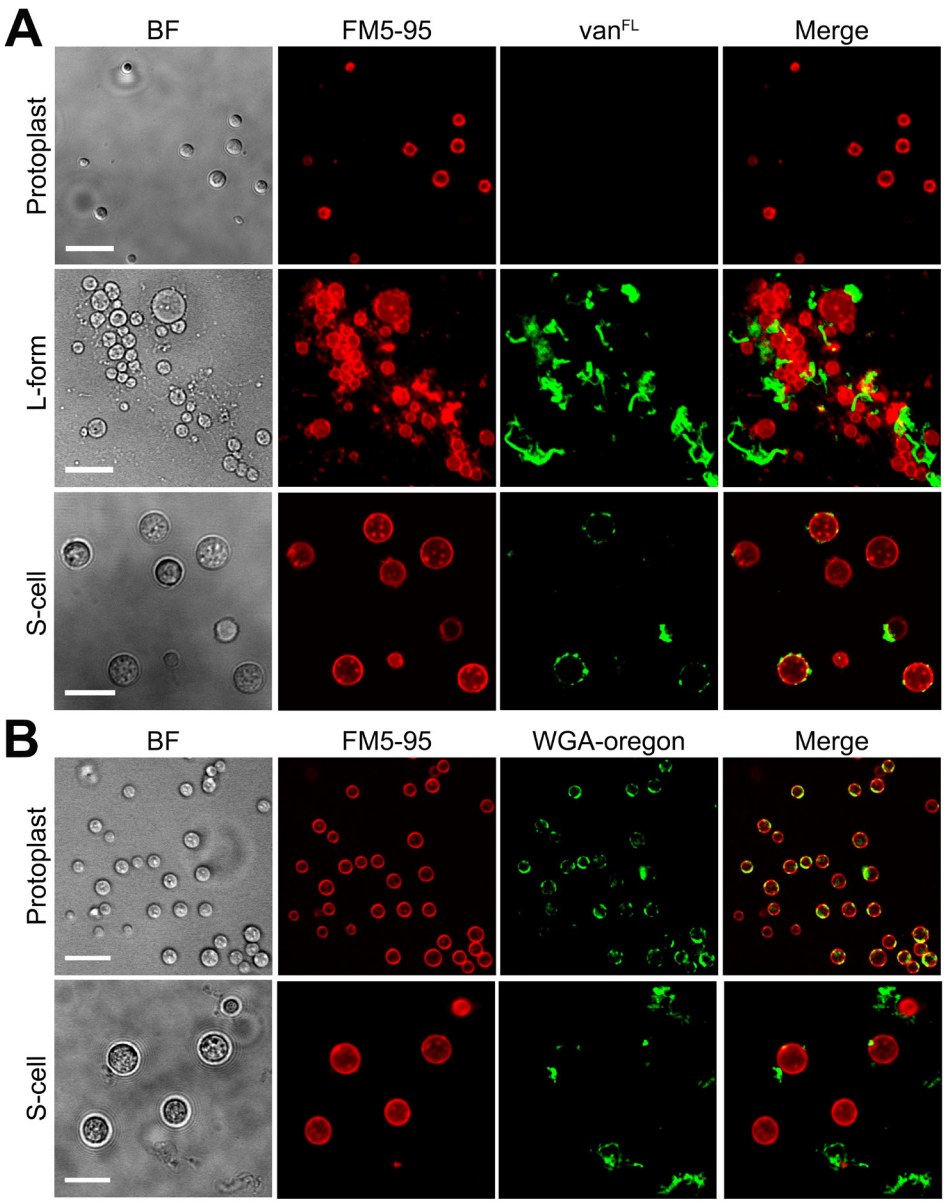


**Figure 2. Comparison between different cell wall-deficient cell types in *K. viridifaciens*.** (**A**) Morphology of freshly made protoplasts (top panels), penicillin-induced L-forms (middle panels) and S-cells (bottom panels). Cells were stained with the membrane dye FM5-95 or fluorescent vancomycin (van$^{FL}$) to detect nascent PG. (**B**) Morphology of protoplasts (top panels) and S-cells (bottom panels) grown for 48 hours in LPB containing 0.6 M sucrose. Cells were stained with the membrane dye FM5-95 or wheat germ agglutinin (WGA-Oregon) to detect PG. Scale bars represents 10 µm.

## Formation of S-cells is common in natural isolates

To see how widespread the formation of S-cells is among natural isolates, we screened our collection of filamentous actinomycetes, obtained from the Himalaya and Qinling mountains[209], using *Streptomyces coelicolor*, *Streptomyces lividans*, *Streptomyces griseus*, and *Streptomyces venezuelae* as the reference strains. We used a cut-off diameter of 2 µm to distinguish small S-cells from spores. Spherical cells, similar to S-cells were evident in hyperosmotic media in *S. venezuelae* and in 7 out of the 96 wild isolates (Supplementary Fig. 4A). The cells were variable in size within the same strains and between strains (Fig. 3A, Supplementary Table 3) and showed differences in the organization of their DNA (Fig. 3A). No S-cells were found in *S. coelicolor*, *S. griseus*, or *S. lividans* under the tested conditions. Phylogenetic analysis based on 16S rRNA (Supplementary Fig. 4B), or the taxonomic marker gene *ssgB* used for classifying morphologically complex actinomycetes[4], revealed that the formation of S-cells is common in at least two genera (Fig. 3B). Moreover, the ability to form S-cells was not restricted to strains that sporulate in liquid-grown cultures. This is based on the observation that MBT86, which is classified as a non-liquid sporulating strain, also generates S-cells (Fig. 3C). Altogether, these results show the ability to generate S-cells, without artificial means such as lysozyme and/or cell wall-targeting antibiotics, is widespread in filamentous actinomycetes.

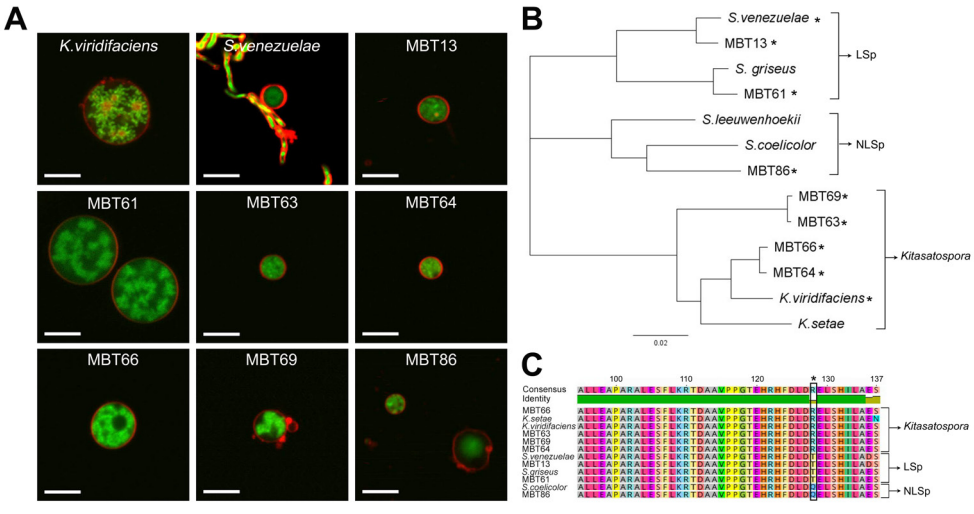

**Figure 3. Formation of S-cells is widespread in filamentous actinomycetes.** (**A**) Morphology of S-cells released by *K. viridifaciens*, *S. venezuelae*, and a number of filamentous actinomycetes from our culture collection (all referred to with the prefix MBT). Cells were stained with FM5-95 (red) and SYTO-9 (green) to visualize membranes and DNA, respectively. (**B**) Phylogenetic tree of filamentous actinomycetes based on the taxonomic marker *ssgB*. Strains with the ability to form S-cells are indicated with an asterisk (*). *Streptomyces* strains that are able to produce spores in liquid-grown cultures are referred to as LSp (for Liquid Sporulation), while those unable to sporulate in liquid environments are called NLSp (No Liquid Sporulation[4]). This classification is based on amino acid residue 128 in the conserved SsgB protein, which is a threonine (T) or glutamine (Q) for LSp and NLSp strains, respectively. Please note that an arginine (R) is present at this position in all *Kitasatospora* strains (**C**). Scale bars represent 5 µm.

## S-cells are able to switch to the mycelial mode-of-growth

To determine where S-cells are generated in the hyphae, we performed live imaging of growing germlings of *K. viridifaciens* (Supplementary Movie 1). Approximately 7 h after the visible emergence of germ tubes, we detected a transient arrest in tip extension of the leading hypha (Fig. 4A, t=400 mins). Shortly thereafter, small S-cells became visible, which were extruded from the hyphal tip (see arrows in Fig. 4A). These cells rapidly increased in size and number. After 545 min a narrow branch (Fig. 4A, arrowhead) was formed in the apical region from which the S-cells were initially extruded. Subapically, other branches became visible approximately 210 minutes after the first appearance of these cells (Supplementary Movie 1, t= 770 min). Notably, such branches frequently also extruded S-cells, similarly to the leading hypha (Supplementary Movie 2). This showed that S-cells are produced at hyphal tips after apical growth was arrested.

Further characterization of S-cells from *K. viridifaciens* revealed that these cells had a granular appearance and contained membrane assemblies that stained with FM5-95 (Fig. 4B, arrows, Supplementary Movie 3). Notably, these assemblies often co-localized with DNA (Fig. 4B, arrows). To study S-cells in more detail, we separated them from the mycelia after 7 days by filtration (see Methods). In agreement with our previous findings, we also detected agglomerates of membrane assemblies in close proximity of the DNA using electron microscopy analysis (Fig. 4C). Additionally, we noticed that S-cells possessed a disorganized surface, characterized by membrane protrusions that appeared to detach from the S-cells (Fig. 4D, E), and an apparent deficiency in normal cell-wall biogenesis (compare to the cell surface of the hypha in Fig. 4F, G).

To establish if S-cells are truly viable cells, they were plated onto plates supplemented with sucrose. After 7 days of growth, many mycelial colonies were found (± $1.6x10^4$ CFUs $ml^{-1}$ of the filtered culture) demonstrating that the cells indeed were viable, and that such cells are only transiently CWD. To exclude that colonies were formed by spores present in the filtrate, we deleted the *ssgB* gene that is required for sporulation[37]. Indeed, this led to a non-sporulating variant of *K. viridifaciens* (Fig. 4H). Like the wild-type strain, the *ssgB* mutant formed cell wall-deficient S-cells in hyperosmotic growth conditions (Fig. 4I). Time-lapse microscopy (Supplementary Movie 4) revealed that S-cells of the *ssgB* mutant were able to initiate filamentous growth and establish mycelial colonies (Fig. 4J). A switch to mycelial growth was also observed when S-cells were inoculated in liquid medium, whether or not the media was supplemented with high levels of sucrose (data not shown). We noticed that the viability of S-cells was reduced by 60% (decreasing from $1.6x10^4$ to $6.7\ x10^3$ CFUs $ml^{-1}$) when these cells were diluted in water before plating, consistent with their cell wall deficiency. Microscopy analysis indicated that the surviving S-cells were those that showed abundant staining with WGA-Oregon (Supplementary Fig. 5). Altogether, these results demonstrate that *K. viridifaciens* generates S-cells that synthesize PG and are able to switch to the mycelial mode-of-growth.

**Figure 4. (in page 49) S-cells are able to switch to the mycelial mode-of-growth.** (**A**) Time-lapse microscopy stills showing the extrusion of S-cells (arrows) from hyphal tips. The arrow heads indicate new branches, while "S" designates the germinated spore. Images were taken from Supplementary Movie 1. (**B**) Z-stack projection of filtered S-cells (taken from Supplementary Movie 3). Cells were stained with Hoechst and FM5-95 to visualize DNA and membranes, respectively. The intracellular membrane assemblies are indicated with white arrows. (**C**) Transmission electron micrographs of S-cell reveal the presence of agglomerates of membrane structures (white arrow) in close proximity to the DNA. Contrary to filamentous cells (**F**, **G**), S-cells possess a disorganized cell surface (**D**, **E**). Deletion of *ssgB* in *K. viridifaciens* blocks the formation of grey-pigmented spores (**H**). (**I**) Transmission electron micrographs indicate that S-cells of the Δ*ssgB* mutant, like those of the wild-type strain, are not surrounded by a cell wall. The arrowhead in the inlay indicates the cell membrane. (**J**) Time-lapse microscopy stills showing the switch of a Δ*ssgB* mutant S-cell (asterisk) to filamentous growth (arrows). Please note that the mycelial outgrowth leads to the collapse of the S-cell at t= 210 mins. Images were taken from Supplementary Movie 4. Scale bars represents 10 µm (**A**, **B**), 5 µm (magnified section in **B**), 2 µm (**C**, **I**), 100 nm (**D**, **E**), 200 nm (**F**, magnified section in **I**), 50 nm (**G**), 20 µm (**J**).

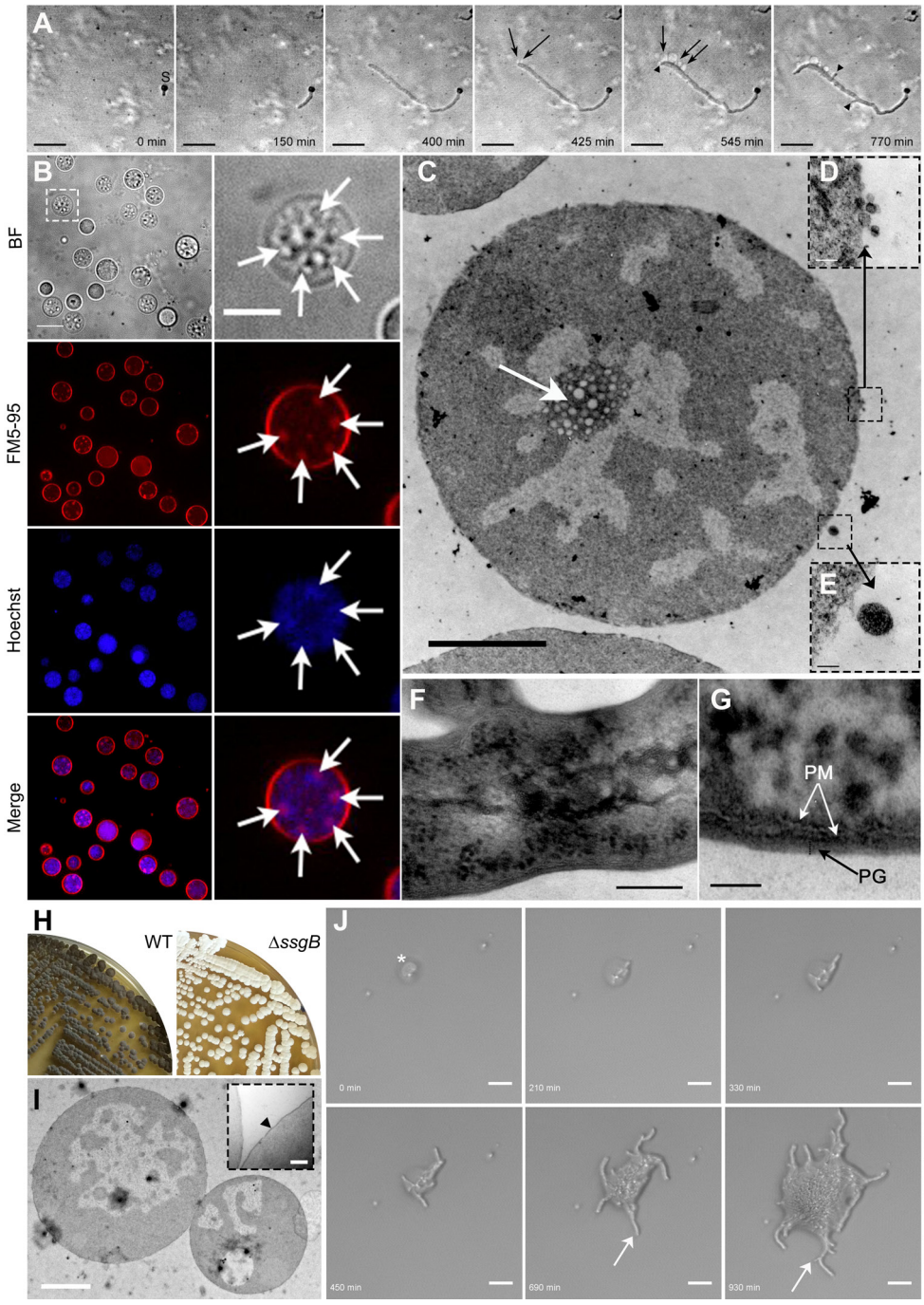
A
S
0 min
150 min
400 min
425 min
545 min
770 min
B
C
D
E
F
G
BF
FM5-95
Hoechst
Merge
PM
PG
H
WT
ΔssgB
I
J
*
0 min
210 min
330 min
450 min
690 min
930 min

## S-cell switching leads to loss of the KVP1 megaplasmid

When S-cells were allowed to switch to mycelium on MYM medium, we identified many colonies with developmental defects (Fig. 5). Most obvious was the frequent occurrence of small, brown-pigmented colonies that neither produced aerial hyphae (which are white) nor grey-pigmented spores (Fig. 5C). These brown-colony variants were also observed when protoplasts were plated (Fig. 5B), but were rare when spores were used (Fig. 5A). Such non-differentiating colonies are referred to as bald, for the lack of the fluffy aerial hyphae[12]. To test if this aberrant phenotype was maintained in subsequent generations, we selected three of these bald colonies (R3-R5), and two grey-pigmented colonies with a near wild-type morphology (R1 and R2) for further analysis. The progeny of the grey colonies developed similarly to the wild-type strain, and sporulated abundantly after 7 days of growth (Fig. 5D). In contrast, strains R3-R5 failed to sporulate after 7 days of growth. This phenotype is reminiscent of the defective sporulation seen in colonies of *Streptomyces clavuligerus* that have lost the large linear plasmid pSCL4 following protoplast formation and regeneration[180].

Given that *K. viridifaciens* also contains a large megaplasmid (KVP1[210]), we reasoned that S-cell formation could increase the frequency of the loss of this plasmid. To test this assumption, we performed quantitative real-time PCR using four genes located on the megaplasmid (*orf1*, *parA*, *tetR*, and *allC*). Of these, *parA* is implied in plasmid segregation, while *orf1* encodes a plasmid-type DNA replication protein[168]. As a control, we included the house-keeping genes *infB* and *atpD*, which encode the translation initiation factor IF-2 and a subunit of the $F_0F_1$ ATP synthase, respectively. Both of these genes are located on the chromosome. Detectable amplification of *infB* and *atpD* was seen after 19 PCR cycles in strains R3-R5, which was similar to the wild-type strain (Fig. 5E). The same was true for the KVP1-specific genes *orf1*, *parA*, *tetR*, and *allC* in the wild-type strain. However, amplification of these plasmid marker genes was only seen after 30 PCR cycles in strain R3-R5 (Fig. 5F). This demonstrates that the KVP1-specific genes represented only a very small fraction of the DNA content of R3-R5 strains (at least $10^4$ times less abundant than the chromosomal genes *infB* and *atpD*) (Fig. 5G). This is consistent with loss of KVP1 in the mycelial colonies obtained after S-cell switching.

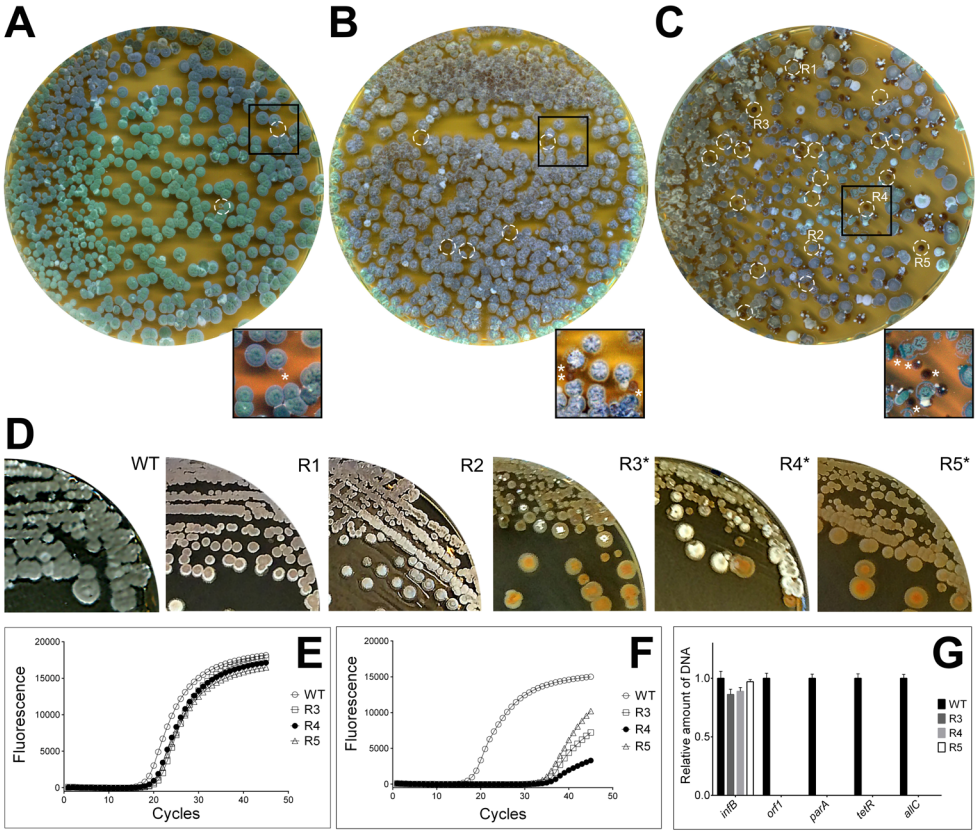


**Figure 5. S-cell switching leads to loss of the linear megaplasmid KVP1.** Morphology of 7-day-old colonies of *K. viridifaciens* on MYM medium obtained after plating spores (**A**), protoplasts (**B**) or S-cells (**C**). The switch of S-cells to the mycelial mode-of-growth yields colonies with different morphologies: besides grey-pigmented colonies (R1, R2), colonies are formed that fail to develop efficiently, and which appear whitish or brown (R3-R5). Brown colonies are also evident when protoplasts are plated (**B**, white circles), but rare when spores are used. (**D**) Subculturing of R1 and R2 leads to the formation of grey colonies that appear similar to the wild type, while subculturing of R3, R4 and R5 yield colonies that are unable to form a robust sporulating aerial mycelium (brown and white colonies). Quantitative real-time PCR of the *infB* (**E**) and *allC* (**F**) genes using gDNA of the wild type and R3-R5 as the template. In all strains, the *infB* gene located on the chromosome is amplified before the 20$^{th}$ cycle. However, the *allC* gene, located on the KVP1 megaplasmid, is amplified in the wild type before the 20$^{th}$ cycle, but in strains R3-R5 after the 30th cycle. Values represent the average of two replicates. (**G**) Quantitative comparison of the relative abundance of four megaplasmid genes (*orf1*, *parA*, *tetR* and *allC*) and the *infB* gene (located on the chromosome) between the wild type and strains R3-R5. The strong reduction in the abundance of the megaplasmid genes are consistent with loss of this plasmid. qPCR data was normalized to the housekeeping gene *atpD*. Error bars indicate the standard error of the mean.

## Prolonged hyperosmotic stress converts S-cells into L-forms

Although the switch to mycelial growth was exclusively observed when young S-cells were cultured in fresh media, we noticed a dramatic change when S-cells had been exposed for prolonged periods to the hyperosmotic stress conditions. In nine out of 15 independent experiments, we found that S-cells switched to mycelial growth, while four times S-cells failed to form a growing culture. Striking, were the two independent occasions where S-cells had proliferated in an apparent cell wall-deficient state. On solid LPMA media, these two independent cell lines, called M1 and M2 (for mutants 1 and 2, respectively, see below), formed viscous colonies, which were morphologically similar to those from an L-form lineage induced by the addition of penicillin. Conversely, filtered S-cells formed compact mycelial colonies on LPMA medium (Fig. 6A). This interesting difference between S-cells and the M1 and M2 lineages suggested that the S-cells represent a transient form of CWD cells, as they formed mycelial colonies even when osmoprotection was available. Consistent with this observation, we observed that the addition of 0.6 $mg \cdot ml^{-1}$ penicillin inhibited the switch of S-cells to mycelial colonies (Fig. 6A). However, the M1 and M2 strains and the L-form lineage were unaffected by the addition of penicillin, and formed viscous colonies composed of spherical cells in the presence of the antibiotic. Remarkably, switched S-cells, but also strains M1, M2 as well as the penicillin-induced L-form lineage were viable on MYM agar plates lacking osmoprotectant (Fig. 6B). Under these conditions, all strains had formed mycelial colonies and exclusively grew in a filamentous manner.

Also, liquid-grown cultures of M1 and M2 exclusively consisted of CWD cells when sucrose and $MgCl_2$ were added (Fig. 6C, BF panels). The spherical cells produced by M1 and M2 were comparable in size to the penicillin-induced L-forms. Further microscopic analysis revealed that the cells from M1 and M2 contained inner vesicles (arrowheads in Fig. 6C) and tubular protrusions emerging from the cell surface (Fig. 6C, inlay). The vast majority of cells contained DNA, although some empty vesicles were also evident in M1 and M2 (Fig. 6C, asterisks). Time-lapse microscopy revealed that both strains proliferated, whereby smaller progeny cells were released following deformation of the mother cell membrane by either vesiculation (Fig. 6D, taken from Supplementary Movie 5), blebbing (Fig. 6E, taken from Supplementary Movie 6) or tubulation (Fig. 6F, taken from Supplementary Movie 7). Altogether these results inferred that strains M1 and M2 morphologically closely resemble L-forms, both in their ability to proliferate in the cell wall-deficient state, and the capacity to grow in the presence of penicillin (see above). However, instead of originating from prolonged exposure to antibiotic and/or lysozyme treatment, they originate from hyperosmotically stress-induced cells.

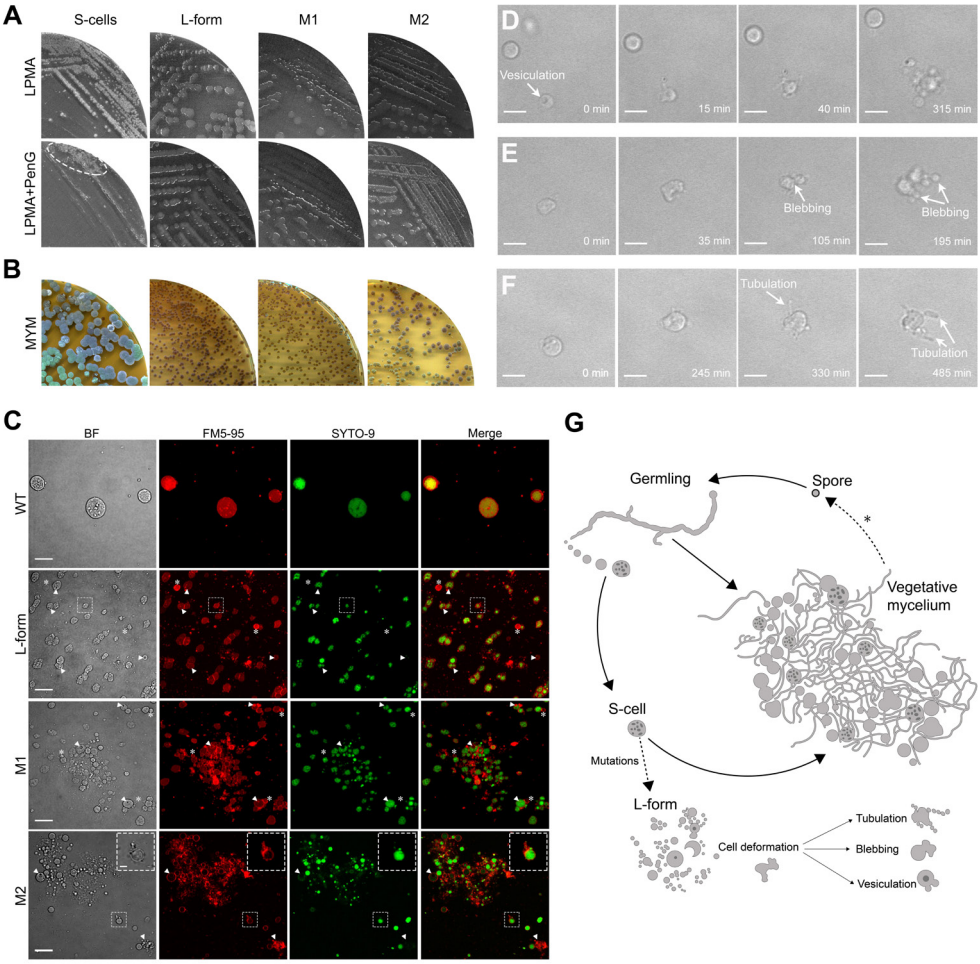


**Figure 6. Hyperosmotic stress conditions are sufficient to isolate L-form strains.** (**A**) Phenotypic differences are evident when S-cells, penicillin-induced L-forms, and cells of the M1 and M2 strains are grown on LPMA medium without (top) and with penicillin (PenG, bottom). Plating S-cells led to the formation of compact mycelial colonies on LPMA medium contrary to the other strains that formed viscous colonies. The addition of 0.6 mg·ml$^{-1}$ penicillin abolished efficient switching of S-cells to the mycelial mode-of-growth. Small mycelial colonies derived from S-cells were only formed in the least diluted part (indicated with a dashed ellipse). In contrast, the addition of penicillin neither effected growth of the penicillin-induced L-forms, nor that of strains M1 and M2. (**B**) All cell wall-deficient cells were able to form mycelial colonies on MYM medium lacking high levels of osmolytes. Unlike the majority of colonies derived from S-cells, the penicillin-induced L-forms and strains M1 and M2 exclusively formed (brown) non-sporulating colonies. (**C**) Morphology of S-cells in comparison to cells of the penicillin-induced L-form strain and strains M1 and M2 grown for 48 hours in LPB medium. Cells were stained with FM5-

95 and SYTO-9 to visualize membranes and DNA, respectively. The arrowheads indicate intracellular vesicles, while empty vesicles are indicated with an asterisk. The inlay in M2 shows a proliferation-associated tubulation event. (**D-F**) Frames from time-lapse microscopy show L-form-like proliferation involving (**D**) vesiculation, (**E**) blebbing, and (**F**) membrane tubulation. (**G**) Formation of S-cells upon prolonged exposure to hyperosmotic stress. Germination of spores under hyperosmotic stress conditions generates germlings, which are able to extrude S-cells. These S-cells are able to switch to the mycelial mode-of-growth, or sporadically acquire mutations that allow them to proliferate like L-forms, which is characterized by tubulation, blebbing or vesiculation. Scale bar represents 10 µm (**C**), 2 µm (inlay panel **C**) or 5 µm (**D-F**).

The low frequency at which the M1 and M2 L-form cell lines had been obtained suggests that M1 and M2 had acquired mutations that enabled these strains to proliferate without a proper cell wall. Real-time qPCR studies revealed that M1 and M2, as well as the penicillin-induced L-form cell line, appeared to have lost the megaplasmid genes *tetR*, *allC*, *orf1* and *parA* (Fig. 7). In agreement, Illumina sequencing revealed a low coverage of KVP1-located sequences (Fig. 7E). However, loss of the megaplasmid is not sufficient to drive the transition from S-cells to L-forms, as strains R3-R5, all of which had also lost the KVP1 megaplasmid, formed mycelia extruding S-cells under hyperosmotic stress conditions (data not shown). Further analyses indicated that M1 and M2 had acquired several other mutations, including both major lesions in the right arm of the chromosome (Fig. 7D, E) and a number of point mutations (Supplementary Table 4, 5). Interestingly, both strains carried a mutation in the gene BOQ63_RS21920, which encodes a putative metal ABC transporter. Transporters are often used to cope with osmotic stress conditions[211]. We also identified mutations in the penicillin-induced L-form strain (Supplementary Table 6). These mutations, however, differed from those observed in the hyperosmotically-induced L-form strains M1 and M2. Notably, the mutations in the penicillin-induced L-form appeared to directly relate to cell wall biogenesis, for example in the case of the mutation in *uppP*. The encoded protein is involved in the recycling pathway of the carrier lipid undecaprenyl phosphate (BOQ63_RS22750), which transports glycan biosynthetic intermediates for cell wall synthesis. Although it is currently not known how all these mutations affect morphology, our results demonstrate that prolonged exposures to hyperosmotic stress are mutagenic conditions through which a filamentous bacterium can be converted into an L-form mutant strain that proliferates without the cell wall.

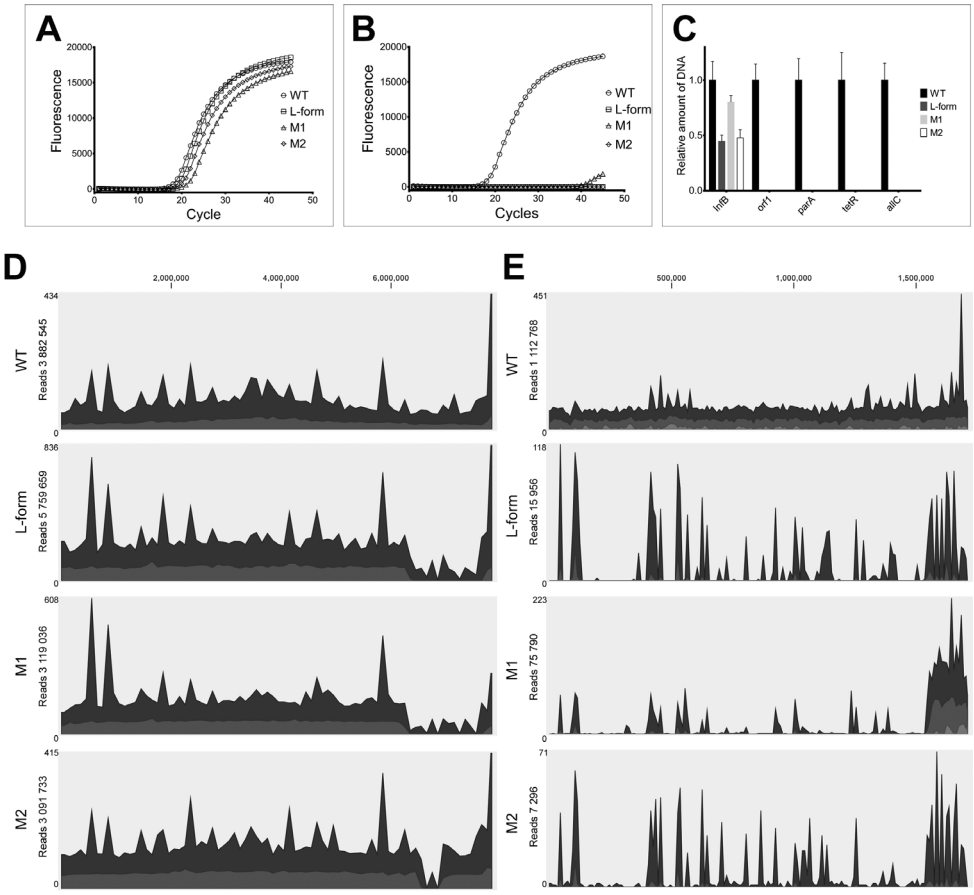


**Figure 7. Strains proliferating as L-forms lack the KVP1 megaplasmid.** Quantitative real-time PCR of the *infB* (**A**) and *allC* (**B**) genes using gDNA of the wild-type strain, the penicillin-induced L-form strain, and strains M1 and M2 that proliferate as L-forms. In all strains, the *infB* gene located on the chromosome is amplified before the 20$^{th}$ cycle. However, the *allC* gene, located on the KVP1 megaplasmid, is only amplified in the wild type strain, but not in any of the other strains. Values represent the average of two replicates. (**C**) Quantitative comparison of the relative abundance of four megaplasmid genes (*orf1*, *parA*, *tetR* and *allC*) and the *infB* gene (located on the chromosome) between wild-type and L-form strains. qPCR data was normalized to the housekeeping gene *atpD*. Error bars indicate the standard error of the mean. (**D**-**E**) Alignment of Illumina reads from the *K. viridifaciens* wild type strain, the penicillin-induced L-form strain, and the M1 and M2 strains against the chromosome (**D**) and the KVP1 megaplasmid (**E**). For all strains, an overall high coverage was observed when reads were aligned against the chromosome (**D**). In contrast, a low coverage was observed when reads were aligned against the megaplasmid KVP1, the wild-type strain being the exception (**E**). Please note that the number of reads corresponding to some parts in the right arms of the chromosomes of the penicillin-induced L-form strain and the M1 and M2 strains is strongly reduced, suggesting major lesions.

## Discussion

Filamentous actinomycetes have been intensely studied for more than 50 years as a model for bacterial development. Here, we provide compelling evidence that S-cells represent a natural and previously unnoticed developmental stage in these organisms when they are exposed to hyperosmotic stress conditions (Fig. 6G). These S-cells are extruded from the hyphal tips, contain DNA and are viable with the ability to grow into mycelial colonies. Furthermore, upon prolonged exposure to hyperosmotic stress, S-cells may also accumulate mutations that enable them to efficiently proliferate in the wall-deficient state we have dubbed hyperosmotically induced-L-forms. Our data show that these L-forms can simply emerge as the product of prolonged exposure of cells to hyperosmotic conditions, without directly requiring cell wall-targeting agents. This work thus provides leads towards dissecting the ecological relevance that such cells may have.

Environmental fluctuations can dramatically influence the availability of water in ecosystems and present osmotic shock conditions to organisms. For instance, microorganisms living in hyperarid regions or hypersaline aquatic environments are frequently exposed to desiccation or hypertonicity[120]. Also, microbes in snow and ice habitats experience low water availability and hypersaline or hyper-acidic environments[119]. Bacteria can adapt to these fluctuations by modulating fatty acid synthesis, accumulating or synthesizing osmoprotectants, protecting their DNA, and secreting extracellular polymeric substance[120,212].

Here, we focused on the adaptation of filamentous actinomycetes, which are common in any soil, to extended periods of hyperosmotic stress. As expected, we detected that these bacteria increased the amount of membrane in the hyphae and condensed their nucleoids. A surprising discovery was the extrusion of cell wall-deficient S-cells. Together with sporulation and the recently discovered explorative mode-of-growth[213], the ability to form S-cells extends the repertoire by which filamentous actinomycetes can thrive in changing environments. Our work reveals that the ability to extrude S-cells is common in filamentous actinomycetes and occurs in both *Streptomyces* and *Kitasatospora* species. We used a stringent selection to assess S-cell formation, which we define as cell wall-deficient cells that contain DNA and which are larger in size than 2 µm (to exclude that these are swollen spores). In this study, strains were solely screened in liquid-grown cultures in hyperosmotic stress conditions. Being this stringent, we anticipate that potentially many more strains are able to make S-cells under influence of other stresses. For instance, it is known that cell wall-deficiency is stimulated by hypoxic, temperature or nutrient stresses[132,214]. These are also conditions that filamentous actinomycetes are frequently exposed to in heterogeneous soil environments.

S-cells are only transiently cell wall-deficient and have the ability to switch to the mycelial mode-of-growth. Strikingly, many of the switched colonies appear to have developmental defects (see Fig. 5C). These developmental phenotypes are reminiscent of those that have been associated with genetic instability in a range of actinomycetes[174,215]. Here, we demonstrated that colonies that were unable to establish reproductive aerial hyphae lacked the KVP1 megaplasmid. This is likely caused by initial differences in the amount and DNA content between S-cells. While the majority of cells will receive one or more KVP1 copies during their formation, a fraction of cells will receive none. Additionally, S-cells may also carry different numbers of chromosomes, based on the range of sizes that S-cells have. Such multinucleated cells are prone to recombination events[216,217], which will furthermore increase diversity. Altogether, we think that these differences in DNA content in S-cells contributes to the morphological heterogeneity observed in the mycelial colonies derived from S-cells.

In addition to switching to mycelial growth, S-cells can have several other fates. As these cells are wall-deficient, they are prone to lysis due to influx of water. Indeed, exposure to water leads to a steep decline in their ability to outgrow into colonies. However, when S-cells lyse, the DNA cargo will be released into the environment. Given the large number of biosynthetic gene clusters (BGCs) that are present in the genomes of filamentous actinomycetes, including their resistance determinants, this release of DNA may be a significant, and previously unknown mechanism by which resistance genes are spread. In contrast to releasing DNA into the environment, we speculate that S-cells may also take up DNA, similar to other cell wall-deficient cell types such as protoplasts or L-forms[218]. Whether S-cells play a role in horizontal gene transfer is under current investigation.

Our work shows that S-cells are extruded from hyphal tips into the environment, coinciding with an arrest in tip growth. Following their release, the extruding hypha reinitiates growth, indicating that the extrusion process occurs in a manner that apparently is not lethal for the filament from which the cells are released. Tip growth in filamentous actinomycetes is coordinated by the polarisome complex, of which the DivIVA protein is a crucial member[82]. Recent work revealed that hyperosmotic stress has a dramatic effect on the polar growth machinery. Following osmotic upshift experiments, tip growth is arrested, followed by relocation of the apical growth machinery to subapical sites. As a consequence, lateral branches emerge from the leading hyphae[193]. We hypothesize that an imbalance between cell wall synthesis and cell wall turnover could locally lead to changes in the thickness or structure of the cell wall, allowing S-cells to escape from the sacculus.

L-forms have been studied for many decades, and only recently are we beginning to understand their exciting biology, especially due to ground-breaking work from the Errington lab. L-form cells have been artificially generated from many different bacteria in many laboratories, invariably aimed at targeting the biosynthesis pathway of the cell wall. To that end, cells are typically exposed to high levels of antibiotics, either or not combined with lysozyme treatment[137,138]. Our work expands on this research by providing for the first-time evidence that CWD strains can emerge solely by exposure to hyperosmotic stress conditions and implies an environmental relevance of this cell type. A crucial and limiting step in the formation of L-forms in *B. subtilis*, as well as in other bacteria, is the escape of a protoplast from the cell-wall sacculus. This process requires lytic activity, which usually comes from lysozyme activity[219]. Our data show that actinomycetes have a natural ability to release such CWD cells when exposed to hyperosmotic conditions. Under prolonged exposure to osmotic stress, some cells are able to acquire mutations allowing these cells to propagate as L-forms. In line with these findings, recent work shows that *B. subtilis* and *S. aureus* both are able to convert to wall-deficient cells[219]. This has been shown in an animal infection model as well as in macrophages, where lysozyme activity from the host converts walled bacteria into CWD cells. Collectively, these results indicate that cell wall-deficient cells represent an adaptive morphology allowing cells to overcome environmental challenges, such as antibiotic treatment or hyperosmotic stress conditions.

In summary, our work provides evidence for a new, cell wall-deficient cell type in the biology of filamentous actinomycetes. It further expands the large diversity in bacterial cell types, and the plasticity that microorganisms employ to handle environmental stresses. It remains to be elucidated how the ability to form S-cells improves fitness in these filamentous actinomycetes, and how this morphogenetic switch is regulated.

## Methods

### Strains and media

Bacterial strains used in this study are shown in Supplementary Table 7. To obtain sporulating cultures, *Streptomyces* and *Kitasatospora* species were grown at 30°C for 4 days on MYM medium[195]. To support growth of CWD cells, strains were grown on solid medium L-Phase Medium (LPMA), containing 0.5% glucose, 0.5% yeast extract, 0.5% peptone, 0.58 M sucrose, 0.01% $MgSO_4 \cdot 7H_2O$, 0.75% Iberian agar (all w/v). After autoclaving, the medium was supplemented with $MgCl_2$ (final concentration of 25 mM) and 5% (v/v) horse serum.

L-Phase Broth (LPB) was used as liquid medium to support growth of wall-deficient cells. LPB contains 0.15%

yeast extract, 0.25% bacto-peptone, 0.15% oxoid malt extract, 0.5% glucose, 0.64 M sucrose, 1.5% oxoid tryptic soy broth powder (all w/v) and 25 mM $MgCl_2$. To test the effect of different sucrose concentrations on mycelial growth and the formation of S-cells, the amount of sucrose in LPB was changed to obtain final concentrations of 0, 0.06, 0.18, 0.50 and 0.64 M. The influence of other osmolytes was analysed by replacing sucrose with NaCl (0.6 M) or sorbitol (1 M). 50 ml cultures were inoculated with $10^6$ spores·$ml^{-1}$ and grown in 250 ml flasks. Cultures were incubated at 30°C, while shaking at 100 rpm.

To prepare protoplasts of *K. viridifaciens*, the wild-type strain was grown for 48 hours in a mixture of TSBS and YEME (1:1 v/v) supplemented with 5 mM $MgCl_2$ and 0.5% glycine. Protoplasts were prepared by incubating the mycelium for three hours in 10 mg·$ml^{-1}$ lysozyme solution[179]. Freshly-made protoplast were diluted and immediately used for fluorescence microscopy.

### Optical density measurements

The growth of *K. viridifaciens* was monitored with the Bioscreen C reader system (Oy Growth Curves AB Ltd). To this end, aliquots of 100 µl of LPB medium with different concentrations of sucrose were added to each well of the honeycomb microplate and inoculated with $10^7$ spores·$ml^{-1}$. Growth was monitored for 24 hours at 30°C, while shaking continuously at medium speed. The OD wide band was measured every 30 min and corrected for the absorbance of liquid medium without inoculum. In total, five replicate cultures were used for each osmolyte concentration. The effect of sodium chloride and sorbitol as osmolyte were tested using the same procedure, with the differences that the final volume of the cultures was 300 µl, and the experiment was run for 96 hours.

### Quantification of the number and size of colonies

Serial dilutions of *K. viridifaciens* spores were plated in triplicate in LPMA (high osmolarity) and LPMA without sucrose, $MgCl_2$ and horse serum (low osmolarity). After 7 days of incubation at 30°C the number of colonies was counted to determine the CFU·$ml^{-1}$. Quantification of the surface area of colonies was done with FIJI[220].

### Screening for strains with the ability to release S-cells

To identify strains that are able to release S-cells, strains from an in-house culture collection[209] were initially grown in flat-bottom polysterene 96-well plates, of which each well contained 200 µl LPB medium and 5 µl of spores. The 96-well plate was sealed with parafilm and incubated at 30°C for 7 days. The cultures were then analysed with light microscopy, and strains with the ability to release S-cells with a diameter larger 2 µm were selected. The selected strains were then grown in 250 mL flasks containing 50

mL LPB medium ($10^6$ spores·$ml^{-1}$) at 30°C while shaking at 100 rpm. After 7 days, aliquots of 50 µl of the bacterial cultures were fluorescently stained with SYTO-9 and FM5-95. The surface area of the S-cells was determined in FIJI[220]. Assuming circularity of these cells, the corresponding diameter D was then calculated as $D = 2 \times \sqrt{(area / \pi)}$

### Filtration of S-cells from *K. viridifaciens*

50 ml LPB cultures of *K. viridifaciens*, inoculated with $10^6$ spores·$ml^{-1}$, were grown for 2 or 7 days at 30°C in an orbital shaker at 100 rpm. To separate the S-cells from the mycelium, the cultures were passed through a sterile filter made from an EcoCloth™ wiper. A subsequent filtration step was done by passing the S-cells through a 5 µm Isopore™ membrane filter. The filtered vesicles were centrifuged at 190 g for 40 mins, after which the supernatant was carefully removed with a 10 mL pipette to avoid disturbance of the S-cells. Same procedure was followed to filtrate S-cells from Δ*ssgB* mutant, although the cultures were inoculated with an individual colony that had been grown on MYM medium for 6 days.

### Viability and subculturing of S-cells from *K. viridifaciens*

To verify the viability of S-cells, the filtered cells were directly plated or incubated in 10 mg·$ml^{-1}$ lysozyme solution[179] for 3 hours at 30°C, while shaking at 100 rpm. The filtered S-cells were then centrifuged at 190 g for 40 mins and resuspended in 1 volume of fresh LPB. Serial dilutions of the S-cells in LPB or water were then plated, in triplicate, on LPMA or MYM medium. The plates were grown for 7 days at 30°C and the CFU values were determined for each treatment.

### Generation of the penicillin-induced L-form cell line

Generation of the *K. viridifaciens* L-form lineage was performed by inoculating the wild-type strain in 50 mL LPB medium, supplemented with lysozyme and/or penicillin G (Sigma), in 250 mL flasks in an orbital shaker at 100 rpm. Every week, 1 mL of this culture was transferred to fresh LPB medium[208]. After the 8$^{th}$ subculture, the inducers were removed from the cultivation medium and the obtained lineage did not revert back to the walled state on LPMA plates or in LPB medium. A single colony obtained after the 8$^{th}$ subculture was designated as penicillin-induced L-forms.

### Construction of the *ssgB* deletion construct pKR1

The *ssgB* (BOQ63_RS34980) mutant was created in *K. viridifaciens* using pKR1, which is a derivative of the unstable plasmid pWHM3 as described[221]. In the *ssgB* mutant, nucleotides +20 to +261 relative to the start codon of *ssgB* were replaced with the *loxP-apra* resistance cassette[222].

### Phylogenetic analysis

The 16S rRNA sequences from strains of the in-house culture collection were previously determined[209]. Homologues of *ssgB* in these strains were identified by BLAST analysis using the *ssgB* sequence from *S. coelicolor* (SCO1541) as the input. For the *Streptomyces* and *Kitasatospora* strains whose genome sequence was not available, the *ssgB* sequence was obtained by PCR with the *ssgB* consensus primers (Supplementary Table 8). Geneious 9.1.7 was used to make alignments of *ssgB* and 16S rRNA, and for constructing neighbour-joining trees.

### Quantitative real time PCR

Filtered S-cells were allowed to regenerate on MYM medium, from which three regenerated bald colonies (R3, R4, and R5) were selected. After two rounds of growth on MYM, bald colonies of the three strains were grown in TSBS for 2 days at 30°C, and genomic DNA was isolated from these strains[179]. Primers were designed to amplify the *infB* (BOQ63_RS29885) and *atpD* (BOQ63_RS19395) genes located in the chromosome, and four genes located on the KVP1 megaplasmid: *allC* (BOQ63_RS01235), *tetR* (BOQ63_RS02930), *parA* (BOQ63_RS04095) and *orf1* (BOQ63_RS04285) (Supplementary Table 8). The PCR reactions were performed in duplicate in accordance with the manufacturer's instructions, using 5 ng of DNA, 5% DMSO and the iTaq Universal SYBR Green Supermix Mix (Bio-Rad). Quantitative real time PCR was performed using a CFX96 Touch Real-Time PCR Detection System (Bio-Rad). To normalize the relative amount of DNA, the wild-type strain was used as a control, using the *atpD* gene as a reference.

### Isolation of the L-form cell lines M1 and M2

Fifteen replicate cultures of *K. viridifaciens* were grown for 7 days in LPB medium. After filtration, the S-cells were transferred to fresh LPB medium. The cultures that had not switched to mycelium after 3 days of cultivation were kept for further analysis. Two cultures turned dark green after 7 days, which after inspection with light microscopy contained proliferating L-form cells. These cell lines were named M1 and M2.

### Microscopy

Bright field images were taken with the Zeiss Axio Lab A1 upright Microscope, equipped with an Axiocam MRc with a resolution of 64.5 nm/pixel. Fluorescent dyes (Molecular Probes™) were added directly to 100 µl aliquots of liquid-grown cultures. For visualization of membranes, FM5-95 was used at a final concentration of 0.02 mg·ml$^{-1}$. Nucleic acids were stained with 0.5 µM of SYTO-9 or 0.05 mg·ml$^{-1}$ of Hoechst 34580. The detection of peptidoglycan was done using 0.02 mg·ml$^{-1}$ Wheat Germ Agglutinin (WGA) Oregon Green, or 1 µg·ml$^{-1}$

BOPIPY FL vancomycin (which stains nascent PG). Prior to visualization, cells and mycelium were applied on a thin layer of LPMA (without horse serum) covering the glass slides. Confocal microscopy was performed using a Zeiss Axio Imager M1 Microscope. Samples were excited using a 488-nm laser, and fluorescence emissions for SYTO-9, and WGA Oregon Green were monitored in the region between 505–600 nm, while a 560 nm long pass filter was used to detect FM5-95.

The characterization of the membrane assemblies in S-cells was done on a Nikon Eclipse Ti-E inverted microscope equipped with a confocal spinning disk unit (CSU-X1) operated at 10,000 rpm (Yokogawa, Japan) using a 100x Plan Fluor Lens (Nikon, Japan) and illuminated in bright-field and fluorescence. Samples were excited at wavelengths of 405 nm and 561 nm for Hoechst and FM5-95, respectively. Fluorescence images were created with a 435 nm long pass filter for Hoechst, and 590-650 nm band pass for FM5-95. Z-stacks shown in Supplementary Movie 3 were acquired at 0.2 µm intervals using a NI-DAQ controlled Piezo element.

Visualization of stained CWD cells for size measurements were done using the Zeiss Axio Observer Z1 microscope. Aliquots of 100 µl of stained cells were deposited in each well of the ibiTreat µ-slide chamber (ibidi®). Samples were excited with laser light at wavelengths of 488, the green fluorescence (SYTO-9, BODIPY FL vancomycin, WGA-Oregon) images were created with the 505-550 nm band pass, while a 650 nm long pass filter was used to detect FM-595.

**Time-lapse imaging**

To visualize the emergence of S-cells, spores of *K. viridifaciens* were pre-germinated in TSBS medium for 5 hours. An aliquot of 10 µl of the recovered germlings was placed on the bottom of an ibiTreat 35 mm low imaging dish (ibidi®), after which an LPMA patch was placed on top of the germlings.

To visualize switching, the S-cells produced by the Δ*ssgB* mutant were collected after 7 days by filtration from a liquid-grown culture. A 50 µl aliquot of the filtrate was placed on the bottom of an ibiTreat 35 mm low imaging dish (ibidi®) with a patch of R5 on top.

To visualize the proliferation of M1 and M2, the strains were grown for 48 hours in LPB. Aliquots of the culture were collected and centrifuged at 7,516 g for 1 min, after which the supernatant was removed, and the cells resuspended in fresh LPB. Serial dilutions of the cells were placed in wells of an ibiTreat µ-slide chamber (ibidi®).

All samples were imaged for ~15 hours using an inverted Zeiss Axio Observer Z1 microscope equipped with a Temp Module S (PECON) stage-top set to 30°C. Z-stacks with a 1 µm spacing were taken every five minutes using a 40x water immersion objective. Aver-

age intensity projections of the in-focus frames were used to compile the final movies. Light intensity over time was equalised using the correct bleach plugin of FIJI.

### Electron microscopy

To visualize the vegetative mycelium of *K. viridifaciens* by transmission electron microscopy (TEM), the strain was grown in TSBS medium for 48 hours. An aliquot of 1.5 ml of the culture was centrifuged for 10 mins at 190 g, after which the supernatant was carefully removed with a pipette. The mycelium was washed with 1X PBS prior to fixation with 1.5% glutaraldehyde for one hour at room temperature. The fixed mycelium was centrifuged with 2% low melting point agarose. The solid agarose containing the embedded mycelium was sectioned in 1 $mm^3$ blocks, which were post-fixed with 1% osmium tetroxide for one hour. The samples were then dehydrated by passing through an ethanol gradient (70%, 80%, 90% and 100%, 15 min per step). After incubation in 100% ethanol, samples were placed in propylene oxide for 15 minutes followed by incubation in a mixture of Epon and propylene oxide (1:1) and pure Epon (each step one hour). Finally, the samples were embedded in Epon and sectioned into 70 nm slices, which were placed on 200-mesh copper grids. Samples were stained using uranyl-430 acetate (2%) and lead-citrate (0.4%), if necessary, and imaged at 70 kV in a Jeol 1010 transmission electron microscope.

To image S-cells, cultures of the *K. viridifaciens* wild-type and the Δ*ssgB* mutant strains that had been grown in LPB medium for 7 days were immediately fixed for one hour with 1.5% glutaraldehyde. Filtered S-cells (see above) were then washed twice with 1X PBS prior to embedding them in 2% low melting agarose. A post-fixation step with 1% $OsO_4$ was performed before samples were embedded in Epon and sectioned into 70 nm slices (as described above). Samples were stained using uranyl-430 acetate (2%) and lead-citrate (0.4%), if necessary, and imaged at 70 kV in a Jeol 1010 transmission electron microscope.

### Image analysis

Image analysis was performed using the FIJI software package. To describe the morphological changes during hyperosmotic stress, we compared mycelium grown in LPB with or without 0.64 M of sucrose (i.e. the concentration in LPB medium). After making average Z-stack projections from mycelia, 10 hyphae derived from independent mycelia projections were further analysed. For each hypha, the total length was measured using the segmented line tool (Supplementary Fig. 1A, H) and the number of branches (asterisks in Supplementary Fig. 1A, H) emerging from that hypha was counted. The hyphal branching ratio was calculated as the number of branches per µm of leading hypha.

To calculate the surface area occupied by membrane in hyphae either or not exposed to 0.64 M sucrose, we

divided the total surface area (Supplementary Fig. 1E, L) that stained with FM5-95 by the total surface area of the hypha (Supplementary Fig. 1C, J). FIJI was also used to measure the average surface area of the nucleoid (using SYTO-9 staining, Supplementary Fig. 1G, N) in both growth conditions. Student's T-tests with two-sample unequal variance were performed to calculate P-values and to discriminate between the samples.

To determine the size of cell wall-deficient (CWD) cells, we compared cells of penicillin-induced L-form to fresh protoplasts and S-cells, all obtained or prepared after 48 hours of growth. Cells were stained with FM5-95 and SYTO-9 and deposited in the wells of an ibiTreat µ-slide chamber (ibidi®). The size of the spherical was determined as the surface area enclosed by the FM5-95-stained membrane. For the particular case of L-forms, where empty vesicles are frequent, only cells that contained DNA were measured. At least 200 cells of each CWD variant were analysed. Proliferating L-forms in which the mother cell could not be separated from the progeny, were counted as one cell.

### Genome sequencing and SNP analysis

Whole-genome sequencing followed by *de novo* assembly (Illumina and PacBio) and variant calling analyses were performed by BaseClear (Leiden, The Netherlands). The unique mutations were identified by direct comparison to the parental strain *Kitasatospora viridifaciens* DSM40239 (GenBank accession number PRJNA353578 [https://www.ncbi.nlm.nih.gov/bioproject/PRJNA353578][210]). The single and multiple nucleotide variations were identified using a minimum sequencing coverage of 50 and a variant frequency of 70%. To reduce the false positives the initial variation list was filtered, and the genes with unique mutations were further analysed. All variants were verified by sequencing PCR fragments (primer sequences in Supplementary Table 8).

### Alignment of Illumina sequences

Alignments of Illumina reads were performed using CLC Genomics Workbench 8.5.1 (Qiagen, the Netherlands). Raw Illumina (Hiseq2500 system) sequences of the wild-type, penicillin-induced L-form, and M1 and M2 strains were imported and mapped to the reference genome of *K. viridifaciens* DSM40239 (GenBank sequence MPLE00000000.1 [https://www.ncbi.nlm.nih.gov/nuccore/MPLE00000000.1/]) through the "Map reads to reference" function in the NGS core tools. Mismatch cost was set to 2 and non-specific matches were handled by mapping them randomly.

## Acknowledgments

We are indebted to Mark Leaver, Roberto Kolter, Danny Rozen, Ben Lugtenberg and Paul Hooykaas for critical reading of the manuscript. This work was supported by a VIDI grant (12957) from the Dutch Applied Research Council to D.C.

## Supplementary information

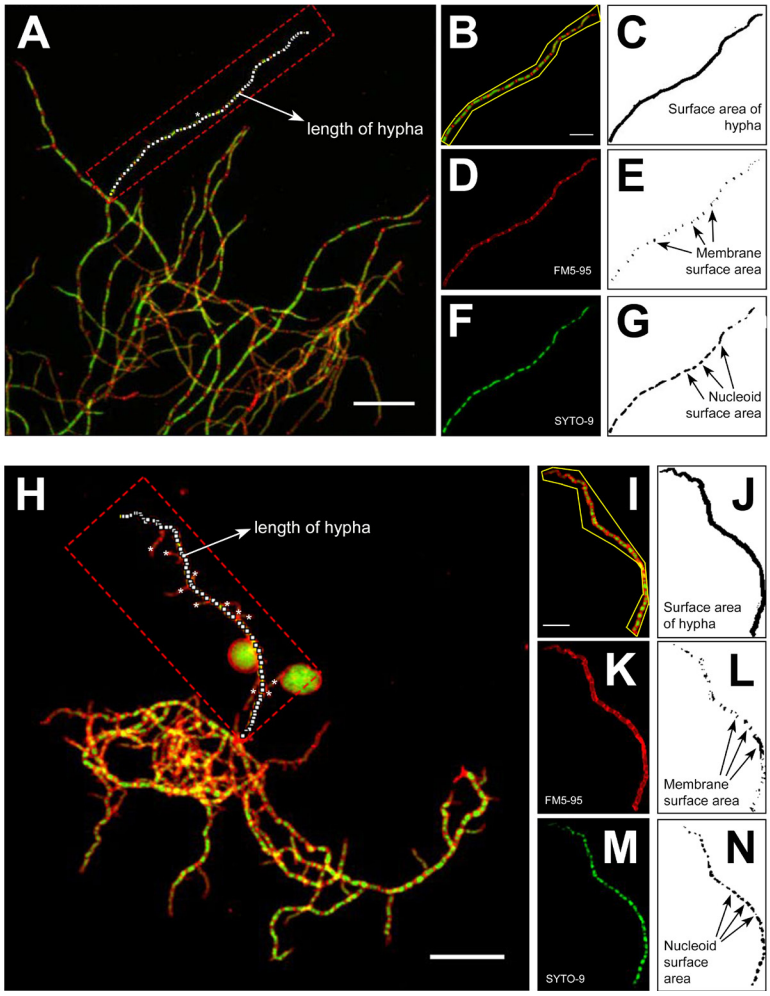


**Supplementary Figure 1. Image analysis of *K. viridifaciens* hyphae.** Average Z-projection of a mycelial particle of *K. viridifaciens* grown in the absence (**A**) or presence (**H**) of 0.64 M sucrose. The red dashed rectangle shows the hypha that was selected for image analysis. Branches emerging from the leading hypha were counted and are indicated with asterisks. The length of the hypha was measured by drawing a segmented line and calculating its length using the FIJI software package. Selected hyphae were cropped from the pellet by drawing a polygon using FIJI (see yellow line in **B**, **I**). The merged pictures of the cropped hyphae were split into the separate channels to show the fluorescence derived from the FM5-95 membrane dye (**D**, **K**) and the fluorescence derived from the SYTO-9 DNA stain (**F**, **M**). The images corresponding to those of the red channel were duplicated to measure the hyphal surface area (**C**, **J**) and the surface area occupied by membranes (**E**, **L**). The green channel was used to measure the area occupied by individual nucleoids. Scale bars represent 20 µm (**A**, **H**) and 10 µm (**B**, **I**).

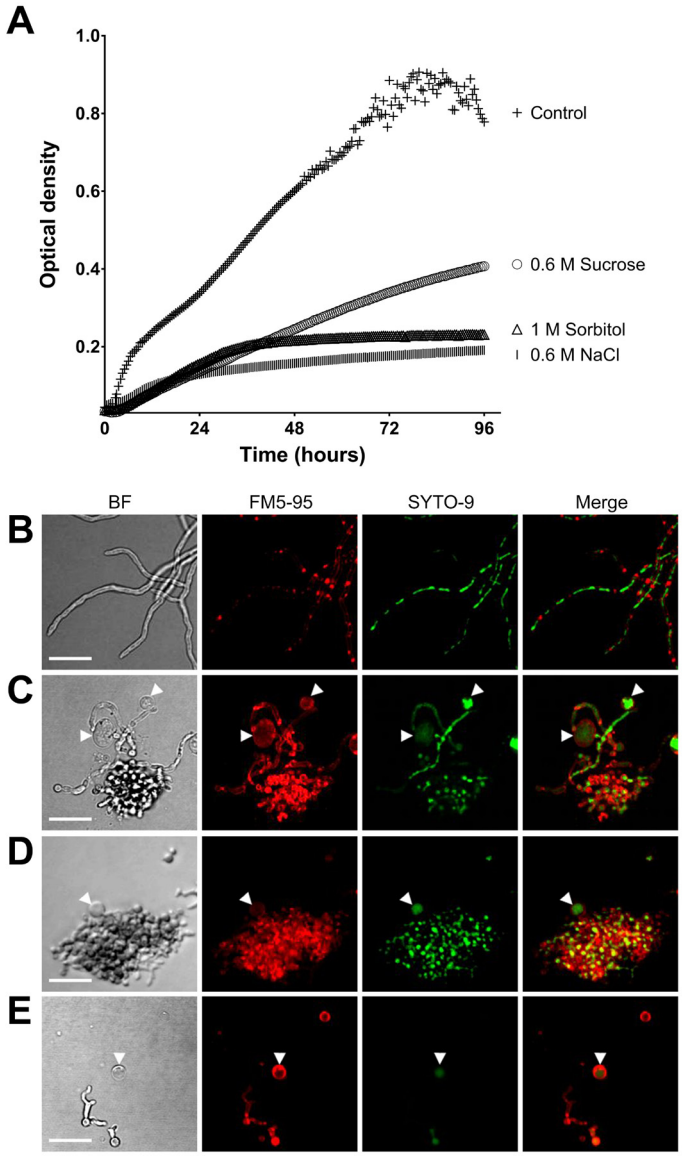


**Supplementary Figure 2. High levels of osmolytes affect growth and lead to S-cell extrusion**. Growth curves of *K. viridifaciens* in LPB medium supplemented with different osmolytes (**A**). Values represent the average of five independent replicate cultures. Unlike in the absence of high levels of osmolytes (**B**), S-cells (arrowheads) were evident after 96 hours of growth in the presence of 0.6 M sucrose (**C**), 0.6 M NaCl (**D**) and 1 M sorbitol (**E**). Mycelium and cells were stained with FM5-95 and SYTO-9 to visualize membranes and DNA, respectively. Scale bars represent 10 µm.

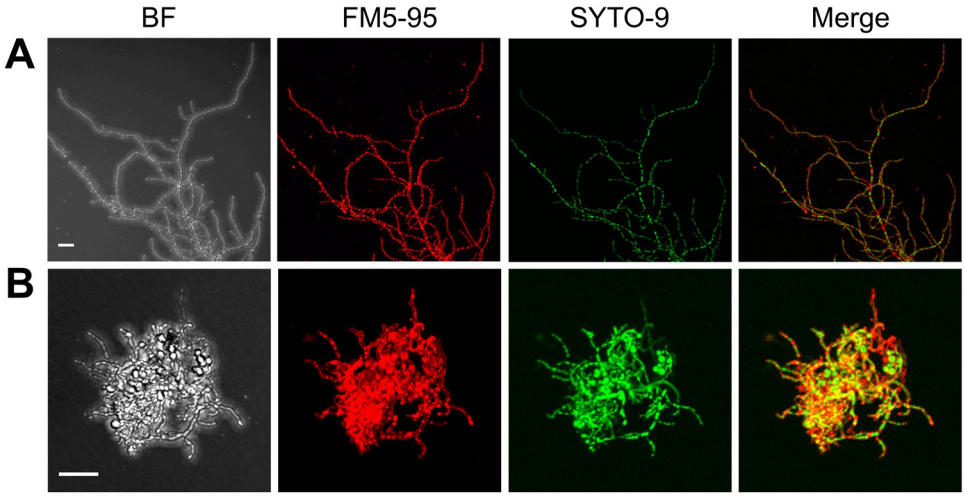


**Supplementary Figure 3. High levels of salt affect pellet morphology in *K. viridifaciens*.** Mycelial morphology of *K. viridifaciens* grown in the absence (**A**) and presence (**B**) of 0.6 M NaCl after 48 hours. Mycelium was stained with FM5-95 and SYTO-9 to visualize membranes and DNA, respectively. Scale bars represent 10 µm.

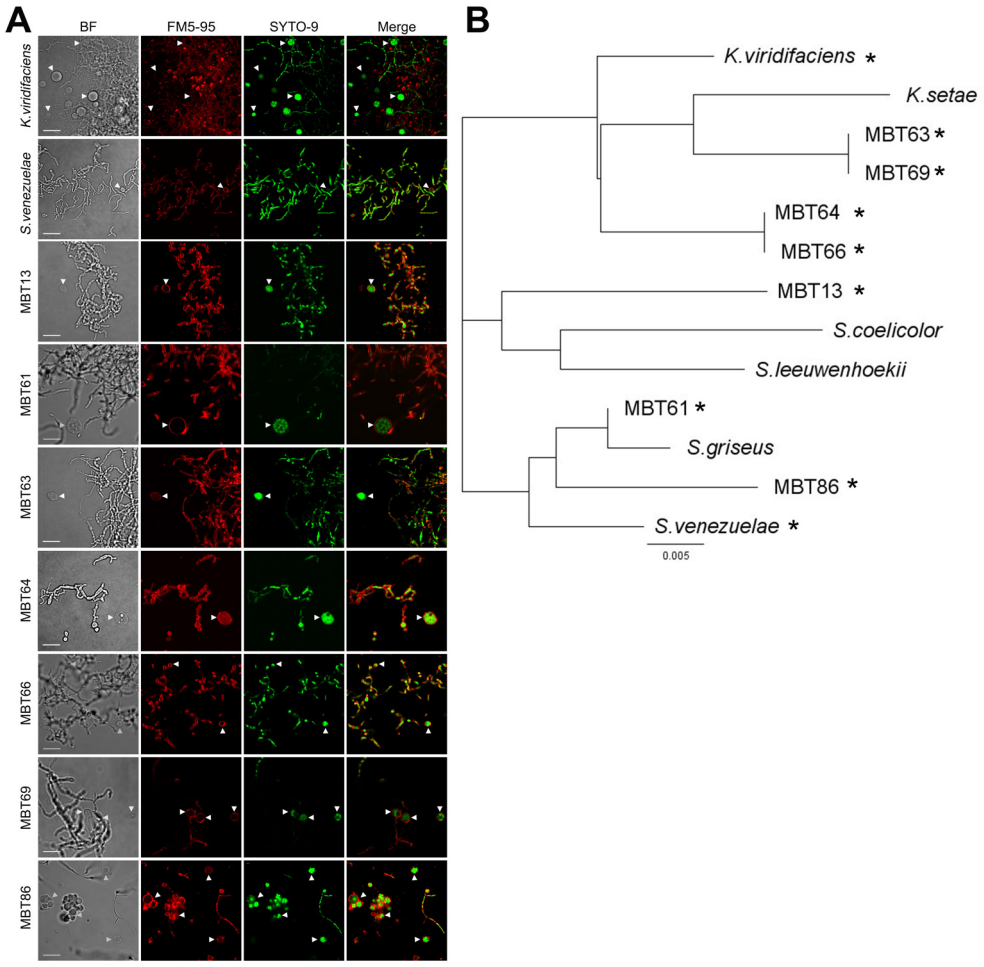


**Supplementary Figure 4. Formation of S-cells is a natural adaptation in filamentous actinomycetes**. (**A**) Microscopic analysis of strains grown for 7 days in liquid medium containing high levels of osmolytes. Cells were stained with FM5-95 and SYTO-9 to visualize membranes and DNA, respectively. Arrowheads indicate S-cells produced by the different strains. (**B**) Phylogenetic tree of filamentous actinomycetes based on the 16S rDNA gene. Strains with the ability to form S-cells are indicated with an asterisk (*). Scale bars represents 10 µm.

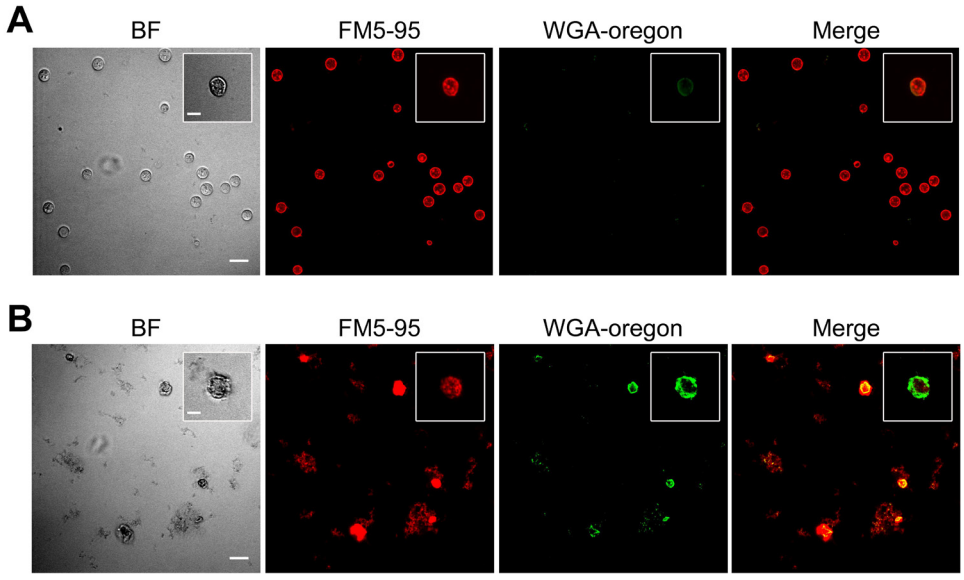


**Supplementary Figure 5. Peptidoglycan surrounding S-cells confers resistance to water treatment**. (**A**) Filtered S-cells were stained with the membrane dye FM5-95 and WGA-Oregon to stain peptidoglycan. The inlay shows an S-cell possessing abundant cell wall material surrounding the cell surface. (**B**) Morphology of S-cells after exposing them to water. While many cells lyse, some S-cells remain intact, which invariably have abundant cell wall material associated with their cell surface (see inlay). Scale bars represents 10 µm, and 5 µm for the inlays.

**Supplementary Table 1**. Image analysis measurements on hyphae formed in the presence of low levels of osmolytes. SD represents the standard deviation. See Fig. S1 for details on the analysis.

| Hypha | Length (µm) | Number of branches | Branching frequency[a] | Membrane fraction[b] | Average nucleoid area[c] (µm$^2$) |
|---|---|---|---|---|---|
| 1 | 86,0180 | 1 | 0,01 | 0,10 | 2,53 |
| 2 | 90,377 | 3 | 0,03 | 0,09 | 2,01 |
| 3 | 72,3597 | 7 | 0,10 | 0,10 | 1,90 |
| 4 | 83,9838 | 0 | 0,00 | 0,10 | 3,02 |
| 5 | 79,0436 | 0 | 0,00 | 0,09 | 3,21 |
| 6 | 65,3853 | 1 | 0,02 | 0,17 | 4,18 |
| 7 | 80,7872 | 7 | 0,09 | 0,07 | 2,11 |
| 8 | 86,3086 | 2 | 0,02 | 0,10 | 3,05 |
| 9 | 76,4282 | 3 | 0,04 | 0,08 | 2,14 |
| 10 | 74,1033 | 2 | 0,03 | 0,12 | 1,71 |
| Average | 79,4795 | 2,6 | 0,03 | 0,10 | 2,59 |
| SD | 7,5857 | 2,5 | 0,03 | 0,03 | 0,77 |

**Supplementary Table 2.** Image analysis measurements on hyphae formed in the presence of high levels of osmolytes. SD represents the standard deviation. See Fig. S1 for details on the analysis.

| Hypha | Length (µm) | Number of branches | Branching frequency[a] | Membrane fraction[b] | Average nucleoid area[c] (µm$^2$) |
|---|---|---|---|---|---|
| 1 | 82,5308 | 11 | 0,13 | 0,22 | 1,35 |
| 2 | 90,9580 | 6 | 0,07 | 0,18 | 2,10 |
| 3 | 88,3428 | 8 | 0,09 | 0,16 | 1,82 |
| 4 | 60,4451 | 12 | 0,20 | 0,29 | 1,86 |
| 5 | 86,0180 | 9 | 0,10 | 0,24 | 2,08 |
| 6 | 76,7188 | 6 | 0,08 | 0,21 | 2,05 |
| 7 | 88,6334 | 6 | 0,07 | 0,22 | 2,34 |
| 8 | 53,4707 | 8 | 0,15 | 0,19 | 1,47 |
| 9 | 69,1631 | 7 | 0,10 | 0,20 | 2,04 |
| 10 | 70,3255 | 2 | 0,03 | 0,21 | 1,15 |
| Average | 76,6606 | 7,5 | 0,10 | 0,21 | 1,83 |
| SD | 12,9242 | 2,8 | 0,05 | 0,03 | 0,38 |

[a] Branching frequency is the number of branches divided by the length of the hypha.
[b] Membrane fraction is the sum of the membrane surface area divided by the total area occupied by the hypha.
[c] Average nucleoid area represents the mean area of all the nucleoids present in the hypha.

**Supplementary Table 3**. Calculated diameters (D) of S-cells released by different filamentous actinomycetes upon hyperosmotic stress. The diameters are indicated in µm.

| Strain | $D_{min}$ | $D_{max}$ | $D_{mean}$ | SD |
|---|---|---|---|---|
| *K. viridifaciens* | 7,77 | 10,04 | 8,91 | 1,60 |
| *S. venezuelae* | 2,06 | 3,68 | 2,87 | 1,15 |
| MBT13 | 2,62 | 4,49 | 3,56 | 1,32 |
| MBT61 | 3,84 | 10,67 | 7,25 | 4,82 |
| MBT63 | 2,52 | 5,21 | 3,86 | 1,91 |
| MBT64 | 2,12 | 4,99 | 3,55 | 2,03 |
| MBT66 | 2,56 | 6,78 | 4,67 | 2,99 |
| MBT69 | 3,87 | 6,27 | 5,07 | 1,70 |
| MBT89 | 2,01 | 6,05 | 4,03 | 2,86 |

**Supplementary Table 4**. Mutations in the hyperosmotic stress-induced L-form strain M1

| Variation | Position | Type | Ref | Allele | Locus | Protein | Effect in protein |
|---|---|---|---|---|---|---|---|
| 1 | 4456932 | SNV | C | G | BOQ63_RS28320 | Acetyl-transferase | L99V |
| 2 | 4876534 | SNV | T | C | BOQ63_RS30295 | Valine-tRNA ligase | V319A |
| 3 | 3219590 | SNV | C | G | NCR | | |
| 4 | 3133612 | SNV | G | A | BOQ63_RS21920 | Metal ABC transporter ATPase | D504N |

SNV: Single Nucleotide Variation, Ref: Reference, L: Leucine, V: Valine, A: Alanine, D: Aspartic Acid, N: Asparagine

**Supplementary Table 5**. Mutations in the hyperosmotic stress-induced L-form strain M2

| Variation | Position | Type | Ref | Allele | Locus | Protein | Effect in protein |
|---|---|---|---|---|---|---|---|
| 1 | 2164717 | SNV | A | G | NCR | - | - |
| 2 | 5054842 | SNV | T | G | BOQ63_RS31145 | XRE family transcriptional regulator | Q332A |
| 3 | 6460621-6460623 | Del | CCA | - | BOQ63_RS37840 | Histidine kinase | T606Del |
| 4 | 3133753^3133754 | Ins | - | C | BOQ63_RS21920 | Metal ABC transporter ATPase | R553fs |

SNV: Single Nucleotide Variation, Del: Deletion, Ins: Insertion, Ref: Reference, Q: Glutamine, A: Alanine, T: Threonine, R: Arginine, fs: frame shift

**Supplementary Table 6.** Mutations in the penicillin-induced L-form

| Variation | Position | Type | Ref | Allele | Locus | Protein | Effect in protein |
|---|---|---|---|---|---|---|---|
| 1 | 546832 | SNV | C | A | NCR | - | - |
| 2 | 3549271 | SNV | G | A | BOQ63_RS23890 | LysX-like protein | T203I |
| 3 | 3297354 | SNV | C | A | BOQ63_RS22750 | UppP | L58M |

SNV: Single Nucleotide Variation, Ref: Reference, LysX: Lysylphosphatidyl-glycerol synthetase, UppP: Undecaprenyl-diphosphate phosophatase, T: Threonine, I: Isoleucine, L: Leucine, M: Methionine

**Supplementary Table 7**. Strains used in this study

| Strains | Genotype | Reference |
|---|---|---|
| ***Streptomyces/Kitasatospora* strains** | | |
| *Streptomyces coelicolor* A3(2) M145 | Wild-type | Lab collection |
| *Streptomyces lividans* 1326 | Wild-type | Lab collection |
| *Streptomyces griseus* | Wild-type | Lab collection |
| *Streptomyces venezuelae* DIVERSA | Wild-type | Lab collection |
| *Kitasatospora viridifaciens* DSM40239 | Wild-type | DSMZ[210] |
| *K. viridifaciens* Δ*ssgB* | DSM40239 *ssgB::apra* | This work |
| *Streptomyces sp.* MBT13 | Wild-type | Lab collection[209] |
| *Streptomyces sp.* MBT61 | Wild-type | Lab collection[209] |
| *Kitasatospora sp.* MBT63 | Wild-type | Lab collection[176] |
| *Kitasatospora sp.* MBT64 | Wild-type | Lab collection[209] |
| *Kitasatospora sp.* MBT66 | Wild-type | Lab collection[176] |
| *Kitasatospora sp.* MBT69 | Wild-type | Lab collection[209] |
| *Streptomyces sp.* MBT86 | Wild-type | Lab collection[209] |
| ***K. viridifaciens* cell wall-deficient strains** | | |
| Penicillin-induced L-form | Mutant | This work |
| Hyperosmotic stress-induced L-form M1 | Mutant | This work |
| Hyperosmotic stress-induced L-form M2 | Mutant | This work |

**Supplementary Table 8**. Primers used in this study

| Primer | Sequence |
|---|---|
| Consensus_*ssgB*-Fw | ATGAACACCACGGTCAGCTG |
| Consensus_*ssgB*-Rv | GCTCTCGGCCAGGATGTG |
| P1-*ssgB*-FW | GACGAATTCAGGCGTCAGAAACGGGTATC |
| P2-*ssgB*-RV | GAAGTTATCCATCACCTCTAGAGCTGACCGTGGTGTTCATAAGC |
| P3-*ssgB*-FW | GAAGTTATCGCGCATCTCTAGACTGAGCTCTCCGGAAGGAGAA |
| P4-*ssgB*-RV | GACAAGCTTTCTACCTGACCGGGCTGTT |
| qPCR_*infB*-Fw | GTCACGTCGACCACGGTAAG |
| qPCR_*infB*-Rv | CACCGATGTGCTGGGTGATG |
| qPCR_*atpD*-Fw | TTCGGACAGCTCGTCCATAC |
| qPCR_*atpD*-Rv | ACATCGCGCAGAACCACTAC |
| qPCR_*parA*-Fw | CGGTCGTCACCCAGTACAAG |
| qPCR-*parA*-Rv | TAACCGAGTTCGAGGGACAG |
| qPCR-*orf1*-Fw | GAGGGAGCCAATCCCGTATC |
| qPCR-*orf1*-Rv | GGCTGTTGGACAGGACCATC |
| qPCR-*allC*-Fw | CGGCGATAGCGGAGACTAAG |
| qPCR-*allC*-Rv | CCACTGGTGGGACCAGAAAG |
| qPCR-*tetR*-Fw | TGCTCGACCAGCTGTTGAAG |
| qPCR-*tetR*-Rv | TGGCGAGCATGAAGTCGTAG |
| BOQ63_RS28320-Fw | CTAGGTCGAAGGACCGATGG |
| BOQ63_RS28320-Rv | CGGACGTGACGCTCTACAAC |
| Seq_RS28320-Rv | GAAATCGGCCAGCGGGTAAG |
| Seq_RS30295-Fw | CTTCAAGCGCCTGTTCGACG |
| Seq_RS30295-Rv | TGTCGACCCAGTCGAAGTAG |
| Seq_NCR-M1-Fw | CGTTGCGGATGTGGTTCTTG |
| Seq_NCR-M1-Rv | GTTCGCTGGCCGAGATGTTC |
| Seq_RS21920-Fw | TGATCGAGGCGATGCCCTTC |
| Seq_RS21920-Rv | CGTTCGATGTTGCCGATCAC |
| Seq_NCR-M2-Fw | AGAGCAGCATGCCGAGCTTG |
| Seq_NCR-M2-Rv | CTTCCTTGGTCGGGAAGTAG |
| Seq_RS31145-Fw | GTGGTGAATCCGTGCCACAG |
| Seq_RS31145-Rv | TGGAACGCCTACTCCATGGG |
| Seq_RS37840-Fw | GATCTCCACGCCGTTGAAAG |
| Seq_RS37840-Rv | GAGTTCGGTGGTTTCGAAGG |
| Seq_NCR-L-form-Fw | GTGGCTCATTCAGGACTCTC |
| Seq_NCR-L-form-Rv | CGCCGCTTCATCTCTGATAC |
| Seq_RS23890-Fw | GAGAAGATCACCGCCTTGTC |
| Seq_RS23890-Rv | ACAGGCACCCGCTCAACTAC |
| Seq_RS22750-Fw | CCGGTGACACCCGGAAATAC |
| Seq_RS22750-Rv | CCGGGATGGTGGAGATGATG |

# Chapter 4
# Exploitation of a shape-shifting *Kitasatospora viridifaciens* strain identifies a MurG-like protein required for peptidoglycan synthesis

K. Ramijan, L. Zhang, V.J. Carrión, L.T van der Aart, J. Willemse, G.P. van Wezel, and D. Claessen.



## Abstract

Bacteria are enveloped by a cell wall structure that provides cellular protection. Despite this critical role, some bacteria are able to shed their wall when exposed to environmental challenges, thereby adopting a cell wall-deficient state. We previously demonstrated that a mutant of the filamentous bacterium *Kitasatospora viridifaciens*, which was designated *alpha*, has the attractive ability to switch between the wall-deficient and filamentous mode-of-growth. Here we show that the *alpha* strain can produce a wild-type cell wall without the canonical MurG, the enzyme that produces the essential cell wall precursor Lipid II. This led to the discovery of a new enzyme, called MurG2, which shares only 29% sequence identity to MurG and which can functionally replace its activity. In the absence of both *murG* and *murG2*, *alpha* cannot switch back to the walled state. Notably, MurG2 occurs in 38% of all *Streptomyces* and *Kitasatospora* strains. These findings highlight MurG2 as a novel and widespread cell-wall biosynthetic enzyme that facilitates switching of cell wall-deficient cells to their walled state.

Manuscript in preparation

## Introduction

Bacteria are surrounded by a cell wall, which is a highly dynamic structure that provides cellular protection and dictates cell shape. A major component of the cell wall is peptidoglycan (PG), which is widely conserved in the bacterial domain. Its biosynthesis has been studied for many decades, reinforced by the notion that many successful antibiotics target important steps in this pathway. The first steps of the PG synthesis pathway occur in the cytoplasm, where the peptidoglycan precursor UDP-MurNAc-pentapeptide is synthesized by the consecutive activity of a number of Mur enzymes (MurA-F)[223]. Next, this pentapeptide precursor is linked to undecaprenyl phosphate (or bactoprenol) residing in the plasma membrane by MurX (or MraY), yielding lipid I. MurG then adds the sugar nucleotide UDP-GlcNAc to lipid I to form lipidII, which is the complete PG subunit that is flipped to the external side of the membrane. Among the candidates to mediate this flipping, FtsW, MurJ and AmJ have been proposed[99,101,102]. Following flipping to the exterior of the cell, the PG subunit is then used to synthesize glycan strands by the activity of transglycosylases, after which these strands are cross-linked using transpeptidases[89,106,107,224].

Several genes required for the biosynthesis of PG are located in the so-called *dcw* gene cluster (for division and cell wall synthesis[225,226] (see Fig. S1). The content and organization of the *dcw* cluster is conserved among species with similar morphologies, indicating a putative role in bacterial cell shape[227]. Some genes in this cluster have gained species-specific functions or have been lost during evolution. Perhaps one of the clearest examples is DivIVA: in *Bacillus subtilis*, this protein is involved in division-site localization by preventing accumulation of the cell division initiator protein FtsZ[228], while DivIVA in actinomycetes is required for cell wall synthesis[78,82,161]. As a consequence, *divIVA* is dispensable in *B. subtilis* but essential in actinomycetes[78,81]. Conversely, *ftsZ* is essential in *B. subtilis*, but is obsolete for normal growth of actinomycetes[29,30].

Despite its important role for the cell's survival, we recently described how certain filamentous actinomycetes are able to release cell wall-deficient cells, called S-cells, in hyperosmotic stress conditions[194]. These S-cells are only transiently wall-deficient and are able to switch to the mycelial mode-of-growth. In some cases, however, prolonged exposure to high levels of osmolytes can lead to the emergence of mutants that are able to proliferate in the wall-deficient state as so-called L-forms[194]. Like S-cells, these L-forms retain the ability to construct functional peptidoglycan based on the observation that removal of the osmolytes from the medium led to the formation of mycelial colonies. L-forms can also be generated in most other bacteria by exposing cells to compounds that target the process of cell wall synthesis[139,208]. Strikingly,

such wall-deficient cells that are able to propagate without the FtsZ-based cell division machinery[139,140,148,229]. Even though the procedures used to generate L-forms can markedly differ, their mode-of-proliferation is conserved across species and largely based on biophysical principles. An imbalance in the cell surface area to volume ratio in cells that increase in size causes strong deformations of the cell membrane, followed by the release of progeny cells by blebbing, tubulation and vesiculation[141,194]. Given that lipid vesicle without any content are able to proliferate in a similar manner to that observed for L-forms, it led to the hypothesis that this mode of proliferation may be comparable to that used by early life forms that existed before the cell wall had evolved[137,230].

Here, we exploit the unique properties of a *Kitasatospora viridifaciens* L-form strain that readily switches between a wall-deficient and filamentous mode-of-growth to discover a novel MurG-like enzyme that is important for building the PG-based cell wall. We find that the switch to the filamentous mode-of-growth is possible in the absence of the highly conserved MurG protein, whose activity is then taken over by the newly identified protein MurG2. Crucially, the absence of MurG2 and MurG abolishes switching to the filamentous mode-of-growth, which highlights MurG2 as an important cell-wall biosynthetic enzyme with the ability to make lipidII in the absence of MurG.

## Results

### Morphological transitions of the shape-shifting strain *alpha*

We recently generated a *K. viridifaciens* L-form lineage by exposing the parental wild-type strain to high levels of penicillin and lysozyme. This strain, designated *alpha*, proliferates indefinitely in the cell wall-deficient state in media containing high levels of osmolytes (Supplementary Table 1). On solid LPMA medium, *alpha* forms green-pigmented viscous colonies, which exclusively contain L-form cells (Fig. 1A). In contrast, the parental strain forms compact and yellowish colonies composed of mycelia and S-cells on LPMA medium (Fig. 1B). Likewise, in liquid LPB medium *alpha* exclusively proliferates in the wall-deficient state, in a manner that is morphologically similar to that described for other L-forms[139,140,146]; (Extended Data Video S1; Fig. 1C). Following strong deformations of the mother cell membrane (see panels of 56, 150, and 200 mins in Fig. 1C); small progeny cells are released after approximately 300 mins. The mother cell, from which the progeny was released (indicated with an asterisk) lysed after 580 minutes. Characterization using transmission electron microscopy (TEM) confirmed that *alpha* possessed no PG-based cell wall when grown on media containing high levels of osmolytes (Fig. 1D). Notably, when *alpha* is plated on MYM medium (lacking high levels of osmolytes) the strain is able to switch to the mycelial mode-of-growth (Fig. 1E). However, unlike the wild-type

strain (Fig. 1F); the mycelial colonies of *alpha* fail to develop aerial hyphae and spores (Fig. 1E). Subsequent transfer of mycelia to LPMA plates stopped filamentous growth and reinitiated wall-deficient growth, during which L-form cells are extruded from stalled hyphal tips (Extended Data Video S2; Fig. 1G). Given the ability of these wall-deficient cells to proliferate, they eventually dominated the culture (not shown). Taken together, these results demonstrate that *alpha* has the ability to switch between a walled and wall-deficient state.



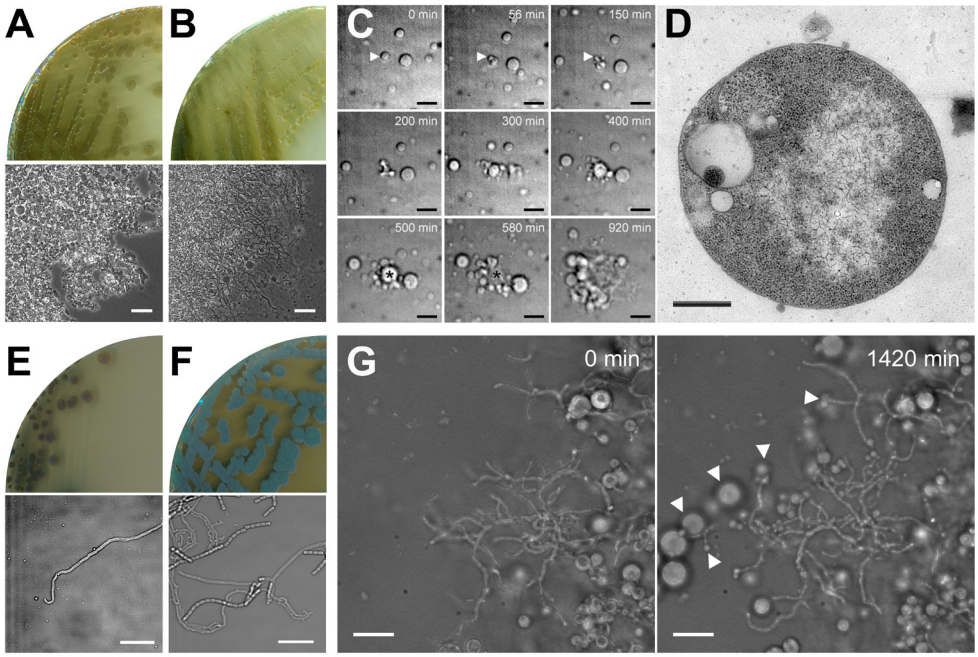


**Figure 1. Morphological transitions of the shape-shifting strain *alpha*.** (**A**) Growth of the *K. viridifaciens alpha* strain on LPMA medium yields green, mucoid colonies exclusively consisting of L-form cells, unlike the wild-type strain that forms yellowish colonies consisting of mycelia and S-cells (**B**). (**C**) Time-lapse microscopy stills of *alpha* proliferating in the wall-deficient state in liquid LPB medium. The arrowhead shows the mother cell, which generates progeny and lyses after 580 min (marked with an asterisk). Stills were taken from Supplementary Movie 1. (**D**) Transmission electron microscopy of a wall-deficient cell of *alpha*. (**E**) Growth of *alpha* on solid MYM medium yields compact, non-sporulating colonies unlike the wild-type strain that forms grey-pigmented sporulating colonies (**F**). (**G**) Time-lapse microscopy stills of mycelium of *alpha* transferred to LPMA medium, which show the extrusion of L-forms by filaments (see arrowheads). Stills were taken from Supplementary Movie 2. Scale bars represent 20 µm (**A**, **B**), 10 µm (**C**, **E**, and **F**) and 500 nm (**D**).

**Deletion of *divIVA* abolishes switching of *alpha* from the wall-deficient to the filamentous mode-of-growth**

We reasoned that the ability of *alpha* to efficiently switch between the walled and wall-deficient state would provide us with a platform to delete genes essential for either mode-of-growth. As a proof of concept, we focused on *divIVA*, which is essential for polar growth in filamentous actinomycetes[78]. In Actinobacteria, *divIVA* is located adjacent to the conserved *dcw* gene cluster (Fig. S1). *divIVA* is present in Gram-positive rod-shaped (*Mycobacterium*, *Corynebacterium*, *Bacillus*), filamentous (*Streptomyces* and *Kitasatospora*) and coccoid (*Staphylococcus* and *Streptococcus*) bacteria, but absent in Gram-negatives such as *Escherichia coli*. In *B. subtilis* and *Staphylococcus aureus*, the DivIVA proteins are only 29% (BSU15420) and 26% (SAOUHSC_01158) identical to the DivIVA from *S. coelicolor*.

To characterize the role of DivIVA in *K. viridifaciens*, we first studied its localization in *alpha* grown in the filamentous state. To this end, we created the pKR2 plasmid that constitutively expresses a C-terminal *eGFP* fusion to DivIVA (Supplementary Table 2). Microscopy analysis revealed that the fusion protein localized to hyphal tips (see arrowheads in Fig. S2A), consistent with earlier findings in streptomycetes[78,231]. When *alpha* was grown in the wall-deficient state in LPB medium, typically one or two foci of DivIVA-*eGFP* were detected per cell (Fig. S2B), which invariably were localized to the membrane. In contrast, no foci were detected in L-form cells containing the empty plasmid (pKR1) or those expressing cytosolic *eGFP* (pGreen[232]). We then constructed the plasmids pKR3 to delete *divIVA* and pKR4 to delete a large part of the *dcw* gene cluster, including *divIVA* (Supplementary Table 2). Introduction of these plasmids into *alpha* by PEG-mediated transformation and a subsequent screening yielded the desired *divIVA* and *dcw* mutants (Fig. S3). Analysis of growth in LPB medium or on solid LPMA plates indicated that the L-form cells proliferated normally in the absence of *divIVA* or part of the *dcw* gene cluster (Fig. 2A, B). However, when L-form cells were plated on MYM medium (lacking osmoprotectants), only the *alpha* strain was able to switch to the mycelial mode-of-growth (Fig. 2B). Introduction of plasmid pKR6, which expresses *divIVA* from the constitutive *gap1* promoter, complemented growth of the *divIVA* mutant on MYM medium (Fig. 2B). In agreement, Western blot analysis using antibodies against DivIVA of *Corynebacterium glutamicum* confirmed the absence of DivIVA in both the *divIVA* and the *dcw* mutant, and also showed the expression was restored in the *divIVA* mutant complemented with pKR6 (Fig. 2C).

To analyse if the switch from the wall-deficient to the walled state in the absence of DivIVA was blocked due to the failure to produce the cytosolic precursors required for peptidoglycan synthesis in the L-form state, we performed a comparative LC-MS analysis (Fig. 2D). We noticed that the LC-MS profiles of the *divIVA* and *dcw* mutant strains were

similar to that of *alpha* with respect to the cytosolic PG building blocks (Fig. 2D). Importantly, MS-MS analysis identified the last cytosolic precursor in the PG biosynthesis pathway, UDP-MurNAc-pentapetide (Mw = 1194.35), in all strains (Fig. 2E). Taken together, these results demonstrate that DivIVA is essential for filamentous growth but not required for synthesis of the cytosolic PG precursors.



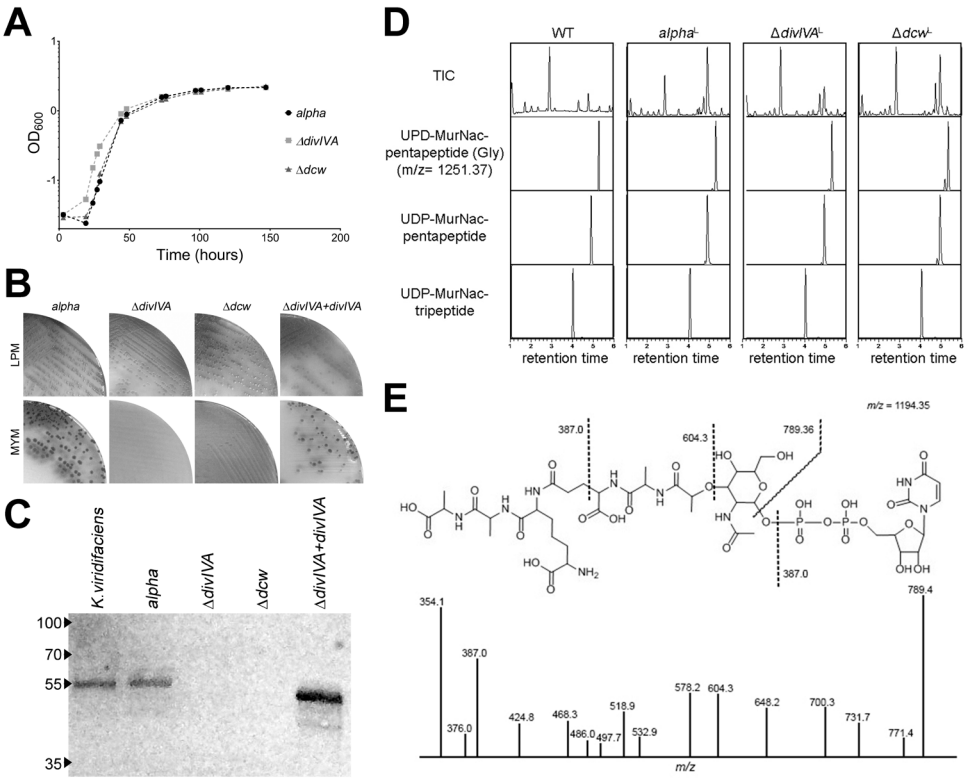


**Figure 2. The absence of DivIVA abolishes switching of *alpha* from the wall-deficient to the filamentous mode-of-growth**. (**A**) Growth curves of *alpha* (black circles), the Δ*divIVA* mutant (grey squares) and the Δ*dcw* mutant (black triangles) in liquid LPB medium. (**B**) While all strains grow on LPMA medium, those lacking *divIVA* are unable to switch to the mycelial mode-of-growth on MYM medium lacking osmoprotectants. (**C**) Western blot analysis using antibodies against the *C. glutamicum* DivIVA protein confirm the absence of DivIVA in the constructed Δ*divIVA* and Δ*dcw* mu-

tants. Reintroduction of *divIVA* under control of the *gap1* promoter restores the expression of DivIVA in the *divIVA* mutant and the ability to form mycelial colonies (see panel **B**). (**D**) Comparative LC-MS analysis of peptidoglycan precursors in *alpha* and the derivative Δ*divIVA* and Δ*dcw* mutants. Similar to the wild-type, all strains produce peptidoglycan precursors including UDP-MurNAc-pentapeptide, which is the last cytosolic precursor in the PG biosynthesis pathway. (**E**) MS-MS analysis demonstrating that the product with a mass of 1194.35 is the precursor UDP-MurNAc-pentapeptide.



The unique capacity of *alpha* to switch back-and-forth between a walled, filamentous mode-of-growth and a wall-less L-form state provided a unique platform to apply an engineering approach to cell morphology design. As a first step towards that goal, we introduced the *dcw* gene cluster from *S. coelicolor* (pKR7) into the *K. viridifaciens dcw* mutant (Fig. 3A). Introduction of this gene cluster restored filamentous growth and reversible metamorphosis (Fig. 3B), demonstrating that DivIVA from *S. coelicolor* ($DivIVA_{SCO}$) can substitute for the function of DivIVA from *K. viridifaciens* ($DivIVA_{KVI}$). Western Blot analysis confirmed the presence of $DivIVA_{SCO}$ protein in the complemented strain, which has a molecular size of 41 kDa as opposed to the 46 kDa for the DivIVA of *K. viridifaciens*. We investigated this size difference *in silico*, and observed that both DivIVA proteins were 70% identical (Fig. S4A). Further inspection of the sequences with SMART (Simple Modular Architecture Research Tool[233]) revealed that the overall architecture of the DivIVA proteins was comparable. Both the *S. coelicolor* and *K. viridifaciens* DivIVA proteins contain a conserved DivIVA domain (grey box), as well as a coiled-coil region and several low complexity domains (pink rectangles, Fig. S4B). The number of low complexity domains largely explains the size difference between $DivIVA_{SCO}$ and $DivIVA_{KVI}$, as the *S. coelicolor* protein lacks two of these domains (see asterisks Fig. S4A and B). Altogether, our data indicate that the ability of *K. viridifaciens* to switch between morphologies is not dictated by specific adaptation in this organism of genes within its *dcw* cluster. These results demonstrate that the mycelium formed by this 'hybrid' bacterium is established by the activity of the macromolecular machinery of two different bacteria belonging to separate genera. This paves the way for extending this principle with *dcw* gene clusters of morphologically distinct bacteria, such as the unicellular actinobacteria *Corynebacterium glutamicum* and *Mycobacterium tuberculosis*.

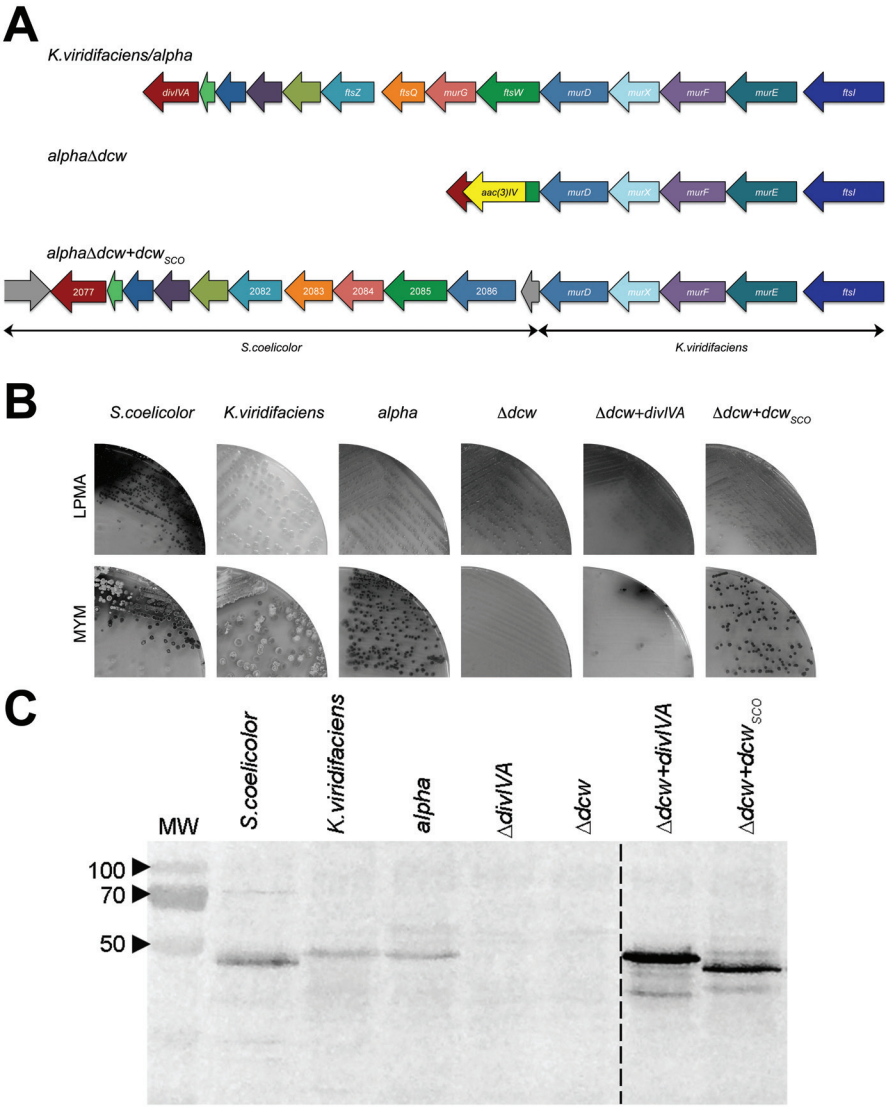


**Figure 3. Orthologous complementation of the *dcw* mutant**. (**A**) Illustration of the *dcw* clusters in *K. viridifaciens alpha*, the Δ*dcw*::*acc(3)IV* mutant, and the Δ*dcw* mutant complemented with the *dcw* cluster from *S. coelicolor*. (**B**) Introduction of the *S. coelicolor dcw* cluster or $divIVA_{KVI}$ restores filamentous growth. (**C**) Western blot analysis showing the presence of DivIVA in the complemented *dcw* mutants. Please note the size difference of the DivIVA proteins between *S. coelicolor* and *K. viridifaciens*.

### Identification of a distant MurG paralogue as a novel lipid II synthase

When we introduced *divIVA* (expressed from the constitutive *gap1* promoter) in the Δ*dcw* mutant, we found that the complemented strain was surprisingly also able to switch to the walled mode-of-growth on solid media lacking osmoprotectants (Fig. 4). The colonies, however, were heterogeneous in appearance and small in size compared to the mycelial colonies formed by *alpha* (Fig. 4A). The complemented Δ*dcw* mutant was not able to grow as filaments in liquid-grown cultures (data not shown).

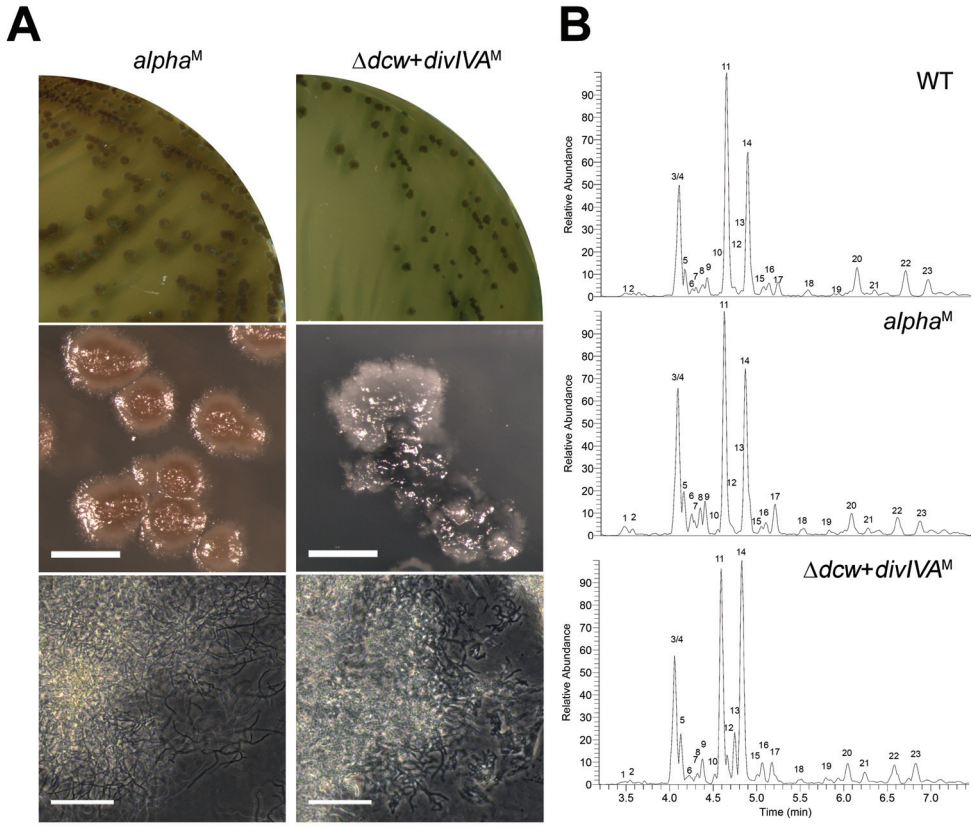


**Figure 4. Reintroduction of DivIVA is sufficient to restore filamentous growth of the Δ*dcw* mutant.** (**A**) Morphological comparison between *alpha* (left) and the *dcw* mutant complemented with $P_{gap1}$-*divIVA* (right) grown on MYM medium. Unlike *alpha*, the complemented *dcw* mutant forms colonies with a heterogeneous appearance. (**B**) Peptidoglycan architecture analysis of mycelium of the wild-type strain (top), *alpha* (middle) and the complemented *dcw* mutant (bottom). The abundance of muropeptides is similar in all strains (see also Table 1). Scale bar represents 40 µm.

To verify that the complemented *dcw* mutant produced normal PG on solid medium, we performed a peptidoglycan architecture analysis (Fig. 4B). The LC-MS analysis revealed that all expected muropeptides were formed in the complemented *dcw* mutant and were comparable in abundance to those formed by *alpha* and the wild-type strain grown as mycelium (Fig. 4B; Table 1).



**Table 1.** Identified muropeptides present in *K. viridifaciens* strains grown as mycelium. The masses are indicated in Da

| Peak | Muropeptide | Retention time (min) | Observed Mass [M+H] | Calculated Mass | WT (%) | *Alpha* (%) | Δ*dcw*+ *divIVA* (%) |
|---|---|---|---|---|---|---|---|
| 1 | Tri (-Gly) | 3.46 | 870.39 | 869.38 | 0.69 | 1.95 | 0.48 |
| 2 | Di [deAc] | 3.54 | 656.30 | 655.29 | 0.48 | 0.10 | 0.59 |
| 3 | Di | 4.07 | 698.31 | 697.30 | 9.39 | 10.74 | 6.55 |
| 4 | Tri | 4.07 | 927.41 | 926.41 | 15.76 | 22.06 | 17.34 |
| 5 | Tetra [Gly4] | 4.13 | 984.44 | 983.43 | 3.03 | 5.16 | 5.45 |
| 6 | TriTri (-GM) | 4.23 | 1355.61 | 1354.60 | 1.16 | 1.67 | 0.47 |
| 7 | Tetra (-Gly) | 4.27 | 941.43 | 940.42 | 1.00 | 1.71 | 0.67 |
| 8 | Tri [Glu] | 4.34 | 928.40 | 927.39 | 1.59 | 0.42 | 1.57 |
| 9 | Penta [Gly5] | 4.38 | 1055.47 | 1054.47 | 21.87 | 4.02 | 2.98 |
| 10 | TetraTetra (-GM) [Gly4] | 4.52 | 1483.67 | 1462.66 | 1.32 | 2.47 | 3.45 |
| 11 | Tetra | 4.58 | 998.45 | 997.44 | 26.66 | 27.63 | 25.82 |
| 12 | TetraTri (-GM) | 4.66 | 1426.65 | 1425.64 | 14.12 | 18.68 | 19.13 |
| 13 | Unidentified peptide | 4.75 | 1055.50 | 1054.47 | 0.00 | 0.00 | 5.76 |
| 14 | Penta | 4.81 | 1069.49 | 1068.48 | 17.49 | 21.81 | 29.76 |
| 15 | TetraTri (-GM) [deAc/Gly4] | 5.01 | 1369.63 | 1368.62 | 6.09 | 5.96 | 5.99 |
| 16 | TetraTetra (-GM) | 5.06 | 1497.39 | 1496.38 | 6.41 | 6.35 | 9.82 |
| 17 | Penta [Glu] | 5.17 | 1070.47 | 1069.47 | 2.05 | 4.40 | 3.03 |
| 18 | TriTri | 5.52 | 1835.81 | 1834.81 | 5.12 | 5.59 | 3.75 |
| 19 | TetraTri [Glu] | 6.11 | 1906.84 | 1905.84 | 4.60 | 7.42 | 2.59 |
| 20 | TetraTri | 6.34 | 1907.83 | 1906.83 | 24.69 | 20.24 | 17.17 |
| 21 | TetraTetra [Glu] | 6.45 | 1977.87 | 1976.88 | 3.97 | 5.19 | 7.51 |
| 22 | TetraTetra | 6.67 | 1978.88 | 1977.86 | 20.50 | 15.85 | 15.20 |
| 23 | PentaTetra [Glu] | 6.94 | 2049.91 | 2048.90 | 12.03 | 10.57 | 14.93 |

monomers and dimers are treated as separate sets

These results demonstrate that filamentous growth of the complemented Δ*dcw* mutant was achieved, even though the strain lacked *murG* in the *dcw* gene cluster (see Fig. S1). This inevitably means that another protein is able to functionally replace the activity of MurG. Blast analysis of the amino acid sequence of $MurG_{SCO}$ (SCO2084) against the genome sequence of *K. viridifaciens* revealed that this actinomycete contains two additional, but distant MurG homologs (Supplementary Table 4). The two additional homologs (BOQ63_RS12640 and BOQ63_RS05415) showed 29 and 24% similarity to the MurG (BOQ63_RS32465) contained in the *dcw* cluster. Further investigation revealed that MurG proteins possess two characteristic domains: an N-terminal domain that contains the lipid I binding site (PF03033)[234], and a C-terminal domain that contains the UDP-GlcNac binding site (PF04101; Fig. S5), both of which are required for the UDP-N-acetyl-glucosamine transferase activity. Of the two distant MurG homologues, only BOQ63_RS12640 contained both domains (Fig. S5).

Remarkably, a broader search of MurG-like proteins in other *Streptomyces* and *Kitasatospora spp*. revealed that 38% of strains possess one, two and sometimes even three MurG-like proteins containing both the necessary N-terminal (PF03033) and C-terminal (PF04101) domains (Fig. 5), in addition to the canonical MurG, which is present in all strains. A sequence similarity network was produced by pairwise comparing the 1553 MurG and MurG-like proteins extracted from all *Streptomyces* and *Kitasatospora spp*., which showed that nearly all MurG proteins encoded in the *dcw* gene clusters grouped together (see pink nodes in Fig. S6).. However, the MurG-like proteins were clustering in many different groups (see green nodes in Fig. S6).

To corroborate that *murG* is not required for filamentous growth, we constructed plasmid pKR8 (Supplementary Table 2) and used this to inactivate *murG* in *alpha*. The genotype of the mutant obtained was verified by PCR (Fig. S7), and in agreement with the results described above, the absence of *murG* had no effect on L-form or filamentous growth (Fig. 6). Likewise, inactivation of *murG2* in *alpha* using construct pKR9 had no effect on L-form growth. In addition, the Δ*murG2* mutant was also able to switch to mycelial growth. However, when we deleted *murG2* in the Δ*murG* mutant, the ability to switch to the filamentous mode-of-growth was dramatically reduced (Fig. 6). Only at very high cell densities infrequent shifters were found (see circled colony in Fig. 6). This is consistent with the notion that we were unable to remove *murG2* in the Δ*murG* mutant completely, perhaps suggesting that low levels of lipid II are essential for these L-forms (see discussion). Nevertheless, our results show that MurG and MurG2 have overlapping activities, whereby MurG2 is able to functionally replace the lipid II synthesis ability of MurG.

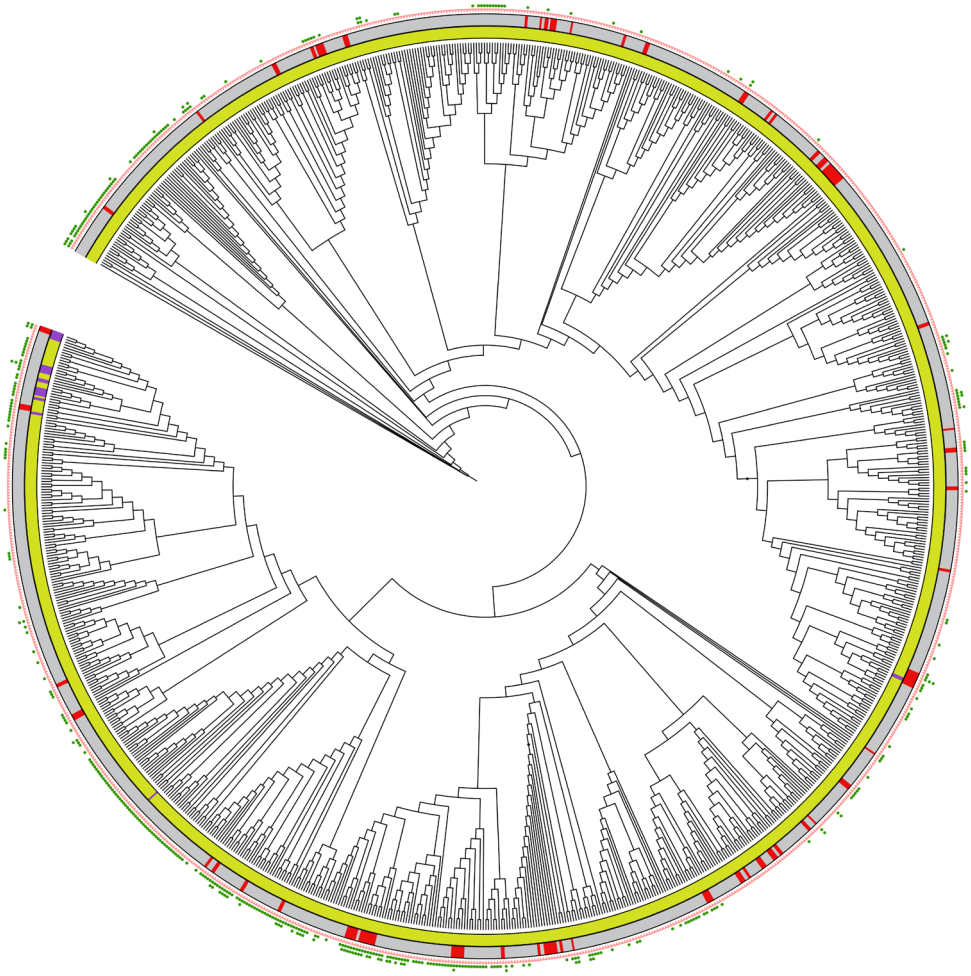

**Figure 5. Overview of MurG and MurG-like proteins present in *Streptomyces* and *Kitasatospora* species**. The phylogenetic tree was constructed on the basis of four conserved housekeeping proteins (AtpD, RecA, TrpB and GyrB). Yellow and purple colors in the inner circle represent *Streptomyces* and *Kitasatospora spp*. strains, respectively. Strains present in the NCBI database are indicated in grey in the middle circle, while those from an in-house collection are indicated in red. The pink triangles represent MurG proteins encoded in the *dcw* gene cluster. The green dots represent distant MurG proteins, whose genes are located elsewhere in the genomes. Phylogenetic trees were constructed using iTOL[235].

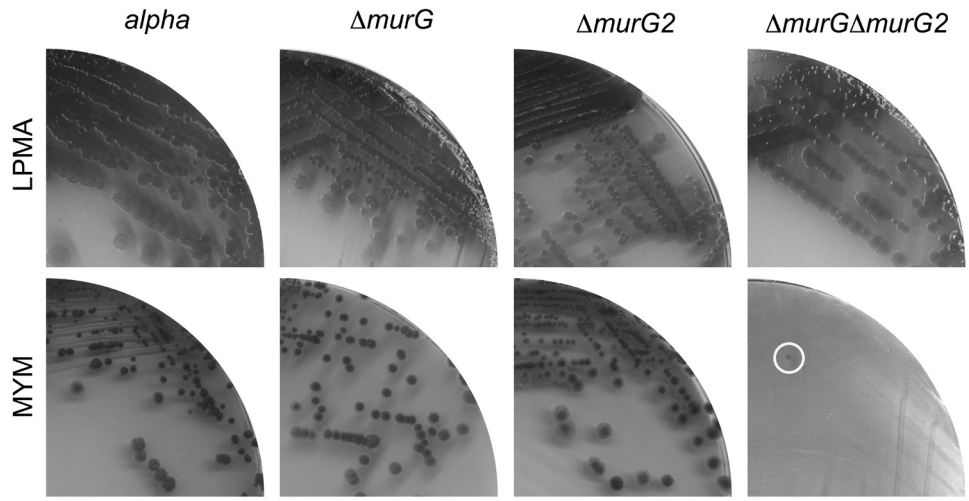


**Figure 6. MurG2 can functionally replace MurG in peptidoglycan synthesis**. Growth of *alpha*, the Δ*murG*, Δ*murG2* and the Δ*murG*Δ*murG2* double mutant as L-forms on LPMA medium (top). With the exception of the Δ*murG*Δ*murG2* double mutant, all strains are able to grow filamentous on MYM medium lacking osmolytes (bottom).

## Discussion

Filamentous actinomycetes are multicellular bacteria that form networks of interconnected hyphae. Furthermore, they have a complex life cycle during which sporulating aerial structures are established after a period of vegetative growth. Over the past decades, we have begun to understand how sporulating aerial hyphae are formed. For instance, previous work in *S. coelicolor* provided compelling evidence that the cell division proteins FtsW, FtsQ, FtsZ, YlmD, YlmE, and SepG are all required for proper sporulation[29,31-33,236,237]. These cell division proteins are encoded by genes located primarily in the conserved *dcw* gene cluster. Notably, none of these genes is essential for filamentous growth. Indeed, we here confirmed these findings by deleting all of these genes in the constructed *dcw* mutant of *K. viridifaciens*, by using a strain (*alpha*) with the ability to switch between a wall-deficient and filamentous mode-of-growth. The power of this strain is its use for identifying the requirements for cell wall synthesis in these filamentous actinomycetes. As a proof-of-concept,

we for the first time deleted the important cytoskeletal gene *divIVA* in a polar-growing bacterium. The absence of *divIVA* arrested growth in the wall-deficient state but had no effect on synthesis of the PG building blocks. This indicates that the block in PG formation is in a late step of the PG biosynthesis pathway. Given that DivIVA of polar-growing bacteria interacts with cell wall polymerases, we expect that the inability to grow filamentous is caused by the inability of cells to properly coordinate and localize PG synthesis.

We surprisingly found that filamentous growth was still possible when *divIVA* was re-introduced in the *dcw* mutant, despite the absence of *ftsW* and *murG*. FtsW is a SEDS protein family member, which were recently found to be cell wall polymerases[106,238]. FtsW is involved in cell division, which explains why this protein is not essential for growth filamentous actinomycetes. After all, cell division is dispensable for filamentous growth[9,29]. MurG on the other hand catalyzes the coupling of GlcNAc to lipid I, yielding the PG precursor lipid II. MurG is present in all bacteria and universally encoded in the *dcw* gene cluster. Analysis of the PG composition showed that normal PG was produced in the absence of the canonical *murG* gene. The ability to make a cell wall with an apparently normal architecture indicates that *K. viridifaciens* also has other enzymes capable of synthesizing lipid II in the absence of *murG*.

An *in silico* search in the genome of *K. viridifaciens* identified *murG2* (BOQ63_RS12640), which is a distant relative of MurG with the likely ability to replace the activity of the canonical MurG. This is based among others on the presence of the two domains that are known to be required for the transfer of GlcNAc to lipid I. Remarkably, many actinomycetes possess multiple proteins carrying these two domains, inferring that MurG2 proteins are common in these bacteria. In fact, some species even contained three MurG-like proteins, in addition to the canonical MurG encoded in the *dcw* gene cluster.

Notably, removing *murG2* in the Δ*murG* strain dramatically reduced the ability to switch to the filamentous mode-of-growth, whereas each of the single mutants switched as efficiently as the parental *alpha* strain. This provides evidence that MurG2 is a new protein involved in cell wall metabolism, which appears to facilitate switching from a wall-deficient to a walled life style. Interestingly, we have so far been unable to remove all *murG2* copies in the *murG* mutant, even after repetitive attempts. L-forms are multinucleated cells, and it appears that mutant cells retain at least some *murG2* genes in the population. This suggests that low levels of lipid II are required for these L-forms. Consistent with this idea is the finding that antibiotics that target lipid II, such as vancomycin, are still killing *alpha* efficiently (our unpublished data).

We hypothesize that this lethality is caused by depletion of the lipid carrier undecaprenyl diphosphate, which is also used in other pathways and which may be essential for L-forms. We are currently investigating this in more detail.



## Methods

### Strains and media

Bacterial strains used in this study are shown in Supplementary Table 1. To obtain sporulating cultures of *K. viridifaciens* and *S. coelicolor*, strains were grown at 30°C for 4 days on MYM medium[195]. For general cloning purposes, *E. coli* strains DH5α and JM109 were used, while *E. coli* ET12567 and SCS110 were used to obtain unmethylated DNA. *E. coli* strains were grown at 37 °C in LB medium, supplemented with chloramphenicol (25 μg·ml$^{-1}$), ampicillin (100 μg·ml$^{-1}$), apramycin (50 μg·ml$^{-1}$), kanamycin (50 μg·ml$^{-1}$), or viomycin (30 μg·ml$^{-1}$), where necessary.

To support growth of wall-deficient cells, strains were grown in liquid LPB medium while shaking at 100 rpm, or on solid LPMA medium at 30°C[194]. To switch from the wall-deficient to the filamentous mode-of-growth, L-form colonies grown on LPMA for seven days were streaked on MYM medium. If needed, mycelial colonies of switched strains were transferred after 4 days to liquid TSBS medium and grown for two days at 30°C, while shaking at 200 rpm.

### Construction of plasmids

All plasmids and primers used in this work are shown in Supplementary Tables 2 and 3, respectively.

*Construction of the DivIVA localization construct pKR2*

To localize DivIVA, we first created plasmid pKR1 containing a viomycin resistance cassette cloned into the unique NheI site of pIJ8630[239]. To this end, the viomycin resistance cassette was amplified from pIJ780[240] with the primers *vph*-FW-NheI and *vph*-RV-NheI. Next, we amplified the constitutive *gap1* promoter as a 450 bp fragment from the genome of *S. coelicolor* with the primers $P_{gap1}$-FW-BglII and $P_{gap1}$-RV-XbaI. We also amplified the *divIVA* coding sequence (the +1 to +1335 region relative to the start codon of *divIVA* (BOQ63_RS32500) from the chromosome of *K. viridifaciens* using primers *divIVA*-FW-XbaI and *divIVA*-Nostop-RV-NdeI. Finally, the promoter and *divIVA* coding sequence were cloned into pKR1 as a BglII/XbaI and XbaI/NdeI fragment respectively, yielding plasmid pKR2.

*Construction of the deletion constructs pKR3, pKR4, pKR8, pKR9 and pKR10*

The *divIVA* mutant was created in *K. viridifaciens* using pKR3, which is a derivative of the unstable plasmid pWHM3[221]. In the *divIVA* mutant, nucleotides +205 to +349 relative to the start codon of *diviVA* were replaced with the *loxP-apra* resistance cassette as described[222]. A similar strategy was used for the deletion of the partial *dcw* cluster (plasmid pKR4), and for the deletion of *murG* (plasmid pKR8) and *murG2* (plasmid pKR9). For the deletion of the partial *dcw* cluster, the chromosomal region from +487 bp relative to the start of the *ftsW* gene (BOQ63_RS32460) until +349 relative to the start of the *divIVA* gene were replaced with the apramycin resistance marker. For the deletion of *murG* (BOQ63_RS32465, located in the *dcw* cluster), the nucleotides +10 to +1077 bp relative to the start codon of *murG* were replaced with the *loxP-apra* resistance cassette, while for the *murG2* (BOQ63_RS12640) deletion the chromosomal region from +18 to +1105 bp relative to the start of *murG2* were replaced with the apramycin resistance marker. To construct the *murG*/*murG2* double mutant, pKR10 was created, replacing the apramycin resistance cassette in pKR8 by a viomycin resistance cassette. To this end, the viomycin resistance cassette was amplified from pIJ780[240] with the primers *vph*-Fw-EcoRI-HindIII-XbaI and *vph*-Rv-EcoRI-HindIII-XbaI. The viomycin resistance cassette contained on the PCR fragment was then cloned into pKR8 using XbaI, thereby replacing the apramycin cassette and yielding pKR10.

*Construction of the complementation constructs pKR6 and pKR7*

For complementation of *divIVA* under control of the strong *gap1* promoter[232], the constructs pKR6 was made. First, we created plasmid pKR5 with the strong *gap1* promoter. The promoter region of *gap1* (SCO1947) was amplified with the primers $P_{gap1}$-FW-BglII and $P_{gap1}$-RV-XbaI using *S. coelicolor* genomic DNA as the template. Next, the *gap1* promoter was cloned as BglII/XbaI fragment into the integrative vector pIJ8600[239] to generate the plasmid pKR5. Afterwards, the *divIVA* coding sequence was amplified from the genome of *K. viridifaciens* with the primers *divIVA*-XbaI-FW and *divIVA*-NdeI-RV. Finally, to create the plasmid pKR6 the XbaI/NdeI fragment containing the *divIVA* coding sequence was cloned in pKR5. For the orthologous complementation of the *dcw* mutant, the *S. coelicolor dcw* cluster contained on cosmid ST4A10[241] was used. The ST4A10 cosmid was cut with BglII and ScaI, followed by gel extraction of a 13,268 bp BglII fragment, encompassing the partial *S. coelicolor dcw* cluster. This fragment was subsequently ligated into BglII-digested pIJ8600[239], yielding pKR7.

### Transformation of L-forms

Transformation of *alpha* essentially followed the protocol for the rapid small-scale transformation of *Streptomyces* protoplasts[179], with the difference that 50 µl cells from a mid-exponential growing L-form culture were used instead of protoplasts. Typically, 1 µg DNA was used for each transformation. Transformants were selected by applying an overlay containing the required antibiotics in P-buffer after 20 hours. Further selection of transformants was done on LPMA medium supplemented with apramycin (50 µg·ml$^{-1}$), thiostrepton (5 µg·ml$^{-1}$), or viomycin (30 µg·ml$^{-1}$), when necessary. Transformants were verified by PCR (Supplementary Table 3).

### Microscopy

Strains grown in LPB or LPMA were imaged using a Zeiss Axio Lab A1 upright microscope equipped with an Axiocam Mrc. A thin layer of LPMA (without horse serum) was applied to the glass slides to immobilize the cells prior to the microscopic analysis.

*Fluorescence microscopy*

Fluorescence microscopy pictures were obtained with a Zeiss Axioscope A1 upright fluorescence microscope equipped with an Axiocam Mrc5 camera. Aliquots of 10 µl of live cells were immobilized on top of a thin layer of LPMA (without horse serum) prior to analysis. Fluorescent images were obtained using a 470/40 nm band pass excitation and a 505/560 band pass detection, using an 100x N.A. 1.3 objective. To obtain a sufficiently dark background, the background of the images was set to black. These corrections were made using Adobe Photoshop CS5.

*Time-lapse microscopy*

To visualize the proliferation of *alpha*, cells were collected and resuspended in 300 µl LPB (containing 4-22% sucrose) and placed in the wells of a chambered 8-well µ-slide (ibidi®). Cells were imaged on a Nikon Eclipse Ti-E inverted microscope equipped with a confocal spinning disk unit (CSU-X1) operated at 10,000 rpm (Yokogawa), using a 40x Plan Fluor Lens (Nikon) and illuminated in bright-field. Images were captured every 2 minutes for 10-15 hours by an Andor iXon Ultra 897 High Speed EM-CCD camera (Andor Technology). Z-stacks were acquired at 0.2-0.5 µm intervals using a NI-DAQ controlled Piezo element. During imaging wall-less cells were kept at 30°C using an INUG2E-TIZ stage top incubator (Tokai Hit).

*Electron microscopy*

For transmission electron microscopy, L-forms obtained from a 7-day-old liquid-grown *alpha* culture were trapped in agarose blocks prior to fixation with 1.5% glutaraldehyde and a post-fixation step with 1% $OsO_4$. Samples were embedded in Epon and sectioned into 70

nm slices. Samples were stained using uranyl-acetate (2%) and lead-citrate (0.4%), if necessary, before being imaged using a Jeol 1010 or a Fei 12 BioTwin transmission electron microscope.

### DivIVA detection using Western blot analysis

To detect DivIVA using Western blot analysis, the biomass of L-form strains was harvested after 7 days of growth in LPB medium, while biomass of mycelial strains was obtained from liquid-grown TSBS cultures after 17 hours. Cell pellets were washed twice with 10% PBS, after which they were resuspended in 50 mM HEPES pH 7.4, 50 mM NaCl, 0.5% Triton X-100, 1 mM PFMS and P8465 protease inhibitor cocktail (Sigma). The cells and mycelia were disrupted with a Bioruptor Plus Sonication Device (Diagenode). Complete lysis was verified by microscopy, after which the soluble cell lysate was separated from the insoluble debris by centrifugation at 13,000 rpm for 10 min at 4°C. The total protein concentration in the cell lysates was quantified by a BCA assay (Sigma-Aldrich). Equal amounts of total proteins were separated with SDS-PAGE using 12,5% gels. Proteins were transferred to polyvinylidene difluoride (PVDF) membranes (GE Healthcare) with the Mini Trans-Blot® Cell (Bio-Rad Laboratories) according to the manufacturer's instructions. DivIVA was detected using a 1:5,000 dilution of polyclonal antibodies raised against *Corynebacterium glutamicum* DivIVA (kindly provided by Professor Marc Bramkamp). The secondary antibody, anti-rabbit IgG conjugated to alkaline phosphatase (Sigma), was visualized with the BCIP/NBT Color Development Substrate (Promega).

### Isolation of cytoplasmic peptidoglycan precursors

For the cytoplasmic PG precursor isolation and identification we used a modification of the method previously described[242]. The *alpha* strain and the *divIVA* and *dcw* mutants were grown in LPB for seven days, while the wild-type *K. viridifaciens* strain was grown for three days in a modified version of LPB lacking sucrose. The cells were harvested by centrifugation at 4°C and washed in 0,9% NaCl. Cells were extracted with 5% cold trichloric acid (TCA) for 30 minutes at 4°C. The extracts were centrifuged at 13,000 rpm for 5 minutes at 4°C, after which the supernatants were desalted on a Sephadex G-25 column (Illustra NAP-10 Columns, GE Healthcare, Pittsburgh) and concentrated by rotary evaporation. The concentrated precursors were dissolved in 200 µl HPLC-grade water.

### Peptidoglycan extraction

The peptidoglycan architecture was analyzed as described[243]. Mycelia of the wild-type strain, *alpha* and the Δ*dcw* mutant complemented with *divIVA* were

grown on top of cellophane discs on modified LPMA medium lacking sucrose and horse serum. Following growth, the mycelial mass was removed from the cellophane, washed in 0.1M Tris-HCl pH 7.5 and lyophilized. 10 mg of the lyophilized biomass was used for PG isolation. Therefore, the biomass was boiled in 0.25% SDS in 0.1 M Tris/HCl pH 6.8, thoroughly washed, sonicated, and treated with DNase, RNase and trypsin. Inactivation of these enzymes was performed by boiling the samples followed by washing with water. Wall teichoic acids were removed with 1 M HCl[244]. PG was digested with mutanolysin and lysozyme. Muropeptides were reduced with sodium borohydride and the pH was adjusted to 3.5-4.5 with phosphoric acid.

### LC-MS analysis of PG precursors and muropeptides

The LC-MS setup consisted of a Waters Acquity UPLC system (Waters, Milford, MA, USA) and an LTQ Orbitrap XL Hybrid Ion Trap-Orbitrap Mass Spectrometer (Thermo Fisher Scientific, Waltham, MA, USA) equipped with an Ion Max electrospray source. Chromatographic separation of muropeptides and precursors was performed on an Acquity UPLC HSS T3 C18 column (1.8 µm, 100 Å, 2.1 × 100 mm). Mobile phase A consisted of 99.9% $H_2O$ and 0,1% formic acid, while mobile phase B consisted of 95% acetonitrile, 4.9% $H_2O$ and 0,1% formic acid. All solvents used were of LC-MS grade or better. The flow rate was set to 0.5 ml $min^{-1}$. The binary gradient program consisted of 1 min 98% A, 12 min from 98% A to 85% A, and 2 min from 85% A to 0% A. The column was then flushed for 3 min with 100% B, after which the gradient was set to 98% and the column was equilibrated for 8 min. The column temperature was set to 30°C and the injection volume used was 5 µL. The temperature of the autosampler tray was set to 8°C. Data was collected in the positive ESI mode with a scan range of m/z 500–2500 in high range mode. The resolution was set to 15.000 (at m/z 400).

### Sequence homology analysis of *dcw* gene clusters

The homology search of the different *dcw* clusters was done using MultiGeneBlast[245]. The query used for the search was the *dcw* cluster from *Streptomyces coelicolor* A3(2), for which the required sequences were obtained from the *Streptomyces* Annotation Sever (StrepDB). The homology search included the loci from SCO2077 (*divIVA*) until SCO2091 (*ftsL*). A database was constructed with genome assemblies obtained from NCBI. The analyzed species have the following accession numbers: NC_003888 (*S. coelicolor* A3(2), NZ_MPLE00000000.1 (*Kitasatospora viridifaciens* DSM40239), CP000480 (*Mycobacterium smegmatis* MC2 155), AL123456 (*Mycobacterium tuberculosis* H37Rv), CP014279 (*Corynebacterium*

*stationis* ATCC 6872), BX927147 (*Corynebacterium glutamicum* ATCC13032), AL009126 (*Bacillus subtilis* subsp.168), U00096 (*Escherichia coli* K-12), CP000253.1 (*Staphylococcus aureus* NTC8325), and AE007317 (*Streptococcus pneumoniae* R6). In the homology search, the Blast parameters were set to a minimal sequence coverage of 25% and a minimal identity of 30%. The first 11 hits of the MultiGeneBlast output are shown in Fig. S1, where homologs genes are represented by arrows with the same colors.

**Phylogeny analysis of *Streptomyces* and *Kitasatospora spp*.**

A set of 1050 *Streptomyces* and *Kitasatospora* genomes was downloaded from NCBI by querying the fasta files in combination with the taxonomic identifier. To this set, 116 unpublished draft genome sequences of an in-house collection of actinomycetes were added[209]. Complete protein sets encoded within the genomes of *Streptomyces* and *Kitasatospora spp*. were extracted. Genes were predicted for the new genomes using prodigal (V2.6.3) and annotation was performed with prokka (1.13.3). The Pfam domains of four housekeeping proteins, AtpD (ATP synthase subunit beta), RecA (recombinase A), TrpB (tryptophan synthase beta chain) and GyrB (DNA gyrase subunit B), were retrieved from https://pfam.xfam.org/ and are annotated as PF00213, PF00154, PF06233 and PF00204, respectively. Using the selected Pfam domains, the HMMsearch program of the HMMER v3.0 package was employed to identify analogous proteins within the chosen species. MAFFT was used to perform a multiple sequence alignment[246]. Aligned sequences were concatenated using SeqKit[247] and maximum likelihood phylogenetic trees were calculated with RAxML[248]. iTOL[235] was used for the visualization of the phylogenetic tree.

**Detection of *murG* genes in *Streptomyces* and *Kitasatospora spp*.**

The domains PF03033 and PF04101 from $MurG_{SCO}$ protein (NP_626343.1) were predicted using the Pfam database[234]. Proteins with these predicted MurG domains were used to search in the complete protein sets encoded within the extracted genomes using HMMsearch. Sequences were retrieved and aligned to their respective HMM profile using HMMalign tool[249]. Pairwise percentage identity was calculated for all hits. Network visualizations were constructed using Cytoscape (v. 3.7.1)[250].

**Acknowledgments**

We would like to thank Marc Bramkamp for providing us with antibodies, and Eveline Ultee, Joeri Wondergem and Doris Heinrich for support with microscopy. This work was supported by a VIDI grant (12957) from the Dutch Applied Research Council to D.C.

## Supplementary information

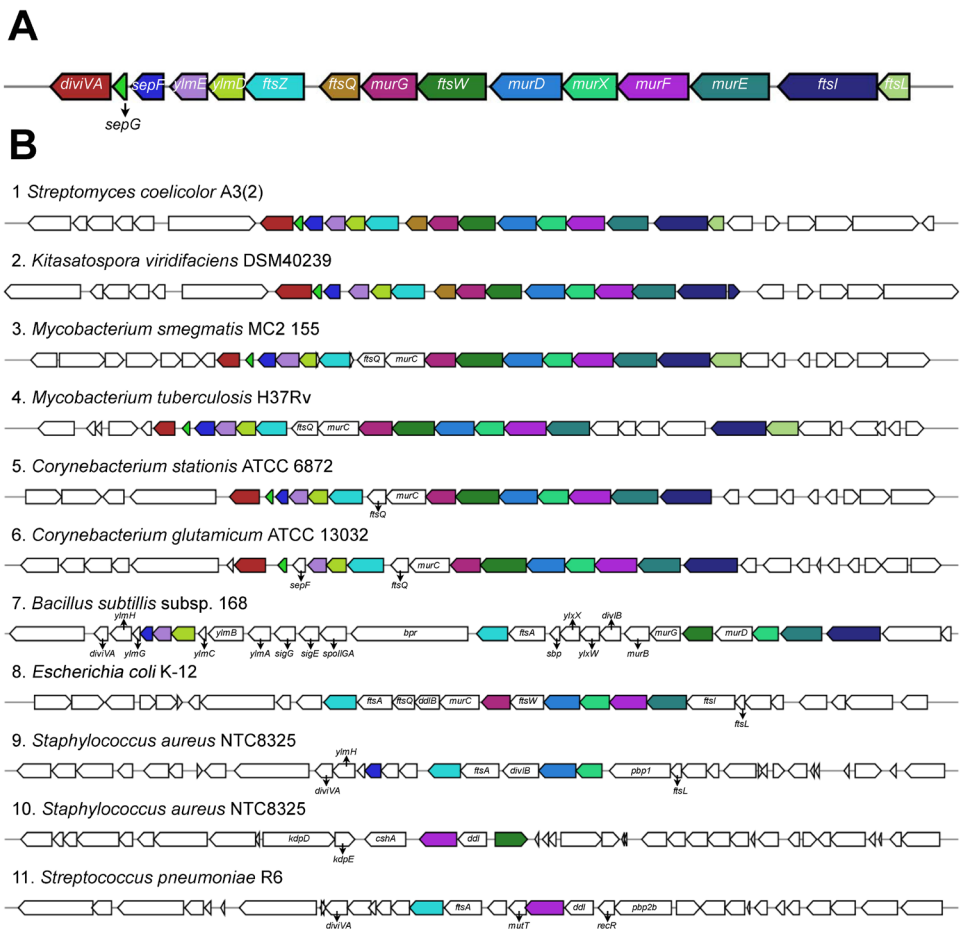


**Supplementary Figure 1. Comparative analysis of *dcw* gene clusters from different bacteria**. (**A**) Organisation and content of the *dcw* gene cluster from *Streptomyces coelicolor* A3(2). (**B**) MultiGeneBlast output showing homologous *dcw* gene clusters with a minimal identity of 30% and minimal sequence coverage of 25% to the *S. coelicolor* cluster.

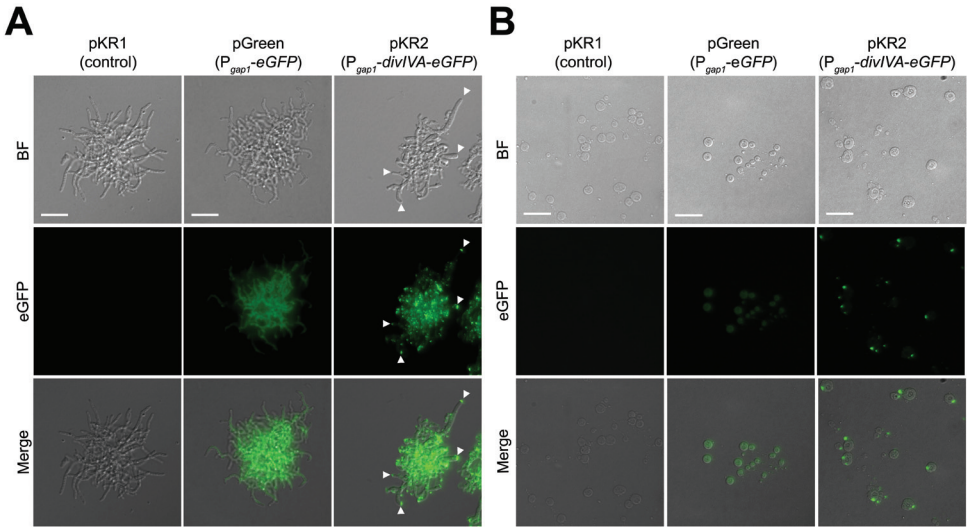


**Supplementary Figure 2. Localization of DivIVA-*eGFP* in *alpha***. (**A**) Fluorescence microscopy analysis of *alpha* grown in TSBS medium as a mycelium and carrying pKR1 (left panels), pGreen (middle panels) or pKR2 (right panels). In mycelium containing pKR2, localization of DivIVA-*eGFP* is found at the hyphal tips (see arrowheads in right panels). No fluorescence is observed in mycelium containing the control plasmid pKR1 (left panels), while a cytosolic signal is observed in *alpha* transformed with pGreen (middle panels). (**B**) Fluorescence microscopy analysis of *alpha* grown in LPB medium in the wall-deficient state and carrying pKR1 (left panels), pGreen (middle panels) and pKR2 (right panels). Cells expressing the DivIVA-*eGFP* fusion protein show distinct foci localized to the membrane (right panels). Like in mycelia, no fluorescence is observed in cells containing the control plasmid pKR1 (left panels), while a cytosolic signal is evident in cells containing pGreen (middle panels). Scale bars represent 10 µm.

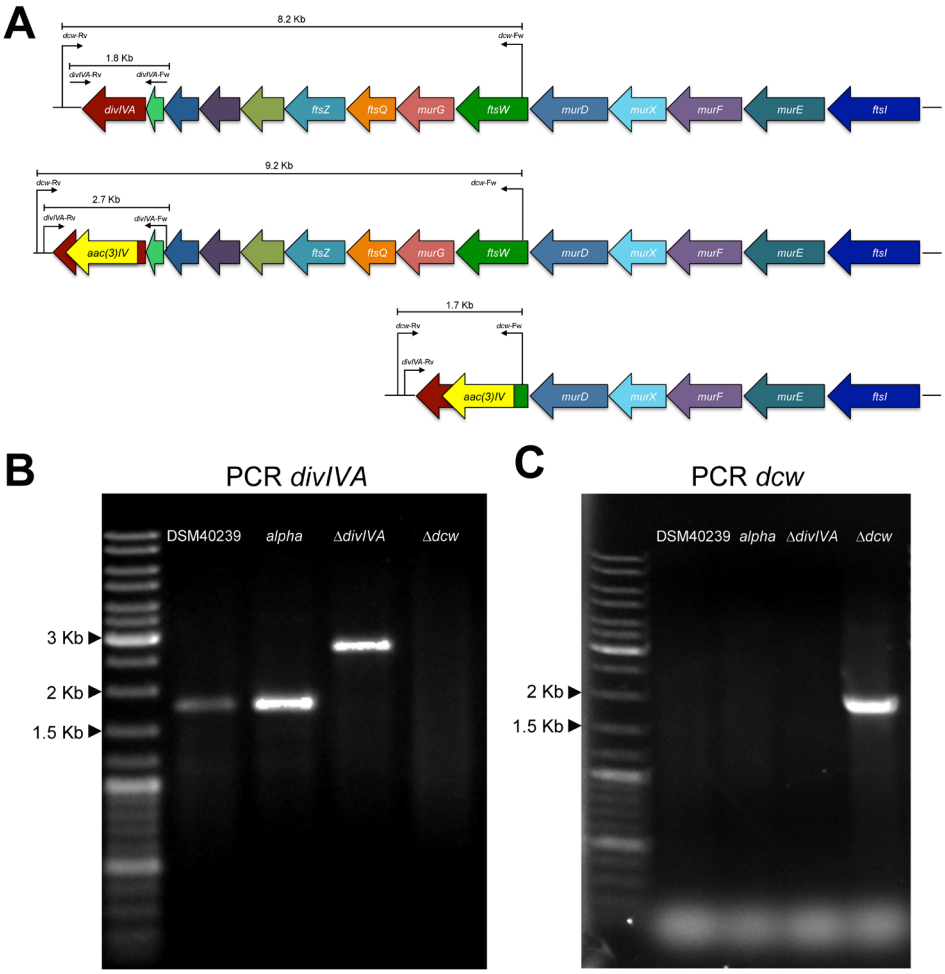


**Supplementary Figure 3. PCR verification of mutants lacking *divIVA* and the partial *dcw* gene cluster**. (**A**) Schematic illustration of the *dcw* clusters in *alpha* (top) and the derivative strains lacking *divIVA* (middle) or part of the *dcw* cluster (bottom). To verify the deletions, PCR analyses were performed using primers *divIVA*-Fw and *divIVA*-Rv (**B**) and *dcw*-Fw and *dcw*-Rv (**C**). (**B**) PCR analysis using primers *divIVA*-Fw and *divIVA*-Rv yielded PCR products of 1.8 Kb when chromosomal DNA of the wild-type strain (DSM40239) or *alpha* were used, while a 2.7 Kb fragment was obtained in the Δ*divIVA* mutant. As expected, no product was obtained with these primers using chromosomal DNA of the Δ*dcw* mutant as the template. (**C**) PCR analysis using primers *dcw*-Fw and *dcw*-Rv only yielded a PCR product of 1.7 Kb when chromosomal DNA of the Δ*dcw* mutant was used as the template. Please note that the sizes of the fragments expected for the wild-type strain and *alpha* (8.2 Kb) and the Δ*divIVA* mutant (9.2 Kb) are too large for efficient amplification.

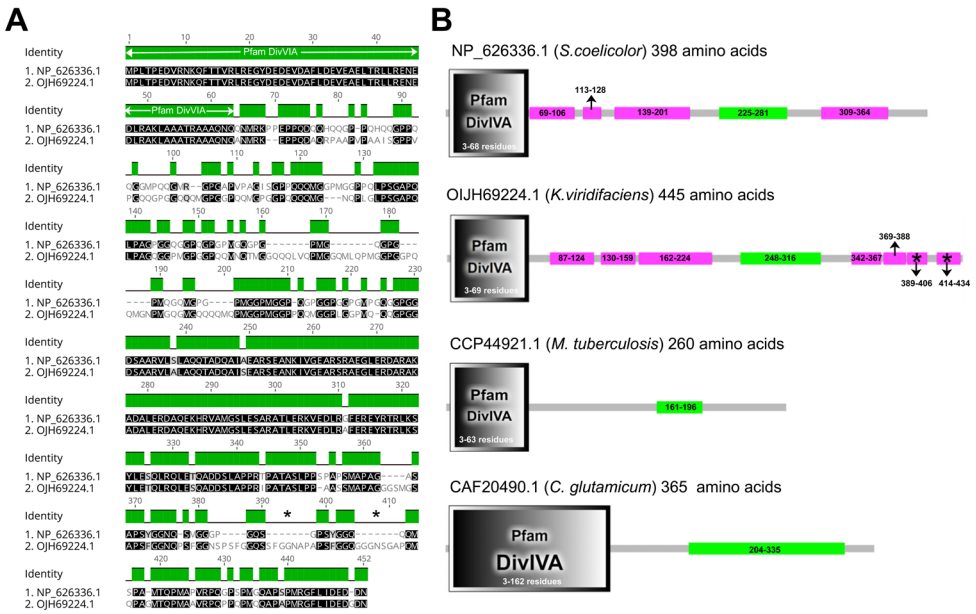


**Supplementary Figure 4. Comparison between DivIVA of *S. coelicolor* and *K. viridifaciens*.** (**A**) Sequence alignment of the DivIVA protein from *S. coelicolor* (NP_626336.1) and *K. viridifaciens* (OIJH69224.1). Green boxes highlight identical regions in both proteins. Please note that the Pfam DivIVA domain is identical in both species. (**B**) Simple Modular Architecture Research Tool (SMART) analysis of DivIVA proteins identified a DivIVA domain (grey), a coiled-coil domain (green), and low complexity domains (pink). Both the DivIVA Pfam domain and the coiled-coil domain is present in the DivIVA proteins of *S. coelicolor* (NP_626336.1), *K. viridifaciens* (OIJH69224.1), *M. tuberculosis* (CCP44921.1) and *C. glutamicum* (CAF20490.1). The low complexity domains are only found in *K. viridifaciens* and *S. coelicolor*. Please note that two of the low complexity domains present in *K. viridifaciens* (indicated with an asterisk) are absent in DivIVA of *S. coelicolor*.

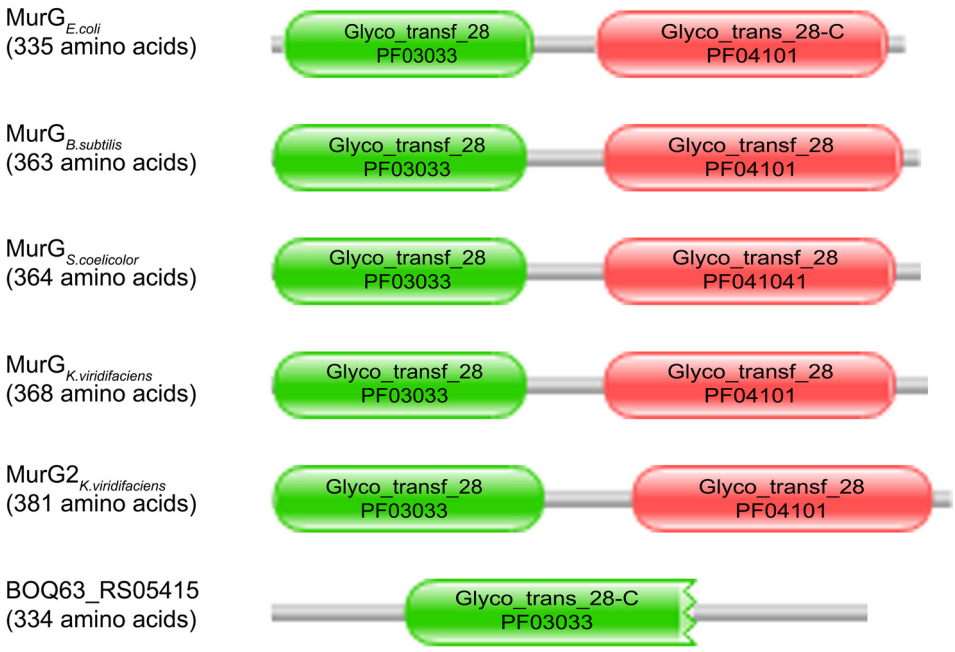


**Supplementary Figure 5. Domain structure of MurG(-like) proteins**. MurG proteins contain an N-terminal domain (PF03033) that binds lipid I and is involved in membrane association. The C-terminal domain (PF04101) contains the UDP-GlcNAc binding site. These domains are found in MurG proteins of *E. coli* (AAC73201.1), *B. subtilis* (CAB13395.2), *S. coelicolor* (NP_626343.1) and *K. viridifaciens* (BOQ63_RS32465). Notably, MurG2 of *K. viridifaciens* (BOQ63_RS12640) also contains both domains. Please note that the protein encoded by the BOQ63_RS05415 gene only contains the N-terminal domain (PF03033), but not the C-terminal (PF04101) domain.

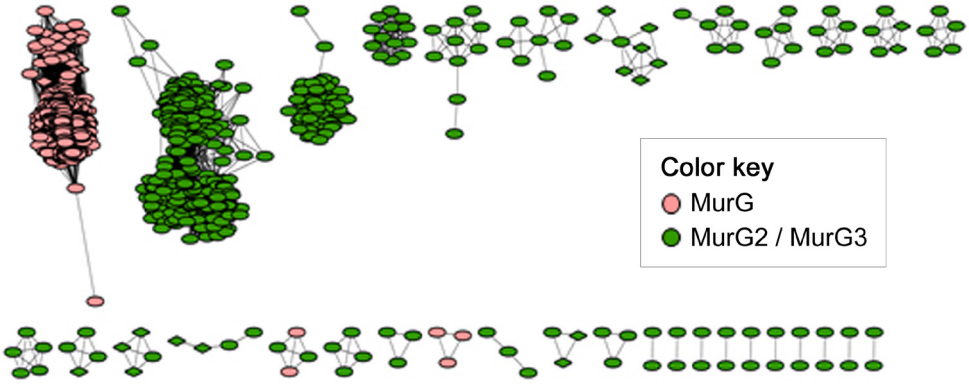


**Supplementary Figure 6. Sequence similarity network of the MurG and MurG-like proteins encoded in the *Streptomyces* and *Kitasatospora spp*. genomes**. Nodes represent MurG proteins and edges highlight similarity (with a threshold set at 0.9). Node colors indicate if the MurG(-like) proteins are encoded in the *dcw* gene cluster (pink) or elsewhere in the genome (green). Circular node shapes are proteins from *Streptomyces spp*., while those from *Kitasatospora spp*. are shown as diamonds. Please note that almost all MurG proteins encoded in the *dcw* cluster group together.

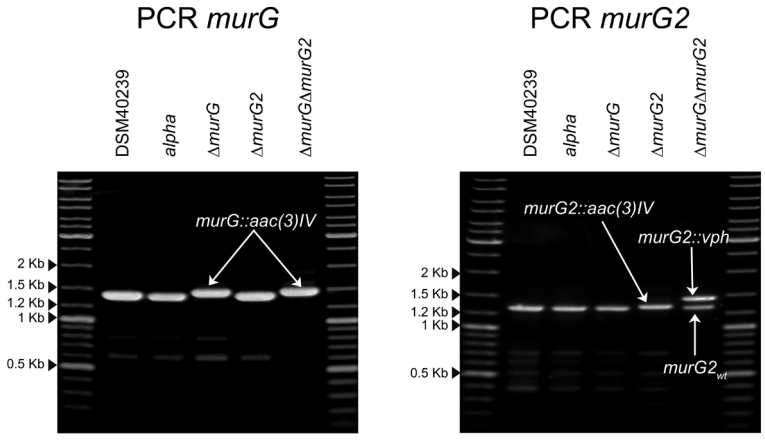


**Supplementary Figure 7. PCR Verification of the *murG* and *murG2* mutants**. The disruption of *murG* and *murG2* was verified by PCR. In strains carrying a wild-type *murG* gene (DSM40239, *alpha* and Δ*murG2*) a fragment of 1.3 Kb is amplified. In contrast, a fragment of 1.4 Kb is found in *murG* mutants (Δ*murG* and Δ*murG*/Δ*murG2*). Likewise, the expected PCR product for strains carrying the *murG2* wild type gene (DSM40239, *alpha*, Δ*murG*) was 1.2 Kb, while replacement of *murG2* by apramycin or viomycin yielded PCR products of 1.3 Kb and 1.5 Kb, respectively. Please note that the wild-type *murG2* gene is still detectable in the Δ*murG*Δ*murG2* double mutant.

**Supplementary Table 1**. Strains used in this study

| Strains | Genotype | Reference |
|---|---|---|
| ***Escherichia coli* strains** | | |
| DH5α | F- Φ80lacZDM15 D(lacZYA-argF)U169 recA1 endA1 hsdR17(rK-, mK-) phoA supE44 thi-1 gyrA96 relA1 λ- | [251] |
| JM109 | *recA1, endAI*, *gyrA*96, *thi, hsdR*17, *supE*44, *relA*1, λ-, Δ(*lac-proAB*), [F', *traD*36, *proAB*, Δ(lacI$^q$ZΔM15] | [252] |
| ET12567 | F-*dam-13::*Tn9 *dcm-6 hsdM hsdR recF143 zjj-202::*Tn10 *galK2 galT22 ara14 lacY1 xyl-5 leuB6 thi-1 tonA31 rpsL136 hisG4 tsx78 mtl-1 glnV44* | [253] |
| SCS110 | *rpsL* (Str$^r$) *thr leu endA thi-1 lacY galK galT ara tonA tsx dam dcm supE*44 Δ(*lac-proAB*) [*F´ traD*36 *proAB lacI$^q$* ZΔM15] | [254] |
| ***Streptomyces/Kitasatospora* strains** | | |
| *S.coelicolor* A3(2) M145 | Wild-type | Lab collection |
| *K.viridifaciens* DSM40239 | Wild-type | DSMZ,[210] |
| ***K. viridifaciens* L-form strains** | | |
| *alpha* | L-form cell line obtained after induction with penicillin and lysozyme | [194] |
| *alpha+pKR1* | *alpha* with promoter-less eGFP | This work |
| *alpha+pKR2* | *alpha* with DivIVA-eGFP | This work |
| *alpha+pGreen* | *alpha* with eGFP | This work |
| Δ*divIVA* | *alpha* lacking *divIVA::aac(3)IV* | This work |
| Δ*dcw* | *alpha* where *ftsW, murG, ftsQ, ftsZ, ylmD, ylmE, sepG, sepF* and *divIVA* replaced by *aac(3)IV* | This work |
| Δ*divIVA+divIVA* | *divIVA* mutant containing *divIVA* under strong promoter | This work |
| Δ*dcw+dcw$_{SCO}$* | *dcw* mutant containing *dcw* from *S.coelicolor: divIVA* (SCO2077), *sepG* (SCO2078), *sepF* (SCO2079), *ylmE* (SCO2080), *ylmD* (SCO2081), *ftsZ* (SCO2082), *ftsQ* (SCO2083), *murG* (SCO2084), *ftsW* (SCO2085), *murD* (SCO2086) | This work |
| Δ*dcw+divIVA* | *dcw* mutant containing *divIVA* under strong promoter | This work |
| Δ*murG* | *alpha* lacking *murG::aac(3)IV* | This work |
| Δ*murG2* | *alpha* lacking *murG2::aac(3)IV* | This work |
| Δ*murG*Δ*murG2* | Δ*murG1::aac(3)IV* lacking *murG2::vph* | This work |

**Supplementary Table 2**. Vectors and constructs used in this study

| Plasmid | Description and relevant features | Ref |
|---|---|---|
| pWHM3 | Unstable, multi-copy and self-replicating S*treptomyces* vector. Contains thiostrepton and ampicillin resistance cassette. | [221] |
| pIJ780 | Plasmid containing a viomycin (*vph*) resistance cassette. | [240] |
| pIJ8600 | *E. coli–Streptomyces* shuttle vector containing the ϕC31 *attP-int* region for genomic integration. Confers resistance to apramycin and thiostrepton. | [239] |
| pIJ8630 | *E. coli–Streptomyces* shuttle vector containing the ϕC31 *attP-int* region for genomic integration. Confers resistance to apramycin | [239] |
| pGreen | pIJ8630 containing the *eGFP* gene under control of the constitutive *gap1* promoter of *S. coelicolor.* | [232] |
| ST4A10 | Supercosmid containing SCO2068-SCO2105 (43,147bp), it confers resistance to ampicillin and kanamycin. | [241] |
| pKR1 | pIJ8630 derivative containing the viomycin resistance cassette from pIJ780 cloned into the unique NheI site. | This work |
| pKR2 | pKR1 derivative containing a C-terminal *eGFP* fusion to *divIVA* of *K. viridifaciens* under control of the *gap1* promoter of *S. coelicolor.* | This work |
| pKR3 | pWHM3 containing the flanking regions of the *K. viridifaciens divIVA* gene interspersed by the *apra-loxP* cassette. | This work |
| pKR4 | pWHM3 derivative containing the flanking regions around the *K. viridifaciens* partial *dcw* gene cluster (*ftsW*, *murG*, *ftsQ*, *ftsZ*, *ylmD*, *ylmE*, *sepF*, *sepG*, *divIVA*) interspersed by the *apra-loxP* cassette. | This work |
| pKR5 | pIJ8600 derivative containing the *gap1* promoter of *S. coelicolor*. | This work |
| pKR6 | pKR5 derivative containing the *divIVA* gene of *K. viridifaciens* under control of the *gap1* promoter of *S. coelicolor*. | This work |
| pKR7 | pIJ8600 containing a 13,268 bp BglII fragment encompassing the *murD*, *ftsW*, *murG*, *ftsQ*, *ftsZ*, *ylmD*, *ylmE*, *sepF*, *sepG* and *divIVA* genes of the *S. coelicolor dcw* gene cluster | This work |
| pKR8 | pWHM3 containing the flanking regions of the *K. viridifaciens murG* gene interspersed by the *apra-loxP* cassette. | This work |
| pKR9 | pWHM3 containing the flanking regions of the *K. viridifaciens murG2* (BOQ63_RS12640) gene interspersed by the *apra-loxP* cassette. | This work |
| pKR10 | pWHM3 containing the flanking regions of the *K. viridifaciens murG2* (BOQ63_RS12640) gene interspersed by the viomycin resistance cassette. | This work |

**Supplementary Table 3**. Primers used in this study

| Primer | Sequence |
|---|---|
| *vph*-Fw-NheI | GACGCTAGCGGCTGACGCCGTTGGATACACCAAG |
| *vph*-Rv-NheI | GACGCTAGCAATCGACTGGCGAGCGGCATCCTAC |
| $P_{aab1}$-Fw-BglII | GATTACAGATCTCCGAGGGCTTCGAGACC |
| $P_{gap1}$-Rv-XbaI | GATGACTCTAGACCGATCTCCTCGTTGGTAC |
| *divIVA*-Fw-XbaI | GTCAAGCTTCTAGAATGCCATTGACCCCCGAGGA |
| *divIVA*-Nostop-Rv-NdeI | GACCATATGGTTGTCGCCGTCCTCGTCAATCAGG |
| P1-*divIVA*-Fw | GACGACGAATTCTGTGATGACCGTCGCTCCACTG |
| P2-*divIVA*-Rv | GACGACTCTAGACTTCCGCATGTTGGCCTGGTTC |
| P1-*dcw*-Fw | GACGAATTCTCCGCGAGGTCACGTACATC |
| P2-*dcw*-Rv | GACTCTAGAAGAGCACCAGTGCGAGCTTG |
| P3-*dcw*-Fw | GACTCTAGAAGCAGCAGATGGGCAACCAG |
| P4-*dcw*-Rv | GATAAGCTTCCCGGCTACAACCTCAGTTGTC |
| Delcheck-*divIVA*-Fw | TGACCCGGCCACGACTTTAC |
| Delcheck-*divIVA*-Rv | GGACGCCCTCAACAAAC |
| Delcheck-*dcw*-Fw | CCAGAACTGGCTGGATTTCG |
| Delcheck-*dcw*-Rv | GTCTCCAGGTACGACTTCAG |
| *divIVA*-XbaI-Fw | GTCAAGCTTCTAGAATGCCATTGACCCCCGAGGA |
| *divIVA*-NdeI-Rv | GATCGAATTCATATGCCCGGCTACAACCTCAGTTGTC |
| *divIVA* seq1-Fw | AGCAGCAGATGGGCAACCAG |
| *divIVA* seq2-Fw | CGCGTCTGAAGTCGTACCTG |
| *divIVA* seq-Rv | ACCTCGTCCTCGTCATAGC |
| SCO2079_F-520 | TCACGGCGCTGTCGAAGGAGGCCG |
| SCO2079_R+1162 | CTCATCGAGGAAGGCATCGACCTC |
| $divIVA_{SCO}$-Fw | AAGGCTACGCCGTACTACAG |
| $divIVA_{SCO}$-Rv | AGATACGGGCTTGCCGAATG |
| P1-*murG*-Fw | CATCGAATTCGATATCTTTCGGCTTCTTCCAGTTCC |
| P2-*murG*-Rv | CATCCATGTCTAGACGACATGCACCGAAATTCAC |
| P3-*murG*-Fw | CATCCATGTCTAGATGGTGTACGAGGCGATCCAG |
| P4-*murG*-Rv | CATGGATATCAAGCTTGACGGATGTCGATGGGTAGG |
| Delcheck-*murG*-Fw | AGCAAGAACTCCCGGATCAG |
| Delcheck-*murG*-Rv | AGCACCGACGAGAAGAACAC |
| P1-*murG2*-Fw | CTGAGAATTCGATATCTTCTCGTGGGAACACCGGGCA |
| P2- *murG2*-Rv | CTGATCTAGAGGTGACGATCAGCCGCATAGG |
| P3- *murG2*-Fw | CTGATCTAGAGACCGTCTCGTGGACGTGCTG |
| P4- *murG2*-Rv | CTGAAAGCTTGATATCGTTCCCGCTACCCGAACGGAAC |
| Delcheck-*murG2*-Fw | CTGAATGTTCCAAGCGTGAACCGGGA |
| Delcheck-*murG2*-Rv | CTGAGCGACTACAAGGCGTACCAGG |
| *vph*-Fw-EcoRI-HindIII-XbaI | GACGAATTCAAGCTTTCTAGAGGCTGACGCCGTTGGATACACCAAG |
| *vph*-Rv-EcoRI-HindIII-XbaI | GACGAATTCAAGCTTTCTAGAAATCGACTGGCGAGCGGCATCCTAC |

**Supplementary Table 4**. *murG* homologs identified in *Kitasatospora viridifaciens*

| Hit | Hit start | Hit end | Locus | E value | Bit-Score | Pairwise Identity (%) | Query coverage (%) |
|---|---|---|---|---|---|---|---|
| 1** | 5334877 | 5335956 | BOQ63_RS32465 | 0 | 604.7 | 84.2 | 98.6 |
| 2** | 1072546 | 1073598 | BOQ63_RS12640 | 6.56e-32 | 125.9 | 31.1 | 90.4 |
| 3* | 1258806 | 1257943 | BOQ63_RS05415 | 1.01e-22 | 98.5 | 32.5 | 80.8 |

*Hit located in KVP1, **Hit located in chromosome

# Chapter 5
# Application of cell wall-deficient variants of the filamentous actinomycete *Kitasatospora viridifaciens* as microbial cell factories

Karina Ramijan, Aimilia Karanatsiou & Dennis Claessen

## Abstract

Filamentous actinomycetes are best known for their ability to produce a vast array of natural products with medical, agricultural and industrial applications. However, filamentous growth leads to the formation of mycelial networks that are unattractive from the industrial fermentation perspective. Here, we have investigated the use of a *Kitasatospora viridifaciens* L-form cell line, *alpha*, as a single cell alternative to strains with mycelial growth. We exploited the shape-shifting capacity of *alpha* to test protein production secretion in both the wall-deficient and the mycelial state. Our results demonstrated that a functional cellulase was produced both in the presence and absence of the cell wall. Secretion of cellulases in the Δ*divIVA* and Δ*dcw* strains demonstrated that DivIVA, the polarity determinant of actinobacteria, is not required for secretion. This is interesting in the light of the notion that secretion takes place at hyphal tips. Altogether, these results indicate that *alpha* can be used for the production of heterologous proteins.

## Introduction

The innovations of the biotechnology industries continue to improve the lives of people worldwide. Industrial biotechnology uses biological systems for the production of chemicals, materials and energy. Important producers are mycelial soil bacteria belonging to the actinobacteria. These multicellular bacteria grow as filaments (hyphae) that form a complex network called a mycelium. When nutrients become limiting, part of the vegetative mycelium is dismantled, concurring with antibiotic production. These secondary metabolites help to protect the pool of nutrients that is released during breakdown of the mycelium, and which is being used for a second phase of growth[160,255]. During this phase, specialized hyphae are formed that grow away from the substrate into the air. This leads to the formation of spores that can survive the adverse environmental conditions. Besides antibiotics, actinomycetes naturally produce other economically valuable metabolites including immunosuppressive agents, anti-cancer drugs and pesticides[2,256].

In industry, streptomycetes are not only being used for the production of important metabolites, but also for the production of enzymes. As saprophytes, these bacteria are an important source for enzymes that are required for the degradation of naturally occurring polymers, such as cellulose, chitin, xylan and starch[257]. Many of these enzymes are industrially relevant, for instance for the conversion of biomass into biofuels, or for various applications in medicine, or the food, feed and textile industries[258]. Advantageously, filamentous actinomycetes have potent secretion systems via which products are directly released into the medium. The vast majority of proteins are secreted by the Sec pathway, which is generally considered to secrete proteins in an unfolded manner[259-261]. In contrast, proteins may also be secreted via the twin arginine translocation (Tat) pathway, which facilitates secretion of folded proteins or those containing cofactors[262]. Specific sequence motifs in the signal peptides direct the proteins to the different transport systems. Secretion of proteins in the culture broth is useful for industrial production because it simplifies downstream processing and may help solving toxicity and production issues, with higher yield as the attractive perspective.

Recent evidence indicates that the Tat secretion machinery localizes at the hyphal tips, which also accommodated the machinery required for apical growth and chromosome segregation[263-267]. A crucial component of the apical growth complex is the cell polarity determinant DivIVA[78,268], which is encoded by the *divIVA* gene in the so-called *dcw* gene cluster. In addition to *divIVA*, this cluster contains various cell division and cell wall synthesis genes[227]. Whether DivIVA is important for protein secretion is unknown, but also inherently difficult to study given the essential role of this protein in polar growth[78,81].

Although actinomycetes are recognized by their multicellularity and filamentous mode-of-growth, unicellular forms of these microorganisms can be isolated. Such variants are called L-forms, which are characterized by the absence of the cell wall[136,137]. L-forms typically have acquired mutations that allow them to proliferate efficiently without the cell wall[194]. Pioneering work indicated that L-forms could have biotechnological potential in the production of heterologous proteins[269,270] and antibiotics[208]. L-forms have been obtained from a range of different actinomycetes, including *S. hygroscopicus*[271], *S. griseus*[272] and *Kitasatospora viridifaciens*[194,208]. We recently generated a cell line, called *alpha* which efficiently proliferates in the L-form state on media containing high levels of osmolytes. Excitingly, when the osmolytes are omitted from the medium *alpha* has the ability to switch morphology and grow filamentous (Chapter 4). Using this strain, we here investigated the ability of L-forms of *K. viridifaciens* to produce and secrete bioactive molecules in the walled and wall-deficient state. We show that secretion can happen in the absence of the cell wall, and furthermore *divIVA* and other members of the *dcw* gene cluster are not required for Tat secretion. Altogether, these data suggest that the localization of the Tat secretion machinery at apices is not required for its activity.

## Results

### Antimicrobial activity in supernatants of walled and wall-deficient variants of *K. viridifaciens*

As previously shown in Chapter 4, we successfully generated a stable *K. viridifaciens* L-form cell line, named *alpha* after exposing the wild-type strain to high levels of penicillin and lysozyme[194]. Growth of *alpha* on LPMA plates leads to the formation of viscous, green-pigmented colonies exclusively consisting of cell wall-deficient (CWD) cells (Fig. 1A). Likewise, *alpha* proliferates in the CWD state in liquid LPB medium (Fig. 1B). In contrast, in TSBS medium, containing 10% sucrose as opposed to the 22% in LPB medium, *alpha* switched to the walled state and formed mycelial aggregates (Fig. 1C). Noticeably, a green pigmentation was evident in both media (Fig. 1B, 1C). When supernatants were tested for antimicrobial activity, it was evident that the wild-type strain and *alpha* produced a metabolite that inhibited growth of *B. subtilis*. Notably, production and secretion of this metabolite was comparable when *alpha* was grown with or without its cell wall (Table 1). The bioactive substance(s) have not been further characterized.

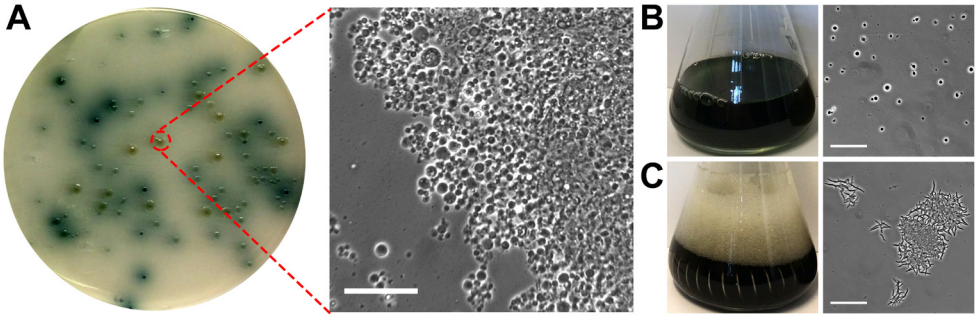


**Figure 1. Production of green pigment by cell line *alpha* in L-form and mycelium shape**. (**A**) *Alpha* grown in LPMA forms green pigmented colonies exclusively consisting of spherical CWD cells. Such CWD cells are also observed in liquid LPB medium (**B**) but not when *alpha* is grown in TSBS medium (**C**). In TSBS medium, only mycelial networks are evident. Scale bar represents 40 µm.



**Table 1.** Antimicrobial activities of walled and wall-deficient *K. viridifaciens* strains against different indicator bacteria. Mycelium-forming strains were grown in TSBS medium, while L-forms were grown in LPB medium. Growth inhibition of indicator bacteria is indicated with a "+".

| ***K. viridifaciens* strain** | **Indicator strain** | | | |
|---|---|---|---|---|
| | ***B. subtilis*** | ***E. coli* JM109** | ***E. coli* ET12567** | ***P. aeruginosa*** |
| Wild-type (mycelium) | + | - | - | - |
| *alpha* (mycelium) | + | - | - | - |
| *alpha* (L-form) | + | - | - | - |

**Figure 2. (in page 109) The morphology of *alpha* depends on the morphology of the inoculum and the sucrose content in the medium**. Pre-cultures of *alpha* grown as L-forms (**A**) or as a mycelium (**B**) were used to inoculate MYM cultures with different amounts of sucrose. After 24 and 96 hours the morphology was analyzed by microscopy. The arrows indicate fibrous material observed in the culture (MYM10%), while the arrowheads in the MYM20% panel highlight L-form cells. Scale bars represents 40 µm.

### A medium to compare protein secretion between walled and wall-deficient cells

The ability of *alpha* to grow as mycelia or as wall-deficient cells prompted us to find the sucrose concentration at which *alpha* grows exclusively in the walled or the wall-deficient state depending on the shape of the pre-culture. We therefore supplemented MYM medium[195] with different amounts of sucrose (5% [MYM5], 10% [MYM10], 15% [MYM15] and 20% [MYM20]) and analysed growth of *alpha* inoculated either as L-forms (Fig. 2A) or as mycelium (Fig. 2B).

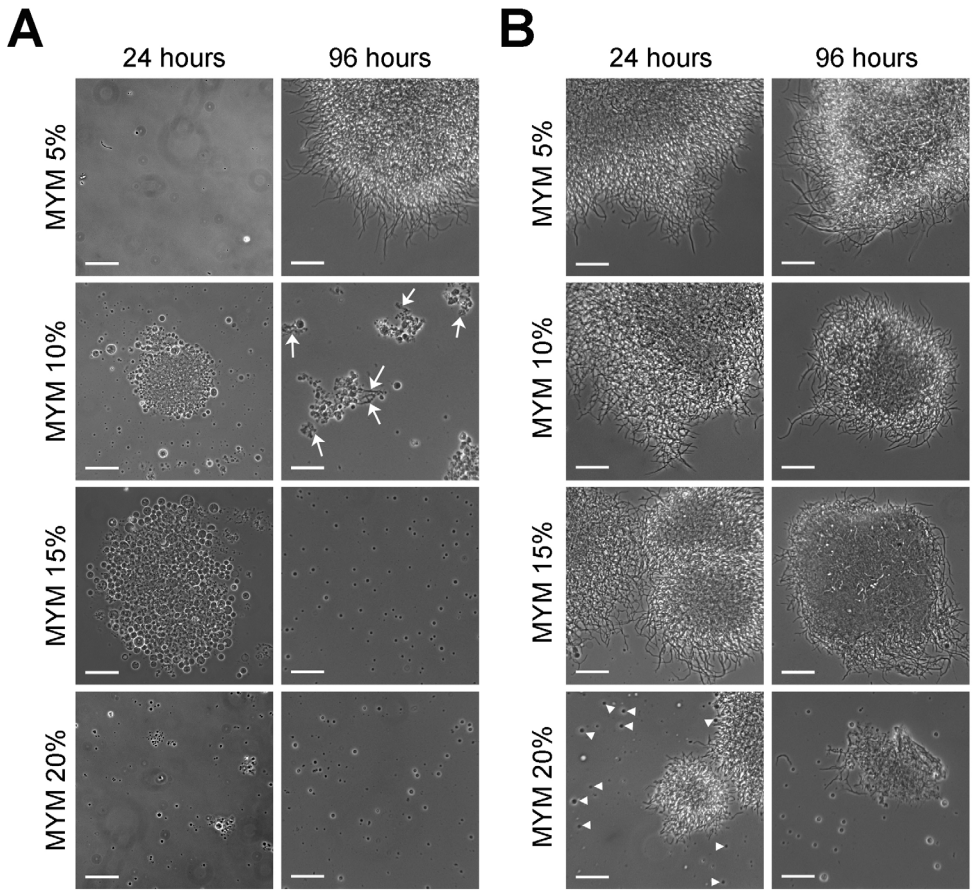

We observed that L-forms inoculated in MYM5 medium were unable to proliferate in the CWD state, which forced *alpha* to switch to the filamentous mode-of-growth (see mycelia after 96 hours). In MYM10, MYM15 and MYM20 *alpha* inoculated as L-forms was able to retain its CWD state. We then tested the morphology of *alpha* inoculated as a mycelium in the different media after 24 and 96 h (Fig. 2B). As expected, growth of *alpha* in MYM5 retained the mycelial morphology of the strain. In fact, L-forms became only apparent when the sucrose concentration in MYM medium was elevated to 20% (see white arrowheads in Fig. 2B at 24 hours). Taken together, these results indicated that *alpha* was able to retain its morphology of the original inoculum at a sucrose concentration between 10 and 15%. Due to the formation of fibrous material in MYM10 (see white arrows in Fig. 2A at 96 hours), we chose MYM15 for subsequent studies.

The ability of *alpha* to retain its original morphology in MYM15 enabled us to study protein secretion in the absence of the cell wall. We therefore transformed the reporter plasmid pSEA4CT-11AG8 to *alpha* and protoplasts of *S. lividans* (which is commonly used for protein secretion studies). This plasmid contains a cellulase gene (*cel12A*), a thiostrepton resistance marker and a *Streptomyces*-specific replicon. The engineered signal sequence ensures secretion of the cellulase in the medium via the Tat secretion machinery. We first analysed the cellulolytic activity of the transformed strains on solid MM medium (lacking osmoprotectants), by visualizing the degradation of carboxymethyl cellulose (CMC) using Congo red staining (Fig. 3A). As shown in Fig. 3A, clearing zones (or halos) are observed on CMC plate surrounding colonies of the strains containing the reporter plasmid. The halos appear more diffuse when *alpha* was grown as mycelium in comparison to *S. lividans*. A small halo was also detected in *S. lividans* without the reporter plasmid, which may be due to the secretion of an endogenous cellulase. In contrast, no halos are formed by *alpha* lacking pSEA4CT-11AG8 or on plates lacking CMC.

To compare the secretion of Cel12A, we analysed the supernatant of the strains after 8 days of growth in MYM15 (Fig. 3B). SDS-PAGE analysis revealed an abundant protein band (black asterisks) between 35 and 40 kDa in the *S. lividans* strain harbouring the pSEA4CT-11AG8 plasmid, which correlates with the predicted size of Cel12A. A similarly sized protein band was also evident in the transformed *alpha* strain, regardless of whether the strain was growing as an L-form or in the canonical mycelial state. Notably, the supernatant of *alpha* grown in the L-form state and containing pSEA4CT-11AG8 revealed an additional protein band (white asterisk), which equates the 40 kDa molecular weight predicted for the cellulase protein still containing its signal sequence. Western Blot analysis of the above mentioned supernatants also indicated the presence of the intracellular

EF-Tu protein in the supernatant of the strains grown as L-forms (Fig. 3C).

To assess whether the intracellular proteins came from potential remaining cells present in the supernatant, we grew *alpha* as L-form in MYM15. After 8 days of growth, we separated the L-forms from the supernatant by ultracentrifugation and plated 1 mL of the supernatant on LPMA plates. Despite ultracentrifugation, 385±49 colony forming units (CFU·ml$^{-1}$) were present in the supernatant. This suggests that the detected putative premature form of cellulase and EF-Tu are a likely consequence of lysis of remaining cells in the supernatants by the loading buffer. Altogether these results demonstrate that *alpha* is capable to produce and secrete a heterologously produced enzyme, both with and without the cell wall.



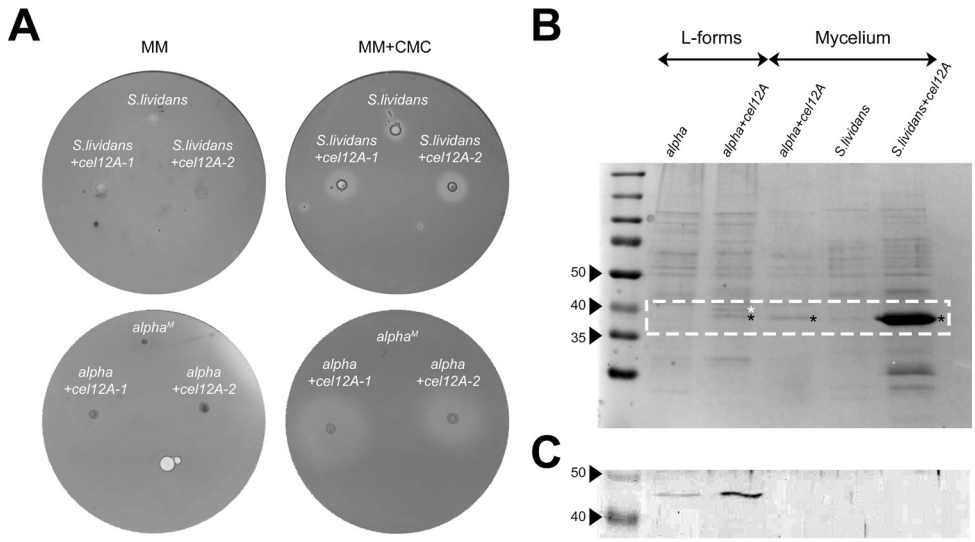


**Figure 3. Cellulase secretion in *alpha* grown with or without the cell wall**. (**A**) Strains carrying the cellulase reporter plasmid pSEA4CT-11AG8 were grown on minimal medium (MM) plates, either or not supplemented with 1% carboxymethyl cellulose (CMC). After 7 days the plates were stained with Congo Red to visualize halos surrounding colonies capable of degrading CMC. The control strains lacking the reporter plasmid are present on the top of each plate. (**B**) SDS-PAGE analysis of supernatants of L-form and mycelial strains expressing the Cel12A cellulase protein. The cellulase band, indicated with black asterisks is exclusively present in strains carrying the reporter plasmid. When *alpha* carrying the reporter plasmid is grown as an L-form, two proteins are evident putatively corresponding to the premature (40 kDa, white asterisk) and mature form of the cellulase (36 kDa). (**C**) Western blot analysis using antibodies against EF-Tu1 indicate the presence of this intracellular protein in the supernatants of the strains grown as L-forms.

## Secretion of the Tat-substrate Cel12A does not depend on DivIVA

The Cel12A secretion by *alpha* grown without its cell wall was the reason for investigating if DivIVA was required for this process. To this end, we introduced the pSEA4CT-11AG8 reporter plasmid into the *divIVA* and *dcw* mutants (Chapter 4). We then examined the secretion of the Cel12A cellulase in solid LPMA plates supplemented with 1% CMC. Although the CMC was not the only carbon source in the medium, we observed cellulase activity surrounding the colonies containing pSEA4CT-11AG8 (Fig. 4A). No halos were observed without the reporter plasmid, or when CMC was omitted from the plates (data not shown). When supernatants obtained from liquid-grown cultures were subsequently analyzed using SDS-PAGE, two protein bands with the sizes expected for the cellulase precursor and the mature cellulase (rectangle Fig. 4B) were evident, which is consistent with the data for *alpha*. Altogether, these results demonstrate that Tat secretion activity does not require DivIVA.

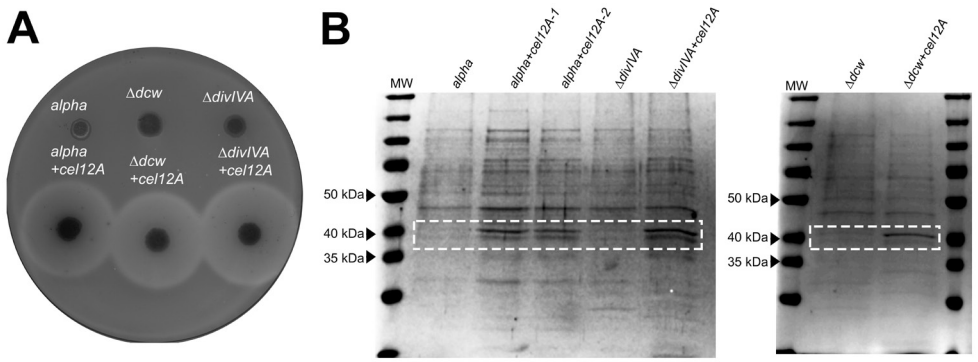


**Figure 4. Secretion of cellulase is not dependent on DivIVA**. (**A**) Strains carrying the cellulase reporter plasmid pSEA4CT-11AG8 were grown on minimal medium (LPMA) plate supplemented with 1% carboxymethyl cellulose. After 7 days the plates were stained with Congo Red to visualize halos surrounding colonies capable of degrading CMC. The control strains lacking the reporter plasmid are present on the top of each plate. (**B**) SDS-PAGE analysis of supernatants of L-form strains expressing the Cel12A cellulase protein. Two protein bands are evident in strains carrying the reporter plasmid, putatively corresponding to the premature (40 kDa) and mature form of the cellulase (36 kDa).

## Discussion

Actinomycetes are prolific producers of natural products, including the majority of the clinically used antibiotics and many industrial relevant enzymes. Most of these natural products are made in large bioreactors. Growth under these conditions leads to the formation of dense mycelial pellets, which from an industrial point-of-view are generally unattractive, given the slow growth rate of pellets and large heterogeneity in their size and physiology[88,273]. This is one of the main reasons why industry still prefers to use unicellular microorganisms, such as *Escherichia coli* and *Saccharomyces cerevisiae*[274]. Many of the products produced by actinomycetes can only be efficiently made in the native host (or a close relative) and cannot be produced in more favored unicellular organisms. An alternative to the limitations of mycelial forming strains would be to use actinomycete derivatives that grow as single cells. Our results have made a first step towards that concept by validating the use of *alpha*, a strain whose morphology can be switched between a walled and wall-deficient state, as a platform for the production of natural products. We have demonstrated that this strain is able to produce and secrete antimicrobial compounds and enzymes, both in the presence and absence of the wall. This provides a unique starting point for further strain optimization.

The cell wall forms a protective barrier surrounding the cell. The ability to limit access to environmental influences also provides a potential barrier for secretion of products into the environment[275]. It was demonstrated that fungi are able to regulate cell wall porosity. Reduced porosity prevents passage of high molecular-weight proteins[276]. As a consequence, such proteins are retained in the cell wall matrix. It is conceivable that bacteria are also able to control cell wall porosity, although little is known about this concept, which provides an exciting opportunity for L-forms to produce large proteins: in contrast to filamentous strains with a wall, proteins secreted by L-forms would not encounter the cell wall barrier and could therefore be more easily secreted into the culture broth.

We here demonstrated that *alpha* is able to produce and secrete a heterologous cellulase in the cell wall-deficient state. Interestingly, we not only observed the expected 35 kDa form of the protein, but also a larger 40 kDa version. This larger version was also evident in the culture broth of L-form strains lacking *divIVA* or the *dcw* gene cluster, but not when *alpha* was grown as mycelium. We expect that this larger form represents the cellulase containing its signal peptide. Besides the high viscosity of MYM15 and accompanying difficulty to harvest the cells from the supernatant, the aberrant proliferation mode of L-form cells often leading to cell lysis could explain how the unprocessed protein is released into the broth. Even in these scenarios, a production

platform could still be considered: initially, cells are grown to high density in the cell-wall deficient state, after which the cells are induced to revert to the mycelial mode-of-growth, leading to the formation of small mycelial particles that will efficiently produce and secrete the product, with the correct posttranslational modification and protein folding machinery operating in the filamentous state. This makes *alpha* an attractive platform in comparison to other L-form cell lines of *E. coli* or *B. subtilis*, which not only lack the actinomycetes-specific machinery for posttranslational modification, but also the unique switching behavior.

In filamentous actinomycetes secretion occurs mainly at the hyphal tip. Remarkably, secretion of the mature Cel12A was possible both in the Δ*divIVA* and Δ*dcw* mutant, suggesting that DivIVA is not required for secretion. However, DivIVA is essential for polar growth and for the assembly of the coiled-coiled proteins from the TIPOC[78,82,161]. This type of polarisome organization is not restricted to bacteria, it is also present in budding yeast[277-279] and in filamentous fungi (Spitzenkörper)[280,281]. Indeed the close relation between polar growth and protein secretion was previously suggested for filamentous fungi[282,283]. Accordingly, in *S. coelicolor*, the Tat complex is dynamically translocated through the hyphae before localizing 2 µm behind the tip[266,267]. Nevertheless, our results suggest secretion of Tat substrates does not require DivIVA.

In addition to production and secretion of enzymes, L-forms are suitable for several other promising applications. These wall-deficient cells are readily transformable and able to take up various forms of DNA, including excessively large DNA fragments, such as those encoding antimicrobial compounds or even entire genomes. As such, wall-deficient cells could provide an interesting platform for production of antimicrobial compounds that target the process of cell wall synthesis. Given that cell wall synthesis is obsolete in L-forms, such strains would potentially allow synthesis of synthetic engineered compounds for which no resistance determinant is available. We here demonstrated that *alpha* is able to produce and secrete an antimicrobial compound as a proof-of-concept. *Mycoplasma* strains, which are naturally cell wall-deficient, have been used successfully for introducing entire synthetic genomes[284]. This work was recently extended by minimizing this genome, yielding a minimal cell consisting of 473 genes[285]. Notably, the obtained minimal cells were proliferating in a manner consistent with L-forms. L-forms may also be exploited to design and build synthetic phages. This concept was recently demonstrated with the assembly of phages for *Bacillus* and *Staphylococcus* in *Listeria monocytogenes* L-forms[218]. Altogether, these results form the basis to further explore the use of L-forms for biotechnological applications.

## Methods

### Strains and media

Bacterial strains used in this study are shown in the Supplementary Table 1. Wall-deficient cells were grown in LPB medium or on LPMA plates[194]. MYM or MS agar plates were used to obtain sporulating cultures of *K. viridifaciens* or *S. lividans*, respectively. For liquid-grown cultures, 100 mL flasks were used, if necessary equipped with a coil. Liquid cultures were grown at 100 (wall-deficient strains) or 200 rpm (walled strains). *E. coli* ET12567 was used to obtain unmethylated plasmids for transformation of L-forms and *S. lividans*.

### Microscopy

Morphology of strains was assessed using a Zeiss Axio Lab A1 upright microscope equipped with an Axiocam Mrc.

### Antimicrobial assay

To assess antimicrobial activity, strains were pre-grown in LPB (*alpha* in L-form) or TSBS (wild-type and *alpha* in mycelium form). After seven days of growth 1 ml of the culture was centrifuged at 9000 rpm for 5 minutes to remove the biomass. 10 µl aliquots of the supernatant were placed on a sterile paper disc on LB plates containing a lawn of the indicator strain (*Bacillus subtilis* 168, *Escherichia coli* JM109, *E. coli* ET12567 and *Pseudomonas aeruginosa* PAO1. Growth inhibition was assessed after overnight incubation at 37°C.

### Transformation procedures

The self-replicating plasmid pSEA4CT-11AG8 plasmid[286] was transformed to *K. viridifaciens* L-forms or protoplasts of *S. lividans* by using the rapid small-scale transformation procedure[179]. For each transformation, 1 µg DNA was added to 50 µl of a mid-exponential *K. viridifaciens* L-form culture. After 20 hours of non-selective growth on LPM or R5 medium for L-forms and protoplasts, respectively, transformants were selected by applying an overlay containing the required antibiotics. Further selection of transformants was done on R5 or LPMA medium supplemented with thiostrepton, using 5 or 10 $\mu g \cdot ml^{-1}$ for L-forms or protoplasts, respectively. Transformants were analysed by colony PCR analysis using primers *cel12A*-292-Fw (5'-GGCATC-GTGCAGAGACAGAC-3)'and *cel12A*-1623-Rv (5'-CTGGGATATGCCGGA-CATGG-3)' directed against the *cel12A* gene contained on pSEA4CT-11AG8.

### Detection of cellulase activity in plates

Qualitative assessment of cellulase activity was performed as previously described[287], with the exception that carboxymethyl cellulose (CMC) was added to minimal medium (MM) or LPMA agar for walled or wall-deficient cells, respectively. To test the degradation of cellulose, plates were inoculated with aliquots of spores, mycelium or L-forms and incubated at 30°C for 7 days. Plates

were then stained for 15 minutes with 0.4% Congo Red (20 ml/plate). Following removal of the Congo Red solution, the plates were washed with distilled water before a final treatment with 1M NaCl (15 ml/plate) for 15 minutes was performed. The presence of halos surrounding the colonies was indicative for cellulase activity.

### Detection of cellulase with SDS-PAGE

SDS-PAGE analysis was used for the detection of the Cel12A cellulase in supernatants. To this end, pre-cultures of *alpha* grown in the wall-deficient or wall-proficient state were obtained after 3 days in LPB and TSBS, respectively. 1 ml of these pre-cultures were then used to inoculate 50 ml of liquid MYM15 medium (i.e. MYM supplemented with 15% sucrose). After eight days of growth, the supernatants were collected by centrifugation at 40,000 rpm for 1 hour (Centrikon T-2070 rotor TFT5038) and mixed with 2X sample buffer (50mM Tris-HCl pH 6.8, 15% glycerol, 1% SDS, 0.01% bromophenolblue, 2% β-mercaptoethanol). The proteins in the supernatant were separated on 12.5% gels at 205 V, 200 mA for 1 hour. The same procedure was employed to analyze the supernatants of the Δ*divIVA* and Δ*dcw* strains transformed with pSEA4CT-11AG8. However, these L-form strains were grown in LPB medium for 7 days before the supernatant was collected.

### EF-Tu detection using Western blot analysis

For Western blot analysis, the supernatant proteins separated by SDS-PAGE were transferred to polyvinylidene difluoride (PVDF) membranes (GE Healthcare) with the Mini Trans-Blot® Cell (Bio-Rad Laboratories) according to the manufacturer's instructions. Antibodies directed against EF-Tu[288] were used in a 1:5,000 dilution as described previously[77].

## Acknowledgments

We would like to thank Sharief Barends from DuPont Industrial Biosciences for providing the pSEA4CT-11AG8 plasmid. We are also thankful to Mariana Avalos for help with the antibiosis assays. Work in this project was supported by a NWO-VIDI grant to D.C.

**Supplementary Table 1**. Strains used in this study

| Strains | Genotype | Reference |
|---|---|---|
| ***Actinomycetes* strains** | | |
| *Kitasatospora viridifaciens* DSMZ40239 | Wild-type | DSMZ, [210] |
| *Streptomyces lividans* 1326 | Wild-type | Lab collection |
| *alpha* | L-form cell line obtained after induction with penicillin and lysozyme | [194] |
| Δ*divIVA* | *alpha* lacking *divIVA::aac(3)IV* | Chapter 4 |
| Δ*dcw* | *alpha* where *ftsW, murG, ftsQ, ftsZ, ylmD, ylmE, sepG, sepF* and *divIVA* replaced by *aac(3)IV* | Chapter 4 |
| *alpha+cel12A-1* | *alpha* with pSEA4CT-11AG8 plasmid clone 1 | This work |
| *alpha+cel12A-1* | *alpha* with pSEA4CT-11AG8 plasmid clone 2 | This work |
| Δ*divIVA+cel12A* | *divIVA* mutant with pSEA4CT-11AG8 plasmid clone 1 | This work |
| Δ*dcw+cel12A* | *dcw* mutant with pSEA4CT-11AG8 plasmid clone 1 | This work |
| **Other strains** | | |
| *Escherichia coli* ET12567 | F-*dam-13::*Tn9 *dcm-6 hsdM hsdR recF143 zjj-202::*Tn10 *galK2 galT22 ara14 lacY1 xyl-5 leuB6 thi-1 tonA31 rpsL136 hisG4 tsx78 mtl-1 glnV44* | [253] |
| *Escherichia coli* JM109 | *recA1, endAI*, *gyrA*96, *thi, hsdR*17, *supE*44, *relA*1, λ-, Δ(*lac-proAB*), [F', *traD*36, *proAB*, Δ(lacI$^q$ZΔM15] | [292] |
| *Bacillus subtilis* 168 | Wild-type | Lab collection |
| *Pseudomonas aeruginosa* PAO1 | Wild-type | Lab collection |

# Chapter 6
# Summary and General Discussion

Filamentous actinomycetes are ubiquitous in virtually all soil and water environments[10]. Their ability to thrive in diverse ecosystems relies on their capacity to produce and secrete many enzymes and specialized metabolites. Hydrolytic enzymes allow them to obtain nutrients from complex polymers, while molecules with antimicrobial properties protect vital resources from competing microorganisms[160]. The actinomycetes are characterized by their multicellular life style, which relies on designated mechanisms for apical growth and morphological differentiation. The actinomycetes studied in this thesis belong to the *Streptomycetaceae*, namely *Kitasatospora* and *Streptomyces*. The developmental program includes the transition from vegetative growth to the formation of reproductive hyphae, which ultimately differentiate into chains of spores.



The work presented in this thesis provides new insights into the biology of these prolific bacteria and demonstrates their ability to switch between the characteristic filamentous mode-of growth into a unicellular and cell wall-deficient state (Fig. 1). The study of single cells revealed information that is otherwise hidden by their multicellular, mycelial life style. **Chapter 2** describes the genetic diversity obtained after segregating the vegetative mycelium into protoplasts in the filamentous actinomycete *Kitasatospora viridifaciens*. Protoplast formation and regeneration revealed significant morphological heterogeneity of the colonies. In addition to grey-pigmented colonies that were similar to the parental strain, numerous bald and white colonies were found that were blocked in aerial growth and sporulation, respectively (Fig. 1). The bald colony phenotype was stable and coincided with loss of a 1.7 Mb megaplasmid, called KVP1, which is present in addition to the chromosome of 7.8 Mb. Further inspection of a bald colony by genome sequencing revealed major genomic rearrangements in the right arm of the chromosome. Notably, this phenotypic and genotypic heterogeneity was also observed in S-cells and L-forms switched from the wall-deficient to the filamentous mode-of growth (Fig. 1 and **Chapter 3**).

It is striking that genome rearrangements and loss of a non-essential replicon have such a drastic fate for filamentous actinomycetes. Indeed, the genome architecture of this organisms contemplates that essential genes are contained in the core of the chromosome and contingency genes, for instance those encoding for secondary metabolites, hydrolytic exoenzymes and conservons are located in the chromosomal arms[163] or on auxiliary plasmids[165,168]. Among the essential loci located in the central region of the chromosome are those required for growth, morphological differentiation, and protein secretion[289]. Indeed, BlastP searches of proteins involved in cell division and morphological differentiation (Table 1 in **Chapter 1**) revealed that neither KVP1 nor the right arm of the *K. viridifaciens* chromosome (6-7.8 Mb) contain any of the genes required for morphological differentiation.

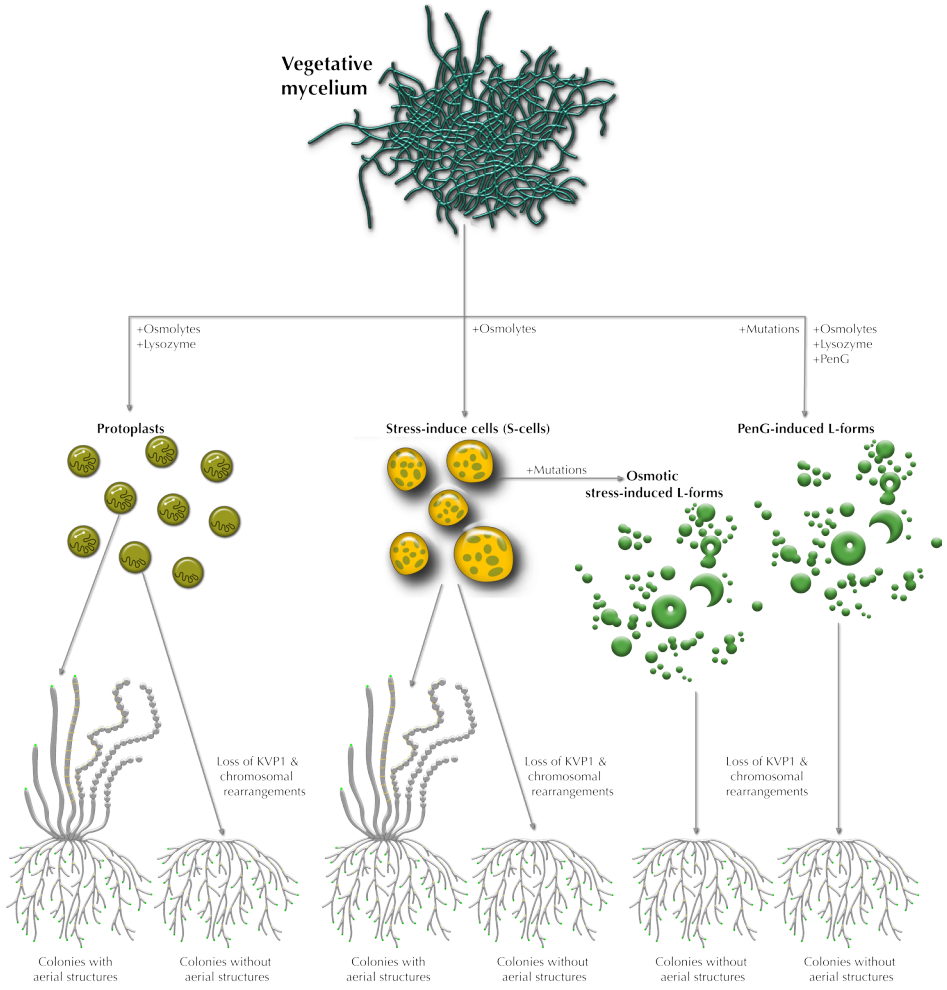


**Figure 1. Summarizing figure highlighting the three types of CWD cell types formed by *K. viridifaciens* and the main findings described in this thesis**. Protoplast formation and regeneration leads to morphological diversity, yielding colonies either with or without aerial structures. The colonies without aerial structures lack the megaplasmid KVP1 (represented as the white dumbbells inside the protoplast) and can also present chromosomal lesions (represented as a shorter black sribble inside the protoplast). In contrast, protoplasts that contain both the chromosome and KVP1 generate colonies that form aerial structures. While protoplasts are formed upon lysozyme treatment, S-cells (for Stress-induced cells) are extruded from the hyphal tips when the mycelium is exposed to hyperosmotic stress. These cells are larger than protoplasts and have the ability to switch to the mycelial mode-of-growth. Like with protoplasts, switching of S-cells generates colonies with different morphologies. Mycelial colonies that fail to form aerial hyphae carry major chromosomal lesions and have also lost KVP1. Prolonged exposure of S-cells to hyperosmotic stress can lead to the formation of L-forms. These osmotic stress-induced L-forms carry additional mutations that allow them to proliferate without their cell wall. Mutations are observed in L-forms derived from exposure to hyperosmotic stress, but also in those formed when mycelium is exposed to lysozyme and antibiotics (PenG-induced L-forms). All L-forms have lost the KVP1 plasmid and can be forced to grow as mycelium again, but exclusively yield colonies lacking aerial structures.

Genomic rearrangements leading to morphological defects are not exclusive for *K. viridifaciens*, as similar results have been reported for *Streptomyces clavuligerus*[290]. The authors demonstrated that the bald phenotype was due to loss of the 1.8 Mb pSCL4 megaplasmid that is present in *S. clavuligerus*. They confirmed this result by deleting the *parA-parB* genes located on pSCL4, which caused loss of the megaplasmid and generated a bald colony phenotype[180]. However, it is unknown if loss of pSCL4 also led to loss of part of the chromosome. Interestingly, large chromosomal rearrangements have been extensively studied before and are known as genetic instability[189,191,291]. Recently, the relevance of this genetic instability was demonstrated in *S. coelicolor*. Although large chromosomal deletions cause cells to become sterile, such profound genetic changes maximize the yield and diversity of antibiotic production. In a multicellular mycelium, compartments with wild-type genomes can focus on reproduction, while those carrying mutant genomes specialize in the production and secretion of costly antibiotics. Given that these antibiotics are mostly secreted, they benefit the entire colony. This thus represents a so-called division-of-labor strategy[185,292].

## Is life without a cell wall an escape from stress?

Although the cell wall is an essential component of virtually all bacteria, species from the bacterial class Mollicutes (*Mycoplasma*, *Spiroplasma*, *Phytoplasma*, *Acholeplasma*) appear to have undergone regressive evolution and lost their cell wall[293]. This adaptation corresponds to their parasitic life style and avoids recognition by the host immune system[294]. Strikingly, in **Chapter 3**, we observed that filamentous actinomycetes possess a natural ability to extrude cell wall-deficient cells, which we called S-cells (for Stress-induced cells). These cells were formed in media containing high levels of sucrose, sorbitol or sodium chloride, which are conditions causing hyperosmotic stress. Such S-cells are capable of switching back to the filamentous mode-of growth. A clear correlation was evident between retardation of filamentous growth and the presence of S-cells. These results indicate that S-cell formation and release is an adaption strategy that is deployed when the filamentous mode-of-growth is impaired by hyperosmotic stress. This stress response can be considered analogous to the process of sporulation, which is triggered when nutrient stress challenges vegetative growth.

Hyphae exposed to hyperosmotic stress show major morphological changes. One of the profound changes was the condensation of the nucleoids (**Chapter 3**,[193]). Chromosome condensation is a generic stress response[295,296], which was suggested to enable bacteria to rapidly and effectively cope with detrimental DNA lesions by facilitating homologous repair of double strand DNA breaks[297].

Likewise, transition to an L-form state may be an escape from stress. When *K. viridifaciens* was exposed to prolonged antibiotic or hyperosmotic stress, three independent L-form (*alpha*, M1, M2) mutant cell lines were isolated. Although these three strains carry different SNPs (see below), their whole genome sequencing revealed they all had lost the KVP1 megaplasmid and contain lesions in the right arm of the chromosome, all of which occurred at a similar site (see **Chapter 3**). Remarkably, the sites of these genomic rearrangements invariably contain insertion sequences (IS), which are the simplest and most widespread mobile genetic elements in prokaryotes[298]. The genome rearrangements may thus be the outcome of transposition events following activation of the IS (**Chapter 2**). Chen *et al* (2002) proposed a model of replicative transposition between linear replicons, which explained the loss of terminal regions and yielding mixed replicons that were an hybrid of the original plasmids and chromosomes[174]. We hypothesize that the replication of a transposable element can create a double stranded break in the DNA, which is later repaired by recombination, possibly by one of the numerous copies of the IS present in the right terminus of the megaplasmid.

Indeed, exposure to hyperosmotic stress or treatment with penicillin could act as an environmental stimulus activating transposable elements in *K. viridifaciens*, thereby generating genetic variability. This variability may allow the bacterium to withstand these stressful conditions and ultimately improve fitness. Bacteria are confronted with several challenging conditions such as a host-specific environment (macrophage, polyamines), radiation, oxidative stress, sub-inhibitory concentrations of metals or antibiotics, high temperatures and conjugative interactions, all of which have been shown to activate IS elements[192]. Notably, the absence of KVP1 and the large genomic rearrangements are not sufficient to promote L-form growth. In **Chapter 2** and **3**, we showed that regenerated protoplasts (B3.1) or switched S-cells (R3-R5) do not proliferate as L-form on media supporting L-form growth. Instead, L-form proliferation seems to be facilitated by certain point mutations that will be discussed in the following section.

## What promotes formation of CWD cells in filamentous actinomycetes?

Filamentous actinomycetes produce various types of CWD cells, such as protoplasts, S-cells and L-forms. Protoplast are formed by hydrolysis of peptidoglycan, which results in the segregation of the vegetative mycelium into uniform CWD cells. L-forms are mutants induced by stress conditions such as Penicillin G or hyperosmotic stress exposure. L-form cells are not homogenous in size, as biophysical mechanisms underlie shape and size differences. S-cells are formed in the presence of high concentrations of ionic (NaCl) or organic (sucrose or sorbitol) osmolytes. The S-cells are released from the hyphal tip as small vesicles, but increase in size over time (unlike protoplasts). However, S-cells do not proliferate in the wall-deficient state, but can do so sometimes when hyperosmotic stress conditions are prolonged. These three cell types have in common that they all lack a uniform cell wall structure, and are thus all susceptible to water and mild detergents. However, protoplasts appear to homogeneously regenerate their cell wall over time, while S-cells and L-forms often have wall material detaching from the cell surface.

Remarkably, *K. viridifaciens* seems to generate CWD cells more easily than other actinomycetes strains. A possible explanation is that *K. viridifaciens* has a genetic background that benefits the production of these CWD cells. For starters, this strain belongs to the *Kitasatospora* genus which has major differences in respect to the cell wall composition and the development regulation, when compared to species belonging to *Streptomyces* genus. While streptomycetes are rich in LL-diaminopimelic acid (DAP), cell wall hydrolysates of *Kitasatospora* strains present similar amounts of both LL-diaminopimelic acid (DAP) and meso-DAP[5,176,299]. Furthermore, representative species from the *Kitasatospora* genus lack *mbl*, *bldB* and *whiJ*, which are conserved genes in the development of *Streptomyces*[176]. Our analysis of *K. viridifaciens* revealed the absence of RdlA, RdlB, and RamS, which are required for production of rodlins and SapB. These proteins with surfactant properties form part of the hydrophobic sheath in aerial hyphae[300,301]. It is possible that absence of bio-surfactant could benefit the formation of CWD cells.

As *K. viridifaciens*, in **Chapter 3** we showed that four *Kitasatospora* strains can also extrude S-cells, however it is still unknown whether the genetic differences mentioned above predispose the hyphae to S-cell extrusion. In the following section, the three CWD cell types produced by *K. viridifaciens* will be compared including the adaptations required for S-cell formation and the mutations that accompany the conversion of S-cells into proliferating L-forms.

*Stress-induced cells (S-cells)*

As outlined above, S-cells are formed upon exposure of hyphae to hyperosmotic stress conditions. These conditions appear to have two effects that potentially contribute to the extrusion of S-cells. The first effect is the escape from the sacculus itself, which in *K. viridifaciens* appears to be a process that can occur naturally. Hyperosmotic conditions cause an arrest of growth at apical sites and extrusion of S-cells at the same hyphal tip (**Chapter 3**). Interestingly, these sites also appear to have a thinner cell wall structure (Eveline Ultee, unpublished results). Hyperosmotic shock causes a redistribution of DivIVA at polar growth site[193]. This redistribution could lead to thinning of the wall and also explains the formation of subapical branches. The hyphal tip is a dynamic structure, where several processes take place, including cell wall synthesis and protein secretion. It is also the site where synthesis of apical glycans occurs. This constant remodeling could contribute to the escape of S-cells, given that it creates a weak spot in the filament.

A second major step is the imbalance between cell wall and membrane synthesis, as hyperosmotic stress appears to stimulate membrane production in the filaments, as demonstrated in **Chapter 3**. The fraction of membrane inside the hyphae increased 11% in the presence of high levels of sucrose. Interestingly, several wild isolates from the Himalaya and Qinling mountains[209] were also capable of forming S-cell under hyperosmotic stress. Microorganisms in cold habitats need to protect themselves against freezing as well as hyperosmolarity, and upregulation of fatty acids biosynthetic genes as well as membrane adaptations are common mechanisms for cold tolerance[120,212].

In summary the two major factors that promote formation of S-cells in *K. viridifaciens* are resulting from the transient adaptation to hyperosmotic stress and do not require mutations.

*Hyperosmotic stress-induced L-forms*

Prolonged hyperosmotic stress promoted the transition of S-cells into L-forms (called M1 and M2), which are able to proliferate without their cell wall (**Chapter 3**). In contrast to S-cells, both L-form strains efficiently propagated in the presence of Penicillin G. Genome sequencing and SNP analysis of M1 and M2 revealed the presence of several point mutations in addition to the more profound changes described above. Remarkably, both cell lines had a mutation in the BOQ63_RS21920 locus, which encodes a putative metal ABC transporter ATPase. Interestingly, this protein has two domains that could be associated with adaptation to osmotic stress: the P-type ATPase and the haloacid dehalogenase (HAD) family domain. In *Mycobacterium tuberculosis*, the P-type ATPases are active transporters of metal cations which are activated under stress-conditions (oxidative stress and

starvation), and have been suggested to play a role in the intraphagosomal survival of this pathogen[302]. The MtlD (mannitol-1-phosphatase dehydrogenase) from *Acinetobacter baylyi* ADP1 has a highly conserved HAD domain at the N-terminus, and it is the enzyme responsible for responding to salinity and osmotic adaptation by synthesizing mannitol as compatible solute[303,304]. If this transporter relates to the ability of these L-form strains to proliferate without their cell wall is currently unknown.

*PenG-induced L-forms*

In the course of this thesis, we also obtained a cell line that was able to proliferate as an L-form but obtained after exposing the wild-type strain to high levels of penicillin and lysozyme. Genome sequence of this PenG-induced L-form cell line, called *alpha* (**Chapter 3**), revealed other types of mutations that could contribute to efficient proliferation in the L-form state. In addition to chromosomal rearrangement and concomitant loss of the megaplasmid KVP1, three SNPs were identified. One of the mutations mapped to a non-coding DNA region (NCR) between two putative genes encoding for a ROK (Repressor Open reading frame Kinase) family protein (BOQ63_RS10195) and an extracellular solute-binding protein (BOQ63_RS10205), respectively. A second mutation was identified in *lysX* (BOQ63_RS23890), which encodes a putative bifunctional phosphatidylglycerol lysyltransferase. The third SNP was in *uppP* (BOQ63_RS22750), which encodes an undecaprenyl-diphosphate phosphatase (UppP). Interestingly, the first mutations were found in the third subculture, during which KVP1 was lost and the point mutation in the non-coding region appeared. In the seventh and ninth subculture the mutations in *lysX* and *uppP* appeared, respectively (unpublished results).

During the L-form induction regime[208] the penicillin concentration was increased 10-fold in the second subculture (6 $mg \cdot ml^{-1}$). This elevated concentration of the antibiotic not only surpassed the Minimal Inhibitory Concentration (MIC) for the wild-type strain (1.5 $mg \cdot ml^{-1}$) but it also caused a noticeable change in the morphology of cells. More specifically, the diameter of the cells in the first subculture were considerably larger (>5µm) than those in the second subculture. The cells in the second subculture more resembled L-form cells in terms of their size. Altogether, these results suggested that mutations emerging in third subculture are probably caused by exposure to Penicillin G (PenG), while mutations acquired in later subcultures could play a role in the stabilization of L-form growth.

The mode of action of beta-lactams antibiotics is the inhibition of the penicillin-binding proteins (PBP) required for cross-linking of PG. However, they can also induce a toxic malfunction of the cell wall synthesis biosynthetic machinery that affects CW degradation[305]. In the tractable L-form system from *B.*

*subtilis* a point mutation in the *ispA* gene promoted L-form growth by counteracting the cellular levels of reactive oxygen species resulting from cell wall synthesis imbalance[143]. In the *K. viridifaciens* L-forms, two mutations could be involved in mitigation of the metabolic imbalance caused by Penicillin. The first one is the SNP located upstream of the ROK protein (BOQ63_RS10195), a kinase with 56% identity to NagK (N-acetylglucosamine kinase)[222], which was suggested to recover the degradation products of peptidoglycan making the recycled amino acids and amino sugars available as energy source[306]. The other SNP located in gene encoding the UppP, which is responsible for the recycling of undecaprenyl phosphate (UP), a lipid carrier required for cell wall assembly[307]. Inhibition of UPP phosphorylation by UppP, has a profound impact on cell envelop because it blocks PG and teichoic acid synthesis[308].

Mutations appearing later in the PenG induction suggest a role in the stability of a L-form, such as the SNP in LysX that could increase membrane rigidity. The *lysX* gene in *K. viridifaciens* has 54% identity to the *M. tuberculosis* LysX protein, which can transfer the lysine residue to the membrane bound phosphatidylglycerol to produce L-PG (lysyl-phosphatidylglicerol). In *M. tuberculosis* LysX-mediated production of L-PG improved membrane integrity by reducing its negative charge, which resulted in an increased resistance against antimicrobial peptides[309]. Likewise, increased positive charge in the membrane surface of *Enterococcus faecalis*, enhanced the rigidification of cell membranes contributing towards resistance[310].

## Can L-forms be exploited to study filamentous growth?

In **Chapter 4** we used *alpha*, the PenG-induced L-form to study the switch from wall-deficient to filamentous growth. This strain has the exceptional hallmark that it can switch from the wall-deficient state to the mycelial state (Fig. 2). We studied the morphological switch in *alpha* by making mutants in genes essential for filamentous actinomycetes. DivIVA is a protein found in Gram-positive bacteria, where it can play different roles; in firmicutes it is involved in cell division, while in actinobacteria DivIVA is required for the incorporation of new cell wall material[311]. Indeed in polar growing strains *divIVA* is an essential gene[78,81,312,313], which makes the *divIVA* null mutant in *alpha* the first example of a true knockout in a polar-growing strain. The deletion of *divIVA* or the partial disruption of the *dcw* gene cluster (*ftsW*, *murG*, *ftsQ*, *ftsZ*, *ylmD*, *ylmE*, *sepF*, *sepG* and *divIVA*), did not affect the growth or morphology of L-forms, but both mutations abolished the formation of mycelial colonies. Strikingly, when *divIVA* was reintroduced in the Δ*dcw* mutant, filamentous growth was restored.

A PG analysis revealed that the complemented mutant had a PG architecture that was similar to that of *alpha*. This also implies that the glycosyltransferase activity required for lipid II formation occurred in a MurG-independent manner. An *in silico* analysis of the *K. viridifaciens* genome revealed the presence of a *murG*-like gene outside the *dcw* cluster, which contained the two domains (PF03033 and PF04101) required for the transferase activity of UDP-N-acetylglucosamine to lipid I. We named this newly identified gene *murG2*. Phylogenetic analyses revealed that *murG2* is present in many filamentous actinomycetes, some of which even appear to have multiple copies. While a *murG* or *murG2* deletion strain was able to grow filamentous, a constructed double mutant (*murG*/*murG2*) blocked filamentous growth. This indicates that MurG2 is able to functionally replace the lipidII synthesis ability in the absence of MurG.

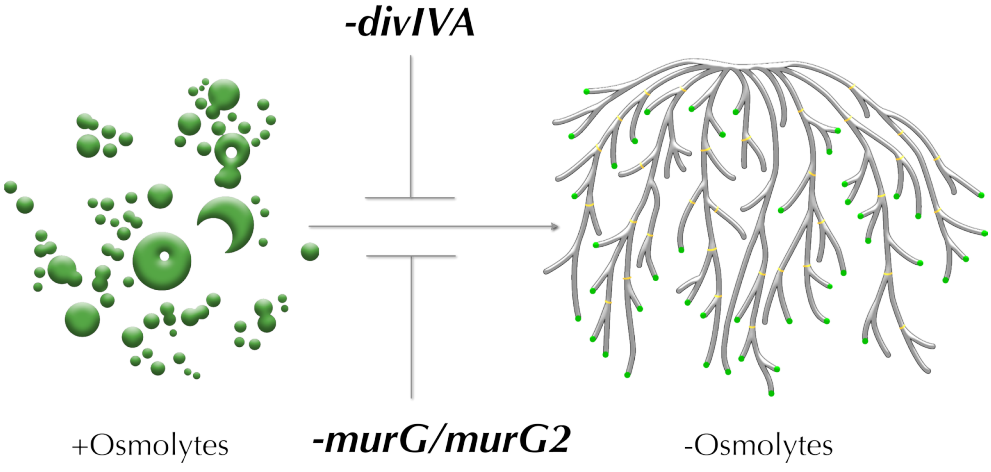


**Figure 2. The use of *alpha* as a platform to study filamentous growth**. The morphological switch from the L-form to the mycelial mode-of-growth occurs in response to the availability of osmolytes in the environment. The transition to filamentous growth is blocked by the deletion of *divIVA* or when both *murG* and *murG2* are absent.

## Are there biotechnological applications of CWD cells?

Another noteworthy result described in **Chapter 4** was the functional complementation of the Δ*dcw* mutant by the *dcw* gene cluster of *S. coelicolor*, which belongs to a different genus than *K. viridifaciens*. The introduction of the orthologous gene cluster restored filamentous growth, indicating that at least DivIVA was functional. Indeed, Western blot analysis using antibodies against DivIVA of *Corynebacterium glutamicum* confirmed the presence of the *S. coelicolor* DivIVA that is 5 kDa smaller than the *K. viridifaciens* DivIVA protein. These results suggest that the ability to switch between the wall-deficient and walled state is not specific to the *K. viridifaciens dcw* cluster. This proof-of-concept study paves the way for a rational morphology design approach. Instead of reintroducing *divIVA* of another filamentous actinomycetes as *S. coelicolor*, we could in the future try to introduce genes of *Mycobacterium* or *Corynebacterium* in *alpha*, in order to engineer a unicellular streptomycete with a cell wall. Unicellular walled streptomycetes could be used as an efficient cell factory in industry overcoming many limitations associated with mycelial growth[88,273].

Our results suggest that *alpha* could be used as screening platform to identify genes involved in this morphological switch or cell wall synthesis. In addition, L-forms are competent cells that can be easily modified genetically with various forms of DNA, such as plasmid, linear and chromosomal (unpublished results). These intrinsic properties of *K. viridifaciens* L-forms makes them attractive strains to study the minimal machinery for filamentous growth, as large deletions from essential genes can be made, and different combinations of cell wall and cell division genes can be tested to find the minimal set that allows the switch from the CWD to the walled state.

**Chapter 5** describes the first attempts to use actinomycetes L-forms as a host for enzyme production and secretion. We gained insight by comparing the secretion of a reporter cellulase Cel12A in both the L-form and mycelial state. The detection of cellulase activity in plates showed that production and secretion of a functional enzyme was possible in the absence of a cell wall. Production of enzymes in L-forms could also overcome in some cases the limited permeability of the cell wall, which sometimes acts as barrier for large molecules[275,314]. Remarkably, the secretion of mature Cel12A was also possible in the Δ*divIVA* and Δ*dcw* L-form mutants, indicating that DivIVA is not required for Tat secretion. In filamentous actinomycetes and fungi, enzyme secretion occurs at the hyphal tip[266,282,283]. Our data indicate that the Tat complex can also work in the absence of a functional tip complex.

The results in **Chapter 5** are promising as a starting point to further improve L-forms as an alternative production platform. Growth of filamentous actinomycetes poses several limitations due to the formation of dense mycelial pellets. As a consequence, this mycelial growth translates in slow growth rates, high viscosity, and culture heterogeneity[88,273]. L-forms, which grow as single cells could potentially overcome some of these disadvantages. Though the challenge to overcome is to make L-forms more robust.

This PhD started out with the characterization of the different types of CWD cells in *K. viridifaciens*. However, several research directions remain to be explored. Perhaps the most urgent questions relate to the ecological relevance of S-cells, and to find conditions and places in nature where this cell type may occur. Actinomycetes have evolved to live in symbiosis with plants, fungi and insects and maybe the conversion to CWD cells could occur in plant tissue. Although the requirements for the switch from L-form to filamentous growth were explored, the mechanism required for proliferation in the wall-less state have not been further characterized. These are important areas for further investigation. And as more studies are done, the importance and potential applications of CWD cells will also take off.

# NL

# Nederlandse Samenvatting

Filamenteuze actinomyceten komen veelvuldig voor in bijna alle ecosystemen[10]. Het succes van bacteriën in h*et al*gemeen komt door de aanwezigheid van een beschermende laag aan de buitenkant van de cellen, wat een celwand genoemd wordt. Daarnaast maken deze micro-organismen specifiek een groot scala aan enzymen en gespecialiseerde metabolieten die bijdragen aan dit succes. Hydrolytische enzymen maken het mogelijk om voedingsstoffen te winnen uit complexe polymeren, terwijl moleculen met antimicrobiële eigenschappen een vitale bescherming bieden tegen concurrerende microben[160]. In vergelijking tot de meeste andere bacteriën hebben veel filamenteuze actinomyceten een multicellulaire levensstijl. De actinomyceten die in dit proefschrift bestudeerd worden behoren tot de *Streptomycetaceae*, namelijk *Kitasatospora* en *Streptomyces*. Deze bacteriën vormen filamenten (hyfen genoemd) die groeien aan hun uiteinde en een complexe levenscyclus hebben. Na een periode van vegetatieve groei worden hyfen gevormd die de lucht in groeien en uiteindelijk differentiëren tot lange ketens van sporen.

Dit proefschrift biedt nieuwe inzichten in de biologie van deze bacteriën en laat zien dat ze kunnen switchen tussen hun kenmerkende filamenteuze manier van groeien en een groeiwijze die gekenmerkt wordt door de afwezigheid van de celwand (Figuur 1). **Hoofdstuk 2** beschrijft de genetische diversiteit die wordt aangetroffen in de filamenteuze actinomyceet *Kitasatospora viridifaciens* na het scheiden van het vegetatieve mycelium in losse cellen, zogenaamde protoplasten. Protoplastvorming en -regeneratie brachten een opvallende morfologische heterogeniteit aan het licht. Naast de grijs gepigmenteerde kolonies die sterk lijken op het wilde type, werden talloze kolonies gevonden die verstoord waren in het differentiatieproces. Zo bleek een groep van mutanten niet meer in staat om luchthyfen te vormen, wat samenviel met het verlies van een megaplasmide van 1,7 Mb (genaamd KVP1); dit plasmide is normaliter naast het chromosoom van 7,8 Mb aanwezig in *K. viridifaciens*. Sequencen van het genoom van één zo'n mutant liet zien dat er grote veranderingen hadden plaatsgevonden in de rechterarm van het chromosoom. Vergelijkbare effecten werden ook waargenomen in andere celtypen die tijdelijk zonder celwand hadden gegroeid (zie Figuur 1 en **Hoofdstuk 3**).

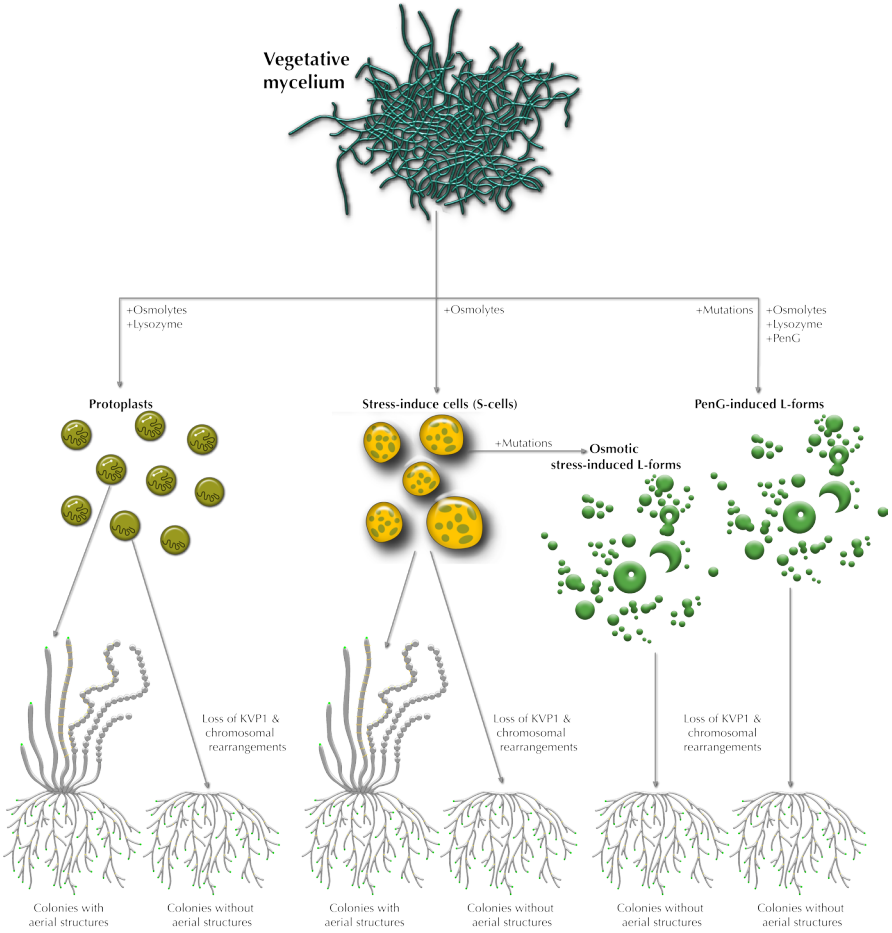


**Figuur 1. Overzicht van de verschillende typen celwandloze cellen van *Kitasatospora viridifaciens* en de belangrijkste bevindingen beschreven in dit proefschrift**. Protoplastvorming en -regeneratie leiden tot morfologische diversiteit, waardoor kolonies gevormd die al dan niet luchtstructuren (luchthyfen en sporen) kunnen vormen. Kolonies die geen luchtstructuren lijken te vormen missen het KVP1 megaplasmide (weergegeven als witte halters binnen protoplasten) en kunnen daarnaast ook grote chromosomale veranderingen vertonen. Daarentegen genereren protoplasten, die zowel het chromosoom als KVP1 bevatten, kolonies met luchtstructuren. Terwijl protoplasten worden gevormd na lysozym behandeling, worden S-cellen (voor Stress-geïnduceerde cellen) uitgescheiden aan de uiteinden van de hyfen wanneer het mycelium aan hyperosmotische stress wordt blootgesteld. Deze cellen zijn groter dan protoplasten en hebben het vermogen om terug te gaan naar mycelium groei. Net als bij protoplasten, leidt deze teruggang vaak tot morfologische heterogeniteit. Kolonies die niet meer in staat zijn om luchthyfen te vormen bevatten vaak grote chromosomale veranderingen en hebben het KVP1 plasmide verloren. Langdurige blootstelling van S-cellen aan hyperosmotische stress kan leiden tot de vorming van L-vormen. Deze door osmotische stress-geïnduceerde L-vormen hebben extra mutaties die hen in staat stellen zonder celwand te prolifereren. Er zijn ook mutaties aanwezig in L-vormen die gemaakt zijn na blootstelling van mycelium aan lysozym en penicilline (zogenaamde PenG-geïnduceerde L-vormen). Alle L-vormen hebben het KVP1-plasmide verloren en kunnen terugveranderen naar een mycelium, hoewel ze uitsluitend leiden tot kolonies die geen luchtstructuren meer kunnen maken.

Het is opvallend dat dergelijke veranderingen in het genoom en het verlies van een megaplasmide zulke drastische effecten hebben op de ontwikkeling van deze filamenteuze actinomyceten. Bestudering van de organisatie van het genoom laat namelijk zien dat de ons bekende essentiële genen die nodig zijn voor groei en morfologische differentiatie in de kern van de chromosoom zitten[163], terwijl de niet-essentiële genen, zoals bijvoorbeeld degene die coderen voor secundaire metabolieten en hydrolytische exo-enzymen, zich veelal in de armen van het chromosoom[289] bevinden of op plasmides[165,168].

Grote genomische veranderingen die leiden tot morfologische defecten zijn niet uniek voor *K. viridifaciens*, ze zijn ook waargenomen in streptomyceten, zoals bijvoorbeeld in *Streptomyces clavuligerus*[290]. De auteurs van dat werk lieten zien dat het onvermogen om te differentiëren het gevolg was van het verlies van het pSCL4 megaplasmide, dat 1.8 Mb groot is. Dit werd aangetoond door de parA-parB-genen op pSCL4 te verwijderen, waardoor het megaplasmide verloren ging[180]. Het is echter niet bekend of het verlies van pSCL4 ook gepaard is gegaan met het verlies van chromosomaal DNA zoals in het geval van *K. viridifaciens*. Grote chromosomale veranderingen zijn eerder uitgebreid bestudeerd en staan bekend als genetische instabiliteit[189,191,291]. Recentelijk werd de relevantie van deze genetische instabiliteit aangetoond in *Streptomyces coelicolor*, een actinomyceet verwant aan *K. viridifaciens*. Ondanks het feit dat cellen steriel lijken te worden door grote chromosomale deleties, zorgen deze ingrijpende genetische veranderingen tegelijkertijd voor een hogere productie en diversiteit van antibiotica. In een multicellulair mycelium kunnen compartimenten met wild-type genomen zich zodoende richten op reproductie, terwijl compartimenten met gemuteerde genomen zich kunnen specialiseren in de productie van dure antibiotica. Doordat deze antibiotica meestal worden uitgescheiden, profiteert uiteindelijk de hele kolonie, wat een klassiek voorbeeld is van een zogenaamde division-of-labor strategie[185,292].

## Is het leven zonder een celwand een ontsnapping aan stress?

Hoewel de celwand een essentieel onderdeel is van vrijwel alle bacteriën, lijken soorten uit de bacterieklasse *Mollicutes* (*Mycoplasma, Spiroplasma, Phytoplasma, Acholeplasma*) een regressieve evolutie te hebben ondergaan waardoor ze hun celwand hebben verloren[293]. Deze aanpassing komt overeen met hun parasitaire levensstijl en zorgt ervoor dat de herkenning door het immuunsysteem van de gastheer wordt vermeden[294]. In **Hoofdstuk 3** wordt aangetoond dat filamenteuze actinomyceten een natuurlijk vermogen hebben om celwand-deficiënte cellen te vormen en uit te scheiden, die we S-cellen hebben genaamd (voor stress-geïnduceerde cellen). Deze cellen worden gevormd in media met hoge hoeveelheden sucrose,

sorbitol of natriumchloride, die hyperosmotische stress veroorzaken en de groei van het mycelium belemmeren. S-cellen zijn tijdelijk celwandloos en in staat om te switchen naar de filamenteuze groeiwijze. Deze resultaten tonen aan dat de vorming van S-cellen een aanpassingsstrategie is die wordt toegepast wanneer de filamenteuze groei wordt aangetast door hyperosmotische stress. Deze stressreactie is in die zin vergelijkbaar met het sporulatieproces, dat geactiveerd wordt wanneer voedingsstress vegetatieve groei belemmert.

Hyfen die worden blootgesteld aan hyperosmotische stress vertonen grote morfologische veranderingen. Een van de opvallendste is de condensatie van de genomen (**Hoofdstuk 3**,[193]). Condensatie van het DNA is een veelvoorkomende stressreactie[295,296], waarvan gedacht wordt dat het bacteriën in staat stelt om snel en effectief om te gaan met nadelige DNA-schade[297]. De vorming van zogenaamde L-vormen – cellen die kunnen prolifereren zonder celwand – lijkt ook een aanpassing te zijn aan stresscondities. Door *K. viridifaciens* bloot te stellen aan langdurige antibiotische of hyperosmotische stress konden drie onafhankelijke L-vorm (*alpha*, M1, M2) cellijnen geïsoleerd worden. Hoewel deze stammen verschillende mutaties bevatten (zie hieronder), bleek na het sequencen van het genoom dat ze allemaal het KVP1-megaplasmide hadden verloren en dat ze grote stukken DNA verloren hadden in de rechterarm van het chromosoom (zie **Hoofdstuk 3**). Opmerkelijk is dat deze genomische veranderingen altijd insertie-sequenties (IS) bevatten, de eenvoudigste en meest wijdverspreide mobiele genetische elementen in prokaryoten[298]. Deze veranderingen kunnen dus het resultaat zijn van transpositie na de activatie van de IS (**Hoofdstuk 2**). Chen *et al*. (2002) hebben een model gepostuleerd hoe zogenaamde replicatieve transpositie tussen lineaire replicons (zoals die aanwezig zijn in deze filamenteuze bacteriën), kunnen leiden tot het verlies van grote stukken DNA in het genoom waarbij tevens hybride replicons worden gevormd die zijn opgebouwd uit stukken DNA van de oorspronkelijke plasmides en chromosomen[174]. We veronderstellen dat de replicatie van een transposon een dubbelstrengsbreuk in het DNA kan veroorzaken, die later wordt hersteld door recombinatie, mogelijk via een van de talrijke IS elementen die aanwezig zijn in de rechterarm van het lineaire megaplasmide. Wellicht dat de blootstelling aan hyperosmotische stress of de behandeling met penicilline stimulerend kunnen werken om dergelijke transponeerbare elementen te activeren. Dit zou de genetische variabiliteit verhogen, waardoor de bacterie stressvolle omstandigheden kan weerstaan en uiteindelijk zijn fitness kan verhogen. Bacteriën worden voortdurend geconfronteerd met uitdagende omstandigheden, zoals gastheer-specifieke omgevingen (macrofagen, polyaminen), straling, oxidatieve stress, schadelijke concentraties van metalen of antibiotica, hoge temperaturen en conjugatieve interacties. Het

is aangetoond dat al deze omstandigheden IS-elementen kunnen activeren[192]. Wat ook is vastgesteld is dat de afwezigheid van KVP1 en de grote genomische veranderingen niet voldoende zijn om de groei van L-vormen mogelijk te maken (zie **Hoofdstuk 2** en **3**). In plaats daarvan lijken bepaalde puntmutaties, die in de volgende alinea staan beschreven, nodig te zijn om proliferatie mogelijk te maken.

## Wat bevordert de vorming van celwand-deficiënte cellen in filamenteuze actinomyceten?

Er zijn nu verschillende typen celwandloze cellen bekend in filamenteuze actinomyceten, zoals protoplasten, S-cellen en L-vormen. Protoplasten worden verkregen door hydrolyse van het peptidoglycaan, waardoor uniforme celwand-deficiënte cellen vrij worden gemaakt uit het vegetatieve mycelium. L-vormen zijn mutanten die geïnduceerd worden door stress-omstandigheden, zoals de aanwezigheid van hoge concentraties penicilline G of hyperosmotische stress. L-vormen zijn niet homogeen in grootte, doordat biofysische mechanismen ten grondslag liggen aan vorm- en grootteverschillen. S-cellen worden gevormd in de aanwezigheid van hoge concentraties van ionische (NaCl) of organische (sucrose of sorbitol) osmolyten. Deze cellen komen vrij uit de hyfetop als kleine vesicles en nemen dan, in tegenstelling tot protoplasten, in grootte toe. S-cellen prolifereren echter niet in de wand-deficiënte toestand en worden slechts waargenomen wanneer hyperosmotische stressomstandigheden lang genoeg duren. Deze drie soorten celtypen hebben gemeen dat ze allemaal een uniforme celwandstructuur missen, waardoor ze gevoelig zijn voor water en detergentia. Protoplasten lijken echter hun celwand na verloop van tijd homogeen te regenereren, terwijl S-cellen en L-vormen wandmateriaal hebben dat vaak loslaat van het celoppervlak.

Opmerkelijk genoeg lijkt *K. viridifaciens* makkelijker S-cellen te produceren dan andere actinomyceten. Een mogelijke verklaring hiervoor is dat *K. viridifaciens* een genetische achtergrond heeft die de productie van S-cellen ten goede komt. Om te beginnen behoort deze stam tot het geslacht *Kitasatospora*, dat grote verschillen vertoont met streptomyceten, onder andere in de samenstelling van de celwanden en de regulatie van differentiatie. Celwandhydrolysaten van *Kitasatospora* stammen bevatten vergelijkbare hoeveelheden van zowel LL-diaminopimelinezuur (LL-DAP) als meso-DAP, terwijl streptomyceten alleen LL-DAP bevatten[5,176,299]. Bovendien missen *Kitasatospora* soorten *mbl, bldB* en *whiJ*, wat geconserveerde genen zijn die cruciaal zijn voor de ontwikkeling van *Streptomyces* soorten[176]. Onze analyse van het *K. viridifaciens* genoom onthulde verder dat de genen coderend voor RdlA, RdlB en RamS afwezig zijn. Deze eiwitten hebben oppervlakte-actieve eigenschappen en zijn onderdeel van de waterafstotende omhulling van luchthyfen[300,301].

Daarnaast worden ze ook uitgescheiden in het medium. Wellicht dat de afwezigheid van deze oppervlakte-actieve moleculen een positief effect heeft op de aanwezigheid van S-cellen.

In **hoofdstuk 3** staat beschreven dat zes andere *Kitasatospora* stammen ook S-cellen kunnen vormen. Het is nog niet bekend of de hierboven genoemde genetische verschillen bijdragen aan de vorming van S-cellen. In de volgende sectie zullen de drie celwandloze celtypen nader worden vergeleken en zullen de mutaties beschreven worden die nodig zijn voor de verandering van S-cellen naar zich delende L-vormen.

*Stress-geïnduceerde cellen (S-cellen)*

Zoals hierboven beschreven is worden S-cellen gevormd bij blootstelling van de hyfen aan hyperosmotische stresscondities. Deze condities lijken twee gevolgen te hebben die mogelijk bijdragen aan de vorming van S-cellen. Het eerste gevolg is het loskomen van de cellen uit de sacculus, een eigenschap die *K. viridifaciens* blijkbaar van nature bezit. Hyperosmotische condities zorgen voor een groeistop bij de apicale delen en uitscheiding van S-cellen aan het uiteinde van de hyfe (**Hoofdstuk 3**). Het interessante is dat deze delen ook een dunnere celwand lijken te hebben (Eveline Ultee, ongepubliceerde resultaten). Een hyperosmotische schok zorgt voor een herverdeling van DivIVA in de hyfen, dat normaliter aanwezig is aan het uiteinde van groeiende hyfen[193]. Deze herverdeling zou kunnen leiden tot het verdunnen van de celwand en verklaart de vorming van sub-apicale zijtakken. Het uiteinde van de hyfe is een dynamische structuur waar verschillende processen plaatsvinden, waaronder celwandsynthese en eiwituitscheiding. Dit is ook de plek waar synthese van glycanen plaatsvindt. Deze constante veranderingen zouden kunnen bijdragen aan het loslaten van de S-cellen, gezien dat dit door deze activiteiten een zwakke plek in het filament is.

Het tweede belangrijke gevolg van hyperosmotische stress is de onbalans tussen celwand- en membraansynthese. De hoge concentraties osmolyten lijken de membraanproductie in filamenten te stimuleren, zoals aangetoond is in **Hoofdstuk 3**. De membraanfractie in de hyfen was 11% hoger wanneer mycelium gegroeid werd in de aanwezigheid van veel sucrose. Een aantal wilde stammen uit het Himalaya of Qinling gebergte[209] bleken ook S-cellen te vormen onder invloed van hyperosmotische stress. Micro-organismen die voorkomen in koude omgevingen zullen zichzelf moeten beschermen tegen bevriezing en hyperosmolariteit. Een toename van lipopolysacchariden of veranderingen in het membraan zijn veelvoorkomende mechanismen van koudetolerantie[120,212]. Dus twee belangrijke factoren die S-cel formatie in *K. viridifaciens* mogelijk maken zijn het resultaat van een tijdelijke aanpassing aan hyperosmotische stress, waar verder geen mutaties voor nodig zijn.

*Hyperosmotische stress-geïnduceerde L-vormen*

Langdurige blootstelling aan hyperosmotische stresscondities induceerde de overgang van S-cellen naar L-vormen (M1 en M2 genoemd), die kunnen prolifereren zonder hun celwand (**Hoofdstuk 3**). Tevens konden deze L-vormen efficiënt prolifereren in de aanwezigheid van penicilline G. Het sequencen van het genoom en de daaropvolgende SNP analyse brachten enkele interessante puntmutaties aan het licht, naast de grote genomische veranderingen zoals die hierboven reeds beschreven zijn. Opmerkelijk is dat beide cellijnen een mutatie hadden in het BOQ63_RS21920 locus, wat codeert voor een mogelijke metaal ABC transporter. Het interessante is dat dit eiwit twee domeinen heeft die geassocieerd kunnen worden met aanpassingen tegen osmotische stress: het P-type ATPase en het halozuur dehalogenase (HAD) domein. In *Mycobacterium tuberculosis* worden P-type ATPases gebruikt voor het actief transport van metaalionen. Deze transporters worden geactiveerd bij stresscondities, zoals oxidatieve stress en uithongering, en zijn mogelijk betrokken bij de intrafagosomale overleving van deze pathogeen[302]. Het MtlD (mannitol-1-fosfatase dehydrogenase) eiwit van *Acinetobacter baylyi* ADP1 heeft een sterk geconserveerd HAD domein in het N-terminale deel, en dit enzym is betrokken bij het proces van osmotische aanpassing door het maken mannitol als “compatibele solute”[303,304]. Of deze transporter iets te maken heeft met het vermogen van L-vormen om te prolifereren zonder celwand is nog onbekend.

*PenG-geïnduceerde L-vormen*

In de loop van dit promotieonderzoek hebben wij ook een cellijn verkregen die zich vermenigvuldigde als een L-vorm maar die echter verkregen was na langdurige blootstelling van het wilde type aan penicilline en lysozym. Deze cellijn werd gemaakt volgens een bepaald inductie regime, waarbij gedurende een periode van enkele maanden wekelijks nieuwe subcultures werden geïnoculeerd in de aanwezigheid van stoffen die de celwandaanmaak verstoren. Het sequencen van het genoom van deze met penicilline geïnduceerde L-vorm cellijn, *alpha* genoemd (**Hoofdsuk 3**), onthulde andere mutaties die mogelijk bijdragen tot het efficiënt kunnen prolifereren als L-vorm. Naast de reeds genoemde grote chromosomale veranderingen en het verlies van KVP1 werden drie puntmutaties (zogenaamde SNPs) geïdentificeerd. Één van de mutaties ligt in de niet-coderende regio van het DNA, tussen twee genen die coderen voor een zogenaamde ROK kinase (BOQ63_RS10195) en een extracellulair oplosstof-bindend eiwit (BOQ63_RS10205). Een tweede mutatie werd geïdentificeerd in *lysX* (BOQ63_RS23890), wat codeert voor een mogelijk bifunctioneel fosfatidylglycerol lysyltransferase enzym. De derde SNP bevond zich in *uppP* (BOQ63_RS22750), die codeert

voor een undecaprenyl-difosfaat fosfatase (UppP). Interessant is dat de eerste mutaties gevonden werden in de derde subcultuur, waarbij naast het verlies van KVP1 ook de puntmutatie in de niet-coderende regio verscheen. In de zevende en negende subcultuur zijn respectievelijk de mutaties in *lysX* en *uppP* verschenen (niet-gepubliceerde resultaten).

Gedurende het gebruikte L-vorm inductie regime[208] werd de penicilline concentratie tienmaal verhoogd in de tweede subcultuur (6 mg·ml-1). Deze verhoogde antibioticum concentratie was ni*et al*leen veel hoger dan de Minimale Inhiberende Concentratie (MIC) van het wilde type (1.5 mg·ml-1), maar leidde ook tot een zichtbare verandering in de morfologie van de cellen. Zo was de diameter van de cellen in de eerste subcultuur significant groter (>5µm) dan die van de tweede subcultuur. De cellen in de tweede subcultuur leken meer op L-vorm cellen wat betreft hun grootte. Deze resultaten suggereren dat de mutaties die ontstaan zijn in de derde subcultuur waarschijnlijk veroorzaakt zijn door blootstelling aan penicilline, terwijl mutaties opgedaan in latere subculturen mogelijk leidden tot efficiënte groei als L-vorm.

Het werkingsmechanisme van beta-lactam antibiotica is het inhiberen van de penicilline-bindende eiwitten (PBP) die betrokken zijn bij het crosslinken van PG[305]. Echter, deze antibiotica kunnen ook een toxische verstoring van de celwand biosynthese systemen teweegbrengen die de celwandafbraak beïnvloed. In *B. subtilis* bevorderde een puntmutatie in het *ispA* gen de L-vorm groei, doordat deze mutatie het ontstaan van zuurstofradicalen tegengaat, die veroorzaakt worden door een onbalans in de celwandsynthese route[143]. In *K. viridifaciens* zijn twee mutaties die mogelijk betrokken zijn bij het compenseren voor de metabolische onbalans veroorzaakt door penicilline. De eerste mutatie is de SNP in het niet-coderende DNA voor het gen BOQ63_RS10195, coderend voor een ROK-kinase die 56% homoloog is aan NagK (N-acetylglucosamine kinase)[222]. NagK is betrokken bij de opname van de afbraakproducten van peptidoglycaan, waardoor gerecyclede aminozuren en aminosuikers weer beschikbaar gemaakt worden als energiebron[306]. De andere SNP ligt in het *uppP* gen, welke verantwoordelijk is voor het recyclen van undecaprenylfosfaat (UP), een lipide transporter benodigd voor de opbouw van de celwand[307]. Remming van UPP forforylering door UppP heeft een sterk effect op de celenvelop omdat het de synthese van PG en teichoinezuren blokkeert[308].

Mutaties die later zijn verschenen zouden een rol kunnen spelen in het verder stabiliseren van de L-vorm, zoals de SNP in LysX, die de stevigheid van het membraan zou kunnen verhogen. Het *lysX* gen in *K. viridifaciens* vertoont 54% homologie met het *M. tuberculosis* LysX eiwit, die een lysine residu aan het membraangebonden fosfatidylglycerol kan koppelen om L-PG te vormen (lysylfosfatidylglycerol). In *M. tuberculosis*

leidde de productie van L-PG voor een verbeterde membraanintegriteit door vermindering van de negatieve lading, wat weer leidde tot een verhoogde resistentie tegen antimicrobiële peptiden[309]. Op een vergelijkbare manier resulteerde een meer positieve lading in het membraanoppervlak van *Enterococcus faecalis* tot meer stevigheid van de celmembraan en een verhoogde resistentie[310].

## Kunnen L-vormen worden gebruikt om filamenteuze groei te bestuderen?

In **Hoofdstuk 4** hebben wij *alpha*, de met penicilline-geïnduceerde L-vorm, gebruikt om de overgang van celwandloze groei naar filamenteuze groei te bestuderen. Deze stam heeft het uitzonderlijke vermogen om over te schakelen van een celwandloze toestand naar groei als een mycelium (Fig. 2). Wij hebben de morfologische overgang in *alpha* bestudeerd door mutanten te creëren in genen die essentieel zijn voor filamenteuze groei. DivIVA is een eiwit dat aanwezig is in Gram-positieve bacteriën, waar het verschillende functies kan hebben; in Firmicutes is het eiwit betrokken bij celdeling, terwijl DivIVA in actinobacteriën nodig is voor de inbouw van nieuw celwandmateriaal[311]. De deletie van *divIVA* of de gedeeltelijke disruptie van het *dcw* gencluster in *alpha* (*ftsW, murG, ftsQ, ftsZ, ylmD, ylmE, sepF, sepG* en *divIVA*) bleek geen effect te hebben op de groei of morfologie van L-vormen, maar beide mutaties blokkeerden een switch naar filamenteuze groei. Verrassenderwijs kon filamenteuze groei hersteld worden wanneer *divIVA* werd teruggeplaatst in de Δ*dcw* mutant. Een PG-analyse liet zien dat de gecomplementeerde mutant eenzelfde PG-architectuur had als *alpha*. Dit suggereert dat de glycosyltransferase-activiteit benodigd voor de vorming van lipid II en normaliter verzorgd door MurG, blijkbaar ook door een ander eiwit tot stand gebracht kan worden. Een in *silico* analyse van het *K. viridifaciens* genoom liet zien dat er een gen buiten het *dcw* cluster lag, coderend voor een MurG-achtig eiwit dat de twee domeinen (PF03033 en PF04101) bleek te bezitten die potentieel nodig zijn voor de koppeling van UDP-N-acetylglucosamine aan lipide I. Dit nieuwgeïdentificeerde gen hebben wij *murG2* benoemd. Een fylogenetische analyse toonde aan dat *murG2* genen aanwezig zijn in tal van filamenteuze actinomyceten, waarbij sommige soorten zelfs meerdere kopieën lijken te hebben. Een genetische analyse liet zien dat mutanten die ofwel *murG* of *murG2* missen in staat zijn over te gaan tot filamenteuze groei. Dit in tegenstelling tot de *murG*/*murG2* dubbel mutant, die alleen kon groeien als L-vorm maar geen mycelium meer kon maken. Dit laat zien dat MurG2 de synthese van lipide II mogelijk maakt in de afwezigheid van MurG.

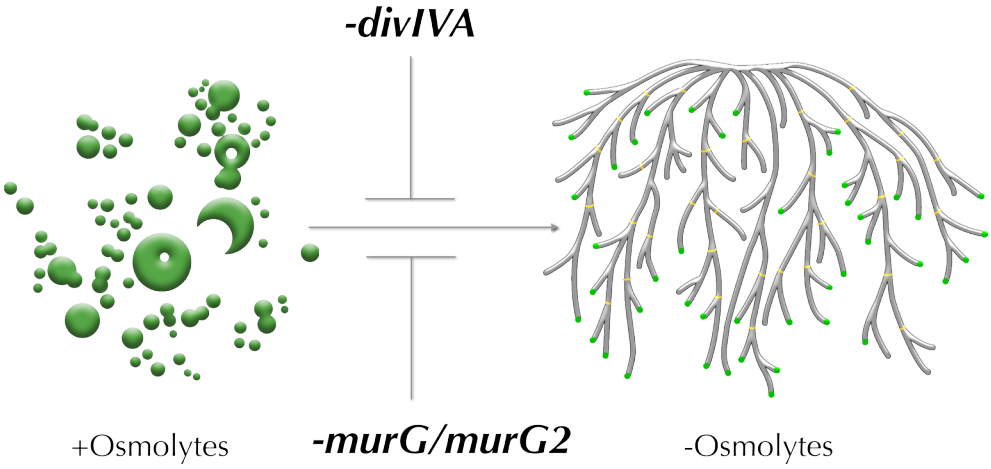


**Figuur 2. Het gebruik van *alpha* om filamenteuze groei te bestuderen.** De morfologische overgang van L-vorm naar filamenteuze groei vindt plaats als reactie op de beschikbaarheid van osmolyten in de omgeving. De transitie naar filamenteuze groei is geblokkeerd in de afwezigheid van *divIVA* of wanneer zowel *murG* als *murG2* afwezig zijn.

## Zijn er biotechnologische toepassingen voor celwandloze cellen?

Een ander opmerkelijk resultaat, beschreven in **Hoofdstuk 4**, was de functionele complementatie van de Δ*dcw* mutant door het dcw gencluster van *S. coelicolor*, welke tot een ander genus behoort dan *K. viridifaciens*. Het introduceren van het orthologe gencluster herstelde filamenteuze groei, wat aanduidt dat in ieder geval DivIVA functioneel tot expressie kwam. Een Western blot analyse bevestigde inderdaad de aanwezigheid van het *S. coelicolor* DivIVA eiwit, wat 5 kDa kleiner is dan het DivIVA eiwit uit *K. viridifaciens*. Deze resultaten suggereren dat het vermogen om te wisselen tussen celwandloze en celwandbevattende groeistatus niet specifiek is voor het *K. viridifaciens dcw* cluster. Deze 'proof-of-concept' studie maakt de weg vrij om de morfologie van filamenteuze bacteriën aan te passen middels een rationele aanpak. Zo zouden we in

de toekomst genen kunnen gaan introduceren van *Mycobacterium* of *Corynebacterium* in *alpha*, om zo een eencellige streptomyceet met een celwand te ontwerpen. Eencellige celwand-bevattende streptomyceten zouden gebruikt kunnen worden als een efficiënte celfabriek, om hiermee de vele beperkingen geassocieerd met myceliumgroei in de industrie te omzeilen[88,273]. Onze resultaten laten tevens zien dat alpha gebruikt zou kunnen worden als screeningsplatform voor het identificeren van genen betrokken bij deze morfologische overgang of celwandsynthese. Daarnaast zijn L-vormen competente cellen die eenvoudig genetisch gemodificeerd kunnen worden met verscheidenen typen van DNA, zoals plasmide, lineair en chromosomaal DNA (niet-gepubliceerde resultaten). Deze eigenschappen maken L-vormen interessante stammen om de minimale machinerie voor filamenteuze groei te bestuderen, gezien er eenvoudig deleties van “essentiële genen” gemaakt kunnen worden, en verschillende combinaties van celwand en celdelingsgenen getest kunnen worden om de minimale set te vinden die de overgang van celwandloze naar celwandbevattende toestand mogelijk maakt.

In **Hoofdstuk 5** wordt beschreven hoe L-vormen van actinomyceten als een gastheer voor enzymproductie te gebruiken zijn. Wij hebben meer inzicht gekregen in dit proces door het vergelijken van de uitscheiding van een reporter cellulase tijdens groei van *alpha* als L-vorm of als mycelium. De aangetoonde cellulase activiteit in platen liet zien dat de productie en secretie van een functioneel enzym mogelijk was zonder celwand. Enzymproductie in L-vormen zou in sommige gevallen de beperkte permeabiliteit van de celwand kunnen omzeilen, die als een barrière kan fungeren voor grote moleculen[275,314]. Opmerkelijk is dat de uitscheiding van functioneel Cel12A ook mogelijk was in de Δ*divIVA* en Δ*dcw* L-vorm mutanten, wat er op duidt dat DivIVA niet nodig is voor secretie van dit Tat-substraat. In filamenteuze actinomyceten en schimmels vindt enzymsecretie plaats aan het uiteinde van de hyfe, waar het Tat secretie complex zich bevindt[266,282,283]. Onze data geeft aan dat het Tat complex ook functioneert zonder functioneel tip complex.

De resultaten in **Hoofdstuk 5** zijn een veelbelovend beginpunt om L-vormen verder te verbeteren als een alternatief productieplatform. Groei van filamenteuze actinomyceten leidt vaak tot de ontwikkeling van compacte pellets. Deze manier van groeien vertaalt zich in een lage groeisnelheid, hoge viscositeit en een heterogene cultuur[88,273]. L-vormen, die als eencelligen groeien, zouden hierbij wellicht een oplossing kunnen zijn. De uitdaging is dan om L-vormen meer robuust te maken, zodat ze ook effectief gebruikt kunnen worden in een fermenter, waar cellen normaliter blootgesteld worden aan hoge shear stress.

Dit onderzoek heeft zich gericht op de karakterisatie van de verschillende typen celwandloze cellen in *K. viridifaciens*. Echter, er zijn nog vele andere onderzoeksrichtingen denkbaar. Wellicht de meest urgente vragen hebben betrekking op de ecologische relevantie van S-cellen, en om de condities en plekken in de natuur te vinden waar deze cellen zouden kunnen voorkomen. Actinomyceten zijn geëvolueerd om in symbiose te leven met planten, schimmels en insecten, en wellicht zou de omschakeling naar celwandloze cellen bijvoorbeeld kunnen plaatsvinden in plantenweefsel. Daarnaast kan toekomstig onderzoek zich richten op de vraag hoe L-vormen van actinomyceten kunnen prolifereren zonder celwand, en wat de rol is van de mutaties die geïdentificeerd zijn in de verschillende L-vorm cellijnen. Op die manier zullen ook het belang en de mogelijke toepassingen van celwandloze cellen inzichtelijk worden.

# RF

# References


**1** Ventura, M. *et al. Genomics of Actinobacteria*: tracing the evolutionary history of an ancient phylum. *Microbiol Mol Biol Rev* **71**, 495-548, doi : 10.1128/MMBR.00005-07 (2007).

**2** Barka, E. A. *et al.* Taxonomy, physiology, and natural products of *Actinobacteria. Microbiol Mol Biol Rev* **80**, 1-43, doi:10.1128/MMBR.00019-15 (2016).

**3** Kämpfer, P. in *The Prokaryotes: Volume 3: Archaea. Bacteria: Firmicutes, Actinomycetes* (eds Martin Dworkin *et al*.) 538-604 (Springer New York, 2006).

**4** Girard, G. *et al*. A novel taxonomic marker that discriminates between morphologically complex actinomycetes. *Open Biol* **3**, 130073, doi:10.1098/rsob.130073 (2013).

**5** Zhang, Z., Wang, Y. & Ruan, J. A proposal to revive the genus *Kitasatospora* (Omura, Takahashi, Iwai, and Tanaka 1982). *Int J Syst Bacteriol* **47**, 1048-1054, doi:10.1099/00207713-47-4-1048 (1997).

**6** Kim, S. B., Lonsdale, J., Seong, C. N. & Goodfellow, M. *Streptacidiphilus* gen. nov., acidophilic actinomycetes with wall chemotype I and emendation of the family *Streptomycetaceae* (Waksman and Henrici (1943) AL) emend. Rainey *et al*. 1997. *Antonie Van Leeuwenhoek* **83**, 107-116 (2003).

**7** Schrempf, H. in *The Prokaryotes: Volume 3: Archaea. Bacteria: Firmicutes, Actinomycetes* (eds Martin Dworkin *et al*.) 605-622 (Springer New York, 2006).

**8** Flärdh, K. & Buttner, M. J. *Streptomyces* morphogenetics: dissecting differentiation in a filamentous bacterium. *Nat Rev Microbiol* **7**, 36-49, doi:10.1038/nrmicro1968 (2009).

**9** McCormick, J. R. Cell division is dispensable but not irrelevant in *Streptomyces*. *Curr Opin Microbiol* **12**, 689-698, doi:10.1016/j.mib.2009.10.004 (2009).

**10** van der Meij, A., Worsley, S. F., Hutchings, M. I. & van Wezel, G. P. Chemical ecology of antibiotic production by actinomycetes. *FEMS Microbiol Rev* **41**, 392-416, doi:10.1093/femsre/fux005 (2017).

**11** Jakimowicz, D. & van Wezel, G. P. Cell division and DNA segregation in *Streptomyces*: how to build a septum in the middle of nowhere? *Mol Microbiol* **85**,393-404, doi:10.1111/j.1365-2958.2012.08107.x (2012).

**12** Merrick, M. J. A morphological and genetic mapping study of bald colony mutants of *Streptomyces coelicolor. J Gen Microbiol* **96**, 299-315 (1976).

**13** Nguyen, K. T. *et al*. Colonial differentiation in *Streptomyces coelicolor* depends on translation of a specific codon within the *adpA* gene. *J Bacteriol* **185**, 7291-7296 (2003).

**14** Hopwood, D. A., Wildermuth, H. & Palmer, H. M. Mutants of *Streptomyces coelicolor* defective in sporulation. *J Gen Microbiol* **61**, 397-408 (1970).

**15** Chater, K. F. A morphological and genetic mapping study of white colony mutants of *Streptomyces coelicolor. J Gen Microbiol* **72**, 9-28 (1972).

**16** Claessen, D., de Jong, W., Dijkhuizen, L. & Wösten, H. A. B. Regulation of *Streptomyces* development: reach for the sky! *Trends Microbiol* **14**, 313-319, doi:10.1016/j.tim.2006.05.008 (2006).

**17** Willey, J. M., Santamaria, R., Guijarro, J., Geistlich, M. & Losick, R. Extracellular complementation of a developmental mutation implicates a small sporulation protein in aerial mycelium formation by *S. coelicolor*. *Cell* **65**, 641-650 (1991).

**18** Claessen, D. *et al*. Two novel homologous proteins of *Streptomyces coelicolor* and *Streptomyces lividans* are involved in the formation of the rodlet layer and mediate attachment to a hydrophobic surface. *Mol Microbiol* **44**, 1483-1492 (2002).

**19** Claessen, D. *et al*. A novel class of secreted hydrophobic proteins is involved in aerial hyphae formation in *Streptomyces coelicolor* by forming amyloid-like fibrils. *Genes & Development* **17**, 1714-1726, doi:10.1101/gad.264303 (2003).

**20** Elliot, M. A. *et al*. The chaplins: a family of hydrophobic cell-surface proteins involved in aerial mycelium formation in *Streptomyces coelicolor*. *Genes Dev* **17**, 1727-1740, doi:10.1101/gad.264403 (2003).

**21** Claessen, D. *et al*. The formation of the rodlet layer of streptomycetes is the result of the interplay between rodlins and chaplins. *Mol Microbiol* **53**, 433-443, doi:10.1111/j.1365-2958.2004.04143.x (2004).

**22** Yang, W. *et al*. The propensity of the bacterial rodlin protein RdlB to form amyloid fibrils determines its function in *Streptomyces coelicolor*. *Sci Rep* **7**, 42867, doi:10.1038/srep42867 (2017).

**23** de Jong, W., Wösten, H. A. B., Dijkhuizen, L. & Claessen, D. Attachment of *Streptomyces coelicolor* is mediated by amyloidal fimbriae that are anchored to the cell surface via cellulose. *Mol Microbiol* **73**, 1128-1140, doi:10.1111/j.1365-2958.2009.06838.x (2009).

**24** Xu, H., Chater, K. F., Deng, Z. & Tao, M. A cellulose synthase-like protein involved in hyphal tip growth and morphological differentiation in *Streptomyces. J Bacteriol* **190**, 4971-4978, doi:10.1128/JB.01849-07 (2008).

**25** Whittaker, M. M. & Whittaker, J. W. *Streptomyces coelicolor* oxidase (SCO2837p): a new free radical metalloenzyme secreted by *Streptomyces coelicolor* A3(2). *Arch Biochem Biophys* **452**, 108-118, doi:10.1016/j.abb.2006.06.020 (2006).

**26** Chaplin, A. K. *et al*. GlxA is a new structural member of the radical copper oxidase family and is required for glycan deposition at hyphal tips and morphogenesis of *Streptomyces lividans*. *Biochem J* **469**, 433-444, doi:10.1042/bj20150190 (2015).

**27** Liman, R., Facey, P. D., van Keulen, G., Dyson, P. J. & Del Sol, R. A laterally acquired galactose oxidase-like gene is required for aerial development during osmotic stress in *Streptomyces coelicolor*. *PLoS One* **8**, e54112, doi:10.1371/journal.pone.0054112 (2013).

**28** Petrus, M. L. C. & Claessen, D. Pivotal roles for *Streptomyces* cell surface polymers in morphological differentiation, attachment and mycelial architecture. *Antonie Van Leeuwenhoek* **106**, 127-139, doi:10.1007/s10482-014-0157-9 (2014).

**29** McCormick, J. R., Su, E. P., Driks, A. & Losick, R. Growth and viability of *Streptomyces coelicolor* mutant for the cell division gene *ftsZ*. *Mol Microbiol* **14**, 243-254 (1994).

**30** Santos-Beneit, F., Roberts, D. M., Cantlay, S., McCormick, J. R. & Errington, J. A mechanism for FtsZ-independent proliferation in *Streptomyces. Nat Commun* **8**, 1378, doi:10.1038/s41467-017-01596-z (2017).

**31** McCormick, J. R. & Losick, R. Cell division gene *ftsQ* is required for efficient sporulation but not growth and viability in *Streptomyces coelicolor* A3(2). *J Bacteriol* **178**, 5295-5301 (1996).

**32** Bennett, J. A. *et al*. Medium-dependent phenotypes of *Streptomyces coelicolor* with mutations in *ftsI or ftsW. J Bacteriol* **191**, 661-664, doi:10.1128/JB.01048-08 (2009).

**33** Mistry, B. V., Del Sol, R., Wright, C., Findlay, K. & Dyson, P. FtsW is a dispensable cell division protein required for Z-ring stabilization during sporulation septation in *Streptomyces coelicolor. J Bacteriol* **190**, 5555-5566, doi:10.1128/JB.00398-08 (2008).

**34** Bennett, J. A., Aimino, R. M. & McCormick, J. R. *Streptomyces coelicolor* genes *ftsL* and *divIC* play a role in cell division but are dispensable for colony formation. *J Bacteriol* **189**, 8982-8992, doi:10.1128/JB.01303-07 (2007).

**35** Kawamoto, S. & Ensign, J. C. Isolation of mutants of *Streptomyces griseus* that sporulate in nutrient rich media: cloning of DNA fragments that suppress the mutations. *Actinomycetologica* **9**, 124-135 (1995).

**36** Kawamoto, S., Watanabe, H., Hesketh, A., Ensign, J. C. & Ochi, K. Expression analysis of the *ssgA* gene product, associated with sporulation and cell division in *Streptomyces griseus. Microbiology* **143**, 1077-1086 (1997).

**37** Keijser, B. J. F., Noens, E. E. E., Kraal, B., Koerten, H. K. & van Wezel, G. P. The *Streptomyces coelicolor ssgB* gene is required for early stages of sporulation. *FEMS Microbiol Lett* **225**, 59-67 (2003).

**38** Sevcikova, B. & Kormanec, J. The *ssgB* gene, encoding a member of the regulon of stress-response sigma factor σH, is essential for aerial mycelium septation in *Streptomyces coelicolor* A3(2). *Arch Microbiol* **180**, 380-384, doi:10.1007/s00203-003-0603-y (2003).

**39** Willemse, J., Borst, J. W., de Waal, E., Bisseling, T. & van Wezel, G. P. Positive control of cell division: FtsZ is recruited by SsgB during sporulation of *Streptomyces. Genes Dev* **25**, 89-99, doi:10.1101/gad.600211 (2011).

**40** Leskiw, B. K., Lawlor, E. J., Fernandez-Abalos, J. M. & Chater, K. F. TTA codons in some genes prevent their expression in a class of developmental, antibiotic-negative, *Streptomyces* mutants. *Proc Natl Acad Sci U S A* **88**, 2461-2465 (1991).

**41** Lawlor, E. J., Baylis, H. A. & Chater, K. F. Pleiotropic morphological and antibiotic deficiencies result from mutations in a gene encoding a tRNA-like product in *Streptomyces coelicolor* A3(2). *Genes Dev* **1**, 1305-1310 (1987).

**42** Pope, M. K., Green, B. & Westpheling, J. The *bldB* gene encodes a small protein required for morphogenesis, antibiotic production, and catabolite control in *Streptomyces coelicolor*. *J Bacteriol* **180**, 1556-1562 (1998).

**43** Eccleston, M., Ali, R. A., Seyler, R., Westpheling, J. & Nodwell, J. Structural and genetic analysis of the BldB protein of *Streptomyces coelicolor*. *J Bacteriol* **184**, 4270-4276 (2002).

**44** Eccleston, M., Willems, A., Beveridge, A. & Nodwell, J. R. Critical residues and novel effects of overexpression of the *Streptomyces coelicolor* developmental protein BldB: evidence for a critical interacting partner. *J Bacteriol* **188**, 8189-8195, doi:10.1128/JB.01119-06 (2006).

**45** Bush, M. J., Chandra, G., Al-Bassam, M. M., Findlay, K. C. & Buttner, M. J. BldC delays entry into development to produce a sustained period of vegetative growth in *Streptomyces venezuelae*. *MBio* **10**, doi:10.1128/mBio.02812-18 (2019).

**46** Hunt, A. C., Servín-González, L., Kelemen, G. H. & Buttner, M. J. The bldC developmental locus of *Streptomyces coelicolor* encodes a member of a family of small DNA-binding proteins related to the DNA-binding domains of the MerR family. *J Bacteriol* **187**, 716-728, doi:10.1128/JB.187.2.716-728.2005 (2005).

**47** Elliot, M. A., Damji, F., Passantino, R., Chater, K. F. & Leskiw, B. K. The *bldD* gene of *Streptomyces coelicolor* A3(2): a regulatory gene involved in morphogenesis and antibiotic production. *J Bacteriol* **180**, 1549-1555 (1998).

**48** Elliot, M. A., Bibb, M. J., Buttner, M. J. & Leskiw, B. K. BldD is a direct regulator of key developmental genes in *Streptomyces coelicolor* A3(2). *Mol Microbiol* **40**, 257-269 (2001).

**49** Kelemen, G. H. *et al*. A connection between stress and development in the multicellular prokaryote *Streptomyces coelicolor* A3(2). *Mol Microbiol* **40**, 804-814 (2001).

**50** Bignell, D. R. D., Warawa, J. L., Strap, J. L., Chater, K. F. & Leskiw, B. K. Study of the *bldG* locus suggests that an anti-anti-sigma factor and an anti-sigma factor may be involved in *Streptomyces coelicolor* antibiotic production and sporulation. *Microbiology* **146**, 2161-2173 (2000).

**51** Sevcikova, B., Rezuchova, B., Homerova, D. & Kormanec, J. The anti-anti-sigma factor BldG is involved in activation of the stress response sigma factor σH in *Streptomyces coelicolor* A3(2). *J Bacteriol* **192**, 5674-5681, doi:10.1128/JB.00828-10 (2010).

**52** Nodwell, J. R., McGovern, K. & Losick, R. An oligopeptide permease responsible for the import of an extracellular signal governing aerial mycelium formation in *Streptomyces coelicolor*. *Mol Microbiol* **22**, 881-893 (1996).

**53** Nodwell, J. R., Yang, M., Kuo, D. & Losick, R. Extracellular complementation and the identification of additional genes involved in aerial mycelium formation in *Streptomyces coelicolor*. *Genetics* **151**, 569-584 (1999).

**54** Akanuma, G., Ueki, M., Ishizuka, M., Ohnishi, Y. & Horinouchi, S. Control of aerial mycelium formation by the BldK oligopeptide ABC transporter in *Streptomyces griseus*. *FEMS Microbiol Lett* **315**, 54-62, doi:10.1111/j.1574-6968.2010.02177.x (2011).

**55** Molle, V. & Buttner, M. J. Different alleles of the response regulator gene *bldM* arrest *Streptomyces coelicolor* development at distinct stages. *Mol Microbiol* **36**, 1265-1278 (2000).

**56** Al-Bassam, M. M., Bibb, M. J., Bush, M. J., Chandra, G. & Buttner, M. J. Response regulator heterodimer formation controls a key stage in *Streptomyces* development. *PLoS Genet* **10**, e1004554, doi:10.1371/journal.pgen.1004554 (2014).

**57** Bibb, M. J., Domonkos, A., Chandra, G. & Buttner, M. J. Expression of the chaplin and rodlin hydrophobic sheath proteins in *Streptomyces venezuelae* is controlled by σ(BldN) and a cognate anti-sigma factor, RsbN. *Mol Microbiol* **84**, 1033-1049, doi:10.1111/j.1365-2958.2012.08070.x (2012).

**58** Bibb, M. J., Molle, V. & Buttner, M. J. σ(BldN), an extracytoplasmic function RNA polymerase sigma factor required for aerial mycelium formation in *Streptomyces coelicolor* A3(2). *J Bacteriol* **182**, 4606-4616 (2000).

**59** Yamazaki, H., Ohnishi, Y. & Horinouchi, S. An A-factor-dependent extracytoplasmic function sigma factor (σ(AdsA)) that is essential for morphological development in *Streptomyces griseus*. *J Bacteriol* **182**, 4596-4605 (2000).

**60** Bush, M. J., Bibb, M. J., Chandra, G., Findlay, K. C. & Buttner, M. J. Genes required for aerial growth, cell division, and chromosome segregation are targets of WhiA before sporulation in *Streptomyces venezuelae*. *mBio* **4**, e00684-00613, doi:10.1128/mBio.00684-13 (2013).

**61** Bush, M. J., Chandra, G., Bibb, M. J., Findlay, K. C. & Buttner, M. J. Genome-wide chromatin immunoprecipitation sequencing analysis shows that WhiB is a transcription factor that cocontrols its regulon with WhiA to initiate developmental cell division in *Streptomyces*. *MBio* **7**, e00523-00516, doi:10.1128/mBio.00523-16 (2016).

**62** Soliveri, J. A., Gomez, J., Bishai, W. R. & Chater, K. F. Multiple paralogous genes related to the *Streptomyces coelicolor* developmental regulatory gene *whiB* are present in *Streptomyces* and other actinomycetes. *Microbiology* **146**, 333-343 (2000).

**63** Molle, V., Palframan, W. J., Findlay, K. C. & Buttner, M. J. WhiD and WhiB, homologous proteins required for different stages of sporulation in *Streptomyces coelicolor* A3(2). *J Bacteriol* **182**, 1286-1295 (2000).

**64** Jakimowicz, P. *et al*. Evidence that the *Streptomyces* developmental protein WhiD, a member of the WhiB family, binds a [4Fe-4S] cluster. *J Biol Chem* **280**, 8309-8315, doi:10.1074/jbc.M412622200 (2005).

**65** Kelemen, G. H. *et al*. Developmental regulation of transcription of *whiE*, a locus specifying the polyketide spore pigment in *Streptomyces coelicolor* A3(2). *J Bacteriol* **180**, 2515-2521 (1998).

**66** Kelemen, G. H. *et al*. The positions of the sigma-factor genes, *whiG* and *sigF,* in the hierarchy controlling the development of spore chains in the aerial hyphae of *Streptomyces coelicolor* A3(2). *Mol Microbiol* **21**, 593-603 (1996).

**67** Liu, S. P. *et al*. Sigma factor $WhiG_{ch}$ positively regulates natamycin production in *Streptomyces* chattanoogensis L10. *Appl Microbiol Biotechnol* **99**, 2715-2726, doi:10.1007/s00253-014-6307-1 (2015).

**68** Ryding, N. J. *et al*. A developmentally regulated gene encoding a repressor-like protein is essential for sporulation in *Streptomyces coelicolor* A3(2). *Mol Microbiol* **29**, 343-357 (1998).

**69** Aínsa, J. A., Parry, H. D. & Chater, K. F. A response regulator-like protein that functions at an intermediate stage of sporulation in *Streptomyces coelicolor* A3(2). *Mol Microbiol* **34**, 607-619 (1999).

**70** Tian, Y., Fowler, K., Findlay, K., Tan, H. & Chater, K. F. An unusual response regulator influences sporulation at early and late stages in *Streptomyces coelicolor*. *J Bacteriol* **189**, 2873-2885, doi:10.1128/JB.01615-06 (2007).

**71** Gehring, A. M., Nodwell, J. R., Beverley, S. M. & Losick, R. Genomewide insertional mutagenesis in *Streptomyces coelicolor* reveals additional genes involved in morphological differentiation. *Proc Natl Acad Sci U S A* **97**, 9642-9647, doi : 10.1073/pnas.170059797 (2000).

**72** Aínsa, J. A., Bird, N., Ryding, N. J., Findlay, K. C. & Chater, K. F. The complex *whiJ* locus mediates environmentally sensitive repression of development of *Streptomyces coelicolor* A3(2). *Antonie Van Leeuwenhoek* **98**, 225-236, doi:10.1007/s10482-010-9443-3 (2010).

**73** Kodani, S. *et al*. The SapB morphogen is a lantibiotic-like peptide derived from the product of the developmental gene *ramS* in *Streptomyces coelicolor*. *Proc Natl Acad Sci U S A* **101**, 11448-11453, doi:10.1073/pnas.0404220101 (2004).

**74** Ma, H. & Kendall, K. Cloning and analysis of a gene cluster from *Streptomyces coelicolor* that causes accelerated aerial mycelium formation in *Streptomyces lividans*. *J Bacteriol* **176**, 3800-3811 (1994).

**75** Nguyen, K. T. *et al*. A central regulator of morphological differentiation in the multicellular bacterium *Streptomyces coelicolor*. *Mol Microbiol* **46**, 1223-1238 (2002).

**76** Blundell, K. L. I. M., Wilson, M. T., Svistunenko, D. A., Vijgenboom, E. & Worrall, J. A. R. Morphological development and cytochrome c oxidase activity in *Streptomyces lividans* are dependent on the action of a copper bound Sco protein. *Open Biol* **3**, 120163, doi:10.1098/rsob.120163 (2013).

**77** Petrus, M. L. C. *et al*. The DyP-type peroxidase DtpA is a Tat-substrate required for GlxA maturation and morphogenesis in *Streptomyces*. *Open Biol* **6**, 150149, doi:10.1098/rsob.150149 (2016).

**78** Flärdh, K. Essential role of DivIVA in polar growth and morphogenesis in *Streptomyces coelicolor* A3(2). *Mol Microbiol* **49**, 1523-1536 (2003).

**79** Edwards, D. H., Thomaides, H. B. & Errington, J. Promiscuous targeting of *Bacillus subtilis* cell division protein DivIVA to division sites in *Escherichia coli* and fission yeast. *EMBO J* **19**, 2719-2727 (2000).

**80** Lenarcic, R. *et al*. Localisation of DivIVA by targeting to negatively curved membranes. *EMBO J* **28**, 2272-2282, doi:10.1038/emboj.2009.129 (2009).

**81** Letek, M. *et al*. DivIVA is required for polar growth in the MreB-lacking rod-shaped actinomycete *Corynebacterium glutamicum*. *J Bacteriol* **190**, 3283-3292, doi:10.1128/JB.01934-07 (2008).

**82** Holmes, N. A. *et al*. Coiled-coil protein Scy is a key component of a multiprotein assembly controlling polarized growth in *Streptomyces*. *Proc Natl Acad Sci U S A* **110**, E397-406, doi:10.1073/pnas.1210657110 (2013).

**83** Ausmees, N. Coiled coil cytoskeletons collaborate in polar growth of *Streptomyces*. *Bioarchitecture* **3**, 110-112 (2013).

**84** Edwards, D. H. & Errington, J. The *Bacillus subtilis* DivIVA protein targets to the division septum and controls the site specificity of cell division. *Mol Microbiol* **24**, 905-915 (1997).

**85** Perry, S. E. & Edwards, D. H. The *Bacillus subtilis* DivIVA protein has a sporulation-specific proximity to Spo0J. *J Bacteriol* **188**, 6039-6043 (2006).

**86** Celler, K., Koning, R. I., Willemse, J., Koster, A. J. & van Wezel, G. P. Cross-membranes orchestrate compartmentalization and morphogenesis in *Streptomyces*. *Nat Commun* **7**, ncomms11836, doi:10.1038/ncomms11836 (2016).

**87** Yagüe, P. *et al*. Subcompartmentalization by cross-membranes during early growth of *Streptomyces* hyphae. *Nat Commun* **7**, 12467, doi:10.1038/ncomms12467 (2016).

**88** Zacchetti, B., Wösten, H. A. B. & Claessen, D. Multiscale heterogeneity in filamentous microbes. *Biotechnol Adv* **36**, 2138-2149, doi:10.1016/j.biotechadv.2018.10.002 (2018).

**89** Scheffers, D. J. & Pinho, M. G. Bacterial cell wall synthesis: new insights from localization studies. *Microbiol Mol Biol Rev* **69**, 585-607 (2005).

**90** Adams, D. W. & Errington, J. Bacterial cell division: assembly, maintenance and disassembly of the Z ring. *Nat Rev Microbiol* **7**, 642-653, doi:10.1038/nrmicro2198 (2009).

**91** Wu, L. J. & Errington, J. Coordination of cell division and chromosome segregation by a nucleoid occlusion protein in *Bacillus subtilis*. *Cell* **117**, 915-925 (2004).

**92** Bernhardt, T. G. & de Boer, P. A. J. SlmA, a nucleoid-associated, FtsZ binding protein required for blocking septal ring assembly over chromosomes in *E. coli. Mol Cell* **18**, 555-564 (2005).

**93** Dajkovic, A., Lan, G., Sun, S. X., Wirtz, D. & Lutkenhaus, J. MinC spatially controls bacterial cytokinesis by antagonizing the scaffolding function of FtsZ. *Curr Biol* **18**, 235-244, doi:10.1016/j.cub.2008.01.042 (2008).

**94** Höltje, J. V. Growth of the stress-bearing and shape-maintaining murein sacculus of *Escherichia coli*. *Microbiol Mol Biol Rev* **62**, 181-203 (1998).

**95** Cava, F. & de Pedro, M. A. Peptidoglycan plasticity in bacteria: emerging variability of the murein sacculus and their associated biological functions. *Curr Opin Microbiol* **18**, 46-53, doi:10.1016/j.mib.2014.01.004 (2014).

**96** Vollmer, W., Blanot, D. & de Pedro, M. A. Peptidoglycan structure and architecture. *FEMS Microbiol Rev* **32**, 149-167, doi:10.1111/j.1574-6976.2007.00094.x (2008).

**97** Barreteau, H. *et al*. Cytoplasmic steps of peptidoglycan biosynthesis. *FEMS Microbiol Rev* **32**, 168-207, doi:10.1111/j.1574-6976.2008.00104.x (2008).

**98** Typas, A., Banzhaf, M., Gross, C. A. & Vollmer, W. From the regulation of peptidoglycan synthesis to bacterial growth and morphology. *Nat Rev Microbiol* **10**, 123-136, doi:10.1038/nrmicro2677 (2012).

**99** Mohammadi, T. *et al*. Identification of FtsW as a transporter of lipid-linked cell wall precursors across the membrane. *EMBO J*, **30**, 1425-1432, doi:10.1038/emboj.2011.61 (2011).

**100** Ruiz, N. Bioinformatics identification of MurJ (MviN) as the peptidoglycan lipid II flippase in *Escherichia coli*. *Proc Natl Acad Sci U S A* **105**, 15553-15557, doi:10.1073/pnas.0808352105 (2008).

**101** Sham, L. T. *et al*. MurJ is the flippase of lipid-linked precursors for peptidoglycan biogenesis. Science **345**, 220-222, doi:10.1126/science.1254522 (2014).

**102** Meeske, A. J. *et al*. MurJ and a novel lipid II flippase are required for cell wall biogenesis in *Bacillus subtilis*. *Proc Natl Acad Sci U S A* **112**, 6437-6442, doi:10.1073/pnas.1504967112 (2015).

**103** Sauvage, E., Kerff, F., Terrak, M., Ayala, J. A. & Charlier, P. The penicillin-binding proteins: structure and role in peptidoglycan biosynthesis. *FEMS Microbiol Rev* **32**, 234-258, doi:10.1111/j.1574-6976.2008.00105.x (2008).

**104** Vollmer, W. & Bertsche, U. Murein (peptidoglycan) structure, architecture and biosynthesis in *Escherichia coli*. *Biochim Biophys Acta* **1778**, 1714-1734, doi:10.1016/j.bbamem.2007.06.007 (2008).

**105** Leclercq, S. *et al*. Interplay between Penicillin-binding proteins and SEDS proteins promotes bacterial cell wall synthesis. *Sci Rep* **7**, 43306, doi:10.1038/srep43306 (2017).

**106** Meeske, A. J. *et al*. SEDS proteins are a widespread family of bacterial cell wall polymerases. *Nature* **537**, 634-638, doi:10.1038/nature19331 (2016).

**107** Cho, H. *et al*. Bacterial cell wall biogenesis is mediated by SEDS and PBP polymerase families functioning semi-autonomously. *Nat Microbiol* **1**, 16172, doi:10.1038/nmicrobiol.2016.172 (2016).

**108** Emami, K. *et al*. RodA as the missing glycosyltransferase in *Bacillus subtilis* and antibiotic discovery for the peptidoglycan polymerase pathway. *Nat Microbiol* **2**, 16253, doi:10.1038/nmicrobiol.2016.253 (2017).

**109** Curtis, P. D. & Brun, Y. V. Getting in the loop: regulation of development in *Caulobacter crescentus*. *Microbiol Mol Biol Rev* **74**, 13-41, doi:10.1128/MMBR.00040-09 (2010).

**110** Kearns, D. B. A field guide to bacterial swarming motility. *Nat Rev Microbiol* **8**, 634-644, doi:10.1038/nrmicro2405 (2010).

**111** Verstraeten, N. *et al*. Living on a surface: swarming and biofilm formation. Trends Microbiol **16**, 496-506, doi:10.1016/j.tim.2008.07.004 (2008).

**112** Ultee, E., Ramijan, K., Dame, R. T., Briegel, A. & Claessen, D. Stress-induced adaptive morphogenesis in bacteria. *Advances in Microbial Physiology* **74** (2019).

**113** Jordan, S., Hutchings, M. I. & Mascher, T. Cell envelope stress response in Gram positive bacteria. *FEMS Microbiol Rev* **32**, 107-146, doi:10.1111/j.1574-6976.2007.00091.x (2008).

**114** Raivio, T. L. Envelope stress responses and Gram-negative bacterial pathogenesis. *Mol Microbiol* **56**, 1119-1128, doi:10.1111/j.1365-2958.2005.04625.x (2005).

**115** Stock, A. M., Robinson, V. L. & Goudreau, P. N. Two-component signal transduction. *Annu Rev Biochem* **69**, 183-215, doi:10.1146/annurev.biochem.69.1.183 (2000).

**116** Möker, N. *et al*. Deletion of the genes encoding the MtrA-MtrB two-component system of *Corynebacterium glutamicum* has a strong influence on cell morphology, antibiotics susceptibility and expression of genes involved in osmoprotection. *Mol Microbiol* **54**, 420-438, doi:10.1111/j.1365-2958.2004.04249.x (2004).

**117** Via, L. E. *et al*. Elements of signal transduction in Mycobacterium tuberculosis: in vitro phosphorylation and in vivo expression of the response regulator MtrA. *J Bacteriol* **178**, 3314-3321 (1996).

**118** Cangelosi, G. A. *et al*. The two-component regulatory system *mtrAB* is required for morphotypic multidrug resistance in *Mycobacterium avium*. *Antimicrob Agents Chemother* **50**, 461-468, doi:10.1128/AAC.50.2.461-468.2006 (2006).

**119** Maccario, L., Sanguino, L., Vogel, T. M. & Larose, C. Snow and ice ecosystems: not so extreme. *Res Microbiol* **166**, 782-795, doi:10.1016/j.resmic.2015.09.002 (2015).

**120** Lebre, P. H., De Maayer, P. & Cowan, D. A. Xerotolerant bacteria: surviving through a dry spell. *Nat Rev Microbiol* **15**, 285-296, doi:10.1038/nrmicro.2017.16 (2017).

**121** Chen, X. M. *et al*. Regulation of expression of trehalose-6-phosphate synthase during cold shock in *Arthrobacter* strain A3. *Extremophiles* **15**, 499-508, doi:10.1007/s00792-011-0380-5 (2011).

**122** Chen, X. *et al*. A trehalose biosynthetic enzyme doubles as an osmotic stress sensor to regulate bacterial morphogenesis. *PLOS Genetics* **13**, e1007062, doi:10.1371/journal.pgen.1007062 (2017).

**123** Jan, G., Leverrier, P., Pichereau, V. & Boyaval, P. Changes in protein synthesis and morphology during acid adaptation of *Propionibacterium freudenreichii*. *Appl Environ Microbiol* **67**, 2029-2036, doi:10.1128/AEM.67.5.2029-2036.2001 (2001).

**124** Pinto, D., Santos, M. A. & Chambel, L. Thirty years of viable but nonculturable state research: unsolved molecular mechanisms. *Crit Rev Microbiol* **41**, 61-76, doi:10.3109/1040841X.2013.794127 (2015).

**125** Yang, D. C., Blair, K. M. & Salama, N. R. Staying in shape: the impact of cell shape on bacterial survival in diverse environments. *Microbiol Mol Biol Rev* **80**, 187-203, doi:10.1128/MMBR.00031-15 (2016).

**126** Mizoguchi, H. *et al*. Diversity in protein synthesis and viability of *Helicobacter pylori* coccoid forms in response to various stimuli. *Infect Immun* **66**, 5555-5560 (1998).

**127** Costa, K. *et al*. The morphological transition of *Helicobacter pylori* cells from spiral to coccoid is preceded by a substantial modification of the cell wall. *J Bacteriol* **181**, 3710-3715 (1999).

**128** Chaput, C. *et al*. Role of AmiA in the morphological transition of *Helicobacter pylori* and in immune escape. *PLoS Pathog* **2**, e97, doi:10.1371/journal.ppat.0020097 (2006).

**129** Sowers, K. R., Boone, J. E. & Gunsalus, R. P. Disaggregation of *Methanosarcina* spp. and growth as single cells at elevated osmolarity. *Appl Environ Microbiol* **59**, 3832-3839 (1993).

**130** Williams, T. J. *et al*. Cold adaptation of the Antarctic haloarchaea *Halohasta litchfieldiae* and *Halorubrum lacusprofundi*. *Environ Microbiol* **19**, 2210-2227, doi:10.1111/1462-2920.13705 (2017).

**131** Monahan, L. G. *et al*. Rapid conversion of *Pseudomonas aeruginosa* to a spherical cell morphotype facilitates tolerance to carbapenems and penicillins but increases susceptibility to antimicrobial peptides. *Antimicrob Agents Chemother* **58**, 1956-1962, doi:10.1128/AAC.01901-13 (2014).

**132** Slavchev, G., Michailova, L. & Markova, N. Stress-induced L-forms of *Mycobacterium bovis*: a challenge to survivability. *New Microbiol* **36**, 157-166 (2013).

**133** Klieneberger, E. The natural occurrence of pleuropneumonia-like organisms in apparent symbiosis with *Streptobacillus moniliformis* and other bacteria. *J Pathol Bacteriol* **40**, 93-105 (1935).

**134** Onwuamaegbu, M. E., Belcher, R. A. & Soare, C. Cell wall-deficient bacteria as a cause of infections: a review of the clinical significance. *J Int Med Res* **33**, 1-20 (2005).

**135** Ferguson, C. M. J., Booth, N. A. & Allan, E. J. An ELISA for the detection of *Bacillus subtilis* L-form bacteria confirms their symbiosis in strawberry. *Lett Appl Microbiol* **31**, 390-394 (2000).

**136** Allan, E. J., Hoischen, C. & Gumpert, J. Bacterial L-forms. *Adv Appl Microbiol* **68**, 1-39, doi:10.1016/S0065-2164(09)01201-5 (2009).

**137** Errington, J. L-form bacteria, cell walls and the origins of life. *Open Biol* **3**, 120143, doi:10.1098/rsob.120143 (2013).

**138** Errington, J., Mickiewicz, K., Kawai, Y. & Wu, L. J. L-form bacteria, chronic diseases and the origins of life. *Phil Trans R Soc B* **371**, 20150494, doi : 10.1098/rstb.2015.0494 (2016).

**139** Leaver, M., Dominguez-Cuevas, P., Coxhead, J. M., Daniel, R. A. & Errington, J. Life without a wall or division machine in *Bacillus subtilis*. *Nature* **457**, 849-853, doi:10.1038/nature07742 (2009).

**140** Mercier, R., Kawai, Y. & Errington, J. General principles for the formation and proliferation of a wall-free (L-form) state in bacteria. *Elife* **3**, 04629, doi:10.7554/eLife.04629 (2014).

**141** Mercier, R., Kawai, Y. & Errington, J. Excess membrane synthesis drives a primitive mode of cell proliferation. *Cell* **152**, 997-1007, doi:10.1016/j.cell.2013.01.043 (2013).

**142** Cronan, J. E., Jr. & Waldrop, G. L. Multi-subunit acetyl-CoA carboxylases. *Prog Lipid Res* **41**, 407-435 (2002).

**143** Kawai, Y. *et al*. Cell growth of wall-free L-form bacteria is limited by oxidative damage. *Curr Biol* **25**, 1613-1618, doi:10.1016/j.cub.2015.04.031 (2015).

**144** Domínguez-Cuevas, P., Mercier, R., Leaver, M., Kawai, Y. & Errington, J. The rod to L-form transition of *Bacillus subtilis* is limited by a requirement for the protoplast to escape from the cell wall sacculus. *Mol Microbiol* **83**, 52-66, doi:10.1111/j.1365-2958.2011.07920.x (2012).

**145** Briers, Y. *et al*. Intracellular vesicles as reproduction elements in cell wall-deficient L-form bacteria. *PLoS One* **7**, e38514, doi:10.1371/journal.pone.0038514 (2012).

**146** Cambré, A. *et al*. Metabolite profiling and peptidoglycan analysis of transient cell wall-deficient bacteria in a new *Escherichia coli* model system. *Environ Microbiol* **17**, doi:10.1111/1462-2920.12594 (2014).

**147** Dell'Era, S. *et al*. *Listeria monocytogenes* L-forms respond to cell wall deficiency by modifying gene expression and the mode of division. *Mol Microbiol* **73**, 306-322, doi:10.1111/j.1365-2958.2009.06774.x (2009).

**148** Studer, P. *et al*. Proliferation of *Listeria monocytogenes* L-form cells by formation of internal and external vesicles. *Nat Commun* **7**, 13631, doi:10.1038/ncomms13631 (2016).

**149** Mercier, R., Dominguez-Cuevas, P. & Errington, J. Crucial role for membrane fluidity in proliferation of primitive cells. *Cell Rep* **1**, 417-423, doi:10.1016/j.celrep.2012.03.008 (2012).

**150** Almenoff, P. L., Johnson, A., Lesser, M. & Mattman, L. H. Growth of acid fast L forms from the blood of patients with sarcoidosis. *Thorax* **51**, 530-533 (1996).

**151** Mattman, L. H. & Mattman, P. E. L-Forms of *Streptococcus fecalis* in septicemia. *Arch Intern Med* **115**, 315-321 (1965).

**152** Barile, M. F., Graykowski, E. A., Driscoll, E. J. & Riggs, D. B. L-Form of Bacteria Isolated from Recurrent Aphthous Stomatitis Lesions. *Oral Surg Oral Med Oral Pathol* **16**, 1395-1402 (1963).

**153** Belsheim, M. R., Darwish, R. Z., Watson, W. C. & Schieven, B. Bacterial L-form isolation from inflammatory bowel disease patients. *Gastroenterology* **85**, 364-369 (1983).

**154** Chiodini, R. J., Van Kruiningen, H. J., Thayer, W. R. & Coutu, J. A. Spheroplastic phase of mycobacteria isolated from patients with Crohn's disease. *J Clin Microbiol* **24**, 357-363 (1986).

**155** Dimova, T. *et al*. Mother-to-newborn transmission of mycobacterial L-forms and Vδ2 T-cell response in placentobiome of BCG-vaccinated pregnant women. *Sci Rep* **7**, 17366, doi:10.1038/s41598-017-17644-z (2017).

**156** Paton, A. M. & Innes, C. M. J. Methods for the establishment of intracellular associations of L-forms with higher plants. *J Appl Microbiol* **71**, 59-64 (1991).

**157** Verma, S. K. *et al*. Bacterial endophytes from rice cut grass (*Leersia oryzoides* L.) increase growth, promote root gravitropic response, stimulate root hair formation, and protect rice seedlings from disease. *Plant Soil* **422**, 223-238, doi:10.1007/s11104-017-3339-1 (2018).

**158** White, J. F. *et al*. Disease protection and allelopathic interactions of seed-transmitted endophytic pseudomonads of invasive reed grass (*Phragmites australis*). *Plant Soil* **422**, 195-208, doi:10.1007/s11104-016-3169-6 (2018).

**159** Kronheim, S. *et al*. A chemical defence against phage infection. *Nature* **564**, 283-286, doi:10.1038/s41586-018-0767-x (2018).

**160** van der Heul, H. U., Bilyk, B. L., McDowall, K. J., Seipke, R. F. & van Wezel, G. P. Regulation of antibiotic production in Actinobacteria: new perspectives from the post-genomic era. *Nat Prod Rep* **35**, 575-604, doi:10.1039/c8np00012c (2018).

**161** Flärdh, K., Richards, D. M., Hempel, A. M., Howard, M. & Buttner, M. J. Regulation of apical growth and hyphal branching in *Streptomyces*. *Curr Opin Microbiol* **15**, 737-743, doi:10.1016/j.mib.2012.10.012 (2012).

**162** Chater, K. F. Regulation of sporulation in *Streptomyces coelicolor* A3(2): a checkpoint multiplex? *Curr Opin Microbiol* **4**, 667-673 (2001).

**163** Bentley, S. D. *et al*. Complete genome sequence of the model actinomycete *Streptomyces coelicolor* A3(2). *Nature* **417**, 141-147, doi:10.1038/417141a (2002).

**164** Ichikawa, N. *et al*. Genome sequence of *Kitasatospora setae* NBRC 14216T: an evolutionary snapshot of the family *Streptomycetaceae*. *DNA Res* **17**, 393-406, doi:10.1093/dnares/dsq026 (2010).

**165** Kinashi, H. Giant linear plasmids in *Streptomyces*: a treasure trove of antibiotic biosynthetic clusters. *J Antibiot* **64**, 19-25, doi:10.1038/ja.2010.146 (2011).

**166** Chater, K. F. & Kinashi, H. in *Microbial Linear Plasmids* (eds Friedhelm Meinhardt & Roland Klassen) 1-31 (Springer Berlin Heidelberg, 2007).

**167** Mochizuki, S. *et al*. The large linear plasmid pSLA2-L of *Streptomyces rochei* has an unusually condensed gene organization for secondary metabolism. *Mol Microbiol* **48**, 1501-1510 (2003).

**168** Medema, M. H. *et al*. The sequence of a 1.8-mb bacterial linear plasmid reveals a rich evolutionary reservoir of secondary metabolic pathways. *Genome Biol Evol* **2**, 212-224, doi:10.1093/gbe/evq013 (2010).

**169** Kirby, R. & Chen, C. W. in *Streptomyces*: *Molecular Biology & Biotechnology* (ed P Dyson) 5-26 (Caister Academic Press, 2011).

**170** Chen, C. W. Complications and implications of linear bacterial chromosomes. *Trends Genet* **12**, 192-196 (1996).

**171** Hopwood, D. A. Soil to genomics: the *Streptomyces* chromosome. *Annu Rev Genet* **40**, 1-23, doi:10.1146/annurev.genet.40.110405.090639 (2006).

**172** Nindita, Y. *et al*. The *tap-tpg* gene pair on the linear plasmid functions to maintain a linear topology of the chromosome in *Streptomyces rochei*. *Mol Microbiol* **95**, 846-858, doi:10.1111/mmi.12904 (2015).

**173** Hoff, G., Bertrand, C., Piotrowski, E., Thibessard, A. & Leblond, P. Genome plasticity is governed by double strand break DNA repair in *Streptomyces*. *Sci Rep* **8**, 5272, doi:10.1038/s41598-018-23622-w (2018).

**174** Chen, C. W., Huang, C. H., Lee, H. H., Tsai, H. H. & Kirby, R. Once the circle has been broken: dynamics and evolution of *Streptomyces* chromosomes. *Trends Genet* **18**, 522-529 (2002).

**175** Leblond, P. & Decaris, B. New insights into the genetic instability of *Streptomyces*. *FEMS Microbiol Lett* **123**, 225-232 (1994).

**176** Girard, G. *et al*. Analysis of novel *kitasatosporae* reveals significant evolutionary changes in conserved developmental genes between *Kitasatospora* and *Streptomyces*. *Antonie Van Leeuwenhoek* **106**, 365-380, doi:10.1007/s10482-014-0209-1 (2014).

**177** Redenbach, M., Bibb, M., Gust, B., Seitz, B. & Spychaj, A. The linear plasmid SCP1 of *Streptomyces coelicolor* A3(2) possesses a centrally located replication origin and shows significant homology to the transposon *Tn4811*. *Plasmid* **42**, 174-185, doi:10.1006/plas.1999.1419 (1999).

**178** Weber, T. *et al*. antiSMASH 3.0-a comprehensive resource for the genome mining of biosynthetic gene clusters. *Nucleic Acids Res* **43**, W237-243, doi:10.1093/nar/gkv437 (2015).

**179** Kieser, T., Bibb, M. J., Buttner, M. J., Chater, K. F. & Hopwood, D. A. Practical *Streptomyces genetics*. (The John Innes Foundation, 2000).

**180** Álvarez-Álvarez, R. *et al*. A 1.8-Mb-reduced *Streptomyces clavuligerus* genome: relevance for secondary metabolism and differentiation. *Appl Microbiol Biotechnol* **98**, 2183-2195, doi:10.1007/s00253-013-5382-z (2014).

**181** Bibb, M. J., Ward, J. M. & Hopwood, D. A. Transformation of plasmid DNA into *Streptomyces* at high frequency. *Nature* **274**, 398-400 (1978).

**182** Lu, C., Wu, H., Su, X. & Bai, L. Elimination of indigenous linear plasmids in *Streptomyces hygroscopicus var. jinggangensis* and *Streptomyces* sp. FR008 to increase validamycin A and candicidin productivities. *Appl Microbiol Biotechnol* **101**, 4247-4257, doi:10.1007/s00253-017-8165-0 (2017).

**183** Charusanti, P. *et al*. Exploiting adaptive laboratory evolution of *Streptomyces clavuligerus* for antibiotic discovery and overproduction. *PLoS One* **7**, e33727, doi:10.1371/journal.pone.0033727 (2012).

**184** Hsu, C. C. & Chen, C. W. Linear plasmid SLP2 is maintained by partitioning, intrahyphal spread, and conjugal transfer in *Streptomyces*. *J Bacteriol* **192**, 307-315, doi:10.1128/JB.01192-09 (2010).

**185** Zhang, Z. *et al*. Antibiotic production is organized by a division of labour in *Streptomyces*. *bioRxiv*, 560136, doi:10.1101/560136 (2019).

**186** Lin, Y. S. & Chen, C. W. Instability of artificially circularized chromosomes of *Streptomyces lividans*. *Mol Microbiol* **26**, 709-719 (1997).

**187** Daveran-Mingot, M. L., Campo, N., Ritzenthaler, P. & Le Bourgeois, P. A natural large chromosomal inversion in *Lactococcus lactis* is mediated by homologous recombination between two insertion sequences. *J Bacteriol* **180**, 4834-4842 (1998).

**188** Gaffé, J. *et al*. Insertion sequence-driven evolution of *Escherichia coli* in chemostats. *J Mol Evol* **72**, 398-412, doi:10.1007/s00239-011-9439-2 (2011).

**189** Gravius, B., Bezmalinović, T., Hranueli, D. & Cullum, J. Genetic instability and strain degeneration in *Streptomyces rimosus*. *Appl Environ Microbiol* **59**, 2220-2228 (1993).

**190** Redenbach, M. *et al*. The *Streptomyces lividans* 66 chromosome contains a 1 MB deletogenic region flanked by two amplifiable regions. *Mol Gen Genet* **241**, 255-262 (1993).

**191** Leblond, P. *et al*. Hypervariability, a new phenomenon of genetic instability, related to DNA amplification in *Streptomyces ambofaciens*. *J Bacteriol* **171**, 419-423 (1989).

**192** Vandecraen, J., Chandler, M., Aertsen, A. & Van Houdt, R. The impact of insertion sequences on bacterial genome plasticity and adaptability. *Crit Rev Microbiol* **43**, 709-730, doi:10.1080/1040841X.2017.1303661 (2017).

**193** Fuchino, K., Flärdh, K., Dyson, P. & Ausmees, N. Cell-biological studies of osmotic shock response in *Streptomyces* spp. *J Bacteriol* **199**, e00465-00416, doi:10.1128/JB.00465-16 (2017).

**194** Ramijan, K. *et al*. Stress-induced formation of cell wall-deficient cells in filamentous actinomycetes. *Nat Commun* **9**, 5164, doi:https://doi.org/10.1101/094037 (2018).

**195** Stuttard, C. Temperate phages of *Streptomyces venezuelae*: lysogeny and host specificity shown by phages SV1 and SV2. *J Gen Microbiol* **128**, 115-121 (1982).

**196** Chikhi, R. & Medvedev, P. Informed and automated k-mer size selection for genome assembly. *Bioinformatics* **30**, 31-37, doi:10.1093/bioinformatics/btt310 (2014).

**197** Chaisson, M. J. & Tesler, G. Mapping single molecule sequencing reads using basic local alignment with successive refinement (BLASR): application and theory. *BMC Bioinformatics* **13**, 238, doi:10.1186/1471-2105-13-238 (2012).

**198** Boetzer, M. & Pirovano, W. SSPACE-LongRead: scaffolding bacterial draft genomes using long read sequence information. *BMC Bioinformatics* **15**, 211, doi:10.1186/1471-2105-15-211 (2014).

**199** Boetzer, M. & Pirovano, W. Toward almost closed genomes with GapFiller. *Genome Biol* 1**3**, R56, doi:10.1186/gb-2012-13-6-r56 (2012).

**200** Sleator, R. D. & Hill, C. Bacterial osmoadaptation: the role of osmolytes in bacterial stress and virulence. *FEMS Microbiol Rev* **26**, 49-71 (2002).

**201** Poolman, B., Spitzer, J. J. & Wood, J. M. Bacterial osmosensing: roles of membrane structure and electrostatics in lipid–protein and protein–protein interactions. *Biochimica et Biophysica Acta (BBA) - Biomembranes* **1666**, 88-104, doi:https://doi.org/10.1016/j.bbamem.2004.06.013 (2004).

**202** Kysela, D. T., Randich, A. M., Caccamo, P. D. & Brun, Y. V. Diversity takes shape: understanding the mechanistic and adaptive basis of bacterial morphology. *PLoS Biol* **14**, e1002565, doi:10.1371/journal.pbio.1002565 (2016).

**203** Szwedziak, P. & Löwe, J. Do the divisome and elongasome share a common evolutionary past? *Curr Opin Microbiol* **16**, 745-751, doi:10.1016/j.mib.2013.09.003 (2013).

**204** Claessen, D. *et al*. Control of the cell elongation-division cycle by shuttling of PBP1 protein in *Bacillus subtilis*. *Mol Microbiol* **68**, 1029-1046, doi:10.1111/j.1365-2958.2008.06210.x (2008).

**205** Claessen, D., Rozen, D. E., Kuipers, O. P., Søgaard-Andersen, L. & van Wezel, G. P. Bacterial solutions to multicellularity: a tale of biofilms, filaments and fruiting bodies. *Nat Rev Microbiol* **12**, 115-124, doi:10.1038/nrmicro3178 (2014).

**206** Alvarez, H. M. *et al*. Physiological and morphological responses of the soil bacterium *Rhodococcus opacus* strain PD630 to water stress. *FEMS Microbiology Ecology* **50**, 75-86, doi:10.1016/j.femsec.2004.06.002 (2004).

**207** Frenkel, A. & Hirsch, W. Spontaneous development of L forms of Streptococci requiring secretions of other bacteria or sulphydryl compounds for normal growth. *Nature* **191**, 728-730 (1961).

**208** Innes, C. M. J. & Allan, E. J. Induction, growth and antibiotic production of *Streptomyces viridifaciens* L-form bacteria. *J Appl Microbiol* **90**, 301-308 (2001).

**209** Zhu, H. *et al*. Eliciting antibiotics active against the ESKAPE pathogens in a collection of actinomycetes isolated from mountain soils. *Microbiology* **160**, 1714-1725, doi:10.1099/mic.0.078295-0 (2014).

**210** Ramijan, K., van Wezel, G. P. & Claessen, D. Genome sequence of the filamentous actinomycete *Kitasatospora viridifaciens*. *Genome Announc* **5**, doi:10.1128/genomeA.01560-16 (2017).

**211** Kempf, B. & Bremer, E. Uptake and synthesis of compatible solutes as microbial stress responses to high-osmolality environments. *Arch Microbiol* **170**, 319-330 (1998).

**212** de Maayer, P., Anderson, D., Cary, C. & Cowan, D. A. Some like it cold: understanding the survival strategies of psychrophiles. *EMBO Rep* **15**, 508-517, doi:10.1002/embr.201338170 (2014).

**213** Jones, S. E. *et al*. *Streptomyces* exploration is triggered by fungal interactions and volatile signals. *Elife* **6**, doi:10.7554/eLife.21738 (2017).

**214** Markova, N., Slavchev, G., Michailova, L. & Jourdanova, M. Survival of *Escherichia coli* under lethal heat stress by L-form conversion. *Int J Biol Sci* **6**, 303-315 (2010).

**215** Leblond, P., Demuyter, P., Simonet, J. M. & Decaris, B. Genetic instability and hypervariability in *Streptomyces ambofaciens*: towards an understanding of a mechanism of genome plasticity. *Mol Microbiol* **4**, 707-714 (1990).

**216** Bos, J. *et al*. Emergence of antibiotic resistance from multinucleated bacterial filaments. *Proc Natl Acad Sci U S A* **112**, 178-183, doi:10.1073/pnas.1420702111 (2015).

**217** Suzuki, T., Yamada, M. & Sakaguchi, S. Occurrence of chromosome rearrangements during the fusion process in the imperfect yeast *Candida albicans*. *Microbiology* **140** (12), 3319-3328, doi : 10.1099/13500872-140-12-3319 (1994).

**218** Kilcher, S., Studer, P., Muessner, C., Klumpp, J. & Loessner, M. J. Cross-genus rebooting of custom-made, synthetic bacteriophage genomes in L-form bacteria. *Proc Natl Acad Sci USA* **115**, 567-572, doi:10.1073/pnas.1714658115 (2018).

**219** Kawai, Y., Mickiewicz, K. & Errington, J. Lysozyme counteracts β-Lactam antibiotics by promoting the emergence of L-form bacteria. *Cell* **172**, 1038-1049.e1010, doi:https://doi.org/10.1016/j.cell.2018.01.021 (2018).

**220** Schindelin, J. *et al*. Fiji: an open-source platform for biological-image analysis. *Nat Methods* **9**, 676-682, doi:10.1038/nmeth.2019 (2012).

**221** Vara, J., Lewandowska-Skarbek, M., Wang, Y. G., Donadio, S. & Hutchinson, C. R. Cloning of genes governing the deoxysugar portion of the erythromycin biosynthesis pathway in *Saccharopolyspora erythraea* (*Streptomyces erythreus*). *J Bacteriol* **171**, 5872-5881 (1989).

**222** Świątek, M. A., Tenconi, E., Rigali, S. & van Wezel, G. P. Functional analysis of the N-acetylglucosamine metabolic genes of *Streptomyces coelicolor* and role in control of development and antibiotic production. *J Bacteriol* **194**, 1136-1144, doi:10.1128/JB.06370-11 (2012).

**223** Liu, Y. & Breukink, E. The membrane steps of bacterial cell wall synthesis as antibiotic targets. *Antibiotics (Basel)* **5**, doi:10.3390/antibiotics5030028 (2016).

**224** Pazos, M., Peters, K. & Vollmer, W. Robust peptidoglycan growth by dynamic and variable multi-protein complexes. *Curr Opin Microbiol* **36**, 55-61, doi:10.1016/j.mib.2017.01.006 (2017).

**225** Vicente, M. & Errington, J. Structure, function and controls in microbial division. *Mol Microbiol* **20**, 1-7 (1996).

**226** Tamames, J., González-Moreno, M., Mingorance, J., Valencia, A. & Vicente, M. Bringing gene order into bacterial shape. *Trends Genet* **17**, 124-126 (2001).

**227** Mingorance, J., Tamames, J. & Vicente, M. Genomic channeling in bacterial cell division. *J Mol Recognit* **17**, 481-487, doi:10.1002/jmr.718 (2004).

**228** Marston, A. L., Thomaides, H. B., Edwards, D. H., Sharpe, M. E. & Errington, J. Polar localization of the MinD protein of *Bacillus subtilis* and its role in selection of the mid-cell division site. *Genes Dev* **12**, 3419-3430 (1998).

**229** Mercier, R., Kawai, Y. & Errington, J. Wall proficient *E. coli* capable of sustained growth in the absence of the Z-ring division machine. *Nature Microbiology* **1**, 16091, doi:10.1038/nmicrobiol.2016.91 (2016).

**230** Briers, Y., Walde, P., Schuppler, M. & Loessner, M. J. How did bacterial ancestors reproduce? Lessons from L-form cells and giant lipid vesicles: multiplication similarities between lipid vesicles and L-form bacteria. *Bioessays* **34**, 1078-1084, doi:10.1002/bies.201200080 (2012).

**231** Schlimpert, S., Flärdh, K. & Buttner, M. Fluorescence Time-lapse Imaging of the complete *S. venezuelae* life cycle using a microfluidic device. *J Vis Exp*, **108**, 53863, doi:10.3791/53863 (2016).

**232** Zacchetti, B. *et al*. Aggregation of germlings is a major contributing factor towards mycelial heterogeneity of *Streptomyces*. *Sci Rep* **6**, 27045, doi:10.1038/srep27045 (2016).

**233** Letunic, I. & Bork, P. 20 years of the SMART protein domain annotation resource. *Nucleic Acids Res* **46**, D493-D496, doi:10.1093/nar/gkx922 (2018).

**234** El-Gebali, S. *et al*. The Pfam protein families database in 2019. *Nucleic Acids Res* **47**, D427-D432, doi:10.1093/nar/gky995 (2019).

**235** Letunic, I. & Bork, P. Interactive Tree Of Life (iTOL) v4: recent updates and new developments. *Nucleic Acids Res*, doi:10.1093/nar/gkz239 (2019).

**236** Zhang, L., Willemse, J., Hoskisson, P. A. & van Wezel, G. P. Sporulation-specific cell division defects in *ylmE* mutants of *Streptomyces coelicolor* are rescued by additional deletion of *ylmD*. *Sci Rep* **8**, 7328, doi:10.1038/s41598-018-25782-1 (2018).

**237** Zhang, L., Willemse, J., Claessen, D. & van Wezel, G. P. SepG coordinates sporulation-specific cell division and nucleoid organization in *Streptomyces coelicolor*. *Open Biol* **6**, 150164, doi:10.1098/rsob.150164 (2016).

**238** Taguchi, A. *et al*. FtsW is a peptidoglycan polymerase that is functional only in complex with its cognate penicillin-binding protein. *Nat Microbiol* **4**, 587-594, doi:10.1038/s41564-018-0345-x (2019).

**239** Sun, J., Kelemen, G. H., Fernández-Abalos, J. M. & Bibb, M. J. Green fluorescent protein as a reporter for spatial and temporal gene expression in *Streptomyces coelicolor* A3(2). *Microbiology* **145**, 2221-2227 (1999).

**240** Gust, B., Challis, G. L., Fowler, K., Kieser, T. & Chater, K. F. PCR-targeted *Streptomyces* gene replacement identifies a protein domain needed for biosynthesis of the sesquiterpene soil odor geosmin. *Proc Natl Acad Sci U S A* **100**, 1541-1546, doi:10.1073/pnas.0337542100 (2003).

**241** Redenbach, M. *et al*. A set of ordered cosmids and a detailed genetic and physical map for the 8 Mb *Streptomyces coelicolor* A3(2) chromosome. *Mol Microbiol* **21**, 77-96 (1996).

**242** van der Aart, L. T., Lemmens, N., van Wamel, W. J. & van Wezel, G. P. Substrate inhibition of VanA by d-alanine reduces vancomycin resistance in a VanX-dependent manner. *Antimicrob Agents Chemother* **60**, 4930-4939, doi:10.1128/AAC.00276-16 (2016).

**243** van der Aart, L. T. *et al*. High-resolution analysis of the peptidoglycan composition in *Streptomyces coelicolor*. *J Bacteriol* **200**, doi:10.1128/JB.00290-18 (2018).

**244** Kühner, D., Stahl, M., Demircioglu, D. D. & Bertsche, U. From cells to muropeptide structures in 24 h: peptidoglycan mapping by UPLC-MS. *Sci Rep* **4**, 7494, doi:10.1038/srep07494 (2014).

**245** Medema, M. H., Takano, E. & Breitling, R. Detecting sequence homology at the gene cluster level with MultiGeneBlast. *Mol Biol Evol* **30**, 1218-1223, doi:10.1093/molbev/mst025 (2013).

**246** Katoh, K. & Standley, D. M. MAFFT multiple sequence alignment software version 7: improvements in performance and usability. *Mol Biol Evol* **30**, 772-780, doi:10.1093/molbev/mst010 (2013).

**247** Shen, W., Le, S., Li, Y. & Hu, F. SeqKit: a cross-platform and ultrafast toolkit for FASTA/Q file manipulation. *PLoS One* **11**, e0163962, doi:10.1371/journal.pone.0163962 (2016).

**248** Stamatakis, A. RAxML version 8: a tool for phylogenetic analysis and post-analysis of large phylogenies. *Bioinformatics* **30**, 1312-1313, doi:10.1093/bioinformatics/btu033 (2014).

**249** Eddy, S. R. Accelerated profile HMM searches. *PLoS Comput Biol* **7**, e1002195, doi:10.1371/journal.pcbi.1002195 (2011).

**250** Shannon, P. *et al*. Cytoscape: a software environment for integrated models of biomolecular interaction networks. *Genome Res* 13, 2498-2504, doi:10.1101/gr.1239303 (2003).

**251** Hanahan, D. Studies on transformation of *Escherichia coli* with plasmids. *J Mol Biol* **166**, 557-580 (1983).

**252** Yanisch-Perron, C., Vieira, J. & Messing, J. Improved M13 phage cloning vectors and host strains: nucleotide sequences of the M13mp18 and pUC19 vectors. *Gene* **33**, 103-119 (1985).

**253** MacNeil, D. J. *et al*. Analysis of *Streptomyces avermitilis* genes required for avermectin biosynthesis utilizing a novel integration vector. *Gene* **111**, 61-68 (1992).

**254** Jerpseth, B. & Kretz, B. L. SCS110: *dam-, dcm-, endA-* Epicurian coli® competent cells. *Strategies* **6**, 22 (1993).

**255** Chater, K. F. *Streptomyces* inside-out: a new perspective on the bacteria that provide us with antibiotics. *Philos Trans R Soc Lond B Biol Sci* **361**, 761-768, doi:10.1098/rstb.2005.1758 (2006).

**256** Bérdy, J. Thoughts and facts about antibiotics: where we are now and where we are heading. *J Antibiot* **65**, 385-395, doi:10.1038/ja.2012.27 (2012).

**257** Chater, K. F., Biro, S., Lee, K. J., Palmer, T. & Schrempf, H. The complex extracellular biology of *Streptomyces*. *FEMS Microbiol Rev* **34**, 171-198, doi:10.1111/j.1574-6976.2009.00206.x (2010).

**258** Book, A. J. *et al*. Evolution of high cellulolytic activity in symbiotic *Streptomyces* through selection of expanded gene content and coordinated gene expression. *PLoS Biol* **14**, e1002475, doi:10.1371/journal.pbio.1002475 (2016).

**259** Schaerlaekens, K., Van Mellaert, L., Lammertyn, E., Geukens, N. & J., A. The importance of the Tat-dependent protein secretion pathway in *Streptomyces* as revealed by phenotypic changes in *tat* deletion mutants and genome analysis. *Microbiology* **150**, 21-31 (2004).

**260** Widdick, D. A. *et al*. The twin-arginine translocation pathway is a major route of protein export in *Streptomyces coelicolor*. *Proc Natl Acad Sci U S A* **103**, 17927-17932, doi:10.1073/pnas.0607025103 (2006).

**261** De Keersmaeker, S. *et al*. Functional analysis of TatA and TatB in *Streptomyces lividans*. *Biochem Biophys Res Commun* **335**, 973-982, doi:10.1016/j.bbrc.2005.07.165 (2005).

**262** Anné, J., Maldonado, B., Van Impe, J., Van Mellaert, L. & Bernaerts, K. Recombinant protein production and streptomycetes. *J Biotechnol* **158**, 159-167, doi:10.1016/j.jbiotec.2011.06.028 (2012).

**263** Ditkowski, B. *et al*. Dynamic interplay of ParA with the polarity protein, Scy, coordinates the growth with chromosome segregation in *Streptomyces coelicolor*. *Open Biol* **3**, 130006, doi:10.1098/rsob.130006 (2013).

**264** Kois-Ostrowska, A. *et al*. Unique function of the bacterial chromosome segregation machinery in apically growing *Streptomyces* - targeting the chromosome to new hyphal tubes and its anchorage at the tips. *PLoS Genet* **12**, e1006488, doi:10.1371/journal.pgen.1006488 (2016).

**265** Flärdh, K. Growth polarity and cell division in *Streptomyces*. *Curr Opin Microbiol* **6**, 564-571 (2003).

**266** Willemse, J. *et al*. Dynamic localization of Tat protein transport machinery components in *Streptomyces coelicolor*. *J Bacteriol* **194**, 6272-6281, doi:10.1128/JB.01425-12 (2012).

**267** Celler, K., van Wezel, G. P. & Willemse, J. Single particle tracking of dynamically localizing TatA complexes in *Streptomyces coelicolor*. *Biochem Biophys Res Commun* **438**, 38-42, doi:10.1016/j.bbrc.2013.07.016 (2013).

**268** Flärdh, K. Cell polarity and the control of apical growth in *Streptomyces*. *Curr Opin Microbiol* **13**, 758-765, doi:10.1016/j.mib.2010.10.002 (2010).

**269** Gumpert, J., Cron, H., Plapp, R., Niersbach, H. & Hoischen, C. Synthesis and secretion of recombinant penicillin G acylase in bacterial L-forms. *J Basic Microbiol* **36**, 89-98 (1996).

**270** Gumpert, J. & Hoischen, C. Use of cell wall-less bacteria (L-forms) for efficient expression and secretion of heterologous gene products. *Curr Opin Biotechnol* **9**, 506-509 (1998).

**271** Baudler, E. & Gumpert, J. Isolation of a protoplast-type L-form from *Streptomyces hygroscopicus*. *Z Allg Mikrobiol* **19**, 363-365 (1979).

**272** Gumpert, J. Growth characteristics and ultrastructure of protoplast type L-forms from streptomycetes. *Z Allg Mikrobiol* **22**, 617-627 (1982).

**273** van Dissel, D., Claessen, D. & van Wezel, G. P. Morphogenesis of *Streptomyces* in submerged cultures. *Adv Appl Microbiol* **89**, 1-45, doi:10.1016/B978-0-12-800259-9.00001-9 (2014).

**274** Gustavsson, M. & Lee, S. Y. Prospects of microbial cell factories developed through systems metabolic engineering. *Microb Biotechnol* **9**, 610-617, doi:10.1111/1751-7915.12385 (2016).

**275** Casadevall, A., Nosanchuk, J. D., Williamson, P. & Rodrigues, M. L. Vesicular transport across the fungal cell wall. *Trends Microbiol* **17**, 158-162, doi:10.1016/j.tim.2008.12.005 (2009).

**276** Klis, F. M., Boorsma, A. & De Groot, P. W. Cell wall construction in *Saccharomyces cerevisiae*. *Yeast* **23**, 185-202, doi:10.1002/yea.1349 (2006).

**277** Zizlsperger, N. & Keating, A. E. Specific coiled-coil interactions contribute to a global model of the structure of the spindle pole body. *J Struct Biol* **170**, 246-256, doi:10.1016/j.jsb.2010.01.022 (2010).

**278** Zizlsperger, N., Malashkevich, V. N., Pillay, S. & Keating, A. E. Analysis of coiled-coil interactions between core proteins of the spindle pole body. *Biochemistry* **47**, 11858-11868, doi:10.1021/bi801378z (2008).

**279** Moseley, J. B. & Goode, B. L. The yeast actin cytoskeleton: from cellular function to biochemical mechanism. *Microbiol Mol Biol Rev* **70**, 605-645, doi:10.1128/MMBR.00013-06 (2006).

**280** Virag, A. & Harris, S. D. The Spitzenkörper: a molecular perspective. *Mycol Res* **110**, 4-13, doi:10.1016/j.mycres.2005.09.005 (2006).

**281** Steinberg, G. Hyphal growth: a tale of motors, lipids, and the Spitzenkörper. *Eukaryot Cell* **6**, 351-360, doi:10.1128/EC.00381-06 (2007).

**282** Wösten, H. A. B., Moukha, S. M., Sietsma, J. H. & Wessels, J. G. H. Localization of growth and secretion of proteins in *Aspergillus niger*. *J Gen Microbiol* **137**, 2017-2023 (1991).

**283** Peberdy, J. F. Protein secretion in filamentous fungi - trying to understand a highly productive black box. *Trends Biotechnol* **12**, 50-57, doi:10.1016/0167-7799(94)90100-7 (1994).

**284** Lartigue, C. *et al*. Genome transplantation in bacteria: changing one species to another. *Science* **317**, 632-638, doi:10.1126/science.1144622 (2007).

**285** Hutchison, C. A., 3rd *et al*. Design and synthesis of a minimal bacterial genome. *Science* 351, aad6253, doi:10.1126/science.aad6253 (2016).

**286** Bao, K., Wang, H. & Genencor International Inc. Neutral cellulase catalytic core and method of producing same. United States patent *US20060154843A1* (2006).

**287** Teather, R. M. & Wood, P. J. Use of Congo Red-polysaccharide interactions in enumeration and characterization of cellulolytic bacteria from the bovine rumen. *Appl Environ Microbiol* **43**, 777-780 (1982).

**288** Vijgenboom, E. *et al*. Three *tuf*-like genes in the kirromycin producer *Streptomyces ramocissimus*. *Microbiology* **140** (4), 983-998, doi:10.1099/00221287-140-4-983 (1994).

**289** Zhou, Z., Gu, J., Li, Y. Q. & Wang, Y. Genome plasticity and systems evolution in *Streptomyces*. *BMC Bioinformatics* **13**, S8, doi:10.1186/1471-2105-13-S10-S8 (2012).

**290** Lorenzana, L. M., Pérez-Redondo, R., Santamarta, I., Martín, J. F. & Liras, P. Two oligopeptide-permease-encoding genes in the clavulanic acid cluster of *Streptomyces clavuligerus* are essential for production of the β-lactamase inhibitor. *J Bacteriol* **186**, 3431-3438, doi:10.1128/JB.186.11.3431-3438.2004 (2004).

**291** Altenbuchner, J. & Cullum, J. DNA amplification and an unstable arginine gene in *Streptomyces lividans* 66. *Mol Gen Genet* **195**, 134-138 (1984).

**292** Zhang, Z., Claessen, D. & Rozen, D. E. Understanding microbial divisions of labor. *Front Microbiol* **7**, 2070, doi:10.3389/fmicb.2016.02070 (2016).

**293** Trachtenberg, S. Mollicutes - Wall-less bacteria with internal cytoskeletons. *J Struct Biol* **124**, 244-256, doi:10.1006/jsbi.1998.4063 (1998).

**294** Razin, S., Yogev, D. & Naot, Y. Molecular biology and pathogenicity of mycoplasmas. *Microbiology and Molecular Biology Reviews* **62**, 1094-1156 (1998).

**295** Scutigliani, E. M. *et al*. Interfering with DNA decondensation as a strategy against mycobacteria. *Front Microbiol* **9**, 2034, doi:10.3389/fmicb.2018.02034 (2018).

**296** Delmas, S., Duggin, I. G. & Allers, T. DNA damage induces nucleoid compaction via the Mre11-Rad50 complex in the archaeon *Haloferax volcanii*. *Mol Microbiol* **87**, 168-179, doi:10.1111/mmi.12091 (2013).

**297** Shechter, N. *et al*. Stress-induced condensation of bacterial genomes results in repairing of sister chromosomes: implications for double strand DNA break repair. *J Biol Chem* **288**, 25659-25667, doi:10.1074/jbc.M113.473025 (2013).

**298** Siguier, P., Gourbeyre, E. & Chandler, M. Bacterial insertion sequences: their genomic impact and diversity. *FEMS Microbiology Reviews* **38**, 865-891, doi:10.1111/1574-6976.12067 (2014).

**299** Takahashi, Y. Genus *Kitasatospora*, taxonomic features and diversity of secondary metabolites. *J Antibiot* **70**, 506-513, doi:10.1038/ja.2017.8 (2017).

**300** de Jong, W., Vijgenboom, E., Dijkhuizen, L., Wösten, H. A. B. & Claessen, D. *FEMS Microbiol Lett Vol.* 329(2) 154-159 (2012).

**301** Willey, J. M., Willems, A., Kodani, S. & Nodwell, J. R. Morphogenetic surfactants and their role in the formation of aerial hyphae in *Streptomyces coelicolor*. *Mol Microbiol* **59**, 731-742, doi:10.1111/j.1365-2958.2005.05018.x (2006).

**302** Novoa-Aponte, L. & Soto Ospina, C. Y. *Mycobacterium tuberculosis* P-type ATPases: possible targets for drug or vaccine development. *Biomed Res Int* **2014**, 296986, doi:10.1155/2014/296986 (2014).

**303** Sand, M. *et al*. Mannitol-1-phosphate dehydrogenases/phosphatases: a family of novel bifunctional enzymes for bacterial adaptation to osmotic stress. *Environ Microbiol* **17**, 711-719, doi:10.1111/1462-2920.12503 (2015).

**304** Sand, M., Mingote, A. I., Santos, H., Müller, V. & Averhoff, B. Mannitol, a compatible solute synthesized by *Acinetobacter baylyi* in a two-step pathway including a salt-induced and salt-dependent mannitol-1-phosphate dehydrogenase. *Environ Microbiol* **15**, 2187-2197, doi:10.1111/1462-2920.12090 (2013).

**305** Cho, H., Uehara, T. & Bernhardt, T. G. Beta-lactam antibiotics induce a lethal malfunctioning of the bacterial cell wall synthesis machinery. *Cell* **159**, 1300-1311, doi:10.1016/j.cell.2014.11.017 (2014).

**306** Park, J. T. & Uehara, T. How bacteria consume their own exoskeletons (turnover and recycling of cell wall peptidoglycan). *Microbiol Mol Biol Rev* **72**, 211-227, table of contents, doi:10.1128/MMBR.00027-07 (2008).

**307** Radeck, J., Lautenschlager, N. & Mascher, T. The essential UPP phosphatase pair BcrC and UppP connects cell wall homeostasis during growth and sporulation with cell envelope stress response in *Bacillus subtilis*. *Front Microbiol* **8**, 2403, doi:10.3389/fmicb.2017.02403 (2017).

**308** Schneider, T. & Sahl, H. G. An oldie but a goodie - cell wall biosynthesis as antibiotic target pathway. *Int J Med Microbiol* **300**, 161-169, doi:10.1016/j.ijmm.2009.10.005 (2010).

**309** Maloney, E. *et al*. The two-domain LysX protein of *Mycobacterium tuberculosis* is required for production of lysinylated phosphatidylglycerol and resistance to cationic antimicrobial peptides. *PLoS Pathog* **5**, e1000534, doi:10.1371/journal.ppat.1000534 (2009).

**310** Kumariya, R., Sood, S. K., Rajput, Y. S., Saini, N. & Garsa, A. K. Increased membrane surface positive charge and altered membrane fluidity leads to cationic antimicrobial peptide resistance in *Enterococcus faecalis*. *Biochim Biophys Acta* **1848**, 1367-1375, doi:10.1016/j.bbamem.2015.03.007 (2015).

**311** Halbedel, S. & Lewis, R. J. Structural basis for interaction of DivIVA/GpsB proteins with their ligands. *Mol Microbiol*, **111**, 1404-1415, doi:10.1111/mmi.14244 (2019).

**312** Kang, C. M., Nyayapathy, S., Lee, J. Y., Suh, J. W. & Husson, R. N. Wag31, a homologue of the cell division protein DivIVA, regulates growth, morphology and polar cell wall synthesis in mycobacteria. *Microbiology* **154**, 725-735, doi:10.1099/mic.0.2007/014076-0 (2008).

**313** Ramos, A. *et al*. Involvement of DivIVA in the morphology of the rod-shaped actinomycete *Brevibacterium lactofermentum*. *Microbiology* **149**, 3531-3542, doi:10.1099/mic.0.26653-0 (2003).

**314** Kim, B. H., Andersen, C. & Benz, R. Identification of a cell wall channel of *Streptomyces griseus*: the channel contains a binding site for streptomycin. *Mol Microbiol* **41**, 665-673 (2001).

# CV

# Curriculum vitae

Karina Ramijan was born on the 18th of June 1985, in San José, Costa Rica. In 2002, she graduated from the Liceo Laboratorio Emma Gamboa in Moravia. In February 2003 she started a bachelor program on Biotechnology Engineering, at the Technological Institute of Costa Rica (TEC). As part of her undergraduate training she did a 6-months research internship at the Public Intellectual Property Resource for Agriculture (PIPRA), an international initiative hosted by the University of California at Davis (UC Davis). During her time at PIPRA she completed her Bachelor thesis, entitled "Development of Biotechnological tools for the genetic transformation of crops with agronomic and economical interest for Costa Rica". After her graduation in July 2007, she continued working at UC Davis as a Junior Specialist for another year. In 2009 she moved to Germany and started a Master program in Chemical and Bioprocess Engineering from Hamburg University of Technology (TUHH). She did her MSc thesis entitled "Role of highly conserved hisitidines in the catalytic site of a glucose dehydrogenase form *Penicillium chrysogenum*" in the Institute of Technical Microbiology. Prior to her PhD she worked as a Junior Researcher in Abengoa, a highly technological multinational company based in Spain. In 2013 she accepted a PhD position in the Microbial Biotechnology and Health cluster at Leiden University. The work she compiled as PhD student is presented in this thesis: "Off the wall: characterisation and exploitation of a cell wall-deficient life style in filamentous actinomytecess". This thesis was performed under the supervision of Dr. Dennis Claessen and Prof. Gilles van Wezel.

# PB

# Publications

**Ramijan**, K., van Wezel, G. P. & Claessen, D. Genome sequence of the filamentous actinomycete *Kitasatospora viridifaciens*. *Genome Announc* **5** (2017).

**Ramijan**, K. *et al*. Stress-induced formation of cell wall-deficient cells in filamentous actinomycetes. *Nat Commun* **9**, 5164 (2018).

Ultee, E., **Ramijan**, K., Dame, R. T., Briegel, A. & Claessen, D. Stress-induced adaptive morphogenesis in bacteria. *Advances in Microbial Physiology* **74**, 97-141 (2019).